Commun. Math. Phys. (2024) 405:105
Digital Object Identifier (DOI) https://doi.org/10.1007/s00220-024-04956-1

Communications in
Mathematical
Physics

Phase Space Mixing of a Vlasov Gas in the Exterior of a Kerr Black Hole

Paola Rioseco[1], **Olivier Sarbach**[2]

[1] Departamento de Ingeniería Matemática and Centro de Modelamiento Matemático, Universidad de Chile, Beauchef 851, Santiago, Chile
[2] Instituto de Física y Matemáticas, Universidad Michoacana de San Nicolás de Hidalgo, Edificio C-3, Ciudad Universitaria, 58040 Morelia, Michoacán, México. E-mail: olivier.sarbach@umich.mx

Received: 28 February 2023 / Accepted: 1 February 2024

Abstract: We study the dynamics of a collisionless kinetic gas whose particles follow future-directed timelike and spatially bound geodesics in the exterior of a sub-extremal Kerr black hole spacetime. Based on the use of generalized action-angle variables, we analyze the large time asymptotic behavior of macroscopic observables associated with the gas. We show that, as long as the fundamental frequencies of the system satisfy a suitable non-degeneracy condition, these macroscopic observables converge in time to the corresponding observables determined from an averaged distribution function. In particular, this implies that the final state is characterized by a distribution function which is invariant with respect to the full symmetry group of the system, that is, it is stationary, axisymmetric and Poisson-commutes with the integral of motion associated with the Carter constant. As a corollary of our result, we demonstrate the validity of the strong Jeans theorem in our setting, stating that the distribution function belonging to a stationary state must be a function which is independent of the generalized angle variables. An analogous theorem in which the assumption of stationarity is replaced with the requirement of invariance with respect to the Carter flow is also proven. Finally, we prove that the aforementioned non-degeneracy condition holds if the black hole is rotating. This is achieved by providing suitable asymptotic expansions for the energy and Carter constant in terms of action variables for orbits having sufficiently large radii, and by exploiting the analytic dependency of the fundamental frequencies on the integrals of motion.

Contents

Published online: 16 April 2024

1. Introduction

In recent years there has been much interest on the properties of solutions of the Einstein-Vlasov system (see [1] for a review). Even neglecting its self-gravity, studying the properties of a collisionless gas on a fixed (but curved) background leads to interesting problems and phenomena. In particular, it has been argued that, as a consequence of the integrability properties of the underlying geodesic flow [2,3], the Vlasov equation on a Kerr background admits an explicit solution representation in terms of generalized action-angle variables [4]. Based on this representation, it has been possible to study accretion problems which constitute the kinetic analogue of the popular hydrodynamic Bondi-Michel [5,6] and Bondi-Hoyle-Lyttleton [7,8] models by analytic methods [9–14]. These accretion models are based on a careful analysis of the relativistic phase space

corresponding to future-directed timelike geodesics of the Schwarzschild spacetime which are unbounded in the spatial directions. By imposing suitable boundary conditions at spatial infinity (describing, typically, a state in thermodynamic equilibrium) one can show that under reasonable assumptions on the initial datum, the gas configuration settles down to a steady-state configuration whose one-particle distribution function (DF) depends only on the integrals of motion. This is not surprising, since a gas particle following an unbound orbit either falls into the black hole in finite proper time or disperses to infinity, implying that a stationary observer perceives a steady-state configuration after long enough time. At the mathematical level, this translates into the fact that the DF describing this scenario converges pointwise in time to the DF specified at spatial infinity [9]. For recent related work analyzing the steady-state accretion of a Vlasov gas in the equatorial plane of a Kerr black hole, see [15].

The complementary region of phase space, describing spatially bound future-directed timelike geodesics in a Schwarzschild or Kerr black hole exterior spacetime, leads to (non-accreting) gas clouds surrounding the black hole. As long as the gas is collisionless, it is sufficient to focus ones attention to the free-particle flow in the bound region of phase space to understand such configurations. Unlike the unbounded case, a DF whose support lies inside the bound region does not converge pointwise since the geodesic motion is quasi-periodic in this region. Interestingly however, the macroscopic observables associated with the gas, which we define by "smearing out" the DF by multiplying it with a suitable test function and integrating over phase space, may nevertheless converge as time goes to infinity, due to phase space mixing [16,17]. This effect, which plays a fundamental role in diverse fields of physics, including stellar dynamics (see e.g. [18–22]) nonlinear Landau damping in plasma physics [23,24] and quantum physics [25–27], is based on the fact that orbits belonging to neighboring invariant tori have, in general, slightly different fundamental frequencies associated with them, implying that the flow spreads in the angle directions. As a consequence, from the point of view of the macroscopic observables, the DF can be replaced with the angle-averaged DF at large times; in other words, the DF converges weakly to its angle-average [28,29]. Recently, based on the explicit solution representation of the DF in terms of action-angle variables, we have analyzed this mixing phenomena for the restricted case in which the gas particles were confined to equatorial orbits in a Kerr black hole exterior, and we provided evidence that the macroscopic observables do relax in time to a stationary and axisymmetric state [30]. In the present article, we extend the results of our previous work to the case in which the gas particles are free to follow any spatially bound, future-directed timelike geodesic trajectory in the exterior of a Kerr black hole, and we prove that as long as the black hole is rotating, phase space mixing also occurs in this more general case.

In the next subsection we provide an overview of the different steps and intermediate results (many of them having an interest on their own) involved in establishing our result. We emphasize that we restrict ourselves to a kinetic gas consisting of massive particles; the behavior of a massless Vlasov gas propagating on a fixed black hole background has been studied in Refs. [31,32] and leads to decay. See also [33] for self-gravitating static solutions describing a Schwarzschild black hole surrounded by a finite shell of massless Vlasov matter.

1.1. Organization of the article and description of the main results. In section 2 we start with a compilation of relevant results (most of them which are known) regarding the Hamiltonian flow associated with the geodesic motion in the Kerr spacetime. For

definiteness, we restrict our attention to the sub-extremal case in which the rotation parameter's magnitude is strictly smaller than the black hole mass. For generality and in view of potential future applications to the accretion problem, we describe these results in terms of a coordinate chart based on Kerr coordinates, which covers the future event horizon and a part of the black hole interior in addition to the exterior region. In particular, we list the four integrals of motion, show that they satisfy (almost everywhere) the hypotheses for an integrable system and characterize the region Γ_{bound} of phase space corresponding to spatially bound future-directed timelike geodesics which are confined to the exterior region.[1] This region Γ_{bound} is naturally foliated by the invariant subsets on which all integrals of motion are constant, and we show that (after subtracting a zero measure set from Γ_{bound}), these subsets are smooth manifolds with topology $\mathbb{R} \times T^3$. Here, the presence of the non-compact factor $\mathbb{R}$ is a consequence of the fact that we work on (the fully covariant) relativistic phase space.

Next, in section 3 we focus our attention on Γ_{bound} and introduce generalized action-angle variables (J_α, Q^α). Although such variables have been introduced and used previously in the literature, see e.g. [35–37], we are not aware of rigorous results regarding their global properties on Γ_{bound}. Two difficulties arise; the first one is related to the fact that the invariant sets are not compact, such that one cannot immediately apply the Liouville-Arnold theorem to construct action-angle variables. However, by showing that the Hamiltonian vector fields associated with the integrals of motion are complete on each invariant set, one can generalize the construction of the Liouville-Arnold theorem [38] and construct (J_α, Q^α) in an open neighborhood of any invariant set. Whereas the action variables J_1, J_2, J_3 are topological invariants associated with each invariant set, there is an ambiguity in the choice for J_0, originating from the presence of its non-compact factor. In this article, we choose J_0 equal to the integral of motion corresponding to the rest mass of the particle, and we explain the advantages of our choice. By construction, on each invariant set the variables J_α are constant while the variables Q^α are globally well-defined coordinates on this set, Q^1, Q^2, and Q^3 providing angles parametrizing the torus T^3 and Q^0 parametrizing the non-compact factor $\mathbb{R}$. The second difficulty is related to the question of whether or not the action variables J_α uniquely characterize each invariant set; that is, whether the variables (J_α, Q^α) provide a global chart of Γ_{bound}. Although this can be established in some limiting cases, like the Schwarzschild limit or when restricting to orbits with sufficiently large radii, we do not address this question in the present article. To circumvent this problem, we replace the J-variables with the variables P_α describing the constants of motion, and work with the globally-defined (but non-canonical) variables (P_α, Q^α) instead of (J_α, Q^α). The main results of section 3 are summarized in Theorems 1 and 2. Finally, in this section we also express the variables (J_α, Q^α) explicitly in terms of Legendre's elliptic integrals, we compute the fundamental frequencies ω^α characterizing the motion and discuss their meaning, and we show that the free-particle (Liouville) flow on Γ_{bound} is trivialized.

Section 4 is devoted to the main results of this article and states the strong Jeans and mixing theorems. To this purpose, we start with a reduction to a problem on a six-dimensional phase space foliated by invariant tori T^3, for which the motion is characterized by the standard winding around the tori with associated frequencies $\boldsymbol{\omega} = (\omega^1, \omega^2, \omega^3)$. This reduction is performed by fixing the particles' rest mass, by considering constant Boyer-Lindquist time hypersurfaces and by identifying points lying on the same Killing orbit generated by the asymptotically timelike unit Killing vector

[1] A similar characterization has recently been worked out in Ref. [34].

field.[2] The reduced problem allows one to easily prove that the Cauchy problem associated with the Vlasov equation on Γ_{bound} is well-posed and that its propagator is described by a strongly continuous unitary group. Next, we introduce the *A-nondegeneracy condition* which essentially states that the Jacobian of $\boldsymbol{\omega}$ is almost everywhere invertible and show that this implies that the frequencies are non-resonant for almost all values of the constants of motion.[3] Based on these observations, we first formulate the strong Jeans theorem for our setting (Theorem 3), stating that a stationary DF is independent of all angle variables if the A-nondegeneracy condition holds. A similar theorem (Theorem 4) is proven stating that under an analogous *B-nondegeneracy condition*, invariance of the DF under the Carter flow implies that it must be independent of the angle variables. The mixing theorem is stated in Theorem 5, and we formulate it for any dual pair (F, G), where F denotes the initial distribution function and G the test function. Our theorem only requires very mild regularity conditions on F and G; in particular it works for any $F \in L^p$, $1 < p < \infty$, and G lying in the dual space L^q with $1/p + 1/q = 1$.

Next, in section 5 we provide a more detailed analysis in the *Keplerian limit* of orbits lying far from the black hole. To this purpose we first show that the relevant quantities are analytic in the parameter μ, which represents the inverse square root of the *semi-latus rectum* of the orbit, in a vicinity of $\mu = 0$. Next, we show that for small enough $|\mu|$, the energy, Carter constant and the action variables can be expressed in the form of convergent power series in μ. Further, we prove that for small enough $|\mu|$, the mapping from the constants of motion to the action variables can be inverted, and using this result, we express the energy and Carter constant as a power series of the action variables, up to the desired accuracy in μ. We perform this expansion including terms of the order of μ^5 in the energy and terms of the order of μ^2 in the Carter constant. This allows one to compute the fundamental frequencies $\boldsymbol{\omega}$ including terms of the order μ^6 and to prove that both the A- and B-degeneracy conditions are satisfied for small enough values of $\mu > 0$ (see Theorem 6), provided the rotation parameter of the black hole is nonzero. This shows that mixing is taking place in the far exterior region of a rotating Kerr black hole. The validity of the non-degeneracy conditions for generic bound orbits then follows from the analytic dependency of the fundamental frequency on the constants of motion.

Finally, in section 6 we summarize our results and formulate the main conclusion of this paper, namely the mixing theorem for the Kerr case (Theorem 7). We also give several remarks regarding possible generalizations and open problems that, we hope, will be addressed in future work. Several technical points, such as a thorough analysis of the effective potentials describing the motion in the polar and radial directions, the parametrization of orbits and the explicit evaluation of the generalized action-angle variables (J_α, Q^α) are discussed in appendices A–E.

1.2. Notation and conventions. Throughout this article, we use the same notation as in Ref. [9]. In particular, T^*M denotes the cotangent bundle associated with the spacetime manifold (M, g) (which is assumed to be a smooth and time-oriented Lorentz manifold), the relativistic one-particle phase space corresponding to a simple gas of massive particles is the subspace

$$\Gamma := \{(x, p) \in T^*M : p^\sharp \text{ is future-directed timelike}\}, \tag{1}$$

[2] An alternative approach which does not rely on the introduction of a specific foliation has been discussed in [30].

[3] Resonant orbits and their implications for perturbations of Kerr black holes have been analyzed in Refs. [39,40].

where $p^\sharp := g_x^{-1}(p, \cdot)$ denotes the vector associated with the momentum covector $p \in T_x^*M$ at $x \in M$, and the Liouville equation, which describes the evolution of a collisionless DF $f : \Gamma \to \mathbb{R}$, is

$$X_H[f] := g^{\mu\nu}(x)p_\nu \frac{\partial f}{\partial x^\mu} - \frac{1}{2}p_\alpha p_\beta \frac{\partial g^{\alpha\beta}(x)}{\partial x^\mu}\frac{\partial f}{\partial p_\mu} = 0, \tag{2}$$

in adapted local coordinates (x^μ, p_μ) on T^*M. Here, X_H refers to the Liouville vector field which can be defined invariantly as the Hamiltonian vector field associated with the free-particle Hamiltonian $H(x, p) := \frac{1}{2}g_x^{-1}(p, p)$ and the natural symplectic form $\Omega_s = dp_\mu \wedge dx^\mu$ on T^*M. Recall that for an arbitrary smooth function $F : T^*M \to \mathbb{R}$, the associated Hamiltonian vector field X_F is the unique vector field on T^*M such that $dF = \Omega_s(\cdot, X_F)$, and it is given explicitly by

$$X_F = \frac{\partial F}{\partial p_\mu}\frac{\partial}{\partial x^\mu} - \frac{\partial F}{\partial x^\mu}\frac{\partial}{\partial p_\mu}. \tag{3}$$

The Poisson-bracket between two smooth functions $F, G : T^*M \to \mathbb{R}$ is defined as

$$\{F, G\} := \Omega_s(X_F, X_G) = \frac{\partial F}{\partial p_\mu}\frac{\partial G}{\partial x^\mu} - \frac{\partial F}{\partial x^\mu}\frac{\partial G}{\partial p_\mu} = dG(X_F). \tag{4}$$

Note that the symplectic form can be expressed as the exterior differential of the Poincaré one-form

$$\Theta = p_\mu dx^\mu, \tag{5}$$

see, for instance, Eq. (2) in Ref. [9] for a coordinate-invariant definition of Θ. Finally, recall that Γ is equipped with the volume form

$$\begin{aligned}\eta_\Gamma &:= -\frac{1}{4!}\Omega_s \wedge \Omega_s \wedge \Omega_s \wedge \Omega_s \\ &= -dx^0 \wedge dx^1 \wedge dx^2 \wedge dx^3 \wedge dp_0 \wedge dp_1 \wedge dp_2 \wedge dp_3,\end{aligned} \tag{6}$$

which is invariant with respect to the Liouville flow: $\pounds_{X_H}\eta_\Gamma = 0$. For a recent review on the geometric structures of the cotangent bundle which are relevant for relativistic kinetic theory, see [41].

2. Geodesic Motion on a Kerr Black Hole as an Integrable Hamiltonian System

This section is devoted to a review of some of the most important results regarding the geodesic motion on a Kerr spacetime which are relevant for this article. We consider the spacetime (M, g) describing a Kerr black hole of mass M_H and rotation parameter a_H satisfying $a_H^2 < M_H^2$. Using horizon-penetrating coordinates $(t, r, \vartheta, \varphi)$ which are related to the standard Kerr coordinates $(\tilde{V}, r, \theta, \tilde{\phi})$ (see, for instance [42]) through the relations $\tilde{V} = t + r$, $\theta = \vartheta$, $\tilde{\phi} = \varphi$, the Kerr metric is given by

$$\begin{aligned}g = &-dt^2 + dr^2 - 2a_H \sin^2\vartheta dr d\varphi + \left(r^2 + a_H^2\right)\sin^2\vartheta d\varphi^2 + \rho^2 d\vartheta^2 \\ &+ \frac{2M_H r}{\rho^2}\left(dt + dr - a_H \sin^2\vartheta d\varphi\right)^2,\end{aligned} \tag{7}$$

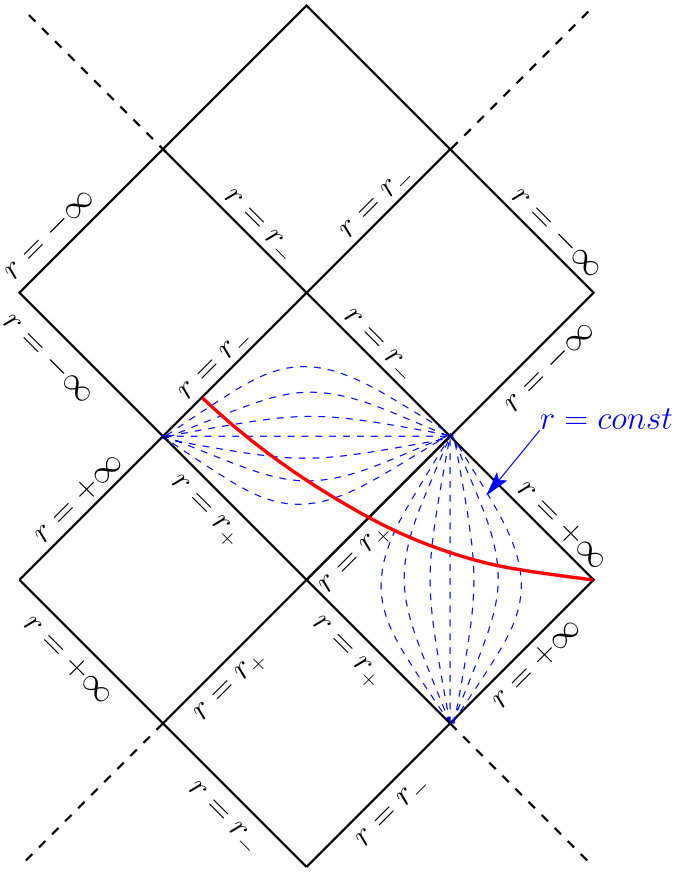

Fig. 1. Penrose diagram of the symmetry axis of the Kerr spacetime. The spacetime (M, g) considered in this article corresponds to the two causal diamonds showing the dashed blue $r = const$ lines. The continuous red line illustrates the qualitative behavior of a $t = const$ hypersurface in the region $r > r_-$

with the function $\rho^2 = \rho^2(r, \vartheta) := r^2 + a_H^2 \cos^2 \vartheta$. The representation of the metric in these coordinates is regular for all $r > 0$ and $0 < \vartheta < \pi$,[4] in particular it is regular at the inner and outer horizons $r_\pm := M_H \pm \sqrt{M_H^2 - a_H^2}$. For the following, we restrict ourselves to the region of the (maximally extended) Kerr spacetime corresponding to $r > r_-$ which contains the future event horizon $r = r_+$, see Fig. 1. For brevity, we shall denote this spacetime region by (M, g).

Note that the $t = const.$ hypersurfaces have the normal vector field

$$N := -g^{\mu\nu}(\nabla_\mu t)\frac{\partial}{\partial x^\nu} = \left(1 + \frac{2M_H r}{\rho^2}\right)\frac{\partial}{\partial t} - \frac{2M_H r}{\rho^2}\frac{\partial}{\partial r}, \tag{8}$$

[4] The coordinate singularities at the poles $\vartheta = 0, \pi$ could be removed by introducing Kerr-Schild coordinates (x, y, z) defined by $x + iy = (r + ia_H)\sin\vartheta e^{i\varphi}$, $z = r\cos\vartheta$, see Ref. [42]. In this article, we shall not consider polar orbits, i.e. bound orbits which cross the symmetry axis, such that we do not need to introduce Kerr-Schild coordinates.

which satisfies $g(N,N) = -(1+2M_H r/\rho^2) < 0$; hence N is timelike and the hypersurfaces $t = const.$ are spacelike, and N provides a time orientation on (M,g). Instead of N, it will result more convenient to use the vector fields[5]

$$X := (r^2 + a_H^2)\frac{\partial}{\partial t} + a_H \frac{\partial}{\partial \varphi} \quad \text{and} \quad Y := 2M_H r \frac{\partial}{\partial t} + a_H \frac{\partial}{\partial \varphi} + \Delta \frac{\partial}{\partial r} \tag{9}$$

with the function $\Delta = \Delta(r) := r^2 - 2M_H r + a_H^2$. They satisfy $-g(X,X) = g(Y,Y) = \rho^2\Delta$, $g(X,Y) = 0$ and $dt(X) > 0$, $dt(Y) > 0$; hence X is future-directed timelike in the region $r > r_+$ and Y is future-directed timelike in the region $r_- < r < r_+$.

The free-particle Hamiltonian for the metric (7) is

$$H(x,p) = \frac{1}{2\rho^2}\left[-\left(\rho^2 + 2M_H r\right)p_t^2 + 4M_H r p_t p_r + 2a_H p_r p_\varphi + \Delta p_r^2 + p_\vartheta^2 + \frac{p_\varphi^2}{\sin^2\vartheta}\right]. \tag{10}$$

Since the underlying spacetime is stationary and axisymmetric, the following quantities are conserved along the particle trajectories:

$$m = \sqrt{-2H} \quad \text{(rest mass)}, \tag{11}$$

$$E = -p_t \quad \text{(energy)}, \tag{12}$$

$$L_z = p_\varphi \quad \text{(azimuthal angular momentum)}. \tag{13}$$

Remarkably, there exists a fourth conserved quantity, discovered by Carter by separating the Hamilton-Jacobi equation [2], which is defined by[6]

$$\mathcal{K} := p_\vartheta^2 + \left(\frac{L_z}{\sin\vartheta} - E a_H \sin\vartheta\right)^2 + m^2 a_H^2 \cos^2\vartheta \qquad \text{(Carter constant)}. \tag{14}$$

Note that this constant is manifestly positive, and moreover, in the Schwarzschild limit $a_H = 0$ it reduces to the square of the total angular momentum L^2. For these reasons, we shall use the notation L^2 instead of $\mathcal{K}$ (and L instead of $\sqrt{\mathcal{K}}$) even in the rotating case.

For the following, we introduce the smooth functions $F_0, F_1, F_2, F_3 : T^*M \to \mathbb{R}$ on the cotangent bundle which define these integrals of motion:

$$F_0(x,p) := -H(x,p), \quad F_1(x,p) := -p_t, \quad F_2(x,p) := p_\varphi,$$

$$F_3(x,p) := p_\vartheta^2 + \left(\frac{p_\varphi}{\sin\vartheta} + a_H \sin\vartheta\, p_t\right)^2 - 2a_H^2 \cos^2\vartheta\, H(x,p). \tag{15}$$

The presence of these four functions imply that the geodesic motion in the Kerr spacetime yields an integrable Hamiltonian system.[7] The precise formulation of this statement is contained in the following two proposition whose proof will be given below.

[5] With respect to Boyer-Lindquist coordinates the vector field Y is just $\Delta\frac{\partial}{\partial r}$.

[6] In Kerr-Schild coordinates one has $L_z = xp_y - yp_x$ and

$$\mathcal{K} = (r^2 + a_H^2)(p_x^2 + p_y^2 + p_z^2) - (xp_x + yp_y + zp_z)^2 - 2a_H E L_z + \frac{a_H^2}{r^2}\left[(r^2 - z^2)E^2 - r^2 p_z^2 + m^2 z^2\right],$$

which shows that $\mathcal{K}$ is everywhere regular for $r > 0$ including at the axis $\vartheta = 0, \pi$ where $x = y = 0$.

[7] A Hamiltonian vector field X_H on a $2n$-dimensional symplectic manifold is called integrable if there exists n smooth functions F_j such that $\{H, F_j\} = \{F_j, F_k\} = 0$ for all $j,k = 1,2,\ldots,n$ and $dF_1, dF_2, \ldots, dF_n$ are linearly independent at each point. See, for instance, chapter V in [43] for more details.

Proposition 1. *The functions F_α defined in Eq. (15) Poisson-commute with each other:*

$$\{F_\alpha, F_\beta\} = 0, \qquad \alpha, \beta = 0, 1, 2, 3.$$

Proposition 2. *The differentials dF_0, dF_1, dF_2, dF_3 are linearly independent from each other at each $x \in \Gamma_0$, where $\Gamma_0 \subset \Gamma$ is a dense subset of the phase space Γ which is invariant with respect to the flows generated by the Hamiltonian vector fields $X_\alpha := X_{F_\alpha}$, $\alpha = 0, 1, 2, 3$.*

Next, one considers for each given value of (m, E, L_z, L) the (possibly empty) subset

$$\begin{aligned}\Gamma_{m,E,L_z,L} := \{(x, p) \in \Gamma : F_0(x, p) = m^2/2, F_1(x, p) = E,\\ F_2(x, p) = L_z, F_3(x, p) = L^2\}\end{aligned} \tag{16}$$

of the one-particle phase space Γ, which by definition is invariant with respect to the Hamiltonian flows associated with F_0, F_1, F_2 and F_3. As a corollary of Propositions 1 and 2 one has

Corollary 1. *Suppose $\Gamma_{m,E,L_z,L} \subset \Gamma_0$ is contained in the set Γ_0 appearing in the statement of the previous proposition. Then, $\Gamma_{m,E,L_z,L}$ is a four-dimensional smooth submanifold of Γ whose tangent spaces are spanned by the vectors $X_\alpha|_{(x,p)}$, $\alpha = 0, 1, 2, 3$, at each point $(x, p) \in \Gamma_{m,E,L_z,L}$. Furthermore, the restriction of the Poincaré one-form Θ to $\Gamma_{m,E,L_z,L}$ is closed.*

Proof. Since $\Omega_s(X_\alpha, X_\beta) = \{F_\alpha, F_\beta\} = 0$ for all $\alpha, \beta = 0, 1, 2, 3$ and the vectors $X_\alpha|_{(x,p)}$ span the tangent spaces of $\Gamma_{m,E,L_z,L}$, it follows that the restriction of $\Omega_s = d\Theta$ on $\Gamma_{m,E,L_z,L}$ vanishes. □

Remark 1. The Hamiltonian vector fields $X_\alpha = X_{F_\alpha}$ have the following interpretation: $-X_0$ is the Liouville vector field, $-X_1$ is the complete lift[8] of the asymptotically timelike Killing vector field ∂_t and X_2 the complete lift of the Killing vector field ∂_φ. The vector field X_3 generates the Carter flow, that is, the symmetry flow associated with the Carter constant, and it cannot be written as the complete lift of any spacetime vector field.

For the following, we focus our attention on spatially bound orbits. This leads to the restriction of phase space Γ on which the invariant submanifolds $\Gamma_{m,E,L_z,L}$ have topology $\mathbb{R} \times T^3$. The next proposition characterizes the range for the parameters this subset corresponds to.

Proposition 3. *Let $\alpha := a_H/M_H \in [0, 1)$ and denote for each $\beta \in (-1, 1)$ by $L_{ms}(\alpha, \beta)$, $E_{min}(\alpha, \beta, L)$ and $E_{max}(\alpha, \beta, L)$ the quantities (whose precise form is unimportant for the moment) corresponding to the dimensionless quantities λ_{ms}, ε_{min}, ε_{max} defined in Lemma 21 in appendix B. Finally, denote by Ω the open set of four-tuples (m, E, L_z, L) satisfying*

$$\begin{aligned}m > 0, \quad L > L_{ms}(\alpha, \beta), \quad E_{min}(\alpha, \beta, L) < E < \min\{m, E_{max}(\alpha, \beta, L)\},\\ L_z = \beta L + a_H E \neq 0,\end{aligned} \tag{17}$$

for some $\beta \in (-1, 1)$.

Then, $\Gamma_{m,E,L_z,L}$ has a unique connected component which lies entirely in the exterior region $r > r_+$. This component, which we denote by $\Gamma^{(ext)}_{m,E,L_z,L}$ in the following, has topology $\mathbb{R} \times T^3$.

The remaining part of this section is devoted to the proofs of Propositions 1, 2 and 3. Some of the intermediate results in these proofs will be used in the next section as well.

[8] See, for instance, Ref. [9] for a definition and a summary on the properties of the complete lift.

2.1. Proof of Proposition 1. The only commutator whose vanishing is not immediately evident is $\{F_0, F_3\}$. To compute it, we rewrite F_3 in the form

$$F_3 = p_\vartheta^2 + Q^2 - 2a_H^2 \cos^2\vartheta H, \qquad Q := \frac{p_\varphi}{\sin\vartheta} + a_H \sin\vartheta p_t. \tag{18}$$

Using the identity $\{H, AB\} = \{H, A\}B + A\{H, B\}$ we obtain first

$$\{F_0, F_3\} = -2\{H, p_\vartheta\}p_\vartheta - 2\{H, Q\}Q + 2a_H^2\{H, \cos^2\vartheta\}H. \tag{19}$$

Next, an explicit computation reveals that

$$\{H, p_\vartheta\} = -\frac{\partial H}{\partial\vartheta} = \frac{\cot\vartheta}{\rho^2}\left[\frac{p_\varphi^2}{\sin^2\vartheta} - a_H^2\sin^2\vartheta(2H + p_t^2)\right], \tag{20}$$

$$\{H, Q\} = \frac{\partial H}{\partial p_\vartheta}\frac{\partial Q}{\partial\vartheta} = -\cot\vartheta\frac{p_\vartheta}{\rho^2}\left[\frac{p_\varphi}{\sin\vartheta} - a_H\sin\vartheta p_t\right], \tag{21}$$

$$\{H, \cos^2\vartheta\} = \frac{\partial H}{\partial p_\vartheta}\frac{\partial\cos^2\vartheta}{\partial\vartheta} = -2\cos\vartheta\sin\vartheta\frac{p_\vartheta}{\rho^2}, \tag{22}$$

from which one concludes easily that $\{F_0, F_3\} = 0$. □

2.2. Proof of Proposition 2. The proof of Proposition 2 and the determination of the dense invariant subset Γ_0 is more involved than the proof of the previous proposition. In order to proceed, we consider for each given value of (m, E, L_z, L) the (possibly empty) subset $\Gamma_{m,E,L_z,L} \subset \Gamma$ defined in Eq. (16), which by definition is invariant with respect to the Hamiltonian flows generated by F_0, F_1, F_2 and F_3. Clearly, each point $(x, p) \in \Gamma$ is contained in precisely one of these invariant sets. Furthermore, $(x, p) \in \Gamma_{m,E,L_z,L}$ if and only if p is future-directed and if the conjugate pairs (t, p_t), (φ, p_φ), (ϑ, p_ϑ), (r, p_r) fulfill the following restrictions:

$$(t, p_t) : p_t = -E, \tag{23}$$

$$(\varphi, p_\varphi) : p_\varphi = L_z, \tag{24}$$

$$(\vartheta, p_\vartheta) : p_\vartheta^2 + K(\vartheta) = L^2, \qquad K(\vartheta) := \left(\frac{L_z}{\sin\vartheta} - a_H\sin\vartheta E\right)^2 + a_H^2 m^2\cos^2\vartheta, \tag{25}$$

$$\begin{aligned}(r, p_r) : \Delta p_r^2 - 2(2M_H E r - a_H L_z)p_r - (r^2 + a_H^2 + 2M_H r)E^2 \\ +2a_H E L_z + L^2 + m^2 r^2 = 0,\end{aligned} \tag{26}$$

where the last of these restrictions is an immediate consequence of the following identity:

$$\begin{aligned}2r^2 H(x, p) = \Delta p_r^2 + 2(a_H p_\varphi + 2M_H r p_t)p_r - (r^2 + a_H^2 + 2M_H r)p_t^2 \\ -2a_H p_t p_\varphi + F_3(x, p).\end{aligned} \tag{27}$$

As long as $\Delta \neq 0$ Eq. (26) is equivalent to

$$\begin{aligned}(\Delta p_r - 2M_H E r + a_H L_z)^2 = R(r), \\ R(r) := \left[E(r^2 + a_H^2) - a_H L_z\right]^2 - \Delta\left(L^2 + m^2 r^2\right).\end{aligned} \tag{28}$$

Note that Hamilton's equations of motion imply that

$$\dot{r} = \frac{\partial H}{\partial p_r} = \frac{1}{\rho^2}\left(\Delta p_r - 2M_H E r + a_H L_z\right), \tag{29}$$

and hence the expression inside the parenthesis on the left-hand side of Eq. (28) is just ρ^2 times the radial velocity $\dot{r}$. When $\Delta = 0$, Eq. (26) reduces to

$$2(2M_H E r - a_H L_z)(p_r + E) = L^2 + m^2 r^2. \tag{30}$$

The next lemma characterizes the set of points in phase space Γ for which the differentials dF_0, dF_1, dF_2 and dF_3 fail to be linearly independent from each other:

Lemma 1. *Let $(x, p) \in \Gamma_{m,E,L_z,L}$ be such that $0 < \vartheta < \pi$. Then, dF_0, dF_1, dF_2, dF_3 are linearly independent unless one (or both) of the following cases occur:*

(a) $p_\vartheta = 0$ and $K'(\vartheta) = 0$,
(b) $r > r_+$ and $R(r) = R'(r) = 0$.

Remark 2. Case (a) corresponds to particle trajectories which are confined to the equatorial plane or to certain cones of constant ϑ (see appendix A), while case (b) corresponds to spherical trajectories.

Proof of Lemma 1. We note first that $dF_1 = -dp_t \neq 0$ and $dF_2 = dp_\varphi \neq 0$ are linearly independent from each other. Next, we consider instead of $dF_0 = -dH$ and dF_3 the one-forms

$$\Lambda_0 := 2r^2 dH - dF_3, \qquad \Lambda_3 := dF_3 + 2a_H^2 \cos^2\vartheta\, dH. \tag{31}$$

The linear transformation that maps (dH, dF_3) to (Λ_0, Λ_3) has determinant equal to $2\rho^2 > 0$, and thus it is invertible. Consequently, the statement of the Lemma is equivalent to the verification that the one-forms dF_1, dF_2, Λ_0, Λ_3 are linearly independent from each other.

An explicit calculation taking into account the definition of Q defined in Eq. (18) reveals that[9]

$$\Lambda_3 = 2p_\vartheta dp_\vartheta + 2Q\left(\frac{dp_\varphi}{\sin\vartheta} + a_H \sin\vartheta\, dp_t\right) + K'(\vartheta)d\vartheta, \tag{32}$$

which shows that Λ_3 is linearly independent from dF_1 and dF_2 unless the conditions in case (a) are met. In order to analyze Λ_0, it is convenient to introduce the quadratic form

$$\begin{aligned}\mathcal{Q}(r, p_r) :=\ & \Delta p_r^2 - 2(2M_H E r - a_H L_z)p_r - (r^2 + a_H^2 + 2M_H r)E^2 \\ & + 2a_H E L_z + L^2 + m^2 r^2,\end{aligned} \tag{33}$$

such that $\mathcal{Q}(r, p_r) = 0$ if $(x, p) \in \Gamma_{m,E,L_z,L}$, see Eq. (26). Using the identity (27) one finds

$$\Lambda_0 = \frac{\partial \mathcal{Q}}{\partial p_r}(r, p_r)dp_r + \frac{\partial \mathcal{Q}}{\partial r}(r, p_r)dr + (\ldots)\, dp_t + (\ldots)\, dp_\varphi, \tag{34}$$

[9] Using Kerr-Schild coordinates one finds the following expression for Λ_3 on the symmetry axis:

$$\Lambda_3|_{(x,y)=(0,0)} = 2z\left[-p_z(p_x dx + p_y dy) + (p_x^2 + p_y^2)dz\right] + 2(r^2 + a_H^2)(p_x dp_x + p_y dp_y) + 2a_H p_t dp_\varphi,$$

which shows that Λ_3 is linearly independent from dp_t and dp_φ unless $(p_x, p_y) = (0, 0)$, that is, the motion is confined to the axis.

which shows that Λ_0 is linearly independent form dF_1, dF_2 and Λ_3 unless

$$\frac{\partial \mathcal{Q}}{\partial p_r}(r, p_r) = 2\,(\Delta p_r - 2M_H E r + a_H L_z) = 0 \text{ and } \frac{\partial \mathcal{Q}}{\partial r}(r, p_r) = 0. \tag{35}$$

When $\Delta = 0$ the first of these equations and Eq. (30) imply that $L^2 + m^2 r^2 = 0$ which is a contradiction since $m > 0$ and $r > r_-$. When $\Delta \neq 0$ the first equation and Eq. (28) imply $R(r) = 0$; however, this situation cannot occur when $r_- < r < r_+$ since in this case $\Delta < 0$ and thus $R(r) > 0$. When $r > r_+$, the quadratic form $\mathcal{Q}$ can also be written as

$$\mathcal{Q}(r, p_r) = \frac{1}{\Delta}\left[(\Delta p_r - 2M_H E r + a_H L_z)^2 - R(r)\right], \tag{36}$$

and differentiating both sides with respect to r shows that when $R(r) = 0$, the second condition in Eq. (35) is equivalent to $R'(r) = 0$. □

To conclude the proof of the Proposition, we define Γ_0 to be the set of points $(x, p) \in \Gamma$ for which dF_0, dF_1, dF_2, dF_3 are linearly independent from each other. It follows from Lemma 1 that the complement $\Gamma \setminus \Gamma_0$ is a zero measure set in (Γ, η_Γ) since the sets $\{p_\vartheta = 0\}$ and $\{R(r) = 0\} = \{\Delta p_r = -2M_H r p_t + a_H p_\varphi\}$ are already zero measure sets. Finally, it is not difficult to verify that $\Gamma \setminus \Gamma_0$ is invariant with respect to the flows generated by X_{F_α}. □

2.3. Proof of Proposition 3. As discussed previously, $(x, p) \in \Gamma_{m,E,L_z,L}$ if and only if p is future-directed and if the pairs (t, p_t), (φ, p_φ), (ϑ, p_ϑ), (r, p_r) satisfy Eqs. (23–26). From these conditions it is clear that the time coordinate t and the azimuthal angle φ are free, giving rise to one $\mathbb{R} \times S^1$ factor.

Next, one uses the qualitative features of the function $K : (0, \pi) \to \mathbb{R}$ which are summarized in appendix A. For the present case in which $|L_z - a_H E| < L$ and $0 < E_{ms} < E < m$ with $E_{ms} := m\varepsilon_{sph}(x_{ms})$ the energy of the marginally stable orbits it turns out that K decreases monotonously from ∞ to $(L_z - a_H E)^2$ and then increases monotonously again to ∞ as ϑ increases from 0 to $\pi/2$ to π. Consequently, the projections of the sets $\Gamma_{m,E,L_z,L}$ onto the (ϑ, p_ϑ)-plane are closed curves which are topologically equivalent to S^1.

Finally, we analyze the projection of the set $\Gamma_{m,E,L_z,L}$ onto the (r, p_r)-plane. When $r \neq r_+$ (that is, $\Delta \neq 0$), this set is described by Eq. (28), where the function R is a fourth order polynomial in the variable r, which depends on the six parameters a_H, M_H, m, L_z, L and E. In the following, we determine the r-intervals on which this polynomial is non-negative. To perform this analysis, we first note that for $r_- < r < r_+$ the function $R(r)$ is manifestly positive and hence Eq. (28) has always two solutions given by $p_r = p_{r\pm}(r)$ with

$$\begin{aligned} p_{r\pm}(r) &:= \frac{2M_H E r - a_H L_z \pm \sqrt{R(r)}}{\Delta} \\ &= -\frac{(r^2 + a_H^2 + 2M_H r)E^2 - 2a_H E L_z - (L^2 + m^2 r^2)}{2M_H E r - a_H L_z \mp \sqrt{R(r)}}, \end{aligned} \tag{37}$$

where the second representation is useful to understand the limits when $r \to r_\pm$. The next lemma shows that only the solution corresponding to $p_r = p_{r-}(r)$ yields a future-directed momentum p and is relevant for the purpose of this work.

Lemma 2. *Let* $(x, p) \in \Gamma_{m,E,L_z,L}$ *such that* $r_- < r < r_+$. *Then* $p_r = p_{r-}(r)$.

Proof. Consider the vector field Y defined in Eq. (9) which is future-directed timelike in the region $\Delta < 0$. Since $(x, p) \in \Gamma_{m,E,L_z,L}$, p must be future-directed and thus

$$0 < -p(Y) = 2M_H Er - a_H L_z - \Delta p_r = \mp\sqrt{R},$$

where we have used the fact that $p_r = p_{r\pm}(r)$ in the last step. This proves that only the lower sign is possible as claimed. □

Remark 3. As $r \to r_\pm$, the relevant function $p_{r-}(r)$ has a well-defined limit provided $2M_H Er_\pm - a_H L_z > 0$.

Next, we restrict our attention to the region $r > r_+$. For this, it is convenient to replace L_z with the new parameter

$$\hat{L}_z := L_z - a_H E, \tag{38}$$

whose square corresponds to the minimal value of the function $K(\vartheta)$ when $a_H^2(E^2 - m^2) \le L_z^2$, see appendix A. With this change we can rewrite the function R in the form

$$R(r) = r^4[E - W_+(r)][E - W_-(r)], \tag{39}$$

where

$$W_\pm(r) := \frac{a_H \hat{L}_z}{r^2} \pm \frac{\sqrt{\Delta\left(m^2 r^2 + L^2\right)}}{r^2}. \tag{40}$$

Since $W_+(r) > W_-(r)$ for $r > r_+$ it follows that $R(r) \ge 0$ if and only if r lies in either one of the disjoint sets

$$\{r > r_+ : W_+(r) \le E\} \text{ or } \{r > r_+ : W_-(r) \ge E\}.$$

However, as shown in the following Lemma, only the first of these two sets corresponds to future-directed trajectories and hence belongs to the invariant set $\Gamma_{m,E,L_z,L}$:

Lemma 3. *Let* $(x, p) \in \Gamma_{m,E,L_z,L}$ *such that* $r > r_+$. *Then,* $W_+(r) \le E$.

Proof. If $(x, p) \in \Gamma_{m,E,L_z,L}$, then p is, by definition, future-directed. On the other hand, the vector field X defined in Eq. (9) is also timelike future-directed in the region $\Delta > 0$. Therefore, we must have

$$0 < -p(X) = (r^2 + a_H^2)E - a_H L_z = r^2 E - a_H \hat{L}_z.$$

However, if $E \le W_-(r)$ then

$$r^2 E - a_H \hat{L}_z \le -\sqrt{\Delta(m^2 r^2 + L^2)} < 0,$$

so in this case p is past-directed and we obtain a contradiction. On the other hand, if $E \ge W_+(r)$ then

$$r^2 E - a_H \hat{L}_z \ge +\sqrt{\Delta(m^2 r^2 + L^2)} > 0,$$

and p is future-directed. □

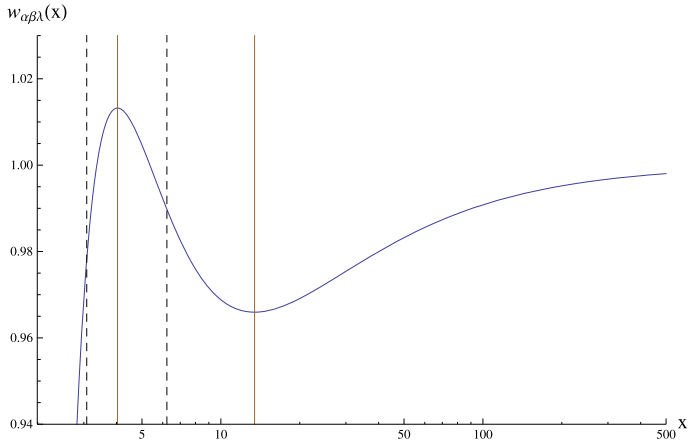

Fig. 2. The effective potential $w_{\alpha,\beta,\lambda}(x) = W_+(r)/m$ as a function of $x = r/M_H$ for the parameter values $\alpha = 0.12$, $\beta = -0.61$ and $\lambda = 4.25$. The vertical solid lines show the locations of the maximum and minimum, $r_{max}/M_H \approx 4.034$ and $r_{min}/M_H \approx 13.45$. The dashed vertical lines indicate the locations of $r_{ph}/M_H \approx 3.077$ and $r_{ms}/M_H \approx 6.223$

Remark 4. It follows from Lemmas 2 and 3 that the projection of $\Gamma_{m,E,L_z,L}$ onto the (r, p_r)-plane consists of the points for which

$$r_- < r < r_+ \text{ and } p_r = p_{r-}(r) \text{ or } r \geq r_+ \text{ and } W_+(r) \leq E \text{ and } p_r = p_{r\pm}(r),$$

with $p_{r\pm}(r)$ given by Eq. (37). In the limit $r \to r_+$ one obtains the condition $E \geq W_+(r_+) = a_H\hat{L}_z/r_+^2$ which implies that $2M_HEr_+ - a_HL_z = (2M_Hr_+ - a_H^2)E - a_H\hat{L}_z = r_+^2E - a_H\hat{L}_z \geq 0$; hence for values of E such that $E > a_H\hat{L}_z/r_+^2$ the curve $p_r = p_{r-}(r)$ intersects the event horizon. This curve corresponds to infalling particles that are absorbed by the black hole.

Remark 5. The properties of the projection of $\Gamma_{m,E,L_z,L}$ onto the (r, p_r)-plane in the region $r > r_+$ depend on the shape of the effective potential W_+ for a given energy level E. A detailed analysis of the qualitative features of the function W_+ is given in appendix B. We summarize the relevant results in the following Lemma.

Lemma 4. *Suppose that $|a_H| < M_H$ and $|\hat{L}_z| < L$ and let $L_{ms} := M_Hm\lambda_{ms}(\alpha, \beta)$, $r_{ms} := M_Hx_{ms}(\alpha, \beta)$, $r_{ph} := M_Hx_{ph}(\alpha, \beta)$, be defined as in appendix B (in particular, see Lemmas 19 and 20 for the definitions of x_{ph} and x_{ms}). Then, the function $W_+ : [r_+, \infty) \to \mathbb{R}$ defined by Eq. (40) satisfies the following properties:*

- *When $L \leq L_{ms}$ the function W_+ is monotonously increasing.*
- *For each $L > L_{ms}$ the function W_+ has a unique local maximum (the centrifugal barrier) located at $r_{max} \in (r_{ph}, r_{ms})$ and it has a potential well with a local minimum located at $r_{min} \in (r_{ms}, \infty)$ which is enclosed between the centrifugal barrier and its asymptotic value m (see Fig. 2).*
- *As L increases from L_{ms} to ∞, r_{max} decreases monotonously from r_{ms} to r_{ph} and $W_+(r_{max})$ increases monotonously from E_{ms} to ∞ while r_{min} increases monotonously from r_{ms} to ∞ and $W_+(r_{min})$ increases monotonously from E_{ms} to m.*

It follows from this Lemma that for the given ranges for L and E in the hypothesis of the proposition, there are closed trajectories giving rise to the remaining S^1-factor in the topology of $\Gamma^{(ext)}_{m,E,L_z,L}$. This concludes the proof of the proposition. □

3. Generalized Action-Angle Variables on Γ_{bound}

This section is devoted to the construction of generalized action-angle variables which provide new symplectic coordinates[10] (J_α, Q^α) on the subset of the relativistic one-particle phase space Γ corresponding to bound orbits in the Kerr exterior region. The construction largely follows standard methods from classical mechanics, see for instance [43,44]. Nevertheless, one should point out that in our case the invariant sets $\Gamma^{(ext)}_{m,E,L_z,L}$ are not compact, such that one cannot directly apply the famous Liouville-Arnold theorem. However, by showing that the Hamilton vector fields X_α associated with the integrals of motion F_α defined in Eq. (15) are complete, it is not difficult to generalize the proof to the present case, obtaining one extended coordinate $Q^0 \in \mathbb{R}$ in addition to the 2π-periodic angle variables Q^1, Q^2, Q^3. For a generalization of the Liouville-Arnold theorem to non-compact invariant manifolds of completely (or partially) integrable systems, see [38].

For the following, we recall the set Ω defined by the conditions (17) in Proposition 3, and we introduce the following subset of Γ:

$$\Gamma_{bound} := \bigcup_{(m,E,L,L_z)\in\Omega} \Gamma^{(ext)}_{m,E,L_z,L}, \tag{41}$$

which (with the exception of the special orbits characterized in Lemma 1) describes the phase space of bound orbits in the exterior Kerr spacetime. In the next subsection, we provide a formal definition for the construction of the generalized action-angle variables (J_α, Q^α). In subsection 3.2 we determine the action variables and analyze the local invertibility of the transformation $\mathbb{I}$ which maps the conserved quantities (m, E, L_z, L) to the action variables. Next, in subsection 3.3 we show that the Hamiltonian vector fields X_α associated with F_α are complete in Γ_{bound}. This allows one to show in subsection 3.4 that the (multi-valued) Q^α-variables are globally well-defined, and leads to the main theorems 1,2 of this section. Finally, in subsection 3.5 we provide explicit expressions for the variables (J_α, Q^α) in terms of Legendre's elliptic integrals.

From now on we shall introduce the following notation: $C = (C_\alpha) := (m, E, L_z, L)$ denotes the conserved quantities, whereas $P := (P_\alpha) : \Gamma_{bound} \to \Omega \subset \mathbb{R}^4$ refers to the corresponding integrals of motion

$$(P_\alpha(x, p)) := \left(\sqrt{2F_0(x, p)}, F_1(x, p), F_2(x, p), \sqrt{F_3(x, p)}\right), \qquad (x, p) \in \Gamma_{bound}. \tag{42}$$

Hence, according to Eq. (16), one has $P_\alpha(x, p) = C_\alpha$ if and only if $(x, p) \in \Gamma^{(ext)}_{m,E,L_z,L}$ for all $C = (m, E, L_z, L) \in \Omega$ and $(x, p) \in \Gamma_{bound}$.

3.1. Formal definition of the action-angle variables. Recall that each set $\Gamma^{(ext)}_{m,E,L_z,L}$ in the union (41) is invariant under the Liouville flow and topologically of the form $\mathbb{R} \times T^3$. We have also seen that the torus T^3 is naturally generated by the three S^1-factors corresponding to the motion in the azimuthal, polar and radial directions, respectively. Each of these S^1 factors gives rise to the variable

$$I_k(m, E, L_z, L) := \frac{1}{2\pi} \oint_{\gamma_k} \Theta, \qquad k = 1, 2, 3, \tag{43}$$

[10] This means that (J_α, Q^α) are local coordinates satisfying $\Omega_s = dJ_\alpha \wedge dQ^\alpha$.

where γ_k denotes a closed curve confined to $\Gamma^{(ext)}_{m,E,L_z,L}$ which circumscribes once the k'th factor S^1 and can be contracted to a single point with respect to the other S^1 factors. Since the restriction of the Poincaré one-form Θ to $\Gamma^{(ext)}_{m,E,L_z,L}$ is closed (see Corollary 1), the variables I_k are invariant with respect to deformations of the curves γ_k within $\Gamma^{(ext)}_{m,E,L_z,L}$, and thus they describe topological invariants of $\Gamma^{(ext)}_{m,E,L_z,L}$.

The choice for I_0 is more subtle. One could imagine defining I_0 in analogy with Eq. (43) to be proportional to

$$\int_{\gamma_0} \Theta,$$

with γ_0 a curve in $\Gamma^{(ext)}_{m,E,L_z,L}$ which is contractible to a single point with respect to each S^1 factor. However, since $\mathbb{R}$ is not compact, in general the result depends on the end points of γ_0 and fails to represent an invariant quantity.[11] For this reason, we adopt a different choice for I_0, already proposed by us in [29], which turns out the be convenient for our purposes, namely

$$I_0(m, E, L_z, L) := m. \tag{44}$$

The quantities $(I_\alpha) := (I_0, I_1, I_2, I_3)$ defined by Eqs. (43,44) yield a smooth map $\mathbb{I} : \Omega \to \mathbb{R}^4$ which, as we show below, is (at least) locally invertible. The generalized action variables $J_\alpha : \Gamma_{bound} \to \mathbb{R}$ are defined by the functions

$$J_\alpha(x, p) := I_\alpha(P(x, p)) = I_\alpha\left(\sqrt{-2H(x, p)}, F_1(x, p), F_2(x, p), \sqrt{F_3(x, p)}\right), \quad (x, p) \in \Gamma_{bound}, \qquad \alpha = 0, 1, 2, 3. \tag{45}$$

Note that unlike J_1, J_2 and J_3 which have the units of an action (mass squared in geometrized units), J_0 has units of mass. Consequently, the conjugate variable Q^0 (defined below) has units of length whereas the angle variables Q^1, Q^2 and Q^3 are dimensionless. The main advantage for the choice in Eq. (44) lies in the fact that the one-particle Hamiltonian (10) and Liouville vector field assume the simple form

$$H = -\frac{1}{2}J_0^2, \qquad X_H = -J_0\frac{\partial}{\partial Q^0}. \tag{46}$$

An immediate consequence is that any DF satisfying the collisionsless Boltzmann equation whose support lies in the closure $\overline{\Gamma_{bound}}$ of Γ_{bound} can be represented by a suitable function depending only on the variables $(Q^1, Q^2, Q^3, J_0, J_1, J_2, J_3)$, provided they are globally well-defined on Γ_{bound}.

The generalized angle variables Q^α can be formally defined as

$$Q^\alpha(x, p) = \left.\frac{\partial S}{\partial I_\alpha}\right|_x (\gamma_x; J_0(x, p), J_1(x, p), J_2(x, p), J_3(x, p)), \qquad (x, p) \in \Gamma_{bound}, \tag{47}$$

[11] In our case, this integral is equal to $-E(t_2 - t_1)$ with $E = -p_t$ the conserved energy and t_1 and t_2 the times at the endpoints of the curve γ_0. One possibility of getting rid of the dependency of the end points is to restrict γ_0 to be an integral curve of the complete lift of the Killing vector field ∂_t and divide the resulting integral by the time interval $(t_2 - t_1)$, where t is interpreted as the time-parameter along this integral curve. Up to a sign, this corresponds to the choice made in previous work [30,35,36].

where the generating function S is given by

$$S(\gamma_x; I_0, I_1, I_2, I_3) := \int_{\gamma_x} \Theta, \qquad (I_0, I_1, I_2, I_3) \in \mathbb{I}(\Omega). \tag{48}$$

Here, the line integral is performed along a curve γ_x which is confined to the set $\Gamma^{(ext)}_{m,E,L_z,L}$ with $\mathbb{I}(m, E, L_z, L) = (I_0, I_1, I_2, I_3)$ and connects a given reference point (x_0, p_0) on this set to a point in the intersection between $\Gamma^{(ext)}_{m,E,L_z,L}$ and the fibre over $x \in M$. We choose the reference point (x_0, p_0) as the one parametrized by $(t, p_t) = (t_1, -E)$, $(\varphi, p_\varphi) = (\varphi_1, L_z)$, $(\vartheta, p_\vartheta) = (\vartheta_1, \sqrt{L^2 - K(\vartheta_1)})$ and $(r, p_r) = (r_1, p_{r+}(r_1) = p_{r-}(r_1))$, where the functions $p_{r\pm}(r)$ are defined in Eq. (37). Here, ϑ_1 and r_1 refer to the left turning points in the (ϑ, p_ϑ) and (r, p_r)-planes, respectively, and the values of t_1 and φ_1 will be determined shortly. We close this subsection by remarking that the generating function S and Q^α-variables are multi-valued, since S depends on the winding of the curve γ_x around the torus T^3. Nevertheless, as we show below, the Q^α-variables are globally well-defined on Γ_{bound}, with Q^1, Q^2, Q^3 being 2π-periodic.

3.2. Generalized action variables and local invertibility. Next, we provide an explicit integral representation for the generalized action variables J_μ and ask whether they provide "good" labels for the invariant sets. In order to do so, we start with the quantities I_α in Eqs. (43,44) which define the action variables. Using the fact that $\Theta = p_t dt + p_\varphi d\varphi + p_r dr + p_\vartheta d\vartheta$ and Eqs. (25,37) we conclude that

$$I_0(m, E, L_z, L) = m, \tag{49}$$

$$I_1(m, E, L_z, L) = L_z, \tag{50}$$

$$I_2(m, E, L_z, L) = \frac{1}{2\pi} \oint p_\vartheta d\vartheta = \frac{1}{\pi} \int_{\vartheta_1}^{\vartheta_2} \sqrt{L^2 - K(\vartheta)} d\vartheta, \tag{51}$$

$$I_3(m, E, L_z, L) = \frac{1}{2\pi} \oint p_r dr = \frac{1}{\pi} \int_{r_1}^{r_2} \frac{\sqrt{R(r)}}{\Delta(r)} dr, \tag{52}$$

where here and in the following $\vartheta_1 < \vartheta_2$ and $r_1 < r_2$ refer to the turning points. Similarly, the generating function (48) yields

$$S(\gamma_x; I_0, I_1, I_2, I_3) = -E(t - t_1) + L_z(\varphi - \varphi_1) + \int_{\gamma_r} p_r dr + \int_{\gamma_\vartheta} p_\vartheta d\vartheta, \tag{53}$$

where the last two integrals should be interpreted as line integrals. More specifically, the first integral is a line integral along the projection γ_r of the curve γ_x onto the (r, p_r)-plane, and similarly, the second integral is a line integral along the projection γ_ϑ of γ_x onto the (ϑ, p_ϑ)-plane. For definiteness, in the following, we restrict the curve γ_x to be such that its projections γ_r and γ_ϑ are oriented clockwise. In order to simplify the calculations, it is useful to represent p_r in the form

$$p_r = \frac{2M_H Er - a_H L_z + V}{\Delta}, \qquad V^2 = R(r), \tag{54}$$

where $R(r)$ was defined in Eq. (28). Then, Eq. (53) can be rewritten as

$$S(\gamma_x; I_0, I_1, I_2, I_3) = -Et_{BL} + L_z\varphi_{BL} + \int_{\gamma_r} V\frac{dr}{\Delta} + \int_{\gamma_\vartheta} p_\vartheta d\vartheta, \tag{55}$$

with $V^2 = R(r)$ and $p_\vartheta^2 = L^2 - K(\vartheta)$ and where

$$t_{BL} := t - 2M_H\int^r \frac{rdr}{\Delta}, \qquad \varphi_{BL} := \varphi - a_H\int^r \frac{dr}{\Delta}, \tag{56}$$

turn out to be the Boyer-Lindquist time and azimuthal coordinates. In deriving these equations, we have adjusted the free constants t_1 and φ_1 determining the reference point (x_0, p_0) such as to absorb a r_1-dependent constant. In subsection 3.5 the line integrals in Eqs. (51,52,55) will be represented more explicitly in terms of Legendre's elliptic integrals.

Before we proceed with the computation of the variables Q^μ we need the following result.

Lemma 5. *The map $\mathbb{I} : \Omega \to \mathbb{R}^4, C \mapsto (I_0, I_1, I_2, I_3)(C)$, is locally invertible in a vicinity of each point $C = (m, E, L_z, L) \in \Omega$.*

Proof. According to the inverse function theorem, it is sufficient to show that the linearization $D\mathbb{I}(C)$ of the map $\mathbb{I}$ is invertible at each $C \in \Omega$. The associated Jacobi matrix has the form

$$\mathbf{M} = \begin{pmatrix} 1 & 0 & 0 & 0 \\ 0 & 0 & 1 & 0 \\ I_{20} & I_{21} & I_{22} & I_{23} \\ I_{30} & I_{31} & I_{32} & I_{33} \end{pmatrix}, \qquad I_{\alpha\beta} := \frac{\partial I_\alpha}{\partial P_\beta}, \tag{57}$$

and its determinant is

$$\det\mathbf{M} = I_{23}I_{31} - I_{21}I_{33} = \frac{\partial I_2}{\partial L}\frac{\partial I_3}{\partial E} - \frac{\partial I_2}{\partial E}\frac{\partial I_3}{\partial L}. \tag{58}$$

Using the expressions (D3,D5,D7,D9) from appendix D and taking into account that $I_2 = S_\vartheta(\vartheta_1)/\pi$ and $I_3 = S_r(r_2)/\pi$, one finds

$$\det\mathbf{M} = \frac{L}{\pi^2}\int_{r_1}^{r_2}\int_{\vartheta_1}^{\vartheta_2}\left[\Delta\rho^2 E + 2M_H r(r^2E - a_H\hat{L}_z)\right]\frac{d\vartheta}{\sqrt{L^2 - K(\vartheta)}}\frac{dr}{\Delta(r)\sqrt{R(r)}}, \tag{59}$$

where we recall that $\hat{L}_z = L_z - a_H E$. Since on Γ_{bound} one has $E > 0$ and $a_H\hat{L}_z + \sqrt{\Delta(m^2r^2 + L^2)} = r^2W_+(r) \le r^2E$, such that $r^2E - a_H\hat{L}_z > 0$, if follows that $\det\mathbf{M}$ is positive. □

Remark 6. Denoting by $\Omega_I := \mathbb{I}(\Omega)$ the image of $\mathbb{I}$, the question regarding the global invertibility of the map $\mathbb{I} : \Omega \to \Omega_I$ is, of course, a difficult question. In the Schwarzschild limit $a_H = 0$, the integral I_2 can be computed explicitly and yields $I_2(C) = L - |L_z|$, which does not depend on E. It is then sufficient to show that for fixed values of (m, L_z, L) the map $E \mapsto I_3(m, E, L_z, L)$ is invertible which is the case since $\partial I_3/\partial E$ is positive. However, in the Kerr case, I_2 is not independent of E, and hence one needs to show that for fixed (m, L_z) the map $(E, L) \mapsto (I_2, I_3)(m, E, L_z, L)$ is invertible. We will not pursue this question further in this work.

3.3. Completeness of the generators and global coordinates on the invariant submanifolds. In this subsection we show:

Lemma 6. *Let $(m, E, L_z, L) \in \Omega$. Then, the Hamiltonian vector fields $X_\alpha = X_{F_\alpha}$ associated with the integrals of motion F_α defined in Eq. (15) are complete on $\Gamma^{(ext)}_{m,E,L_z,L}$.*

Proof. Recall that the fields X_α are tangent to $\Gamma^{(ext)}_{m,E,L_z,L} = \mathbb{R} \times T^3$ and that $-X_1$ and X_2 correspond to the complete lifts of the Killing vector fields, which are complete in the exterior region. By introducing angles χ and ϕ on the S^1-factors corresponding to the radial and polar motions and transporting them along the flows of $-X_1$ and X_2 one obtains a global coordinates system (t, φ, χ, ϕ) on $\Gamma^{(ext)}_{m,E,L_z,L}$, such that

$$X_1 = -\frac{\partial}{\partial t}, \qquad X_2 = \frac{\partial}{\partial \varphi}, \tag{60}$$

and X_0 and X_3 have the form

$$X_\alpha = A_\alpha(\chi, \phi)\frac{\partial}{\partial t} + Y_\alpha, \qquad Y_\alpha = Y^\varphi_\alpha(\chi, \phi)\frac{\partial}{\partial \varphi} + Y^\chi_\alpha(\chi, \phi)\frac{\partial}{\partial \chi} + Y^\phi_\alpha(\chi, \phi)\frac{\partial}{\partial \phi}, \quad \alpha = 0, 3, \tag{61}$$

with components A_α and $Y^\varphi_\alpha, Y^\chi_\alpha, Y^\phi_\alpha$ which are independent of (t, φ). The vector fields Y_α are tangent to the compact manifold T^3, and hence they are complete. Together with the boundedness of A_α, this implies that X_α are also complete. □

For what follows, it turns out to be useful to provide explicit definitions for the angles χ and ϕ. Of course, there are many possibilities for introducing such angles. Our choice has the advantage of allowing one to write the variables Q^μ explicitly in terms of Legendre's elliptic integrals. We start with the definition of the angle χ which has period π and parametrizes the invariant curve in the (r, p_r)-plane according to

$$r = r_4 + \frac{r_1 - r_4}{1 - b^2 \sin^2 \chi}, \tag{62}$$

$$V = \frac{M_H m b^2}{\mathcal{C}}(r_1 - r_4)\frac{\sqrt{1 - k^2 \sin^2 \chi}}{(1 - b^2 \sin^2 \chi)^2} \sin(2\chi), \tag{63}$$

where here $r_3 < r_4 < r_1 < r_2$ denote the roots of the polynomial $R(r)$ defined in Eq. (28) (with $r_1 < r_2$ the turning points, as before), p_r is obtained from V according to Eq. (54), and

$$b := \sqrt{\frac{r_2 - r_1}{r_2 - r_4}}, \qquad k := \sqrt{\frac{r_4 - r_3}{r_1 - r_3}}\, b, \qquad \mathcal{C} := \sqrt{\frac{2M_H(r_1 + r_2 + r_3 + r_4)}{(r_1 - r_3)(r_2 - r_4)}}. \tag{64}$$

It follows from Eqs. (62,63) that

$$\frac{dr}{V} = \frac{\mathcal{C}}{M_H m}\frac{d\chi}{\sqrt{1 - k^2 \sin^2 \chi}}. \tag{65}$$

The invariant curve in the (ϑ, p_ϑ)-plane is parametrized in terms of the 2π-periodic angle ϕ, such that

$$\cos \vartheta = -\cos \vartheta_1 \sin \phi, \tag{66}$$

$$p_\vartheta = \frac{\sqrt{L^2 - \hat{L}_z^2}}{\sin\vartheta}\sqrt{1 - k_1^2 \sin^2\phi}\cos\phi, \tag{67}$$

where here ϑ_1 denotes the left turning point of the polar motion and $k_1 := \zeta_1/\zeta_2$ denotes the ratio between the two positive roots of the polynomial $q(\zeta)$ defined in Eq. (D11). It follows from Eqs. (66,67) that

$$\frac{d\vartheta}{p_\vartheta} = \frac{\cos\vartheta_1}{\sqrt{L^2 - \hat{L}_z^2}}\frac{d\phi}{\sqrt{1 - k_1^2\sin^2\phi}}. \tag{68}$$

The coordinates $(z^\mu) := (t, \varphi, \chi, \phi)$ provide global coordinates on each invariant submanifold $\Gamma^{(ext)}_{m,E,L_z,L}$ with $(m, E, L_z, L) \in \Omega$.

For completeness, we compute the components of the generators $-X_0$ and X_3 of the Liouville and Carter flows with respect to these coordinates. Using $dz^\mu(X_\alpha) = \{F_\alpha, z^\mu\}$ and the fact that $\{F_\alpha, F_\beta\} = 0$ one finds

$$dz^\mu(X_\alpha) = \frac{\partial z^\mu}{\partial x^\nu}\{F_\alpha, x^\nu\} = \frac{\partial F_\alpha}{\partial p_\nu}\frac{\partial z^\mu}{\partial x^\nu}. \tag{69}$$

Taking into account Eqs. (65,68) a straightforward calculation yields

$$\begin{aligned}\rho^2 X_0 = &-\Big[2M_H r(p_r + E) + \rho^2 E\Big]\frac{\partial}{\partial t} - \left(a_H p_r + \frac{L_z}{\sin^2\vartheta}\right)\frac{\partial}{\partial\varphi}\\ &-\frac{M_H m}{\mathcal{C}}\sqrt{1 - k^2\sin^2\chi}\,\frac{\partial}{\partial\chi} - \frac{\sqrt{L^2 - \hat{L}_z^2}}{\cos\vartheta_1}\sqrt{1 - k_1^2\sin^2\phi}\,\frac{\partial}{\partial\phi},\end{aligned} \tag{70}$$

$$\begin{aligned}\rho^2 X_3 = &\,2a_H\Big[-2a_H\cos^2\vartheta M_H r(p_r + E) + \rho^2\hat{L}_z\Big]\frac{\partial}{\partial t}\\ &+2\left[-a_H^3\cos^2\vartheta(p_r + E) + \frac{r^2}{\sin^2\vartheta}(\hat{L}_z + a_H\cos^2\vartheta E)\right]\frac{\partial}{\partial\varphi}\\ &-2\frac{M_H m}{\mathcal{C}}a_H^2\cos^2\vartheta\sqrt{1 - k^2\sin^2\chi}\,\frac{\partial}{\partial\chi} + 2r^2\frac{\sqrt{L^2 - \hat{L}_z^2}}{\cos\vartheta_1}\sqrt{1 - k_1^2\sin^2\phi}\,\frac{\partial}{\partial\phi},\end{aligned} \tag{71}$$

where here r, ϑ and p_r are functions of (χ, ϕ), which are determined by the relations in Eqs. (62,63,54,66).

In the next subsection, a coordinate transformation $(t, \varphi, \chi, \phi) \mapsto (Q^0, Q^1, Q^2, Q^3)$ is introduced which brings the vector fields X_0 and X_3 in simpler form. Before we proceed, we note the following consequence of Lemma 6 which will turn out to be useful later. Denote by $\varphi_\alpha^{\lambda^\alpha}$ the flows associated with X_α and define for each $(\lambda^0, \lambda^1, \lambda^2, \lambda^3) \in \mathbb{R}^4$ the map

$$\varphi^\lambda := \varphi_0^{\lambda^0} \circ \varphi_1^{\lambda^1} \circ \varphi_2^{\lambda^2} \circ \varphi_3^{\lambda^3}. \tag{72}$$

Since the vector fields X_α are complete, this map is well-defined for all $\lambda \in \mathbb{R}^4$ and it satisfies $\varphi^0 = \mathrm{id}$ and $\varphi^{\lambda+\mu} = \varphi^\lambda \circ \lambda^\mu$ for all $\lambda, \mu \in \mathbb{R}^4$, due to the fact that the vector fields X_α commute with each other. Therefore, the maps φ^λ define an action of the group $(\mathbb{R}^4, +)$ on Γ_{bound}. Restricting to a particular invariant submanifold $\Gamma^{(ext)}_{m,E,L_z,L}$, one has:

Lemma 7. *Let $(m, E, L_z, L) \in \Omega$ and consider the restriction of the map φ^λ defined in Eq. (72) on $\Gamma^{(ext)}_{m,E,L_z,L}$. Denote by*

$$H_{Iso} := \{\lambda \in \mathbb{R}^4 : \varphi^\lambda(x, p) = (x, p) \text{ for all } (x, p) \in \Gamma^{(ext)}_{m,E,L_z,L}\}$$

the isotropy subgroup. Then, φ^λ provides a diffeomorphism of $\mathbb{R}^4/H_{Iso}$ onto $\Gamma^{(ext)}_{m,E,L_z,L}$.

Proof. Let us abbreviate $\Gamma^{(0)} := \Gamma^{(ext)}_{m,E,L_z,L}$, and let $(x_0, p_0) \in \Gamma^{(0)}$ be fixed. Consider the map

$$G : \mathbb{R}^4 \to \Gamma^{(0)}, \lambda \mapsto G(\lambda) = \varphi^\lambda(x_0, p_0). \tag{73}$$

Its linearization $DG(\lambda)$ maps the vector fields e_α of the standard basis of $\mathbb{R}^4$ to the vectors $X_\alpha|_{\varphi^\lambda(x_0,p_0)}$, which are linearly independent, and hence G is a local diffeomorphism. Consequently, the image of G is both open and closed in $\Gamma^{(0)}$, which implies that $G(\mathbb{R}^4) = \Gamma^{(0)}$. Hence, when restricted to the quotient $\mathbb{R}^4/H_{Iso}$, G provides a diffeomorphism of $\mathbb{R}^4/H_{Iso}$ to $\Gamma^{(0)}$. □

Remark 7. Since $\Gamma^{(ext)}_{m,E,L_z,L} = \mathbb{R} \times T^3$, the isotropy subgroup H_{Iso} is a lattice group generated by three linearly independent vectors $E_\varphi, E_\chi, E_\phi \in \mathbb{R}^4$. They will be computed explicitly in subsection 3.5 below.

3.4. The generalized angle variables. In this subsection we analyze the properties of the Q^α variables which are formally defined by Eq. (47). We first prove that they are locally well-defined and that (J_α, Q^α) are local symplectic coordinates.

Lemma 8. *For each $(x, p) \in \Gamma_{bound}$ there exists an open neighborhood U of (x, p) in Γ_{bound} on which the variables Q^α are well-defined and smooth and the coordinates (J_α, Q^α) are symplectic.*

Proof. Let $(x, p) \in \Gamma_{bound}$ and set $(C_\alpha) := (P_\alpha(x, p)) \in \Omega$. Choose an open neighborhood $\Omega' \subset \Omega$ of (C_α) on which the map $\mathbb{I}$ is injective and consider the corresponding subset

$$\Gamma'_{bound} := \bigcup_{(m,E,L,L_z)\in\Omega'} \Gamma^{(ext)}_{m,E,L_z,L}$$

of Γ_{bound}. Next, rewrite the generating function S in Eq. (55) in the form $S(\gamma_x; I_\alpha) = -Et_{BL} + L_z\varphi_{BL} + S_r(\gamma_r; I_\alpha) + S_\vartheta(\gamma_\vartheta; I_\alpha)$, with the generating functions S_r and S_ϑ corresponding to the radial and polar motion, respectively, defined by

$$S_r(\gamma_r; I_\alpha) = \int_{\gamma_r} V \frac{dr}{\Delta}, \qquad S_\vartheta(\gamma_\vartheta; I_\alpha) := \int_{\gamma_\vartheta} p_\vartheta d\vartheta, \tag{74}$$

where we recall that V and p_ϑ satisfy $V^2 = R(r)$ and $p_\vartheta^2 = L^2 - K(\vartheta)$. Unless (x, p) corresponds to a turning point for the radial or polar motions, we can choose an open neighborhood U of (x, p) in Γ'_{bound} on which S_r and S_ϑ are well-defined functions of (r, I_α) and (ϑ, I_α), respectively. On such a neighborhood, the functions

$$Q^\alpha(x, p) := \left.\frac{\partial S}{\partial I_\alpha}\right|_x (\gamma_x, J_\alpha(x, p)), \qquad (x, p) \in U, \tag{75}$$

are well-defined and the map $(x^\mu, p_\mu) \mapsto (Q^\mu, J_\mu)$, $J_\mu := I_\mu(P(x,p))$, is smooth and symplectic since

$$\Omega_s = dp_\mu \wedge dx^\mu = d\left(\frac{\partial S}{\partial x^\mu}\right) \wedge dx^\mu = \frac{\partial^2 S}{\partial x^\mu \partial I_\alpha} dJ_\alpha \wedge dx^\mu + \frac{\partial^2 S}{\partial x^\mu \partial x^\nu} dx^\nu \wedge dx^\mu$$
$$= dJ_\alpha \wedge d\left(\frac{\partial S}{\partial I_\alpha}\right) = dJ_\alpha \wedge dQ^\alpha. \tag{76}$$

If the point (x, p) corresponds to a turning point of the polar motion, say, we use p_ϑ instead of ϑ to parametrize the curve γ_ϑ which leads to an alternative generating function $S'_\vartheta(p_\vartheta, I_\alpha)$. Specifically, we rewrite

$$S_\vartheta(\gamma_\vartheta; I_\alpha) = p_\vartheta \vartheta + S'_\vartheta(p_\vartheta, I_\alpha), \qquad S'_\vartheta(p_\vartheta, I_\alpha) = -\int_{\gamma_{p_\vartheta}} \vartheta dp_\vartheta,$$

and notice that for points away from the turning point

$$\left.\frac{\partial S_\vartheta}{\partial I_\alpha}\right|_\vartheta = \left(\vartheta + \frac{\partial S'_\vartheta}{\partial p_\vartheta}\right)\frac{\partial p_\vartheta}{\partial I_\alpha} + \frac{\partial S'_\vartheta}{\partial I_\alpha} = \frac{\partial S'_\vartheta}{\partial I_\alpha},$$

such that Q^α can be obtained by the same equation (75) replacing S_ϑ with S'_ϑ in the generating function. Again, the transformation $(x^\mu, p_\mu) \mapsto (Q^\mu, J_\mu)$ is symplectic. A similar procedure is used if (x, p) is a turning point of the radial motion. □

Although they are locally well-defined, the variables Q^α are not globally uniquely defined on Γ'_{bound}, due to their dependency on the winding of the curve γ_x connecting the reference point (x_0, p_0) to the end point (x, p). If γ_x and γ'_x are two curves connecting (x_0, p_0) and (x, p), one has, according to Eqs. (43,48):

$$S(\gamma'_x; I_\alpha) = S(\gamma_x; I_\alpha) + 2\pi \sum_{j=1}^{3} n^j I_j, \tag{77}$$

with $n = (n^1, n^2, n^3) \in \mathbb{Z}^3$ the difference in the winding numbers between the two curves. As a consequence, the corresponding Q^α-variables are related to each other by

$$(Q')^\alpha(x,p) = Q^\alpha(x,p) + 2\pi \delta^\alpha{}_j n^j, \tag{78}$$

that is, the variables Q^j with $j = 1, 2, 3$ are 2π-periodic, whereas Q^0 is independent of the winding. We conclude this subsection by proving that (taking into account the periodicity of the angle variables Q^j) the Q^α variables provide global coordinates on each invariant set $\Gamma^{(ext)}_{m,E,L_z,L}$.

Lemma 9. *Let $(m, E, L_z, L) \in \Omega$. Then, $\mathcal{Q} : \Gamma^{(ext)}_{m,E,L_z,L} \to \mathbb{R} \times T^3, (x,p) \mapsto (Q^0(x,p), Q^1(x,p), Q^2(x,p), Q^3(x,p))$ is a diffeomorphism.*

Proof. Denote by $Z_\alpha := X_{J_\alpha}$ the Hamiltonian vector fields associated with J_α. Due to the fact that (J_α, Q^α) are symplectic coordinates, they satisfy

$$Z_\alpha[Q^\beta] = \{J_\alpha, Q^\beta\} = \delta^\beta{}_\alpha. \tag{79}$$

Furthermore, it follows from $J_\alpha = I_\alpha(m, E, L_z, L)$ and $F_0 = m^2/2$ $F_1 = E$, $F_2 = L_z$, $F_3 = L^2$ on $\Gamma^{(ext)}_{m,E,L_z,L}$ (see Eq. (16)) that

$$\Omega_s(\cdot, Z_\alpha) = dJ_\alpha = \mathbf{N}_\alpha{}^\beta dF_\beta = \mathbf{N}_\alpha{}^\beta \Omega_s(\cdot, X_\beta), \tag{80}$$

with $\mathbf{N} := \mathbf{M} \circ \mathbf{D}^{-1}$, where $\mathbf{M}$ is the matrix defined in Eq. (57) which is invertible as has been shown in the proof of Lemma 5, and $\mathbf{D} = \mathrm{diag}(m, 1, 1, 2L)$. It follows from Eq. (80) that $Z_\alpha = \mathbf{N}_\alpha{}^\beta X_\beta$, and as a consequence of Lemma 6 and the fact that $\mathbf{N}$ is constant on each $\Gamma^{(ext)}_{m,E,L_z,L}$, these fields Z_α are complete and satisfy $[Z_\alpha, Z_\beta] = \{J_\alpha, J_\beta\} = 0$. Next, denote by $\psi_\alpha^{\lambda^\alpha}$ the flow associated with Z_α and define for each $\lambda = (\lambda^0, \lambda^1, \lambda^2, \lambda^3) \in \mathbb{R}^4$ the map

$$\psi^\lambda := \psi_0^{\lambda^0} \circ \psi_1^{\lambda^1} \circ \psi_2^{\lambda^2} \circ \psi_3^{\lambda^3}, \tag{81}$$

in analogy with Eq. (72). Denote by (x_0, p_0) the reference point of $\Gamma^{(ext)}_{m,E,L_z,L}$, and introduce the map[12]

$$G' : \mathbb{R}^4 \to \Gamma^{(ext)}_{m,E,L_z,L}, \lambda \mapsto G'(\lambda) := \psi^\lambda(x_0, p_0). \tag{83}$$

As in the proof of Lemma 7 it follows that G' defines a diffeomorphism of $\mathbb{R}^4/H'_{Iso}$ onto $\Gamma^{(ext)}_{m,E,L_z,L}$, where H'_{Iso} denotes the isotropy subgroup of ψ^λ. We claim that this map is the inverse of $\mathcal{Q}$. To prove this, it is sufficient to observe that $Q^\mu(x_0, p_0) = 0$ and

$$\frac{\partial}{\partial \lambda^\beta} Q^\alpha(G'(\lambda)) = Z_\beta[Q^\alpha]\big|_{G'(\lambda)} = \delta^\alpha{}_\beta,$$

which implies that $Q^\alpha(G'(\lambda)) = \lambda^\alpha$ for all $\lambda \in \mathbb{R}^4$ and that $H'_{Iso} = \{\lambda = (0, \mathbf{n}) : \mathbf{n} \in 2\pi\mathbb{Z}^3\}$. □

Lemmas 5, 8 and 9 imply:

Theorem 1. *Let $\Omega' \subset \Omega$ be an open subset of Ω on which the map $\mathbb{I}$ is injective and consider the corresponding subset*

$$\Gamma'_{bound} := \bigcup_{(m,E,L,L_z)\in\Omega'} \Gamma^{(ext)}_{m,E,L_z,L} \tag{84}$$

of Γ_{bound}. Then, the map $\Phi : \Gamma'_{bound} \to \mathbb{R} \times T^3 \times \mathbb{I}(\Omega')$ defined by

$$\begin{aligned}\Phi(x, p) := (&Q^0(x, p), Q^1(x, p), Q^2(x, p), Q^3(x, p), J_0(x, p),\\ &J_1(x, p), J_2(x, p), J_3(x, p)), \qquad (x, p) \in \Gamma'_{bound},\end{aligned} \tag{85}$$

is a diffeomorphism which satisfies $\Omega_s = dJ_\alpha \wedge dQ^\alpha$.

[12] Note that this map is related to the corresponding map G defined in Eq. (73) through

$$G'(\lambda) = G(\mathbf{N}^T\lambda), \qquad \lambda \in \mathbb{R}^4. \tag{82}$$

As mentioned previously, it is not a priori clear whether or not the map $\mathbb{I}$ defined in Lemma 5 is globally invertible, such that it is a priori not clear either whether or not the map Φ can be extended to all Γ_{bound}. To bypass this problem, one can work with the variables (Q^α, P_α) instead of (Q^α, J_α) which are globally well-defined on Γ_{bound} as follows from Lemma 9. These variables are not symplectic anymore; however the symplectic form Ω_s still has a simple representation.

Theorem 2. *The map* $\Psi : \Gamma_{bound} \to \mathbb{R} \times T^3 \times \Omega$ *defined by*

$$\Psi(x, p) := (Q^0(x, p), Q^1(x, p), Q^2(x, p), Q^3(x, p), P_0(x, p), P_1(x, p), P_2(x, p), P_3(x, p)), \qquad (x, p) \in \Gamma_{bound}, \tag{86}$$

is a diffeomorphism which satisfies $\Omega_s = \mathbf{M}_\alpha{}^\beta dP_\beta \wedge dQ^\alpha$, *with* $\mathbf{M}$ *the Jacobi matrix defined in Eq. (57).*

Proof. The fact that Ψ defines a diffeomorphism follows from Lemmas 8 and 9. To prove the validity of the claimed expression for the symplectic form, we take a subset Γ'_{bound} on which the previous theorem applies and note that

$$dJ_\alpha = \mathbf{M}_\alpha{}^\beta dP_\beta,$$

which implies that $\Omega_s = \mathbf{M}_\alpha{}^\beta dP_\beta \wedge dQ^\alpha$ on Γ'_{bound}. Since $\mathbf{M}_\alpha{}^\beta$ only depends on the constants of motion C_α and Γ_{bound} can be covered by sets of the form Γ'_{bound} as in the previous theorem, the claim follows. □

3.5. Explicit expressions for the generalized action-angle variables in terms of Legendre's elliptic integrals. As mentioned above, the variables J_α and Q^α can be computed explicitly. We provide more details of the calculations in appendix D; the explicit representation is based on the roots of the polynomial $R(r)$ defined in Eq. (28), those of the polynomial $q(\zeta)$ in Eq. (D11) and the angles χ and ϕ defined through Eqs. (62,63,66,67). In terms of the functions $\mathbb{G}^\alpha(\phi)$ and $\mathbb{H}^\alpha(\chi)$ defined in Eqs. (D16–D19,D23–D26) and the abbreviations $\mathbb{G}^\alpha := \mathbb{G}^\alpha(\pi/2)$ and $\mathbb{H}^\alpha := \mathbb{H}^\alpha(\pi/2)$, the action variables can be written as

$$J_0 = m, \tag{87}$$

$$J_1 = L_z, \tag{88}$$

$$J_2 = \frac{1}{\pi}\left[M_H m\mathbb{G}^0 + M_H\mathbb{G}^1 + L_z\mathbb{G}^2 + L\mathbb{G}^3\right], \tag{89}$$

$$J_3 = \frac{1}{\pi}\left[M_H m\mathbb{H}^0 + M_H\mathbb{H}^1 + L_z\mathbb{H}^2 + L\mathbb{H}^3\right], \tag{90}$$

where it is understood that $(m, E, L_z, L) = (C_\alpha) = (P_\alpha(x, p))$. The angle variables Q^α defined in Eq. (47) can be computed by applying the chain rule:

$$Q^\alpha = \frac{\partial S}{\partial I_\alpha} = \frac{\partial S}{\partial P_\beta}\frac{\partial P_\beta}{\partial I_\alpha} = (\mathbf{M}^{-T})^\alpha{}_\beta \tilde{Q}^\beta, \qquad \tilde{Q}^\beta := \frac{\partial S}{\partial P_\beta}, \tag{91}$$

with $\mathbf{M}$ the Jacobi matrix of the map $\mathbb{I} : \Omega \to \mathbb{R}^4$ and $\mathbf{M}^{-T} := (\mathbf{M}^{-1})^T$ its inverse transposed. The partial derivatives of the generating function S with respect to P_β give

$$\tilde{Q}^0 = \frac{\partial S}{\partial m} = M_H\left[\mathbb{G}^0(\phi) + \mathbb{H}^0(\chi)\right], \tag{92}$$

$$\tilde{Q}^1 = \frac{\partial S}{\partial E} = -t_{BL} + M_H \left[\mathbb{G}^1(\phi) + \mathbb{H}^1(\chi)\right], \tag{93}$$

$$\tilde{Q}^2 = \frac{\partial S}{\partial L_z} = \varphi_{BL} + \mathbb{G}^2(\phi) + \mathbb{H}^2(\chi), \tag{94}$$

$$\tilde{Q}^3 = \frac{\partial S}{\partial L} = \mathbb{G}^3(\phi) + \mathbb{H}^3(\chi), \tag{95}$$

and it can be verified that these quantities satisfy $X_\alpha\left[\tilde{Q}^\beta\right] = 0$ for $\alpha \neq \beta$ and $X_0[\tilde{Q}^0] = m$, $X_1[\tilde{Q}^1] = 1$, $X_2[\tilde{Q}^2] = 1$, $X_3[\tilde{Q}^3] = 2L$, with X_α the Hamiltonian vector field associated with F_α. Hence, $\tilde{Q}^0/m$, $\tilde{Q}^1$, $\tilde{Q}^2$ and $\tilde{Q}^3/(2L)$ are transported along the Hamiltonian flows associated with X_α which implies that they are locally well-defined and multi-valued functions on each invariant set $\Gamma^{(ext)}_{m,E,L_z,L}$. However, they do not have the correct period: under full revolutions $\varphi \mapsto \varphi + 2\pi$, $\chi \mapsto \chi + \pi$, and $\phi \mapsto \phi + 2\pi$ about the S^1 factors, these variables change according to $\tilde{Q}^\alpha \mapsto \tilde{Q}^\alpha + E^\alpha_a$, with $E_\varphi, E_\chi, E_\phi/(2L) \in \mathbb{R}^4$ the generators of the isotropy group H_{Iso} (see the remark below Lemma 7), given by $E_\varphi = (0, 0, 2\pi, 0)$, $E_\chi = 2(M_H\mathbb{H}^0, M_H\mathbb{H}^1, \mathbb{H}^2, \mathbb{H}^3)$, and $E_\phi = 2(M_H\mathbb{G}^0, M_H\mathbb{G}^1, \mathbb{G}^2, \mathbb{G}^3)$.

The matrix $\mathbf{M}$ and its inverse transposed read

$$\mathbf{M} = \frac{1}{\pi}\begin{pmatrix} \pi & 0 & 0 & 0 \\ 0 & 0 & \pi & 0 \\ M_H\mathbb{G}^0 & M_H\mathbb{G}^1 & \mathbb{G}^2 & \mathbb{G}^3 \\ M_H\mathbb{H}^0 & M_H\mathbb{H}^1 & \mathbb{H}^2 & \mathbb{H}^3 \end{pmatrix}, \qquad \mathbf{M}^{-T} = \begin{pmatrix} 1 & \omega^0 & 0 & M_H\eta^0 \\ 0 & \omega^1 & 1 & M_H\eta^1 \\ 0 & \omega^2 & 0 & M_H\eta^2 \\ 0 & \omega^3 & 0 & M_H\eta^3 \end{pmatrix}, \tag{96}$$

with

$$\omega^0 = -\frac{\mathbb{G}^0\mathbb{H}^3 - \mathbb{G}^3\mathbb{H}^0}{\mathbb{G}^1\mathbb{H}^3 - \mathbb{G}^3\mathbb{H}^1}, \quad \omega^1 = -\frac{1}{M_H}\frac{\mathbb{G}^2\mathbb{H}^3 - \mathbb{G}^3\mathbb{H}^2}{\mathbb{G}^1\mathbb{H}^3 - \mathbb{G}^3\mathbb{H}^1}, \quad \omega^2 = \frac{\pi}{M_H}\frac{\mathbb{H}^3}{\mathbb{G}^1\mathbb{H}^3 - \mathbb{G}^3\mathbb{H}^1},$$
$$\omega^3 = -\frac{\pi}{M_H}\frac{\mathbb{G}^3}{\mathbb{G}^1\mathbb{H}^3 - \mathbb{G}^3\mathbb{H}^1}, \tag{97}$$

and

$$\eta^0 = -\frac{\mathbb{G}^1\mathbb{H}^0 - \mathbb{G}^0\mathbb{H}^1}{\mathbb{G}^1\mathbb{H}^3 - \mathbb{G}^3\mathbb{H}^1}, \quad \eta^1 = -\frac{1}{M_H}\frac{\mathbb{G}^1\mathbb{H}^2 - \mathbb{G}^2\mathbb{H}^1}{\mathbb{G}^1\mathbb{H}^3 - \mathbb{G}^3\mathbb{H}^1}, \quad \eta^2 = -\frac{\pi}{M_H}\frac{\mathbb{H}^1}{\mathbb{G}^1\mathbb{H}^3 - \mathbb{G}^3\mathbb{H}^1},$$
$$\eta^3 = \frac{\pi}{M_H}\frac{\mathbb{G}^1}{\mathbb{G}^1\mathbb{H}^3 - \mathbb{G}^3\mathbb{H}^1}. \tag{98}$$

Note that according to the proof of Lemma 5 one has $0 < \det(\mathbf{M}) = -M_H(\mathbb{G}^1\mathbb{H}^3 - \mathbb{G}^3\mathbb{H}^1)/\pi^2$, such that these quantities are well-defined. Furthermore, note that $\mathbf{M}^{-T}E_\varphi = 2\pi(0, 1, 0, 0)$, $\mathbf{M}^{-T}E_\phi = 2\pi(0, 0, 1, 0)$ and $\mathbf{M}^{-T}E_\chi = 2\pi(0, 0, 0, 1)$, such that the variables Q^1, Q^2 and Q^3 have the correct period, as is expected from their definition. Explicitly, one finds $Q^\alpha = q^\alpha - \omega^\alpha t_{BL}$ with

$$q^0 = M_H\left\{\frac{\mathbb{H}^1\mathbb{G}^{03}(\phi) + \mathbb{H}^3\mathbb{G}^{10}(\phi) + \mathbb{H}^0\mathbb{G}^{31}(\phi)}{\mathbb{G}^1\mathbb{H}^3 - \mathbb{G}^3\mathbb{H}^1} - \frac{\mathbb{G}^1\mathbb{H}^{03}(\chi) + \mathbb{G}^3\mathbb{H}^{10}(\chi) + \mathbb{G}^0\mathbb{H}^{31}(\chi)}{\mathbb{G}^1\mathbb{H}^3 - \mathbb{G}^3\mathbb{H}^1}\right\}, \tag{99}$$

$$q^1 = \frac{\mathbb{H}^1\mathbb{G}^{23}(\phi) + \mathbb{H}^2\mathbb{G}^{31}(\phi) + \mathbb{H}^3\mathbb{G}^{12}(\phi)}{\mathbb{G}^1\mathbb{H}^3 - \mathbb{G}^3\mathbb{H}^1} - \frac{\mathbb{G}^1\mathbb{H}^{23}(\chi) + \mathbb{G}^2\mathbb{H}^{31}(\chi) + \mathbb{G}^3\mathbb{H}^{12}(\chi)}{\mathbb{G}^1\mathbb{H}^3 - \mathbb{G}^3\mathbb{H}^1} + \varphi_{BL}, \tag{100}$$

$$q^2 = \pi \frac{\mathbb{H}^3\mathbb{G}^1(\phi) - \mathbb{H}^1\mathbb{G}^3(\phi) - \mathbb{H}^{13}(\chi)}{\mathbb{G}^1\mathbb{H}^3 - \mathbb{G}^3\mathbb{H}^1}, \tag{101}$$

$$q^3 = \pi \frac{\mathbb{G}^1\mathbb{H}^3(\chi) - \mathbb{G}^3\mathbb{H}^1(\chi) + \mathbb{G}^{13}(\phi)}{\mathbb{G}^1\mathbb{H}^3 - \mathbb{G}^3\mathbb{H}^1}, \tag{102}$$

where we have introduced the functions $\mathbb{G}^{\alpha\beta}(\phi) := \mathbb{G}^\alpha\mathbb{G}^\beta(\phi) - \mathbb{G}^\beta\mathbb{G}^\alpha(\phi)$ and $\mathbb{H}^{\alpha\beta}(\chi) := \mathbb{H}^\alpha\mathbb{H}^\beta(\chi) - \mathbb{H}^\beta\mathbb{H}^\alpha(\chi)$ which are invariant with respect to the transformations $\phi \mapsto \phi + \pi/2$ and $\chi \mapsto \chi + \pi/2$. Like (Q^1, Q^2, Q^3), the variables (q^1, q^2, q^3) are angle coordinates associated with the azimuthal, polar and radial motion, respectively, and ω^1, ω^2 and ω^3 are the corresponding frequencies (called the fundamental frequencies [35]) describing their changes with respect to the Boyer-Lindquist time coordinate t_{BL}.[13] Finally, note that q^0, q^2 and q^3 only depend on the integrals of motion P_α and the angles χ and ϕ, while q^1 depends, in addition, on the azimuthal angle φ_{BL}.

In the limit $\beta^2 \to 1$ of equatorial orbits, it follows that $\mathbb{G}^0 = 0$, $\mathbb{G}^1 = -\alpha\mathbb{G}^2$ and $\mathbb{G}^3 = -\beta\mathbb{G}^2$ which implies that $J_2 = 0$ and $\mathbb{G}^{\alpha\beta}(\phi) = 0$, such that the above expressions for q^0, q^1 and q^3 simplify and become independent of ϕ.

In the non-rotating limit $a_H = 0$ it follows that $\mathbb{G}^0 = \mathbb{G}^1 = \mathbb{H}^2 = 0$ and $\mathbb{G}^2(\phi) = -\beta\Pi_*(\phi, 1-\beta^2, 0)$, $\mathbb{G}^3(\phi) = \phi + \pi/2$ and the expressions in Eq. (97) simplify considerably:

$$\omega^0 = -\frac{\mathbb{H}^0}{\mathbb{H}^1}, \qquad \pm\omega^1 = \omega^2 = -\frac{1}{M_H}\frac{\mathbb{H}^3}{\mathbb{H}^1}, \qquad \omega^3 = \frac{\pi}{M_H}\frac{1}{\mathbb{H}^1}, \tag{103}$$

the $\pm$ sign corresponding to the sign of L_z. The fact that ω^1 and ω^2 are equal in magnitude reflects the fact that the motion is confined to a plane. Further, one finds $J_2 = L - |L_z|$ and

$$\begin{aligned} q^0 &= -M_H\frac{\mathbb{H}^{01}(\chi)}{\mathbb{H}^1}, \quad q^1 = -\frac{1}{\pi}\mathbb{G}^{23}(\phi) + \mathrm{sign}(\beta)\frac{\mathbb{H}^{13}(\chi)}{\mathbb{H}^1} + \varphi_{BL}, \\ q^2 &= \frac{\mathbb{H}^{13}(\chi)}{\mathbb{H}^1} + \phi + \pi/2, \quad q^3 = \pi\frac{\mathbb{H}^1(\chi)}{\mathbb{H}^1}. \end{aligned} \tag{104}$$

Before closing this section, for completeness, we provide the explicit expressions for the Hamiltonian vector fields X_α in terms of the generalized action-angle variables (P_α, Q^α). Using Theorem 2, the definition (42) and the relation $(C_\alpha) = (m, E, L_z, L) = (P_\alpha(x, p))$ one finds

$$X_0 = P_0\frac{\partial}{\partial Q^0}, \qquad X_1 = \omega^\alpha\frac{\partial}{\partial Q^\alpha}, \qquad X_2 = \frac{\partial}{\partial Q^1}, \qquad X_3 = 2M_H P_3\eta^\alpha\frac{\partial}{\partial Q^\alpha}. \tag{105}$$

[13] A coordinate-independent definition of these quantities is provided by noting that $\omega^\alpha = X_1[Q^\alpha]$ with X_1 the Hamiltonian vector field associated with the integral of motion F_1, which corresponds to minus the complete lift of the Killing vector field ∂_t, see the remark below Corollary 1.

4. Mixing and Strong Jeans Theorem

In this section we apply the results from the previous section to analyze the late time dynamics of the solutions f of the Liouville equation (2), assuming that f is supported in $\overline{\Gamma_{bound}}$, the subset of relativistic phase space consisting of bound timelike geodesic orbits in the Kerr exterior. According to the results from the previous section, the set Γ_{bound} is diffeomorphic to $\mathbb{R} \times T^3 \times \Omega$ and in terms of the coordinates (Q^α, P_α) the Liouville vector field is simply $-P_0 \frac{\partial}{\partial Q^0}$, which implies that f is a function depending only of the angle variables Q^1, Q^2, Q^3 and the integrals of motion P_α.

For what follows, we consider a kinetic gas consisting of identical massive particles of fixed rest mass $m > 0$. We introduce a foliation S_T of the Kerr exterior by three-dimensional hypersurfaces of constant Boyer-Lindquist time $t_{BL} = T$ and the associated six-dimensional subsets

$$\Sigma_T := \{(x, p) \in \Gamma_{bound} : x \in S_T, g_x(p, p) = -m^2\} \tag{106}$$

of Γ_{bound}. Owing to the fact that the Kerr exterior is stationary, the flow of the Killing vector field ∂_t provides an isometry between the different sets S_T. Likewise, the flow φ^t associated with the complete lift of ∂_t provides a symplectic diffeomorphism between the different sets Σ_T, such that each of these sets can be naturally identified with Σ_0, say.

In the next subsection we show how to reduce the considerations of the previous section to Σ_0, and we reformulate the Liouville equation (2) as a Cauchy problem on Σ_0. Next, in subsection 4.3 we discuss the strong Jeans theorem and in subsection 4.4 we formulate sufficient conditions for phase space mixing to hold.

4.1. Reduction to six-dimensional phase space and Cauchy problem. We denote by $\hat{\Omega}$ the set of 3-tuples (E, L_z, L) for which $(m, E, L_z, L) \in \Omega$. Each Σ_T is foliated by the sets

$$\hat{\Gamma}_{E,L_z,L} := \{(x, p) \in \Sigma_T : F_1(x, p) = E, F_2(x, p) = L_z, F_3(x, p) = L^2\}, \quad (E, L_z, L) \in \hat{\Omega}, \tag{107}$$

which are topologically equal to T^3, and it follows from the results of the previous section that the variables $(\mathbf{P}, \mathbf{q}) := (P_a, q^a)$, $a = 1, 2, 3$, on Σ_T are adapted to this foliation, where on each set $\hat{\Gamma}_{E,L_z,L}$, (P_1, P_2, P_3) is constant equal to (E, L_z, L) and the quantities q^1, q^2, q^3 defined by Eqs. (100,101,102) are angles. When restricted to Σ_T the map Ψ from Theorem 2 induces a diffeomorphism $\hat{\Psi}_T : \Sigma_T \to T^3 \times \hat{\Omega}$ which is explicitly given by

$$\hat{\Psi}_T(x, p) = (Q^1(x, p), Q^2(x, p), Q^3(x, p), P_1(x, p), P_2(x, p), P_3(x, p)), \quad (x, p) \in \Sigma_T, \tag{108}$$

with $Q^a = q^a - T\omega^a$, $a = 1, 2, 3$. In terms of adapted local coordinates (x^μ, p_μ) such that $x^0 = T$ the symplectic form Ω_s and volume form η_Γ induce the forms

$$\hat{\Omega}_s = dp_i \wedge dx^i = \hat{\mathbf{M}}_a{}^b dP_b \wedge dq^a, \tag{109}$$

and

$$\begin{aligned}\hat{\eta} &= dx^1 \wedge dx^2 \wedge dx^3 \wedge dp_1 \wedge dp_2 \wedge dp_3 \\ &= \det(\hat{\mathbf{M}}) dq^1 \wedge dq^2 \wedge dq^3 \wedge dP_1 \wedge dP_2 \wedge dP_3,\end{aligned} \tag{110}$$

on Σ_T respectively, where $\hat{\mathbf{M}} = (\mathbf{M}_a{}^b)$ denotes the matrix consisting of the spatial components of the Jacobi matrix defined in Eq. (57). Note that both $\hat{\Omega}_s$ and $\hat{\eta}$ are invariant with respect to the complete lift of the Killing vector field ∂_t. For the following, we define $\hat{\Gamma} := T^3 \times \hat{\Omega}$.

Now consider a solution f of the Liouville equation (2) with initial datum f_0 supported on the closure of the set Σ_0. By means of the flow φ^t associated with the complete lift $-X_1$ of the Killing vector field ∂_t, we can describe the time evolution of the DF as a map $f_0 \mapsto f_t$ on $L^1(\Sigma_0, \hat{\eta})$, where

$$f_t(x, p) := f(\varphi^t(x, p)), \qquad t \in \mathbb{R}, \quad (x, p) \in \Sigma_0. \tag{111}$$

On the other hand, it follows from $X_0[f] = 0$, $\frac{d}{dt} f_t = -X_1[f]$ and Eq. (105) that

$$f_t(x, p) = [U(t)F](\hat{\Psi}_0(x, p)), \qquad t \in \mathbb{R}, \quad (x, p) \in \Sigma_0, \tag{112}$$

with $F := f_0 \circ \hat{\Psi}_0^{-1}$ the action-angle representation of the initial datum and where the operator $U(t)$ is defined by

$$(U(t)F)(\mathbf{q}, \mathbf{P}) = F(\mathbf{q} - t\boldsymbol{\omega}(\mathbf{P}), \mathbf{P}), \qquad t \in \mathbb{R}, \quad (\mathbf{q}, \mathbf{P}) \in \hat{\Gamma}, \tag{113}$$

with $\boldsymbol{\omega} := (\omega^1, \omega^2, \omega^3)$ the frequencies defined in Eq. (97). Likewise, we define $\boldsymbol{\eta} := (\eta^1, \eta^2, \eta^3)$ with η^a given in Eq. (98).

For the following, we discuss several properties of the flow map (113) on the function spaces $L^p(\hat{\Gamma}, \hat{\eta})$ with measure $\hat{\eta} = \det(\hat{\mathbf{M}}) d^3q\, d^3P$ and $1 \leq p < \infty$. Unless when stated explicitly otherwise, we shall only employ the following properties:

(i) The maps $\boldsymbol{\omega}, \boldsymbol{\eta} : \hat{\Omega} \to \mathbb{R}^3$ are C^1.
(ii) The map $\hat{\mathbf{M}} : \hat{\Omega} \to \mathrm{Mat}(3 \times 3, \mathbb{R})$ is continuous and $\hat{\mathbf{M}}(\mathbf{P})$ is invertible for all $\mathbf{P} \in \hat{\Omega}$.

Of course, these conditions are satisfied in our model describing bound Kerr geodesics in the exterior spacetime. In fact, it follows from the explicit representations in Eqs. (97,98) which allow one to express $\boldsymbol{\omega}$, $\boldsymbol{\eta}$ in terms of analytic functions of the simple roots of the polynomials $R(r)$ and $q(\zeta)$ (see Eqs. (28,D11)), that these quantities are analytic in $\mathbf{P}$. However, the results in the following subsections can be generalized to any model of the same form as (113) for which $\hat{\Gamma}$ has the form $\hat{\Gamma} = T^d \times \hat{\Omega}$ with $d \in \mathbb{N}$ and $\hat{\Omega}$ an open subset of some $\mathbb{R}^d$ and for which the conditions (i) and (ii) with the dimension 3 replaced with d are satisfied.

4.2. Well-posedness of the Cauchy problem and resonant frequencies. Once it has been brought into the form (113), the well-posedness of the Cauchy problem for the Liouville equation (2) follows from the following standard result whose proof is included for the sake of completeness of the presentation.

Lemma 10. *The map $U(t)$ defined by Eq. (113) gives rise to a strongly continuous unitary group on $L^p(\hat{\Gamma}, \hat{\eta})$.*

Proof. The group properties $U(0) = \mathrm{id}$ and $U(t) \circ U(s) = U(t+s)$ for all $t, s \in \mathbb{R}$ are obvious. Next, for $F \in L^p(\hat{\Gamma}, \hat{\eta})$ and $t \in \mathbb{R}$ it follows that

$$\int_{\hat{\Gamma}} |[U(t)F](\mathbf{q}, \mathbf{P})|^p \, \hat{\eta} = \int_{\hat{\Omega}} \int_{T^3} |F(\mathbf{q} - t\boldsymbol{\omega}(\mathbf{P}), \mathbf{P})|^p d^3q \det(\hat{\mathbf{M}}) d^3P = \int_{\hat{\Gamma}} |F(\mathbf{q}, \mathbf{P})|^p \hat{\eta},$$

and hence, $U(t) : L^p(\hat{\Gamma}, \hat{\eta}) \to L^p(\hat{\Gamma}, \hat{\eta})$ is a well-defined linear map which preserves the norm. Since $U(t)^{-1} = U(-t)$ it follows that it is unitary. Finally, to show strong continuity, first take F to lie in the space $C_0(\hat{\Gamma})$ of continuous functions with compact support. Then, $U(t)F \to F$ as $t \to 0$ follows from Lebesgue's dominated convergence theorem. By the density of $C_0(\hat{\Gamma})$ in $L^p(\hat{\Gamma}, \hat{\eta})$ the same property holds for arbitrary $F \in L^p(\hat{\Gamma}, \hat{\eta})$. □

Remark 8. It follows from Eq. (105) that the DF is axisymmetric if and only if F is independent of q^1. Furthermore, it is stationary if and only if F is invariant with respect to the flow of $\omega^a \frac{\partial}{\partial q^a}$. Finally, F is invariant under the Carter flow if and only if is invariant with respect to the flow associated with $\eta^a \frac{\partial}{\partial q^a}$. In the next subsection we show that the last two symmetry requirements have rather strong implications.

For what follows, we consider the two continuous maps $\mathbf{A}, \mathbf{B} : \hat{\Omega} \to \mathrm{Mat}(3 \times 3, \mathbb{R})$ defined by

$$\mathbf{A}^{ab} := \frac{\partial \omega^a}{\partial P_c} (\hat{\mathbf{M}}^{-1})_c{}^b, \qquad \mathbf{B}^{ab} := \frac{\partial \eta^a}{\partial P_c} (\hat{\mathbf{M}}^{-1})_c{}^b, \tag{114}$$

where we recall that ω^a and η^a, $a = 1, 2, 3$, refer to the quantities defined in Eqs. (97,98) and $\hat{\mathbf{M}} = (\mathbf{M}_a{}^b)$ denotes the spatial components of the Jacobi matrix in Eq. (57).

Lemma 11. $\mathbf{A}$ *and* $\mathbf{B}$ *map* $\hat{\Omega}$ *smoothly on the space of symmetric matrices, i.e.* $\mathbf{A}^{ab} = \mathbf{A}^{ba}$ *and* $\mathbf{B}^{ab} = \mathbf{B}^{ba}$.

Proof. Let $\hat{\Omega}' \subset \hat{\Omega}$ be an open subset on which the restriction of the map $\mathbb{I}$ defined in Lemma 5 on $\hat{\Omega}$ is injective. On this set we have (see Eq. (96))

$$\omega^a = \frac{\partial E}{\partial I_a}, \qquad M_H \eta^a = \frac{\partial L}{\partial I_a}, \tag{115}$$

such that

$$\mathbf{A}^{ab} = \frac{\partial \omega^a}{\partial P_c} (\hat{\mathbf{M}}^{-1})_c{}^b = \frac{\partial \omega^a}{\partial I_b} = \frac{\partial^2 E}{\partial I_a \partial I_b}. \tag{116}$$

Likewise,

$$\mathbf{B}^{ab} = \frac{\partial \eta^a}{\partial I_b} = M_H^{-1} \frac{\partial^2 L}{\partial I_a \partial I_b}, \tag{117}$$

which implies the statement of the lemma. □

The determinants of the maps $\mathbf{A}$ and $\mathbf{B}$ will play a fundamental role in the following two subsections. More precisely, we shall consider the following conditions:

Definition 1. We shall say that a measurable subset $\hat{C}$ in $\hat{\Omega}$ satisfies the A-nondegeneracy condition if

$$\{\det(\mathbf{A}) = 0\} \cap \hat{C} \tag{118}$$

has zero Lebesgue-measure in $\mathbb{R}^3$. Likewise, we say $\hat{C}$ satisfies the B-nondegeneracy condition if Eq. (118) with $\mathbf{A}$ replaced by $\mathbf{B}$ holds.

Remark 9. Clearly, if $\hat{C} \subset \hat{\Omega}$ satisfies the A-nondegeneracy condition, so does any measurable subset of $\hat{C}$.

Remark 10. For the Kerr problem which is the main focus of this article, the functions $\det(\mathbf{A})$, $\det(\mathbf{B}) : \hat{\Omega} \to \mathbb{R}$ are real analytic functions, as already noted before. In this case, the following proposition implies that either $\det(\mathbf{A})$ is identically zero or otherwise the A-nondegeneracy condition is satisfied on the whole set $\hat{\Omega}$. As we will prove in the next section, $\det(\mathbf{A})$ and $\det(\mathbf{B})$ cannot be identically zero when $a_H \neq 0$, and hence it follows that both the A and B-nondegeneracy conditions are satisfied on $\hat{\Omega}$ in the rotating Kerr case.

Proposition 4. *Let $U \subset \mathbb{R}^d$ be an open connected subset of $\mathbb{R}^d$ and let $F : U \to \mathbb{R}$ be real analytic. Then, either F is identically zero, or the set $\{x \in U : F(x) = 0\}$ has zero Lebesgue-measure in $\mathbb{R}^d$.*

Proof. See, for instance, Ref. [45]. □

For the next result we formulate the following well-known definition and result.

Definition 2. A three-tuple of frequencies $\mathbf{w} \in \mathbb{R}^3$ is called resonant if there exists $\mathbf{k} \in \mathbb{Z}^3 \setminus \{\mathbf{0}\}$ such that $\mathbf{k} \cdot \mathbf{w} = 0$. Otherwise, $\mathbf{w}$ is called non-resonant.

Lemma 12. *Suppose $\hat{C} \subset \hat{\Omega}$ satisfies the A-nondegeneracy condition. Then, the frequencies $\boldsymbol{\omega}(\mathbf{P})$ are non-resonant for almost all $\mathbf{P} \in \hat{C}$.*

Proof. Since this result is well-known (cf. [44]) we only sketch the proof. First, it is not difficult to verify that the set $\mathcal{M}$ of resonant three-tuples $\mathbf{w}$ is a zero measure set in $\mathbb{R}^3$. Next, we denote by $\boldsymbol{\omega}'$ the restriction of $\boldsymbol{\omega}$ on $\hat{C}' := \hat{C} \setminus \{\det(\mathbf{A}) = 0\}$. Because $\hat{C}$ satisfies the A-nondegeneracy condition, the statement of the lemma follows if we can show that the inverse image of $\mathcal{M}$, $(\boldsymbol{\omega}')^{-1}(\mathcal{M}) \subset \hat{C}'$, is also a zero-measure set in $\mathbb{R}^3$.

To show this, we use the inverse function theorem and cover the set $\hat{C}'$ with a countable number of open sets U_n on which $\boldsymbol{\omega}'$ is a local diffeomorphism. Since each set

$$(\boldsymbol{\omega}')^{-1}(\mathcal{M}) \cap U_n$$

has zero measure and

$$(\boldsymbol{\omega}')^{-1}(\mathcal{M}) \subset \bigcup_n (\boldsymbol{\omega}')^{-1}(\mathcal{M}) \cap U_n,$$

the lemma follows. □

4.3. Strong Jeans theorem. The strong Jeans theorem [46,47] states that a stationary solution of the Liouville equation depends only on the constants of motion E, L and L_z. A priori, this statement appears to be surprising since a function F depending on the combination $\omega^3 q^2 - \omega^2 q^3$, say, is independent of time. However, the requirement for F to be 2π-periodic in q^2 and q^3 implies that there cannot be a nontrivial dependency on any of such combinations, if the A-nondegeneracy condition holds. This is shown in the next theorem.

Definition 3. Let $F \in L^p(\hat{\Gamma}, \hat{\eta})$ with $p \geq 1$. We denote by

$$S(F) := \{\mathbf{P} \in \hat{\Omega} : (\mathbf{q}, \mathbf{P}) \in \mathrm{supp}(F) \text{ for some } \mathbf{q} \in T^3\} \tag{119}$$

the support of F in $\hat{\Omega}$. We say that F satisfies the A-nondegeneracy condition if the set $S(F)$ satisfies the A-nondegeneracy condition. Likewise, F satisfies the B-nondegeneracy condition if $S(F)$ satisfies the B-nondegeneracy condition.

Theorem 3. *(Strong Jeans theorem) Suppose $F \in L^1(\hat{\Gamma}, \hat{\eta})$ satisfies the A-nondegeneracy condition, and suppose in addition that it gives rise to a stationary DF. Then F is independent of the angle variables q^1, q^2 and q^3.*

Proof. Denote by $\hat{F}_k$ the Fourier coefficients of F:

$$\hat{F}_k(\mathbf{P}) := \frac{1}{(2\pi)^{3/2}} \int_{T^3} F(\mathbf{q}, \mathbf{P}) e^{-i\mathbf{k}\cdot\mathbf{q}} d^3q, \qquad \mathbf{k} \in \mathbb{Z}^3, \quad \mathbf{P} \in \hat{\Omega}. \tag{120}$$

According to the assumptions, $\hat{F}_k \in L^1(\hat{\Omega}, \det(\hat{\mathbf{M}}) d^3P)$ and $\mathrm{supp}(\hat{F}_k) \subset S(F)$ for all $\mathbf{k} \in \mathbb{Z}^3$. Moreover, since $S(F)$ satisfies the A-degeneracy condition, Lemma 12 implies that $\boldsymbol{\omega}(\mathbf{P})$ are non-resonant for almost all $\mathbf{P} \in S(F)$. Since

$$\begin{aligned} \widehat{U(t)F}_k(\mathbf{P}) &= \frac{1}{(2\pi)^{3/2}} \int_{T^3} F(\mathbf{q} - t\boldsymbol{\omega}(\mathbf{P}), \mathbf{P}) e^{-i\mathbf{k}\cdot\mathbf{q}} d^3q \\ &= \frac{1}{(2\pi)^{3/2}} \int_{T^3} F(\mathbf{q}, \mathbf{P}) e^{-it\mathbf{k}\cdot\boldsymbol{\omega}(\mathbf{P})} e^{-i\mathbf{k}\cdot\mathbf{q}} d^3q = e^{-it\mathbf{k}\cdot\boldsymbol{\omega}(\mathbf{P})} \hat{F}_k(\mathbf{P}), \end{aligned} \tag{121}$$

the stationarity assumption implies that

$$e^{-it\mathbf{k}\cdot\boldsymbol{\omega}(\mathbf{P})} \hat{F}_k(\mathbf{P}) = \hat{F}_k(\mathbf{P}) \tag{122}$$

for all $t \in \mathbb{R}$, $\mathbf{k} \in \mathbb{Z}^3$ and almost all $\mathbf{P} \in \hat{\Omega}$. This equality is obviously satisfied for the zero mode $\mathbf{k} = (0, 0, 0)$. For $\mathbf{k} \in \mathbb{Z}^3 \setminus \{(0, 0, 0)\}$, differentiate both sides with respect to t and evaluate at $t = 0$, giving

$$\mathbf{k} \cdot \boldsymbol{\omega}(\mathbf{P}) \hat{F}_k(\mathbf{P}) = 0 \tag{123}$$

for almost all $\mathbf{P} \in \hat{\Omega}$. Since $\mathbf{k} \cdot \boldsymbol{\omega}(\mathbf{P}) \neq 0$ for almost all $\mathbf{P} \in S(F)$, this implies that $\hat{F}_k(\mathbf{P}) = 0$ for almost all $\mathbf{P} \in \hat{\Omega}$ and thus $\hat{F}_k = 0$ in $L^1(\hat{\Omega})$ for all $\mathbf{k} \in \mathbb{Z}^3 \setminus \{\mathbf{0}\}$. Since an L^1-function is uniquely determined by its Fourier coefficients, this implies that

$$F(\mathbf{q}, \mathbf{P}) = \frac{1}{(2\pi)^{3/2}} \hat{F}_0(\mathbf{P}) = \frac{1}{(2\pi)^3} \int_{T^3} F(\mathbf{q}, \mathbf{P}) d^3q, \tag{124}$$

which is independent of q. Note that the right-hand side is the angle-average of F. □

In complete analogy with the previous theorem, one has the following result which shows that invariance with respect to the Carter flow and the satisfaction of the B-nondegeneracy condition also imply that the DF is independent of the angle variables:

Theorem 4. *Suppose $F \in L^1(\hat{\Gamma}, \hat{\eta})$ satisfies the B-nondegeneracy condition, and suppose in addition that F is invariant with respect to the Carter flow. Then F is independent of the angle variables q^1, q^2 and q^3.*

4.4. Phase space mixing. Phase space mixing can be interpreted as a dynamical version of the strong Jeans theorem, and states that the macroscopic observables associated with a (time-dependent) DF converge in time to those of the angle-averaged DF. Here, we define a "macroscopic observable" to be a time-dependent function of the form

$$N_g(t) := \int_{\Sigma_0} f_t(x, p) g(x, p) \hat{\eta}, \qquad t \in \mathbb{R}, \tag{125}$$

with $g : \Sigma_0 \to \mathbb{R}$ a suitable test function on Σ_0. In view of Eq. (112) this is equivalent to

$$N_g(t) = \int_{\hat{\Gamma}} [U(t)F](\mathbf{q}, \mathbf{P}) G(\mathbf{q}, \mathbf{P}) \hat{\eta}, \tag{126}$$

where $G := g \circ \hat{\Psi}_0$ denotes the action-angle representation of g. The mixing property consists in showing that the macroscopic observable $N_g(t)$ relaxes in time, that is, that the limit $\lim_{t\to\infty} N_g(t)$ exists. The next theorem shows that under suitable regularity assumptions on F and G this is indeed the case provided that F satisfies the A-nondegeneracy condition.

Theorem 5 (Mixing). *Let $1 \le p < \infty$ and $1 < q \le \infty$ be such that $1/p + 1/q = 1$. Define $Y_\infty := C_b(\hat{\Gamma})$, the space of bounded continuous functions on $\hat{\Gamma}$, and $Y_q := L^q(\hat{\Gamma}, \hat{\eta})$ for $q < \infty$. Suppose $F \in L^p(\hat{\Gamma}, \hat{\eta})$ satisfies the A-nondegeneracy condition. Denoting by $\overline{F}$ its angle-average, then for all $G \in Y_q$ one has*

$$\lim_{t\to\infty} \int_{\hat{\Gamma}} [U(t)F](\mathbf{q}, \mathbf{P}) G(\mathbf{q}, \mathbf{P}) \hat{\eta} = \int_{\hat{\Gamma}} \overline{F}(\mathbf{q}, \mathbf{P}) G(\mathbf{q}, \mathbf{P}) \hat{\eta}. \tag{127}$$

Proof. The proof is based on a refinement of the arguments presented in appendix A of Ref. [29] (which only treated the case $p = 1$ and assumed the frequency map $\boldsymbol{\omega}$ to be C^2 instead of C^1) which in turn, are based on work by C. Mitchell [28].

We start with the symmetric case $p = q = 2$. Hence, let $F, G \in L^2(\hat{\Gamma}, \hat{\eta})$ and consider their Fourier coefficients $\hat{F}_k, \hat{G}_k$, see Eq. (120). Using the Cauchy-Schwarz inequality it follows that $\hat{F}_k, \hat{G}_k \in L^2(\hat{\Omega}, \det(\hat{\mathbf{M}}) d^3P)$ and according to Parseval's identity,

$$\sum_{\mathbf{k}\in\mathbb{Z}^3} |\hat{F}_k(\mathbf{P})|^2 = \int_{T^3} |F(\mathbf{q}, \mathbf{P})|^2 d^3q, \qquad \sum_{\mathbf{k}\in\mathbb{Z}^3} |\hat{G}_k(\mathbf{P})|^2 = \int_{T^3} |G(\mathbf{q}, \mathbf{P})|^2 d^3q, \tag{128}$$

for almost all $\mathbf{P} \in \hat{\Omega}$, which implies that for each $\mathbf{k} \in \mathbb{Z}^3$ the function $h_k := \hat{F}_k \hat{G}_k^* : \hat{\Omega} \to \mathbb{C}$ belongs to $L^1(\hat{\Omega}, \det(\hat{\mathbf{M}}) d^3 P)$ and satisfies

$$\sum_{\mathbf{k}\in\mathbb{Z}^3} \|h_k\|_{L^1(\hat{\Omega},\det(\hat{\mathbf{M}})d^3P)} \leq \|F\|_{L^2(\hat{\Gamma},\hat{\eta})} \|G\|_{L^2(\hat{\Gamma},\hat{\eta})}. \tag{129}$$

Using Parseval's identity again and the expression in Eq. (121) for the Fourier coefficients of $U(t)F$ one obtains

$$\lim_{t\to\infty} \int_{\hat{\Gamma}} [U(t)F](\mathbf{q},\mathbf{P}) G(\mathbf{q},\mathbf{P}) \hat{\eta} = \sum_{k\in\mathbb{Z}^3} \lim_{t\to\infty} \int_{\hat{\Omega}} h_k(\mathbf{P}) e^{-it\mathbf{k}\cdot\boldsymbol{\omega}(\mathbf{P})} \det(\hat{\mathbf{M}}) d^3 P, \tag{130}$$

where we have used the fact that the series converges absolutely to interchange the limit with the sum. Lemma 13 below, combined with the observation that the sets $\mathrm{supp}(h_k) \subset \mathrm{supp}(\hat{F}_k) \subset S(F)$ satisfy the A-nondegeneracy condition, implies that for each $\mathbf{k} \neq \mathbf{0}$ the integrand on the right-hand side converges to zero. Consequently,

$$\begin{aligned} \lim_{t\to\infty} \int_{\hat{\Gamma}} [U(t)F](\mathbf{q},\mathbf{P}) G(\mathbf{q},\mathbf{P}) \hat{\eta} &= \int_{\hat{\Omega}} \hat{F}_0(\mathbf{P})^* \hat{G}_0(\mathbf{P}) \det(\hat{\mathbf{M}}) d^3 P \\ &= (2\pi)^3 \int_{\hat{\Gamma}} \overline{F}(\mathbf{q},\mathbf{P}) \overline{G}(\mathbf{q},\mathbf{P}) \hat{\eta}, \end{aligned} \tag{131}$$

where we have used the identity $\hat{F}_0(\mathbf{P}) = (2\pi)^{3/2} \overline{F}(\mathbf{q},\mathbf{P})$ in the last step. This proves the theorem for $p = q = 2$.

The proof for the remaining cases uses a density argument. According to Hölder's inequality,

$$\langle F, G \rangle := \int_{\hat{\Gamma}} F(\mathbf{q},\mathbf{P}) G(\mathbf{q},\mathbf{P}) \hat{\eta}$$

is well-defined and satisfies $|\langle F, G\rangle| \leq \|F\|_{L^p} \|G\|_{L^q}$ for all $F \in L^p(\hat{\Gamma}, \hat{\eta})$ and $G \in L^q(\hat{\Gamma}, \hat{\eta})$. With this notation, the statement is equivalent to proving that

$$\lim_{t\to\infty} \langle U(t)F - \overline{F}, G \rangle = 0$$

for all $F \in L^p(\hat{\Gamma}, \hat{\eta})$ and $G \in Y_q$. Since we already know that the theorem is true for $p = 2$ it holds, in particular, for any $F, G \in C_0(\hat{\Gamma})$. We first extend the statement to $G \in Y_q$. If $F \in C_0(\hat{\Gamma})$ and $G \in C_b(\hat{\Gamma})$ we take $\chi \in C_0(\hat{\Gamma})$ which is invariant with respect to $U(t)$ and such that $\chi = 1$ on the support of F. Then,

$$\langle U(t)F - \overline{F}, G \rangle = \langle U(t)F - \overline{F}, \chi G \rangle \to 0 \tag{132}$$

as $t \to \infty$, since $\chi G \in C_0(\hat{\Gamma})$. If $F \in C_0(\hat{\Gamma})$ and $G \in L^q(\hat{\Gamma})$ with $1 < q < \infty$ we take a sequence G_n in $C_0(\hat{\Gamma})$ such that $G_n \to G$ in $L^q(\hat{\Gamma}, \hat{\eta})$ and note:

$$\begin{aligned} |\langle U(t)F - \overline{F}, G\rangle| &\leq |\langle U(t)F - \overline{F}, G - G_n\rangle| + |\langle U(t)F - \overline{F}, G_n\rangle| \\ &\leq 2\|F\|_{L^p} \|G - G_n\|_{L^q} + |\langle U(t)F - \overline{F}, G_n\rangle|, \end{aligned}$$

where in the second step we have used the unitarity of $U(t)$ and the estimate $\|\overline{F}\|_{L^p} \leq \|F\|_{L^p}$ which follows from Hölder's inequality. By first choosing n large, and then t large, we can make the right-hand side arbitrarily small, which proves the theorem for $p > 1$, $F \in C_0(\hat{\Gamma})$ and $G \in L^q(\hat{\Gamma}, \hat{\eta})$. Finally, let $F \in L^p(\hat{\Gamma}, \hat{\eta})$ and let F_n be a sequence in $C_0(\hat{\Gamma})$ such that $F_n \to F$ in $L^p(\hat{\Gamma}, \hat{\eta})$. Then, for any $G \in Y_q$,

$$\begin{aligned} |\langle U(t)F - \overline{F}, G\rangle| &\leq |\langle U(t)(F - F_n), G\rangle + |\langle U(t)F_n - \overline{F}_n, G\rangle| + |\langle \overline{F}_n - \overline{F}, G\rangle| \\ &\leq 2\|F - F_n\|_{L^p}\|G\|_{L^q} + |\langle U(t)F_n - \overline{F}_n, G\rangle|. \end{aligned}$$

Again, by first choosing n sufficiently large and then t large, the right-hand side is made arbitrarily small, and this concludes the proof of the theorem. □

Lemma 13. *(Generalized Riemann-Lebesgue lemma) Let $h \in L^1(\hat{\Omega}, \det(\hat{\mathbf{M}})d^3P)$ and assume supp(h) satisfies the A-nondegeneracy condition. Then, for all $\mathbf{k} \in \mathbb{Z}^3 \setminus \{\mathbf{0}\}$,*

$$\lim_{t\to\infty} \int_{\hat{\Omega}} h(\mathbf{P}) e^{-it\mathbf{k}\cdot\boldsymbol{\omega}(\mathbf{P})} \det(\hat{\mathbf{M}}) d^3P = 0. \tag{133}$$

Proof. According to the assumptions, the set

$$Z := \text{supp}(h) \cap \{\det \mathbf{A} = 0\}$$

is closed and has zero-measure. Hence, it is sufficient to prove the statement for $\hat{\Omega}$ replaced by $\hat{\Omega}_0 := \hat{\Omega} \setminus Z$. By density, we can approximate h by functions $h_n \in C_0(\hat{\Omega}_0)$ with compact support supp$(h_n) \subset$ supp$(h) \cap \hat{\Omega}_0$. Since $\boldsymbol{\omega}$ has no critical points on supp(h_n), we can cover the latter by a finite number of open sets $U_m \subset \hat{\Omega}_0$ on which the maps $W_m : U_m \to \mathbb{R}^3$, $\mathbf{P} \mapsto \boldsymbol{\omega}(\mathbf{P})$ are injective. Using the variable substitution $\mathbf{w} := \boldsymbol{\omega}(\mathbf{P})$ and recalling the definition (114) one finds

$$\int_{U_m} h(\mathbf{P}) e^{-it\mathbf{k}\cdot\boldsymbol{\omega}(\mathbf{P})} \det(\hat{\mathbf{M}}) d^3P = \int_{W_m(U_m)} \left.\frac{h(\mathbf{P})}{|\det(\mathbf{A}(\mathbf{P}))|}\right|_{\mathbf{P}=W_m^{-1}(\mathbf{w})} e^{-it\mathbf{k}\cdot\mathbf{w}} d^3w. \tag{134}$$

By the Riemman-Lebesgue lemma, the right hand side converges to zero as $t \to \infty$ for each $\mathbf{k} \in \mathbb{Z}^3 \setminus \{\mathbf{0}\}$. □

Remark 11. We see from the proof of the previous lemma that the decay rate depends on the smoothness of the functions $\mathbf{P} \mapsto \hat{F}_k(\mathbf{P})\hat{G}_k^*(\mathbf{P})/|\det(\mathbf{A}(\mathbf{P}))|$. This in turn depends on the smoothness properties of the functions F and G along with those of the function $\mathbf{P} \mapsto 1/|\det(\mathbf{A}(\mathbf{P}))|$. Therefore, the zeros of the determinant of $\mathbf{A}$ are expected to play an important role for the determination of the decay rate.

Remark 12. Theorem 5 allows one to provide an alternative proof of the strong Jeans theorem. Indeed, if $F \in L^p(\hat{\Gamma}, \hat{\eta})$ satisfies the A-nondegeneracy condition and is stationary, such that $U(t)F = F$ for all $t \in \mathbb{R}$, then Eq. (127) implies that

$$\int_{\hat{\Gamma}} \left[F(\mathbf{q}, \mathbf{P}) - \overline{F}(\mathbf{q}, \mathbf{P})\right] G(\mathbf{q}, \mathbf{P})\hat{\eta} = 0 \tag{135}$$

for all $G \in Y_q$, which implies that $F = \overline{F}$. In this sense the mixing theorem can be interpreted as a dynamical generalization of the strong Jeans theorem. However, note that Theorem 3 holds under weaker assumptions. Indeed, it is sufficient that almost all frequencies are non-resonant (irrespectively whether or not the non-degeneracy condition holds). For example, it holds even if the frequencies $\boldsymbol{\omega}$ are constant and non-resonant, whereas this property is clearly not sufficient for phase mixing.

In the next section we provide asymptotic expressions for the maps **A** and **B** defined in Eq. (114) in the Keplerian limit, and we prove the validity of both the A and B-nondegeneracy conditions for bound orbits which lie sufficiently far from the black hole, provided that $a_H \neq 0$. Together with Remark 10 this implies that the A- and B-nondegeneracy conditions holds for all bound orbits.

5. Validity of the Nondegeneracy Conditions using the Keplerian Limit

In this section we prove the validity of the A and B-nondegeneracy conditions on $\hat{\Omega}$. In principle this could be done by first expressing the frequencies $\boldsymbol{\omega}$ and $\boldsymbol{\eta}$ defined in Eqs. (97,98) in terms of Legendre's elliptic integrals using the expressions in Eqs. (D17–D19,D24–D26) and then differentiating the result with respect to the integrals of motion (E, L_z, L). However, this would result in rather lengthy expressions for the matrix-valued maps **A** and **B** defined in Eq. (114), and it is not immediately clear if those would be useful to check the conditions of Definition 3.

For this reason, in this section we pursue a slightly different goal and only compute the maps **A** and **B** in the Keplerian limit. In order to do so, we use the parametrization of the bound orbits in terms of the quantities $(\beta, p, e) \in \mathcal{E}_\alpha$ which are discussed in appendix C. Recall that the Keplerian limit corresponds to $p \to \infty$ with β and e kept fixed. The main result of this section is the following:

Theorem 6. *Suppose the dimensionless rotation parameter $\alpha = a_H/M_H$ satisfies $0 < \alpha < 1$, and let $0 < e_0 < e_1 < 1$ and $0 < \beta_0 < \beta_1 < 1$. Then, there exists $p_1 > 0$ sufficiently large such that the set*

$$\mathcal{E}_\alpha^\infty := \{(\beta, p, e) : \beta_0 < |\beta| < \beta_1, p > p_1, e_0 < e < e_1\} \tag{136}$$

is contained in $\mathcal{E}_\alpha$ and such that for any $(\beta, p, e) \in \mathcal{E}_\alpha^\infty$ the corresponding quantity $\mathbf{P} := (E, L_z, L)$ satisfies

$$\det \mathbf{A}(\mathbf{P}) > 0, \qquad |\det \mathbf{B}(\mathbf{P})| > 0. \tag{137}$$

Together with the observations made in remark 10, this theorem implies the following important result:

Corollary 2. *Suppose $0 < \alpha < 1$. Then, both the A- and B-nondegeneracy conditions are satisfied on $\hat{\Omega}$.*

We prove Theorem 6 in several steps. In a first step we collect a few useful formulas that allow one to express the action variables in terms of the quantities (β, p, e). Next, we show that the roots of the polynomials $R(r)$ defined in Eq. (28) and those of the polynomial $q(\zeta)$ defined in Eq. (D11) are analytic in the parameter $\mu := 1/\sqrt{p}$ in a vicinity of $\mu = 0$. This allows one to express all the relevant quantities in power series of μ which converge uniformly for small enough $|\mu|$. The next step consists in expanding the action variables I_1, I_2 and I_3 in terms of μ and to show that for small

enough $\mu > 0$ the map $(\mu, \beta, e) \mapsto (I_1, I_2, I_3)$ is invertible. In the next step one computes the expansions of E and L and expresses the lowest-order terms as a function of (I_1, I_2, I_3). This allows one to compute the frequencies $\omega^a = \partial E/\partial I_a$ and the matrix $A^{ab} = \partial^2 E/(\partial I_a \partial I_b)$ (see Eqs. (115,116)) in the Keplerian limit, up to the desired order of accuracy in μ, and similarly for $\eta^a = \partial L/\partial I_a$ and $B^{ab} = \partial^2 L/(\partial I_a \partial I_b)$. Finally, by means of the resulting expansions for A^{ab} and B^{ab} one shows that their determinants are nonzero for small enough $\mu > 0$.

5.1. Action variables in terms of the quantities (β, p, e). In appendix C we show that the orbits can be parametrized by the quantities $(\beta, p, e) \in \mathcal{E}_\alpha$ instead of the constants of motion $(\beta, \lambda, \varepsilon) \in \mathcal{D}_\alpha$. These quantities allow one to determine the four roots x_1, x_2, x_3 and x_4 (or, equivalently, $x_1, x_2, w_+ = x_3 + x_4$ and $w_\times = x_3 x_4$) of $R(r)$ and (ε, λ) in an explicit manner. From this, one can also compute the roots ζ_1 and ζ_2 of the polynomial $q(\zeta)$ determining the polar motion and their ratio $k_1 = \zeta_1/\zeta_2$. From Eqs. (D12,D13) one finds, taking into account that $\zeta_1^2 \leq \zeta_2^2$ and using Eqs. (C6,C8,C9) the following two expressions:

$$\zeta_1^2 = \frac{2w_\times}{\alpha^2} \frac{1}{Z + \sqrt{Z^2 - \frac{4(1-e^2)}{p^2} w_\times}}, \qquad Z := 1 + \frac{2w_+}{p} + \frac{1-e^2}{p^2} w_\times, \tag{138}$$

$$k_1^2 = \frac{4(1-e^2)w_\times}{p^2} \frac{1}{\left[Z + \sqrt{Z^2 - \frac{4(1-e^2)}{p^2} w_\times}\right]^2}. \tag{139}$$

For the analysis in this section, it is convenient to express the action variables I_1, I_2 and I_3 defined in Eqs. (50–52) as follows. The integral defining I_2 is rewritten in terms of the angle ϕ defined in Eqs. (66,67), while the integral defining I_3 is written in terms of the new angle θ defined by

$$x(\theta) := \frac{x_1 + x_2}{2} + \frac{x_2 - x_1}{2} \sin\theta = \frac{p}{1-e^2}(1 + e\sin\theta). \tag{140}$$

Recalling that $\zeta_1 = \cos\vartheta_1$ and using Eq. (C5) this yields

$$\begin{aligned} I_1 &= M_H m(\beta\lambda + \alpha\varepsilon), \qquad I_2 = M_H m\sqrt{1-\beta^2}\lambda\zeta_1 \mathcal{K}_2(\alpha, \beta, e, p), \\ I_3 &= M_H m\sqrt{1-\varepsilon^2}\frac{pe^2}{1-e^2}\mathcal{K}_3(\alpha, \beta, e, p), \end{aligned} \tag{141}$$

with the integrals

$$\mathcal{K}_2(\alpha, \beta, e, p) := \frac{1}{\pi} \int_{-\pi/2}^{\pi/2} \frac{\sqrt{1 - k_1^2 \sin^2\phi}}{1 - \zeta_1^2 \sin^2\phi} \cos^2\phi d\phi, \tag{142}$$

$$\mathcal{K}_3(\alpha, \beta, e, p) := \frac{1}{\pi} \int_{-\pi/2}^{\pi/2} \frac{\sqrt{(1+e\sin\theta)^2 - \frac{1-e^2}{p}(1+e\sin\theta)w_+ + \frac{(1-e^2)^2}{p^2} w_\times}}{(1+e\sin\theta)^2 - 2\frac{1-e^2}{p}(1+e\sin\theta) + \frac{(1-e^2)^2}{p^2}\alpha^2} \cos^2\theta d\theta. \tag{143}$$

Before we proceed, it is instructive to recall the Kepler case, which can formally be obtained by taking the leading-order contribution for $p \to \infty$ in the above expressions (this limit will be performed in a rigorous manner in the following subsections). In this case, one obtains $w_+ = 2$, $w_\times = \alpha^2(1-\beta^2)$, $\varepsilon = 1-(1-e^2)/(2p)$, $\lambda = \sqrt{p}$, $\zeta_1 = \sqrt{1-\beta^2}$, $k_1 = 0$, such that[14]

$$I_1 = M_H m\beta\sqrt{p}, \qquad I_2 = M_H m(1-|\beta|)\sqrt{p}, \qquad I_3 = M_H m\sqrt{p}\left[\frac{1}{\sqrt{1-e^2}}-1\right]. \tag{144}$$

It is useful to replace I_1, I_2 and I_3 with the dimensionless quantities

$$j_1 := \frac{I_1}{M_H m}, \qquad j_2 := \frac{|I_1|+I_2}{M_H m}, \qquad j_3 := \frac{|I_1|+I_2+I_3}{M_H m}, \tag{145}$$

such that $(j_1, j_2, j_3) = \sqrt{p}(\beta, 1, (1-e^2)^{-1/2})$ and $\varepsilon = 1 - 1/(2j_3^2)$. The fundamental frequencies are

$$\boldsymbol{\omega} = \frac{\partial E}{\partial \mathbf{I}} = \mathbf{S}\frac{\partial(m\varepsilon)}{\partial \mathbf{j}} = \omega_{Kepler}\begin{pmatrix}\mathrm{sign}(\beta)\\ 1\\ 1\end{pmatrix}, \tag{146}$$

where we have defined

$$\mathbf{S} := \frac{1}{M_H m}\begin{pmatrix}1 & \mathrm{sign}(\beta) & \mathrm{sign}(\beta)\\ 0 & 1 & 1\\ 0 & 0 & 1\end{pmatrix}, \qquad \omega_{Kepler} := \frac{1}{M_H}\left[\frac{1-e^2}{p}\right]^{3/2}. \tag{147}$$

5.2. Analytic dependency of the roots on the square root of the inverse semi-latus rectum. The expression for u_+ in Eq. (C37) in the Schwarzschild limit motivates the following ansatz for large values of p or small values of $\alpha > 0$:

$$u_+ = \frac{p-4}{2(1+e)}\left[1+\frac{\alpha}{\sqrt{p}}h_+\right]. \tag{148}$$

Introduced into Eq. (C35) this yields the following equation for h_+:

$$h_+ - 2\beta A(\alpha,\beta,e,\mu)\sqrt{1+\alpha\mu B(\alpha,\beta,e,\mu)h_+} - \alpha\mu C(\alpha,\beta,e,\mu) = 0, \tag{149}$$

[14] The following integrals will be useful in this section:

$$\frac{1}{\pi}\int_{-\pi/2}^{\pi/2}\frac{\cos^2\theta d\theta}{1+e\sin\theta} = \frac{1}{\pi}\int_{-\pi/2}^{\pi/2}\frac{\cos^2\theta d\theta}{1-e^2\sin^2\theta} = \frac{1}{1+\sqrt{1-e^2}},$$

$$\frac{1}{\pi}\int_{-\pi/2}^{\pi/2}\frac{\cos^2\theta d\theta}{(1+e\sin\theta)^2} = \frac{1}{\sqrt{1-e^2}}\frac{1}{1+\sqrt{1-e^2}}.$$

where we recall that $\mu = 1/\sqrt{p}$, $\kappa = \alpha\sqrt{1-\beta^2}$, and where we have set

$$A(\alpha,\beta,e,\mu) := \frac{1}{1-\alpha^2\mu^2}\sqrt{\frac{1-(1-e^2)\mu^2}{(1-4\mu^2)\left[1-\frac{1}{2}\kappa^2(3+e)\mu^2\right]}}\,B(\alpha,\beta,e,\mu)^{-1/2}, \tag{150}$$

$$B(\alpha,\beta,e,\mu) := \left[1+\frac{\mu^2(1-e^2)(1-\kappa^2\mu^2)}{(1-4\mu^2)[1-(1-e^2)\mu^2][1-\frac{1}{2}\kappa^2(3+e)\mu^2]}\right]^{-1}, \tag{151}$$

$$\begin{aligned} C(\alpha,\beta,e,\mu) := {} & \frac{1}{1-\alpha^2\mu^2}\frac{1}{1-\frac{1}{2}\kappa^2(3+e)\mu^2} \\ & \times\left\{1+\frac{1-\beta^2}{2}(3+e)(1-\alpha^2\mu^2)\right. \\ & \left.+\mu^2\frac{1-e^2+(1-\beta^2)\left[3+e^2-\alpha^2(1-e^2)\mu^2\right]}{1-4\mu^2}\right\}. \end{aligned} \tag{152}$$

Note that A, B and C are analytic functions of their arguments which are well-defined and positive as long as $-1<\alpha<1$, $-1<\beta<1$, $0<e<1$ and $|\mu|<1/2$. Furthermore, these functions are even in μ and they satisfy $A(\alpha,\beta,e,0) = B(\alpha,\beta,e,0) = 1$ and $C(\alpha,\beta,e,0) = 1+(1-\beta^2)(3+e)/2$, such that $h_+ = 2\beta$ when $\mu = 0$. An explicit expression for h_+ is obtained by squaring Eq. (149) and solving the resulting quadratic equation. Taking into account that $h_+ = 2\beta$ for $\mu = 0$, this yields the following explicit expression for h_+:

$$h_+ = \alpha\mu\left(C+2\beta^2A^2B\right)+2\beta A\sqrt{1+\alpha^2\mu^2\left(BC+\beta^2A^2B^2\right)}. \tag{153}$$

As a consequence of this, we can formulate:

Lemma 14. *Let $\alpha\in[0,1)$. Then, h_+, w_+, $w_\times$, ζ_1, k_1, ε and $\mu\lambda$ are analytic functions of β, e and μ as long as $(\beta,e)\in(-1,1)\times(0,1)$ and μ is restricted to a small enough open neighborhood of $\mu=0$.*

Proof. The statement for h_+ follows directly from Eq. (153) and the aforementioned properties of the functions A, B and C. Next, using Eqs. (148,C34) yields

$$w_+ = \frac{2}{1-4\mu^2}\frac{1-\kappa^2\mu^2}{1-\frac{1}{2}\kappa^2(3+e)\mu^2}\frac{1}{1+\alpha\mu h_+}, \tag{154}$$

which implies the statement for w_+. Finally, the statements for $w_\times$, ζ_1, ζ_2, and $(\varepsilon,\mu\lambda)$ follow from this using Eqs. (C31), (138), (139), and (C44), respectively. □

Remark 13. To second order in μ one obtains

$$h_+ = 2\beta+\frac{1}{2}\alpha\left[5+e+\beta^2(1-e)\right]\mu+\beta\left[4+4\alpha^2+\kappa^2(2+e)\right]\mu^2+\mathcal{O}(\mu^3), \tag{155}$$

which together with Eqs. (154,C31,138,139) yields $k_1^2 = \mathcal{O}(\mu^4)$ and

$$w_+ = 2\left[1-2\alpha\beta\mu+(4+\alpha^2-3\kappa^2)\mu^2-3\alpha\beta(4-\kappa^2)\mu^3+\mathcal{O}(\mu^4)\right], \tag{156}$$

$$w_\times = \kappa^2\left[1 - 2\alpha\beta\mu + (4 + \alpha^2 - 2\kappa^2)\mu^2 - \alpha\beta(12 - \kappa^2)\mu^3 + \mathcal{O}(\mu^4)\right], \quad (157)$$

$$\zeta_1 = \sqrt{1-\beta^2}\left[1 - \alpha\beta\mu - \frac{1}{2}\kappa^2\mu^2 + 2\alpha\beta\mu^3 + \mathcal{O}(\mu^4)\right]. \quad (158)$$

Combined with Eq. (C44) this also gives

$$\varepsilon = 1 - \frac{1}{2}(1-e^2)\mu^2 + \frac{3}{8}(1-e^2)^2\mu^4 - \alpha\beta(1-e^2)^2\mu^5 + \mathcal{O}(\mu^6), \quad (159)$$

$$\lambda = \frac{1}{\mu}\left[1 - \alpha\beta\mu + \frac{1}{2}(3 + e^2 - \kappa^2)\mu^2 - \frac{1}{2}\alpha\beta(5 + 3e^2)\mu^3 + \mathcal{O}(\mu^4)\right]. \quad (160)$$

5.3. Expansion of the action variables. The next step consists in expanding the action variables I_1, I_2 and I_3 defined in Eqs. (50–52) in powers of μ. For the following we denote by U_0 the open set $U_0 := [(-\beta_1, -\beta_0) \cup (\beta_0, \beta_1)] \times (e_0, e_1)$ with $0 < \beta_0 < \beta_1 < 1$ and $0 < e_0 < e_1 < 1$ the same constants as in the hypothesis of Theorem 6. As a consequence of Lemma 14 one has:

Lemma 15. *Let $\alpha \in [0, 1)$. Then, μI_1, μI_2, μI_3 are analytic functions of β, e and μ as long as $(\beta, e) \in U_0$ and μ is restricted to a small enough open neighborhood of $\mu = 0$.*

Proof. The statement for I_1 is a direct consequence of Lemma 14 and the first identity in Eq. (141). Next, to prove the statement for I_3 we note that, again as a consequence of Lemma 14 and the expansions (156,157), the function $\mathcal{K}_3(\alpha, \beta, e, p = \mu^{-2})$ is analytic in β, e and μ as long as $(\beta, e) \in U_0$ and μ is restricted to a neighborhood of $\mu = 0$. This observation, together with the fact that $\sqrt{1-\varepsilon^2} = \mathcal{O}(\mu)$ implies the statement for I_3. Finally, in order to analyze I_2, we use again Lemma 14 and recall that $k_1^2 = \mathcal{O}(\mu^4)$ and $\zeta_1^2 = (1-\beta^2)(1 + \mathcal{O}(\mu))$, which implies that $\mathcal{K}_2(\alpha, \beta, e, p = \mu^{-2})$ is analytic in β, e and μ as long as $(\beta, e) \in U_0$ and μ is restricted to a vicinity of $\mu = 0$.[15] Now the statement for I_2 follows from these observations and the known behavior of λ and ζ_1 from Lemma 14. □

Remark 14. Since $k_1^2 = \mathcal{O}(\mu^4)$ it follows from Eq. (142) that

$$\mathcal{K}_2(\alpha, \beta, e, \mu^{-2}) = \frac{1}{1 + \sqrt{1 - \zeta_1^2}} + \mathcal{O}(\mu^4), \quad (161)$$

which can easily be expanded up to third order in μ using Eq. (158). Likewise, it follows from Eq. (143) that

$$\mathcal{K}_3(\alpha, \beta, e, \mu^{-2}) = \frac{1}{1 + \sqrt{1-e^2}}\left[1 + \sqrt{1-e^2}\mu^2(1 + 2\alpha\beta\mu) + \mathcal{O}(\mu^4)\right], \quad (162)$$

where we have used footnote 14 to perform this calculation.

[15] Note that it is at this point that we need to exclude $\beta = 0$ from our analysis, since in this case $\zeta_1 = 1$ in the limit $\mu = 0$ (see Eq. (158)) such that the denominator in the integrand of Eq. (142) becomes zero when $\theta = \pm\pi/2$.

From the above, one finds for the variables (j_1, j_2, j_3) defined in Eq. (145) the following expansions:

$$j_1 = \frac{\beta}{\mu}\left\{1 + \frac{\alpha}{\beta}(1-\beta^2)\mu + \frac{1}{2}(3+e^2-\kappa^2)\mu^2 - \frac{\alpha}{2\beta}\left[1 - e^2 + (5+3e^2)\beta^2\right]\mu^3 + \mathcal{O}(\mu^4)\right\}, \tag{163}$$

$$j_2 = \frac{1}{\mu}\left[1 + \frac{1}{2}(3+e^2)\mu^2 - \alpha\beta(3+e^2)\mu^3 + \mathcal{O}(\mu^4)\right], \tag{164}$$

$$j_3 = \frac{1}{\sqrt{1-e^2}}\frac{1}{\mu}\left[1 + \frac{3}{2}\sqrt{1-e^2}\left(2 - \sqrt{1-e^2}\right)\mu^2 - \alpha\beta\sqrt{1-e^2}\left(2 + \sqrt{1-e^2}\right)\mu^3 + \mathcal{O}(\mu^4)\right]. \tag{165}$$

Lemma 16. *Let $\alpha \in [0, 1)$. Then, for $\mu_1 > 0$ sufficiently small, the map $\mathcal{J}_\alpha : (0, \mu_1) \times U_0 \to \mathbb{R}^3$, $(\mu, \beta, e) \mapsto (j_1, j_2, j_3)$ is injective.*

Proof. The idea is to write the map $\mathcal{J}_\alpha$ in the form $\mathcal{J}_\alpha = \mathcal{J}_{Kepler} \circ \mathcal{L}_\alpha$ with $\mathcal{J}_{Kepler}$ the Kepler map defined by Eqs. (144,145) and to prove that both $\mathcal{J}_{Kepler}$ and $\mathcal{L}_\alpha$ are injective when $\mu_1 > 0$ is small enough.

The Kepler map $\mathcal{J}_{Kepler} : D_1 \to D_2$ is defined by

$$\mathcal{J}_{Kepler}(\mu, \beta, e) := \frac{1}{\mu}\begin{pmatrix} \beta \\ 1 \\ \frac{1}{\sqrt{1-e^2}} \end{pmatrix}, \qquad (\mu, \beta, e) \in D_1 \tag{166}$$

with domain $D_1 := (0, \infty) \times (-1, 1) \times (0, 1)$ and image

$$D_2 := \{(j_1, j_2, j_3) \in \mathbb{R}^3 : j_2 > 0, |j_1| < j_2 < j_3\}. \tag{167}$$

Clearly it is invertible; its inverse is given by

$$\mathcal{J}^{-1}_{Kepler}(j_1, j_2, j_3) = \begin{pmatrix} \frac{1}{j_2} \\ \frac{j_1}{j_2} \\ \sqrt{1 - \frac{j_2^2}{j_3^2}} \end{pmatrix}, \qquad (j_1, j_2, j_3) \in D_2. \tag{168}$$

Since I_2 and I_3 are positive it follows that the image of $\mathcal{J}_\alpha$ lies in D_2 (see Eq. (145)); hence the map $\mathcal{L}_\alpha := \mathcal{J}^{-1}_{Kepler} \circ \mathcal{J}_\alpha : (0, \mu_1) \times U_0 \to \mathbb{R}^3$ is a well defined differentiable map for sufficiently small $\mu_1 > 0$. Using Eqs. (163,164,165) one finds

$$\mathcal{L}_\alpha(\mu, \beta, e) = \begin{pmatrix} \mu \\ \beta + \alpha(1-\beta^2)\mu \\ e \end{pmatrix} + \mathcal{O}(\mu^2). \tag{169}$$

Its differential satisfies

$$D\mathcal{L}_\alpha(\mu, \beta, e) = \begin{pmatrix} 1 & 0 & 0 \\ \alpha(1-\beta^2) & 1 & 0 \\ 0 & 0 & 1 \end{pmatrix} + \mathcal{O}(\mu), \tag{170}$$

and hence

$$\sup_{(\mu,\beta,e)\in(0,\mu_1)\times U_0} \|D\mathcal{L}_\alpha(\mu,\beta,e) - \mathbb{1}_3\| < 1 \tag{171}$$

for sufficiently small $\mu_1 > 0$. This condition implies the injectivity of the map $\mathcal{L}_\alpha : (0,\mu_1)\times U_0 \to \mathbb{R}^3$. □

Remark 15. Using the decomposition $\mathcal{J}_\alpha = \mathcal{J}_{Kepler} \circ \mathcal{L}_\alpha$,

$$(D\mathcal{J}_{Kepler})^{-T} = \mu \begin{pmatrix} 0 & 1 & 0 \\ -\mu & -\beta & -e^{-1}(1-e^2) \\ 0 & 0 & e^{-1}(1-e^2)^{3/2} \end{pmatrix} \tag{172}$$

and Eq. (170), one finds that

$$\frac{\partial}{\partial j_a} = -\mathcal{O}(\mu^2)\frac{\partial}{\partial \mu} + \mathcal{O}(\mu)\frac{\partial}{\partial \beta} + \mathcal{O}(\mu)\frac{\partial}{\partial e}, \tag{173}$$

and hence differentiating a power series in μ with respect to j_a augments its order by at least one, that is, $\partial/\partial j_a \mathcal{O}(\mu^n) = \mathcal{O}(\mu^{n+1})$ for all $n \in \mathbb{N}$ and $a = 1, 2, 3$.

5.4. Expansion of energy in terms of the action variables. Using the results from the previous subsection, we are ready to prove the following proposition.

Proposition 5 (Expansion of E in terms of action variables). *Let $\alpha \in [0, 1)$ and suppose $\mu_1 > 0$ is sufficiently small such that the map $\mathcal{J}_\alpha : (0,\mu_1)\times U_0 \to \mathbb{R}^3$ from Lemma 16 is injective. Then,*

$$\varepsilon = 1 - \frac{1}{2j_3^2} - \frac{3}{j_2 j_3^3} + \frac{15}{8j_3^4} + \frac{2\alpha j_1}{j_2^3 j_3^3} + \mathcal{O}(\mu^6), \tag{174}$$

for all (j_1, j_2, j_3) lying in the image of $\mathcal{J}_\alpha$.

Remark 16. The term of order $\mathcal{O}(j^{-2}) = \mathcal{O}(\mu^2)$ is the Kepler term (see below Eq. (145)), whereas the next-order correction terms of order $\mathcal{O}(j^{-4}) = \mathcal{O}(\mu^4)$ are the first relativistic corrections. As we will see, the dominant term that is responsible for the mixing property is the fifth-order correction term $2\alpha j_1/(j_2^3 j_3^3)$.

Proof of Proposition 5. From Eq. (165) we find

$$\begin{aligned} \frac{1}{j_3} = \; & \mu\sqrt{1-e^2}\left[1 - \frac{3}{2}\sqrt{1-e^2}\left(2-\sqrt{1-e^2}\right)\mu^2\right. \\ & \left. +\alpha\beta\sqrt{1-e^2}\left(2+\sqrt{1-e^2}\right)\mu^3 + \mathcal{O}(\mu^4)\right]. \end{aligned} \tag{175}$$

This can be used to eliminate the term which is quadratic in μ in Eq. (159). Specifically, we find

$$\varepsilon - 1 + \frac{1}{2j_3^2} = \left[\frac{15}{8}(1-e^2)^2 - 3(1-e^2)^{3/2}\right]\mu^4 + 2\alpha\beta(1-e^2)^{3/2}\mu^5 + \mathcal{O}(\mu^6). \tag{176}$$

Next, we use Eq. (175) again, $1/j_2 = \mu + \mathcal{O}(\mu^3)$ and $j_1/j_2 = \beta + \mathcal{O}(\mu)$ in order to eliminate the quartic and fifth-order terms. This yields

$$\varepsilon - 1 + \frac{1}{2j_3^2} - \frac{15}{8j_3^4} + \frac{3}{j_2 j_3^3} - \frac{2\alpha j_1}{j_2^3 j_3^3} = \mathcal{O}(\mu^6), \tag{177}$$

which concludes the proof of the proposition. □

Using Eq. (146) and taking into account the previous remark we can compute the corresponding expansion for the fundamental frequencies $\boldsymbol{\omega}$, which yields

$$\boldsymbol{\omega} = \mathbf{S}\frac{\partial E}{\partial \mathbf{j}} = m\mathbf{S}\begin{pmatrix} \frac{2\alpha}{j_2^3 j_3^3} \\ \frac{3}{j_2^2 j_3^3}\left[1 - \frac{2\alpha j_1}{j_2^2}\right] \\ \frac{1}{j_3^3} - \frac{15}{2j_3^5} + \frac{3}{j_2 j_3^4}\left[3 - \frac{2\alpha j_1}{j_2^2}\right] \end{pmatrix} + \mathcal{O}(\mu^7), \tag{178}$$

where the matrix $\mathbf{S}$ is defined in Eq. (147) and where $\mathbf{j} = (j_1, j_2, j_3)$. Re-expressing this result in terms of (β, p, e) using Eqs. (163,164,165) yields

$$\boldsymbol{\omega} = \begin{pmatrix} \mathrm{sign}\beta[\omega_r + \Delta\omega_{perihelion}] + \Delta\omega_{LT} \\ \omega_r + \Delta\omega_{perihelion} \\ \omega_r \end{pmatrix}, \tag{179}$$

where

$$\omega_r = \omega_{Kepler}\left[1 - 3\frac{1-e^2}{p}\left(1 - \frac{\alpha\beta}{\sqrt{p}}\right) + \mathcal{O}\left(\frac{1}{p^2}\right)\right], \tag{180}$$

$$\Delta\omega_{perihelion} = \frac{3\omega_{Kepler}}{p}\left[1 - \frac{2\alpha\beta}{\sqrt{p}} + \mathcal{O}\left(\frac{1}{p}\right)\right], \tag{181}$$

$$\Delta\omega_{LT} = \frac{2\alpha\omega_{Kepler}}{p^{3/2}}\left[1 + \mathcal{O}\left(\frac{1}{\sqrt{p}}\right)\right], \tag{182}$$

and where we recall the frequency ω_{Kepler} of the Kepler trajectories defined in Eq. (147). Hence, as expected, in the limit $p \to \infty$ the three frequencies $\omega_1, \omega_2, \omega_3$ have equal magnitude. The next-order correction term $1/p$ yields a difference between the frequencies corresponding to the polar and radial motions, given by $\Delta\omega_{perihelion}$, and it describes the perihelion precession. The next-order correction term of oder $1/p^{3/2}$ breaks the degeneracy between the frequencies associated with the azimuthal and polar motion. It describes the Lense-Thirring effect which yields a precession of the line of nodes (the line connecting the points at which the trajectory crosses the equatorial plane) which has frequency $\Delta\omega_{LT}$ (see e.g. section 10.4 in Ref. [48]).

Computing the Hessian $D^2\varepsilon$ of ε with respect to $\mathbf{j}$ one finds

$$\mathbf{A} = \mathbf{S}(mD^2\varepsilon)\mathbf{S}^T = m\mathbf{S}\left[\left(\begin{array}{c|c|c} 0 & -\frac{6\alpha}{j_2^4 j_3^3} & -\frac{6\alpha}{j_2^3 j_3^4} \\ \hline -\frac{6\alpha}{j_2^4 j_3^3} & -\frac{6}{j_2^3 j_3^3} + \frac{24\alpha j_1}{j_2^5 j_3^3} & -\frac{9}{j_2^2 j_3^4} + \frac{18\alpha j_1}{j_2^4 j_3^4} \\ \hline -\frac{6\alpha}{j_2^3 j_3^4} & -\frac{9}{j_2^2 j_3^4} + \frac{18\alpha j_1}{j_2^4 j_3^4} & -\frac{3}{j_3^4} - \frac{36}{j_2 j_3^5} + \frac{75}{2j_3^6} + \frac{24\alpha j_1}{j_2^3 j_3^5} \end{array}\right) + \mathcal{O}(\mu^8)\right]\mathbf{S}^T. \tag{183}$$

Note that the dominant term in the matrix comes from the contribution $-3/j_3^4$ in its 33-component, which is of the order μ^4. Since $\det(\mathbf{S}) = 1/(M_H m)^3$ it follows that

$$\det(\mathbf{A}) = \frac{108\alpha^2}{M_H^6 m^3} \frac{1}{j_2^8 j_3^{10}} [1 + \mathcal{O}(\mu)]. \tag{184}$$

As a direct consequence, we have the following lemma which proves the statement of Theorem 6 for **A**:

Lemma 17. *Let $\alpha \in (0, 1)$. Then, for $\mu_1 > 0$ sufficiently small, it follows that* $\det(\mathbf{A}) > 0$ *for all $(\mu, \beta, e) \in (0, \mu_1) \times U_0$.*

5.5. Expansion of Carter constant in terms of the action variables. In this final subsection we repeat the steps performed in the previous subsection for the constant of motion L instead of E and verify the validity of the B-nondegeneracy condition.

Proposition 6. *(Expansion of L in terms of action variables) Let $\alpha \in [0, 1)$ and suppose $\mu_1 > 0$ is sufficiently small such that the map $\mathcal{J}_\alpha : (0, \mu_1) \times U_0 \to \mathbb{R}^3$ from Lemma 16 is injective. Then,*

$$\lambda = j_2 - \frac{\alpha j_1}{j_2} + \frac{\alpha^2}{2j_2}\left(1 - \frac{j_1^2}{j_2^2}\right) + \frac{\alpha j_1}{2j_2}\left[\frac{1}{j_3^2} + \frac{\alpha^2}{j_2^2}\left(1 - \frac{j_1^2}{j_2^2}\right)\right] + \mathcal{O}(\mu^3), \tag{185}$$

for all (j_1, j_2, j_3) lying in the image of $\mathcal{J}_\alpha$.

Proof. We use the same strategy as in the proof of Proposition 5, and successively eliminate the μ-terms in the expansion (160) of λ up to the required order.

First, using Eq. (164) one finds

$$\lambda - j_2 = -\alpha\beta - \frac{1}{2}\kappa^2\mu + \frac{1}{2}\alpha\beta(1 - e^2)\mu^2 + \mathcal{O}(\mu^3). \tag{186}$$

In a next step we use Eqs. (163,164) which give

$$\frac{j_1}{j_2} = \beta + \alpha(1 - \beta^2)\mu - \frac{1}{2}\kappa^2\beta\mu^2 + \mathcal{O}(\mu^3), \tag{187}$$

and one obtains

$$\lambda - j_2 + \frac{\alpha j_1}{j_2} = \frac{1}{2}\kappa^2\mu + \frac{1}{2}\alpha\beta\left[1 - e^2 - \kappa^2\right]\mu^2 + \mathcal{O}(\mu^3). \tag{188}$$

Using $j_2^{-1} = \mu[1 + \mathcal{O}(\mu^2)]$ and again Eq. (187), and recalling that $\kappa^2 = \alpha^2(1 - \beta^2)$ yields

$$\lambda - j_2 + \frac{\alpha j_1}{j_2} - \frac{\alpha^2}{2j_2}\left(1 - \frac{j_1^2}{j_2^2}\right) = \frac{1}{2}\alpha\beta\left[1 - e^2 + \alpha^2(1 - \beta^2)\right]\mu^2 + \mathcal{O}(\mu^3). \tag{189}$$

Now the claim follows using Eq. (187) once again and noting that $(1 - e^2)\mu^2 = 1/j_3^2$. □

Using Eq. (185) we compute

$$\boldsymbol{\eta} = \mathbf{S}\frac{\partial L}{\partial \dot{\mathbf{j}}} = M_H m \mathbf{S} \begin{pmatrix} -\frac{\alpha}{j_2} - \frac{\alpha^2 j_1}{j_2^3} + \frac{\alpha}{2j_2}\left[\frac{1}{j_3^2} + \frac{\alpha^2}{j_2^2}\left(1 - \frac{3j_1^2}{j_2^2}\right)\right] \\ 1 + \frac{\alpha j_1}{j_2^2} - \frac{\alpha^2}{2j_2^2}\left(1 - \frac{3j_1^2}{j_2^2}\right) - \frac{\alpha j_1}{2j_2^2}\left[\frac{1}{j_3^2} + \frac{\alpha^2}{j_2^2}\left(3 - \frac{5j_1^2}{j_2^2}\right)\right] \\ -\frac{\alpha j_1}{j_2 j_3^3} \end{pmatrix} + \mathcal{O}(\mu^4)$$

$$= M_H m \mathbf{S} \begin{pmatrix} -\alpha\mu - \alpha^2\beta\mu^2 + \frac{1}{2}\alpha[4 - \alpha^2(1+\beta^2)]\mu^3 \\ 1 + \alpha\beta\mu + \frac{\alpha^2}{2}(1+\beta^2)\mu^2 - \alpha\beta(2-\alpha^2)\mu^3 \\ -\alpha\beta(1-e^2)^{3/2}\mu^3 \end{pmatrix} + \mathcal{O}(\mu^4), \tag{190}$$

and

$$\mathbf{B} = \mathbf{S}(D^2 L)\mathbf{S}^T = M_H m \mathbf{S}\left[\left(\begin{array}{c|c|c} -\frac{\alpha^2}{j_2^3} - \frac{3\alpha^3 j_1}{j_2^5} & \frac{\alpha}{j_2^2} + \frac{3\alpha^2 j_1}{j_2^4} - \frac{\alpha}{2j_2^2}\tau_{3,15} & -\frac{\alpha}{j_2 j_3^3} \\ \hline \frac{\alpha}{j_2^2} + \frac{3\alpha^2 j_1}{j_2^4} - \frac{\alpha}{2j_2^2}\tau_{3,15} & -\frac{2\alpha j_1}{j_2^3} + \frac{\alpha^2}{j_2^3}\left(1 - \frac{6j_1^2}{j_2^2}\right) + \frac{\alpha j_1}{j_2^3}\tau_{6,15} & \frac{\alpha j_1}{j_2^2 j_3^3} \\ \hline -\frac{\alpha}{j_2 j_3^3} & \frac{\alpha j_1}{j_2^2 j_3^3} & \frac{3\alpha j_1}{j_2 j_3^4} \end{array}\right) + \mathcal{O}(\mu^5)\right]\mathbf{S}^T, \tag{191}$$

where we have abbreviated $\tau_{n,m} := 1/j_3^2 + \alpha^2(n - mj_1^2/j_2^2)/j_2^2$. Taking into account that the dominant terms in the matrix are the contributions α/j_2^2 appearing in the 12- and 21-components and $-2\alpha j_1/j_2^3$ appearing in the 22-component, and recalling that $\det(\mathbf{S}) = 1/(M_H m)^3$, it follows that

$$\det(\mathbf{B}) = -\frac{3\alpha^3}{M_H^3 m^3}\frac{j_1}{j_2}\frac{1}{j_2^4 j_3^4}\left[1 + \mathcal{O}(\mu)\right]. \tag{192}$$

As a direct consequence, we have the following lemma which proves the statement of Theorem 6 for **B**:

Lemma 18. *Let* $\alpha \in (0,1)$. *Then, for* $\mu_1 > 0$ *sufficiently small, it follows that* $|\det(\mathbf{B})| > 0$ *for all* $(\mu, \beta, e) \in (0, \mu_1) \times U_0$.

6. Conclusions

We have analyzed the phase space mixing of a relativistic, collisionless kinetic gas whose individual gas particles follow spatially bound future-directed timelike geodesics in the exterior of a Kerr black hole of mass M_H and with rotation parameter a_H such that $a_H^2 < M_H^2$.

Our method exploits the integrability property of the free-particle Hamiltonian on the cotangent bundle associated with the spacetime manifold, and it relies on the construction of generalized action-angle variables (J_α, Q^α) parametrizing the region of phase space Γ_{bound} corresponding to bound orbits in the Kerr black hole exterior. More precisely, the J-variables label, locally, the invariant sets of topology $\mathbb{R} \times T^3$ in Γ_{bound} while the Q-variables provide global coordinates on each of these sets. We have argued that it is convenient to define J_0 as a function of the free-particle Hamiltonian, whereas the action variables $\mathbf{J} := (J_1, J_2, J_3)$ are topological invariants associated with each S^1-factor of T^3 which are dual to the angle variables $\mathbf{Q} := (Q^1, Q^2, Q^3)$. Whether or not the J-variables provide a globally well-defined labeling of the invariant sets foliating Γ_{bound}

constitutes an open problem which requires a proof that the transformation $\hat{\mathbb{I}} : \mathbf{P} \mapsto \mathbf{J}$ which maps the constants of motion $\mathbf{P} = (E, L_z, L)$ to the action variables $\mathbf{J}$ is globally invertible. Although it can be shown that $\hat{\mathbb{I}}$ is locally invertible (cf. Lemma 5) and globally invertible in the Keplerian limit (cf. Lemma 16) or in the Schwarzschild limit $a_H = 0$, understanding its global invertibility in the general case requires further work, showing, for instance, that this map is proper. To circumvent this problem, we have labeled the invariant sets by the constant of motions, represented by the variables $(P_\alpha) = (m, \mathbf{P})$, instead of (J_α) and worked with the globally-defined (though non-canonical) coordinates (P_α, Q^α) on Γ_{bound}. Based on these coordinates, the free-particle flow on Γ_{bound} still has a simple form which allows one to easily show that the propagator associated with the Vlasov equation is a strongly continuous group. The mixing Theorem 5 can then be established using standard Fourier methods generalizing previous work [28,29], and it shows that mixing takes place for any DF whose initial datum and test function lie in appropriate function spaces, as long as the A-nondegeneracy condition is satisfied (see Definitions 1 and 3).

Theorem 6 and Corollary 2 show that this condition holds if $a_H \neq 0$. To prove Theorem 6 we have shown that the integral of motion corresponding to the energy E of the particle can be expressed in terms of the action variables $\mathbf{J}$ in the Keplerian limit, and that this dependency can be represented in terms of a power law to any desired accuracy of the parameter μ which is related to the inverse square root of the semi-latus rectum of the orbit. The gradient of E with respect to $\mathbf{J}$ yields the fundamental frequencies and its Hessian is the matrix $\mathbf{A}$ whose determinant is relevant for the A-nondegeneracy condition and the mixing. The resulting power-law expansion for the frequency (see Eq. (179)) has an interesting interpretation: to leading order, the three frequencies are equal in magnitude, which reflects the fact that the Kepler orbits are closed. The next-to-leading term removes the degeneracy between the frequencies associated with the radial and polar motions and describes the perihelion shift (the orbit still taking place within a plane if truncated at this order). The effects of the rotation of the black hole appear to the next-to-next-to-leading order and break the degeneracy between the frequencies associated with the azimuthal and polar motions, which describes the Lense-Thirring effect. It is at this order that the determinant of $\mathbf{A}$ is non-zero and that mixing becomes perceivable. An analogous expansion can be performed for the variable L, which represents the square root of the Carter constant. Its Hessian with respect to $\mathbf{J}$ yields the matrix $\mathbf{B}$ whose determinant is relevant for the B-nondegeneracy condition which is the fundamental hypothesis in Theorem 4, stating that the imposition of the Carter symmetry implies that the DF is a function of the integrals of motion only. Our power-law expression for E should have an interest beyond the problems analyzed in this work, especially for astrophysical problems in which a star is orbiting the black hole at a radius much larger than its Schwarzschild radius.

The validity of the A- and B-nondegeneracy conditions in the Kepler limit, combined with the analytic dependency of the fundamental frequencies on the constants of motion and Proposition 4, allows one to conclude that these conditions are actually valid on the whole space Γ_{bound}, as long as $a_H \neq 0$.

Gathering the results we arrive at the main conclusion of this article:

Theorem 7 (Mixing in the exterior of a rotating Kerr black hole). *Let $m > 0$, $M_H > 0$ and $a_H \in (0, M_H)$ and consider the reduced phase space Σ_0 (see Eq. (106)), describing bound geodesic motion in the exterior of a Kerr black hole of mass M_H and rotation parameter a_H, which is diffeomorphic to the space $(\hat{\Gamma}, \hat{\eta})$ under the map $\hat{\Psi}_0$, see subsection 4.1.*

Let $p, q \in (1, \infty)$ be such that $1/p + 1/q = 1$ and let $F \in L^p(\hat{\Gamma}, \hat{\eta})$. Then, under the Liouville flow $U(t)$, $U(t)F$ converges weakly to its angle-average $\overline{F}$, that is,

$$\lim_{t\to\infty} \int_{\hat{\Gamma}} [U(t)F](\mathbf{q}, \mathbf{P}) G(\mathbf{q}, \mathbf{P}) \hat{\eta} = \int_{\hat{\Gamma}} \overline{F}(\mathbf{q}, \mathbf{P}) G(\mathbf{q}, \mathbf{P}) \hat{\eta}, \tag{193}$$

for all $G \in L^q(\hat{\Gamma}, \hat{\eta})$.

Remark 17. As explained in Theorem 5, Eq. (193) also holds for $F \in L^1(\hat{\Gamma}, \hat{\eta})$ and $G \in C_b(\hat{\Gamma})$, the space of continuous and bounded functions on $\hat{\Gamma}$.

Remark 18. Theorem 7 implies that any macroscopic observable $N_g(t)$ of the form (125) for which the initial datum f_0 lies in $L^p(\Sigma_0, \hat{\eta})$ ($p > 1$) and the test function g in the dual space $L^q(\Sigma_0, \hat{\eta})$ converges in time to the same observable in which f_0 is replaced with its angle-average. Physically, this implies that a kinetic gas configuration propagating in the background of a rotating Kerr black hole exterior settles down to a stationary, axisymmetric configuration which is invariant with respect to the Carter flow. Such configurations have recently been constructed and their properties analyzed, see Refs. [49,50]. Furthermore, it has been shown that similar configurations yield stationary and axisymmetric solutions of the full Einstein-Vlasov system bifurcating from the Kerr solution [34]. It should be interesting to investigate the role of phase space mixing for the stability of these self-gravitating solutions with respect to small perturbations.

Remark 19. Related to the previous remark, it is natural to ask whether the statement of the theorem can be generalized to a larger class of test functions g, including distributional ones for which $N_g(t)$ describes components of the current-density or energy-momentum-stress tensor. We leave this problem for future work; however see [29] for a Newtonian model problem.

Remark 20. We emphasize that the mixing property established in Theorem 7 only holds in the rotating case $a_H \neq 0$. When $a_H = 0$ there is only partial mixing, which is due to the fact that the fundamental frequencies degenerate, $\omega^2 = \pm\omega^1$, implying that $q^1 \mp q^2$ is a conserved quantity. As explained in [29] this quantity, together with L_z and L determines the three components of the angular momentum vector which is conserved in any spherically symmetric spacetime.

Remark 21. It is also worthwhile comparing Theorem 7 with the results in [30], in which the restricted problem of a kinetic gas confined to the equatorial plane $\vartheta = \pi/2$ was considered, completely suppressing the polar motion. In this case, $J_2 = 0$ and only the angle variables q^1 and q^3 should be considered, such that the degeneracy $\omega^2 = \pm\omega^1$ in the limit $a_H = 0$ becomes irrelevant. In fact, our results in [30] suggest that mixing takes place in this restricted setting, independently of whether or not a_H is zero. It would be interesting to prove this fact rigorously, using similar arguments than in section 5.

Remark 22. An immediate corollary of our mixing theorem is the strong Jeans theorem for our setting (see Theorem 3), which states that a stationary DF is a function of the integrals of motion only. We stress that this result has been derived under the assumption of a fixed Kerr background, and it should not be mixed up with Jean's theorem for a spherically symmetric self-gravitating kinetic gas which applies to the Vlasov-Poisson system [51] but not for the Einstein-Vlasov one [52].

Remark 23. Although Theorem 5 provides sufficient condition for phase space mixing to take place under rather weak regularity assumptions on the DF and the test function, it provides no information on the decay rates. We have made only brief remarks on what would be involved in showing decay, following the generalized Riemann-Lebesgue lemma 13. However, the proof indicates that, apart from the requirement of stronger regularity, the eigenvalues and eigenvector of the matrix **A** may play an important role when analyzing the decay properties. In this regard, we mention that decay results for toy models have recently been obtained in Refs. [53,54], based on the vector field method.

Acknowledgements We are indebted to many colleagues and friends for stimulating discussions. We particularly thank Eloy Ayón-Beato, Emilio Tejeda, Hanne Van den Bosch, and Thomas Zannias for enlightening discussions. We also thank Emilio Tejeda for bringing to our attention the possible connection between the frequency shift and the Lense-Thirring effect, Hanne Van den Bosch for pointing out to us Ref. [45], and Patryk Mach and Thomas Zannias for comments on a previous version of this manuscript. This research was supported in part by CONAHCyT Network Project No. 376127 "Sombras, lentes y ondas gravitatorias generadas por objetos compactos astrofísicos", and by a CIC Grant to Universidad Michoacana. We also thank the Erwin Schrödinger International Institute for Mathematics and Physics, where part of this work was completed, for hospitality. PR received support from the Center for Mathematical Modeling (Universidad de Chile CNRS IRL 2807) through ANID/Basal projects #FB210005 , #ACE210010, and by FONDECYT-ANID postdoctoral grant #3220767. P.R acknowledges partial support from "Junior research fellowship" and the thematic programme conference "Mathematical Perspectives of Gravitation beyond the Vacuum Regime" from Erwin Schrödinger International Institute for Mathematics and Physics University of Vienna.

Data Availibility Statement Data sharing not applicable to this article as no datasets were generated or analyzed during the current study.

Appendix A: Polar motion

As follows from Eq. (25) the polar motion is confined to the set in the (ϑ, p_ϑ)-plane determined by the equation

$$p_\vartheta^2 + K(\vartheta) = L^2, \tag{A1}$$

where here we rewrite the function $K : (0, \pi) \to \mathbb{R}$ in the form

$$K(\vartheta) = \hat{L}_z^2 + L_z^2 \cot^2\vartheta + a_H^2(m^2 - E^2)\cos^2\vartheta, \tag{A2}$$

where we recall that $\hat{L}_z = L_z - a_H E$, see Eq. (38). For $L_z \neq 0$ the function K diverges as $\vartheta \to 0, \pi$. When $a_H^2(E^2 - m^2) \leq L_z^2$ this function has a global minimum at $\vartheta = \pi/2$, where $K(\pi/2) = \hat{L}_z^2$, so in this case the polar motion is described by a closed curve in the (ϑ, p_ϑ)-plane for each $L > |\hat{L}_z|$.

When $a_H^2(E^2 - m^2) > L_z^2$, the function K has a local maximum at $\vartheta = \pi/2$ and two global minima at $\vartheta = \vartheta_*$ and $\vartheta = \pi - \vartheta_*$, where $\vartheta_* \in (0, \pi/2)$ is determined by the equation

$$\sin^2\vartheta_* = \frac{|L_z|}{|a_H|\sqrt{E^2 - m^2}}. \tag{A3}$$

The value of K at these minima is

$$K(\vartheta_*) = K(\pi - \vartheta_*) = \hat{L}_z^2 - \left(|a_H|\sqrt{E^2 - m^2} - |L_z|\right)^2. \tag{A4}$$

For the scenarios considered in the present article, $E^2 < m^2$, since we only consider bound orbits; hence only the first case where K has a global minimum at $\vartheta = \pi/2$ is relevant.

Appendix B: Radial Motion

In this appendix, we discuss the qualitative properties of the effective potential W_+ defined in Eq. (40) describing the radial motion of future-directed timelike geodesics in the Kerr exterior spacetime. For related discussions, see for example [34,55–57].

In terms of the dimensionless variables

$$x := \frac{r}{M_H}, \qquad \varepsilon := \frac{E}{m}, \qquad \lambda := \frac{L}{M_H m}, \qquad \hat{\lambda}_z := \frac{\hat{L}_z}{M_H m}, \tag{B1}$$

and $\alpha := a_H/M_H$, $\beta := \hat{L}_z/L$ we have $W_+(r) = m w_{\alpha,\beta,\lambda}(x)$ with the smooth function $w_{\alpha,\beta,\lambda} : (x_+, \infty) \to \mathbb{R}$ defined by

$$w_{\alpha,\beta,\lambda}(x) = \frac{\alpha\beta\lambda}{x^2} + \sqrt{\left(1 - \frac{2}{x} + \frac{\alpha^2}{x^2}\right)\left(1 + \frac{\lambda^2}{x^2}\right)}, \qquad x > x_+ := 1 + \sqrt{1 - \alpha^2}. \tag{B2}$$

Notice that $\lim_{x\to x_+} w_{\alpha,\beta,\lambda}(x) = \alpha\beta\lambda/x_+^2$ which can have either sign, while for large x,

$$w_{\alpha,\beta,\lambda}(x) = 1 - \frac{1}{x} + \mathcal{O}\left(\frac{1}{x^2}\right). \tag{B3}$$

Spherical orbits. In order to determine the qualitative properties of $w_{\alpha,\beta,\lambda}$ we first discuss its critical points, corresponding to spherical orbits (that is, orbits taking place within a sphere of constant radial coordinate r). For this, suppose $x > x_+$ is a critical point of $w_{\alpha,\beta,\lambda}$. Then,

$$\begin{aligned} 0 &= x^3\sqrt{(x^2 - 2x + \alpha^2)(x^2 + \lambda^2)}\,\frac{d}{dx} w_{\alpha,\beta,\lambda}(x) \\ &= -2\alpha\beta\lambda\sqrt{(x^2 - 2x + \alpha^2)(x^2 + \lambda^2)} + x^2(x - \alpha^2) - (x^2 - 3x + 2\alpha^2)\lambda^2. \end{aligned} \tag{B4}$$

Taking the square on both sides and eliminating the square root one obtains a bi-quadratic equation for λ of the form

$$A\lambda^4 - 2B\lambda^2 + C = 0, \tag{B5}$$

with coefficients

$$\begin{aligned} A &= x^2(x-3)^2 - 4\alpha^2 x + 4\alpha^2(1-\beta^2)\overline{\Delta}(x), \\ B &= x^4(x-3) + \alpha^2 x^3(x+1) - 2\alpha^2(1-\beta^2)x^2\overline{\Delta}(x), \\ C &= x^4(x-\alpha^2)^2, \end{aligned}$$

where for convenience we have set $\overline{\Delta}(x) := x^2 - 2x + \alpha^2$. The discriminant yields

$$D := B^2 - AC = 4\alpha^2\beta^2 x^4 \overline{\Delta}(x)^2 \left[x - \alpha^2(1-\beta^2)\right], \tag{B6}$$

and is positive since $x > x_+ \geq 1$ and $0 \leq \alpha^2(1-\beta^2) \leq 1$. Therefore, Eq. (B5) has two real solutions for λ^2, given by $\lambda^2 = (B \pm \sqrt{D})/A$. Observing the fact that

$$B + x^2 A = x^2 \overline{\Delta}(x) \left[x(x-3) + 2\alpha^2(1-\beta^2)\right] \tag{B7}$$

and the factorization

$$\begin{aligned} A = &\left[x(x-3) + 2\alpha^2(1-\beta^2) + 2\alpha\beta\sqrt{x - \alpha^2(1-\beta^2)}\right] \\ &\left[x(x-3) + 2\alpha^2(1-\beta^2) - 2\alpha\beta\sqrt{x - \alpha^2(1-\beta^2)}\right], \end{aligned} \tag{B8}$$

one obtains

$$\begin{aligned} \lambda^2 &= x^2 \left[-1 + \frac{\overline{\Delta}(x)}{x(x-3) + 2\alpha^2(1-\beta^2) \mp 2\alpha\beta\sqrt{x - \alpha^2(1-\beta^2)}}\right] \\ &= \frac{x^2\left[\sqrt{x - \alpha^2(1-\beta^2)} \pm \alpha\beta\right]^2}{x(x-3) + 2\alpha^2(1-\beta^2) \mp 2\alpha\beta\sqrt{x - \alpha^2(1-\beta^2)}}. \end{aligned} \tag{B9}$$

Since $\sqrt{x - \alpha^2(1-\beta^2)} > \sqrt{1 - \alpha^2 + \alpha^2\beta^2} \geq |\alpha\beta|$ the numerator in Eq. (B9) is always positive, and hence the denominator needs to be positive as well for $\lambda^2 > 0$ to be well-defined. By introducing Eq. (B9) back into Eq. (B4) one can check that the correct solution is the one belonging to the lower sign. Therefore, we conclude that

$$\lambda = x\frac{\sqrt{x - \alpha^2(1-\beta^2)} - \alpha\beta}{\sqrt{h(x)}}, \qquad h(x) > 0, \tag{B10}$$

with the smooth function $h : (x_+, \infty) \to \mathbb{R}$ defined by

$$h(x) := x(x-3) + 2\alpha^2(1-\beta^2) + 2\alpha\beta\sqrt{x - \alpha^2(1-\beta^2)}, \qquad x > x_+. \tag{B11}$$

The next lemma shows the relevant behavior for the function h that will be used in the following:

Lemma 19. *The function $h : (x_+, \infty) \to \mathbb{R}$ defined by Eq. (B11) has a unique zero at some point $x_{ph} = x_{ph}(\alpha, \beta) > x_+$, and it is strictly negative on the interval (x_+, x_{ph}) and strictly positive on the interval (x_{ph}, ∞) (see Fig. 3).*

Proof. First, we observe that

$$\begin{aligned} \lim_{y \to x_+} h(y) &= -x_+ + \alpha^2 + 2\alpha\beta\left(\sqrt{x_+ - \alpha^2(1-\beta^2)} - \alpha\beta\right) \\ &\leq -(x_+ - \alpha^2) + 2\alpha^2\beta^2\left(\sqrt{1 + \frac{x_+ - \alpha^2}{\alpha^2\beta^2}} - 1\right) < 0, \end{aligned}$$

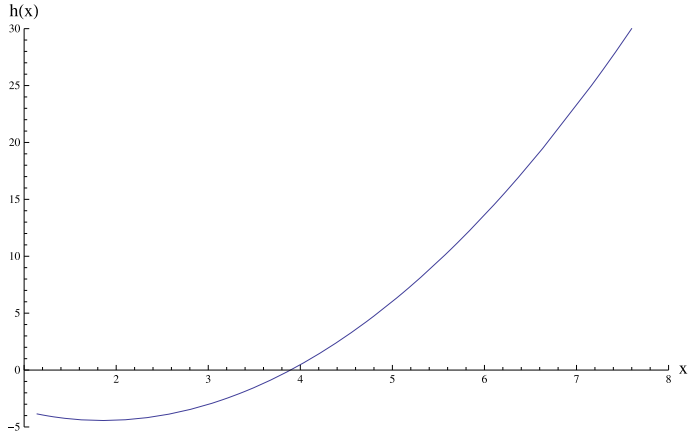

Fig. 3. The function $h : (x_+, \infty) \to \mathbb{R}$ for the parameter values $\alpha = 0.99$ and $\beta = -0.95$. Note that h is not monotonous for these values; nevertheless it has a unique zero

by virtue of the inequality $\sqrt{1+c^2} - 1 < c^2/2$ which holds for all $c > 0$. On the other hand,

$$\lim_{y\to\infty} h(y) = +\infty;$$

hence h has at least one zero on the interval (x_+, ∞). It remains to show that this zero is unique. For this we compute

$$\frac{dh}{dy}(y) = 2y - 3 + \frac{\alpha\beta}{\sqrt{y - \alpha^2(1-\beta^2)}}.$$

Combining this with Eq. (B11) we obtain the identity

$$\begin{aligned} y^3 \frac{d}{dy}\left[\frac{h(y)}{y^2}\right] &= y\frac{dh}{dy}(y) - 2h(y) \\ &= \left[3y - 4\alpha^2(1-\beta^2)\right]\left[1 - \frac{\alpha\beta}{\sqrt{y - \alpha^2(1-\beta^2)}}\right], \qquad y > x_+. \end{aligned}$$

The second parenthesis on the right-hand side is positive since $\sqrt{y - \alpha^2(1-\beta^2)} > |\alpha\beta|$. The first parenthesis is negative for $y < y_1 := 4\alpha^2(1-\beta^2)/3$ and positive for $y > y_1$. Therefore, the function $h(y)/y^2$ decreases for $x_+ < y < y_1$ (as far as this interval is non-empty) and increases for $y > y_1$. Since $h(y)/y^2$ is negative for y close to x_+ this implies that the function h can have only one zero. □

Remark 24. $r = M_H x_{ph}(\alpha, \beta)$ corresponds to the radius of spherical photon orbits.

Concluding from what we have obtained so far, the function $w_{\alpha,\beta,\lambda}$ has a critical point at x only if $x > x_{ph}(\alpha, \beta)$. In this case, the dimensionless Carter constant and energy of the orbit are given by

$$\lambda_{sph}(x) = x\frac{\sqrt{x - \alpha^2(1-\beta^2)} - \alpha\beta}{\sqrt{h(x)}}, \tag{B12}$$

$$\varepsilon_{sph}(x) = \frac{x^2 - 2x + \alpha^2(1-\beta^2) + \alpha\beta\sqrt{x - \alpha^2(1-\beta^2)}}{x\sqrt{h(x)}}$$
$$= \frac{\sqrt{h(x)}}{x} + \frac{\sqrt{x - \alpha^2(1-\beta^2)}}{x^2}\lambda_{sph}(x), \tag{B13}$$

respectively. For large x one finds

$$\lambda_{sph}(x) = \sqrt{x}\left[1 - \frac{\alpha\beta}{\sqrt{x}} + \mathcal{O}\left(\frac{1}{x}\right)\right], \tag{B14}$$

$$\varepsilon_{sph}(x) = 1 - \frac{1}{2x} + \mathcal{O}\left(\frac{1}{x^2}\right), \tag{B15}$$

and the leading order terms coincide with the Newtonian expressions (taking into account the rest energy of the particle), as expected. Note also that $\lambda_{sph}(x)$ and $\varepsilon_{sph}(x)$ are positive for all $x > x_{ph}(\alpha, \beta)$.

Global behavior of the functions λ_{sph} and ε_{sph}. Next, we analyze the behavior of the functions λ_{sph} and ε_{sph} as x increases from x_{ph} to ∞. First, we observe that $\lambda_{sph}(x) \to \infty$ as $x \to x_{ph}$ or $x \to \infty$; hence λ_{sph} must have a global minimum at some $x = x_{ms}$. In order to determine this minimum we compute

$$\lambda'_{sph}(x) = \frac{G(x)}{2h(x)^{3/2}\sqrt{x - \alpha^2(1-\beta^2)}}, \qquad G(x) = x\overline{\Delta}(x) - [h(x) - x(x-1)]^2. \tag{B16}$$

The next lemma gives the required behavior of the function G.

Lemma 20. *The function $G : [x_{ph}, \infty) \to \mathbb{R}$ defined in Eq. (B16) has a unique zero $x_{ms} = x_{ms}(\alpha, \beta)$ in the interval (x_{ph}, ∞). Further, G is negative for $x < x_{ms}$ and positive for $x > x_{ms}$.*

Proof. First, note that G is smooth, diverges to ∞ as $x \to \infty$, and satisfies

$$G(x_{ph}) = \left[x\overline{\Delta}(x) - x^2(x-1)^2\right]_{x=x_{ph}} = -x_{ph}\left[(x_{ph}-1)^3 + 1 - \alpha^2\right] < 0.$$

Hence, it has at least one zero in the interval (x_{ph}, ∞). Next, a short calculation reveals that

$$G'(x) = 3\left[2h(x) - \overline{\Delta}(x)\right]. \tag{B17}$$

Suppose now x is a zero of G. Since

$$h(x) - x(x-1) = -2\sqrt{x - \alpha^2(1-\beta^2)}\left[\sqrt{x - \alpha^2(1-\beta^2)} - \alpha\beta\right] < 0, \tag{B18}$$

it follows from the definition of G in Eq. (B16) that

$$h(x) = x(x-1) - \sqrt{x\overline{\Delta}(x)}, \tag{B19}$$

and thus

$$\frac{1}{3}\,G'(x)\big|_{G(x)=0} = x^2 - \alpha^2 - 2\sqrt{x\overline{\Delta}(x)} =: H(x). \tag{B20}$$

Finally, we claim that $H(x) > 0$ for all $x > x_+$, which implies that the function G can only cross zero from below and hence can have only one zero.

To prove that $H(x)$ is positive for all $x > x_+$ we first notice that $H(x_+) = x_+^2 - \alpha^2 > 0$ and that $H(x) \to \infty$ as $x \to \infty$. Next, let x_0 be a global minimum of H on the interval $[x_+, \infty)$. Since

$$H'(x) = 2x - \frac{1}{\sqrt{x\overline{\Delta}(x)}}(3\overline{\Delta}(x) + 2x - 2\alpha^2), \tag{B21}$$

such that $\lim_{x\to x_+} H'(x) = -\infty$ and $\lim_{x\to\infty} H'(x) = \infty$, this minimum cannot be located at $x = x_+$. Hence, $x_0 > x_+$ satisfies $H'(x_0) = 0$ and

$$H(x_0) = x_0^2 - \alpha^2 - \frac{1}{x_0}(3x_0^2 - 4x_0 + \alpha^2) = \frac{1}{x_0}\left[(x_0-1)^3 + (x_0+1)(1-\alpha^2)\right] > 0, \tag{B22}$$

which proves that $H(x) > 0$ for all $x \geq x_+$. This concludes the proof of the Lemma. □

Remark 25. For equatorial orbits $\beta^2 = 1$, the equation determining x_{ms} simplifies to $2(\sqrt{x_{ms}} - \alpha\beta) = \sqrt{\overline{\Delta}(x_{ms})}$ which implies $h(x_{ms}) = 3(\sqrt{x_{ms}} - \alpha\beta)^2$.

It follows from the previous Lemma that as x increases from x_{ph} to x_{ms} and then from x_{ms} to ∞ the function $\lambda_{sph} : (x_{ph}, \infty) \to \mathbb{R}$ decreases monotonically from ∞ to its global minimum $\lambda_{ms} := \lambda_{sph}(x_{ms})$ and then increases again monotonically to ∞. Next, a somehow long but straightforward calculation reveals that

$$\varepsilon'_{sph}(x) = \frac{\sqrt{x - \alpha^2(1-\beta^2)}}{x^2}\lambda'_{sph}(x), \tag{B23}$$

which shows that as x increases from x_{ph} to x_{ms} and then from x_{ms} to ∞ the function $\varepsilon_{sph} : (x_{ph}, \infty) \to \mathbb{R}$ decreases monotonically from ∞ to $\varepsilon_{ms} := \varepsilon_{sph}(x_{ms})$ and then increases monotonically to 1. The typical behavior of the functions λ_{sph} and ε_{sph} is shown in Fig. 4.

Global behavior of the effective potential $w_{\alpha,\beta,\lambda}$. As a consequence of the inferred behavior for the function $\lambda_{sph} : (x_{ph}, \infty) \to \mathbb{R}$, given any value for $\lambda > \lambda_{ms}$, there exist precisely two spherical orbits at $x_{max} \in (x_{ph}, x_{ms})$ and $x_{min} \in (x_{ms}, \infty)$, respectively, such that

$$\lambda_{sph}(x_{min}) = \lambda_{sph}(x_{max}) = \lambda. \tag{B24}$$

A long calculation shows that

$$w''_{\alpha,\beta,\lambda}(x)\Big|_{\lambda=\lambda_{sph}(x)} = \frac{G(x)}{x^3\sqrt{h(x)\overline{\Delta}(x)}}, \tag{B25}$$

with G the function defined in Eq. (B16). Therefore, x_{max} corresponds to a local maximum of $w_{\alpha,\beta,\lambda}$ and x_{min} to a local minimum. For $\lambda < \lambda_{ms}$ the function $w_{\alpha,\beta,\lambda}$ has no critical points and is monotonously increasing. We summarize our finding in the following

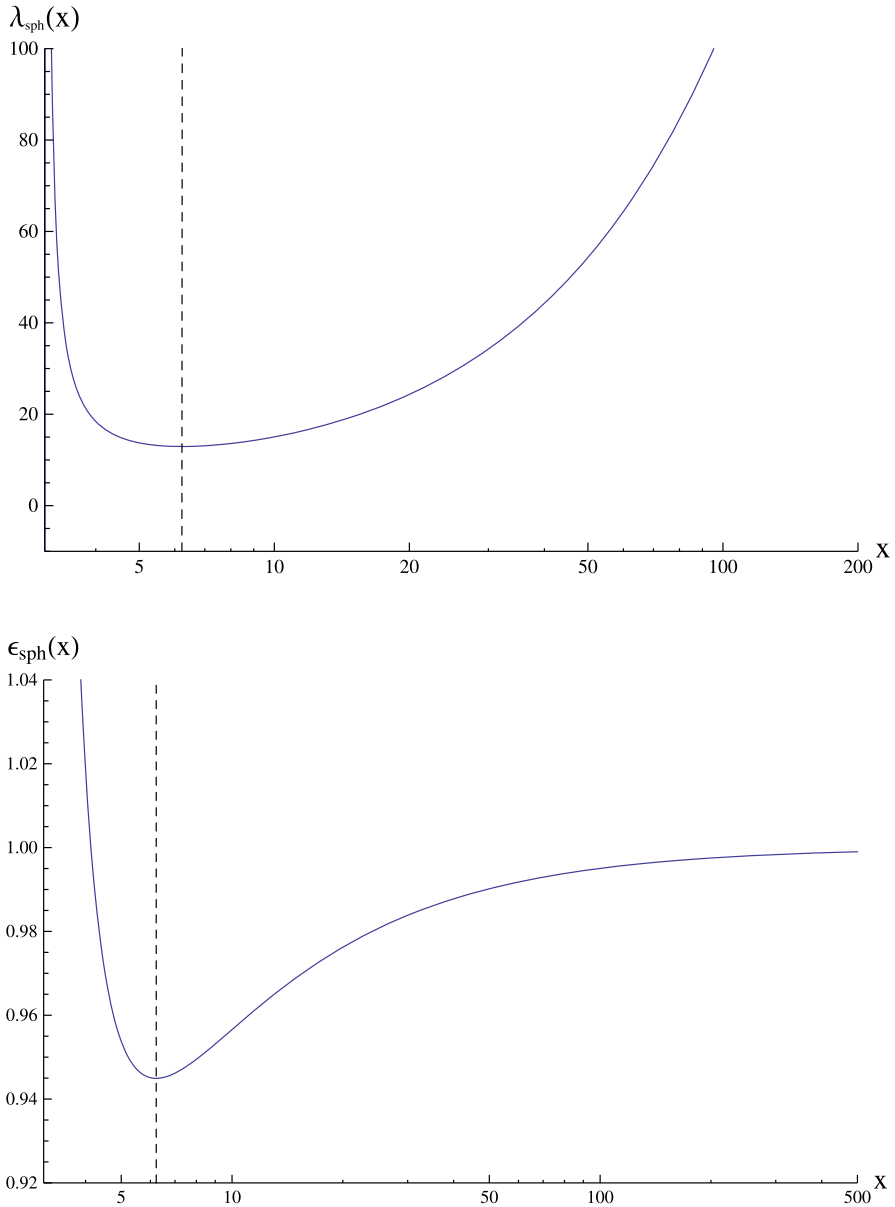

Fig. 4. Plot of the functions $\lambda_{sph}, \varepsilon_{sph} : (x_{ph}, \infty) \to \mathbb{R}$ for the parameter values $\alpha = 0.12$ and $\beta = -0.61$. The vertical dashed lines indicate the location of the marginally stable orbit $x_{ms} \approx 6.223$ for these values, which correspond to the minima of both functions

Lemma 21 *(Global behavior of the effective potential). Let $\alpha \in [0, 1)$ and $\beta \in [-1, 1]$ and denote by $\lambda_{ms} = \lambda_{ms}(\alpha, \beta)$ the global minimum of the function λ_{sph} defined in Eq. (B12). Then, the effective potential $w_{\alpha,\beta,\lambda}$ defined in Eq. (B2) has the following qualitative behavior:*

(i) If $0 < \lambda < \lambda_{ms}$, it is monotonously increasing.

(ii) If $\lambda > \lambda_{ms}$, it has a local maximum at $x_{max} \in (x_{ph}, x_{ms})$ and a local minimum at $x_{min} \in (x_{ms}, \infty)$, where x_{max} and x_{min} are uniquely determined by the equation $\lambda_{sph}(x) = \lambda$. Define the corresponding energy values $\varepsilon_{max} := \varepsilon_{sph}(x_{max})$ and $\varepsilon_{min} := \varepsilon_{sph}(x_{min})$. As λ increases from λ_{ms} to ∞, x_{max} decreases from x_{ms} to x_{ph} and ε_{max} increases from $\varepsilon_{ms} := \varepsilon_{sph}(x_{ms})$ to ∞ while x_{min} increases from x_{ms} to ∞ and ε_{min} increases from ε_{ms} to 1.

Typical examples for the behavior of $w_{\alpha,\beta,\lambda}$ in case (ii) of the lemma are given in Fig. 5. To close this section, we summarize the properties of special orbits we have encountered so far and which play an important role throughout this article. Recall that in our parametrization, we fixed the parameter $\beta = \hat{L}_z/L$, such that the characteristic radii, energies and Carter constants of these orbits depend on α and β.

- **spherical photon orbits**. These correspond to the limit of the unstable spherical orbits as the energy goes to infinity. Their radius $x = x_{ph}$ is determined by the unique zero of the function $h(x)$ defined in Eq. (B11).
- **marginally stable orbits**. These are the spherical orbits with minimum values of λ and ε. Their radius $x = x_{ms}$ is determined by the unique zero of the function G defined in Lemma 20.
- **marginally bound orbits**. These are the unstable spherical orbits whose energy is equal to 1, that is, equal to the asymptotic value of the effective potential. Their radius $x = x_{mb}$ corresponds to the unique root of $\varepsilon_{sph}(x) = 1$ in the interval (x_{ph}, x_{ms}), and it also represents the minimum radius of parabolic-type orbits.
- **innermost stable orbits**. These are the unstable spherical orbits whose energy lies below 1. Their radius $x = x_{max}$ represent the largest lower bound for the radii of bound orbits whose energy lies just below the maximum of the effective potential.

In some limiting cases it is possible to provide explicit expressions for the quantities $x_{ph}, x_{mb}, x_{ms}, \lambda_{mb}, \lambda_{ms}$ and ε_{ms}. In the non-rotating limit $\alpha = 0$ these quantities become independent of β, and they are given by

$$x_{ph}(0, \beta) = 3, \quad x_{mb}(0, \beta) = 4, \quad x_{ms}(0, \beta) = 6, \tag{B26}$$

$$\lambda_{mb}(0, \beta) = 4, \quad \lambda_{ms}(0, \beta) = 2\sqrt{3}, \quad \varepsilon_{ms}(0, \beta) = \sqrt{8/9}. \tag{B27}$$

For equatorial orbits and an arbitrary rotation parameter $\alpha \in (-1, 1)$ one finds [58]

$$x_{ph}(\alpha, \beta = \pm 1) = 2 + 2\cos\left[\frac{2}{3}\arccos(-\alpha\beta)\right], \tag{B28}$$

$$x_{mb}(\alpha, \beta = \pm 1) = \left(1 + \sqrt{1 - \alpha\beta}\right)^2 = 2 - \alpha\beta + 2\sqrt{1 - \alpha\beta}, \tag{B29}$$

$$x_{ms}(\alpha, \beta = \pm 1) = 3 + Z_2 - \beta\sqrt{(3 - Z_1)(3 + Z_1 + 2Z_2)}, \tag{B30}$$

with $Z_1 := 1 + (1 - \alpha^2)^{1/3}[(1 + \alpha)^{1/3} + (1 - \alpha)^{1/3}]$ and $Z_2 := \sqrt{Z_1^2 + 3\alpha^2}$. Using Eqs. (B12,B13,B19) one also obtains from this

$$\lambda_{mb}(\alpha, \beta = \pm 1) = x_{mb}(\alpha, \beta), \tag{B31}$$

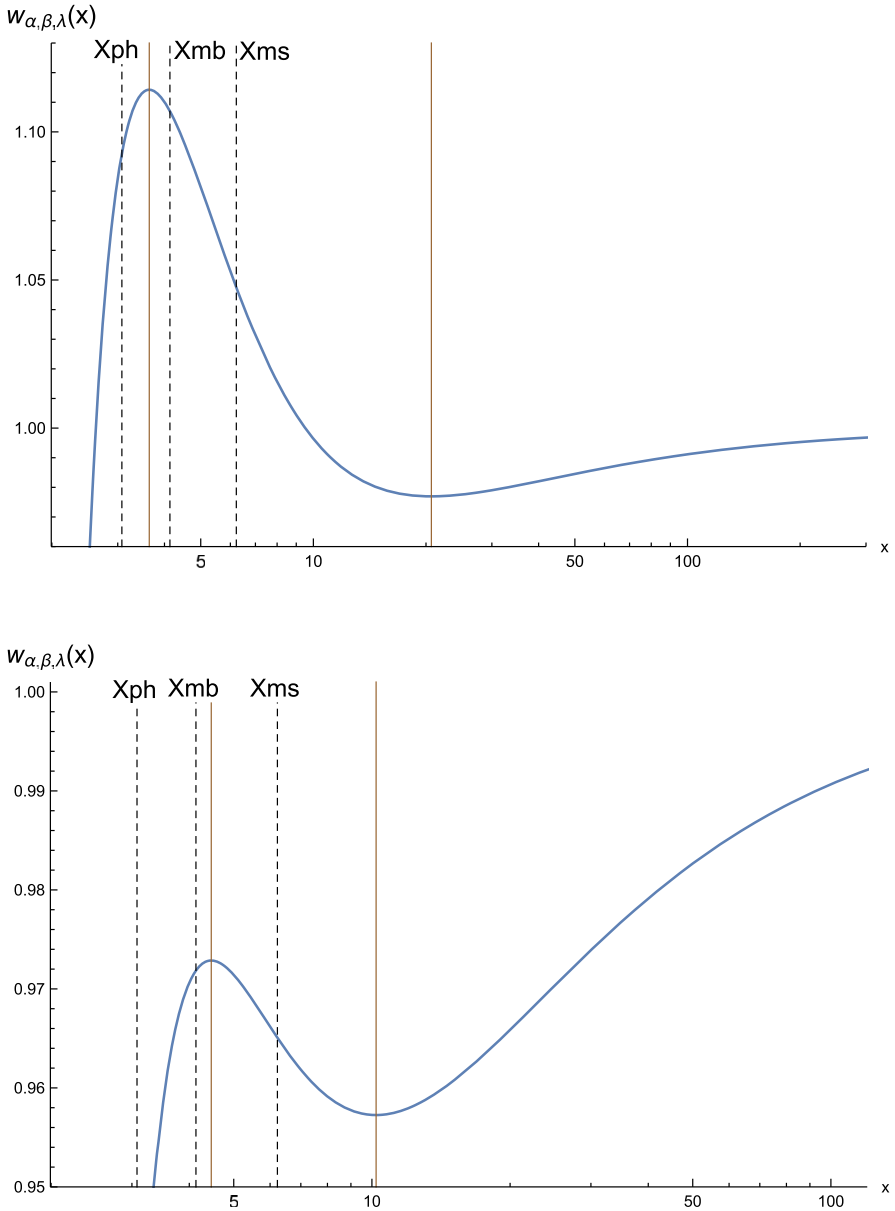

Fig. 5. Plot of the effective potential $w_{\alpha,\beta,\lambda}$ for the parameter values $\alpha = 0.12$, $\beta = -0.61$ and $\lambda = 5$ (top panel) and $\lambda = 3.9$ (bottom panel). Also shown (in vertical dashed lines) are the locations of the photon sphere, the marginally bound orbit, the marginally stable orbit and the locations (in vertical solid lines) of the local maxima and minima of $w_{\alpha,\beta,\lambda}$

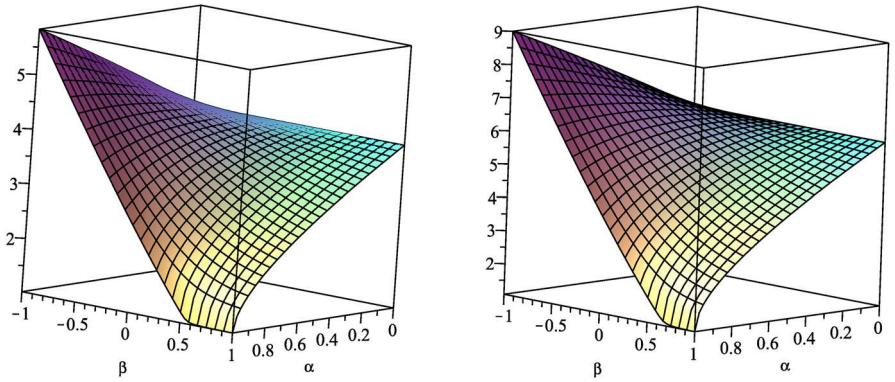

Fig. 6. Plot of the functions $x_{mb}(\alpha, \beta)$ (left panel) and $x_{ms}(\alpha, \beta)$ (right panel)

$$\lambda_{ms}(\alpha, \beta = \pm 1) = \frac{x_{ms}(\alpha, \beta)}{\sqrt{3}}, \qquad \varepsilon_{ms}(\alpha, \beta = \pm 1) = \sqrt{1 - \frac{2}{3x_{ms}(\alpha, \beta)}}. \tag{B32}$$

The behavior of $x_{mb}(\alpha, \beta)$ and $x_{ms}(\alpha, \beta)$ for arbitrary values of $\alpha \in [0, 1)$ and $\beta \in (-1, 1)$ are illustrated in Figs. 6 and indicate that these functions decrease monotonically for fixed α (although this property will not be used here).

Appendix C: Parametrization of the Bound Orbits Through the Parameters (β, p, e)

It follows from Lemma 21 that the parameter range corresponding to bound orbits is described by the set

$$\mathcal{D}_\alpha := \{(\beta, \lambda, \varepsilon) : -1 < \beta < 1, \lambda > \lambda_{ms}(\alpha, \beta), \varepsilon_{min}(\lambda) < \varepsilon < \min\{1, \varepsilon_{max}(\lambda)\}\}. \tag{C1}$$

However, for many applications it is useful to parametrize the bound orbits in terms of the Kepler-type "semi-latus rectum" p and eccentricity e, which are related to the turning points x_1 and x_2 of the radial motion through the transformation [35,40]

$$x_1 = \frac{p}{1+e}, \qquad x_2 = \frac{p}{1-e}. \tag{C2}$$

Here e is restricted to the range $0 < e < 1$, the limits $e \to 0$ and $e \to 1$ corresponding to circular and parabolic-type orbits, respectively. Unlike the Kepler case in which p is an arbitrary positive number, in the Kerr case the range of p is restricted to $p > p_{ISO}(\alpha, \beta, e)$, the limit $p = p_{ISO}(\alpha, \beta, e)$ (determined below) corresponding to the innermost stable orbits, i.e. the orbits with minimal inner radius for given value of λ. Therefore, the quantities (β, p, e) are confined to the open set

$$\mathcal{E}_\alpha := \{(\beta, p, e) : -1 < \beta < 1, 0 < e < 1, p > p_{ISO}(\alpha, \beta, e)\}. \tag{C3}$$

In this subsection, we describe the properties of the function $p_{ISO}(\alpha, \beta, e)$, and we prove that the map $T_\alpha : \mathcal{D}_\alpha \to \mathcal{E}_\alpha, (\beta, \lambda, \varepsilon) \mapsto (\beta, p, e)$ is invertible. To this purpose we first recall the fourth-order polynomial R defined in Eq. (28) and its relation with the effective potentials $W_\pm$ in Eq. (39), which implies that on the interval $r > r_+$ all the

roots of W_+ are also roots of R, with the same multiplicity. Furthermore, we see from the definition of R in Eq. (28) that in the region $r_- < r < r_+$ where Δ is negative, $R(r) > 0$, whereas $R(0) = -a_H^2(L^2 - \hat{L}_z^2) \leq 0$. Therefore, it follows that for $(\beta, \lambda, \varepsilon) \in \mathcal{D}_\alpha$ the function R must have four real roots, two of which are given by the turning points $r_1 < r_2$ of $W_+(r) = E$ and the remaining roots $r_3 < r_4$ satisfying

$$0 \leq r_3 < r_- < r_+ < r_4 < r_1 < r_2, \tag{C4}$$

with $r_3 = 0$ in the limiting case of Schwarzschild or equatorial orbits. In the limit $e \to 0$ the two roots $r_1 = r_2$ fall together and for ISOs the roots $r_4 = r_1$ are equal to each other, with $r_4 = r_1 = r_2$ for marginally stable orbits.

In order to get useful relations between the roots and the conserved quantities, we work again with dimensionless variables, setting $x_i = r_i/M_H$ for $i = 1, 2, 3, 4$. Assuming that $(\beta, \lambda, \varepsilon) \in \mathcal{D}_\alpha$ and writing

$$\begin{aligned} \frac{R(r)}{(M_H^2 m)^2} &= (\varepsilon x^2 - \alpha\beta\lambda)^2 - (x^2 - 2x + \alpha^2)(x^2 + \lambda^2) \\ &= -(1 - \varepsilon^2)(x - x_3)(x - x_4)(x - x_1)(x - x_2), \end{aligned} \tag{C5}$$

one obtains the relations

$$1 - \varepsilon^2 = \frac{2}{x_{1234}}, \tag{C6}$$

$$\lambda^2 = \frac{x_1x_2x_3 + x_1x_2x_4 + x_1x_3x_4 + x_2x_3x_4}{x_{1234}}, \tag{C7}$$

$$\alpha^2(1 - \beta^2)\lambda^2 = \frac{2x_1x_2x_3x_4}{x_{1234}}, \tag{C8}$$

$$\alpha^2 + \lambda^2 + 2\alpha\beta\varepsilon\lambda = 2\frac{x_1x_2 + x_1x_3 + x_1x_4 + x_2x_3 + x_2x_4 + x_3x_4}{x_{1234}}, \tag{C9}$$

where we have introduced the abbreviation $x_{1234} := x_1 + x_2 + x_3 + x_4$. These equations allow one to determine the conserved quantities $(\varepsilon, \lambda, \beta)$ from the roots x_1, x_2, x_3, x_4. Since there are more equations than unknowns, the roots cannot be independent from each other. In fact, we will show that the knowledge of β, x_1 and x_2 is sufficient to determine the other roots x_3 and x_4 and the constants of motion (ε, λ).

Before doing so, we note two immediate conclusions that can be drawn from Eqs. (C6–C9). First, in the limit of marginally stable orbits, for which $x_4 = x_1 = x_2 = x_{ms}$, one obtains

$$1 - \varepsilon_{ms}^2 = \frac{2}{3x_{ms} + x_3}, \qquad \lambda_{ms}^2 = x_{ms}^2\frac{x_{ms} + 3x_3}{3x_{ms} + x_3}. \tag{C10}$$

For equatorial orbits, $x_3 = 0$, and these expressions reduce to Eq. (B32). Second, for marginally bound orbits, one has $x_2 \to \infty$ with $x_4 = x_1 = x_{mb}$ remaining bounded, which yields $\varepsilon \to 1$ and

$$\lambda_{mb}^2 = x_{mb}(x_{mb} + 2x_3). \tag{C11}$$

This simplifies to the corresponding expression (B31) when $x_3 = 0$.

With these observations at hand, one can prove the following general property of the effective potential $w_{\alpha,\beta,\lambda}(x)$ defined in Eq. (B2):

Lemma 22. *Let $\alpha \in [0,1)$, $\beta \in [-1,1]$ and $x \geq x_{mb}(\alpha,\beta)$ be fixed and set $\lambda_1 := \lambda_{sph}(x)$. Then, the function $(\lambda_1,\infty) \to \mathbb{R}$, $\lambda \mapsto w_{\alpha,\beta,\lambda}(x)$ is increasing and unbounded.*

Proof. From Eq. (B2) one easily finds

$$\frac{\partial}{\partial\lambda} w_{\alpha,\beta,\lambda}(x) = \frac{\lambda w_{\alpha,\beta,\lambda}(x) + \alpha\beta}{x^2+\lambda^2}. \tag{C12}$$

The right-hand side is manifestly positive for prograde orbits $\alpha\beta \geq 0$. However, in the retrograde case the right-hand side is certainly not positive for arbitrary values of $x > x_+$, since $w_{\alpha,\beta,\lambda}(x)$ becomes negative when $x \to x_+$.

We treat de retrograde case as follows. First, it follows from the properties of the effective potential established in Lemma 21 that for each $\lambda > \lambda_1$ the point x lies inside the potential well of $w_{\alpha,\beta,\lambda}$. Therefore, using Eq. (C10) one finds $w_{\alpha,\beta,\lambda}(x)^2 \geq \varepsilon_{ms}^2 \geq 1 - 2/(3x_{ms})$ and $\lambda^2 \geq \lambda_{ms}^2 \geq x_{ms}^2/3$ which imply

$$\lambda w_{\alpha,\beta,\lambda}(x) \geq \frac{x_{ms}}{\sqrt{3}}\sqrt{1-\frac{2}{3x_{ms}}}. \tag{C13}$$

Next, we claim that for retrograde orbits, $x_{ms}(\alpha,\beta) \geq 4$, the equality being achieved for $\alpha = 1$ and $\beta = 0$. To prove this assertion, we recall that x_{ms} is determined by the unique root of the function G on the interval $x > x_{ph}$, and that $G'(x) > 0$ at this root, see Lemma 20. Using Eqs. (B16,B18) a short computation reveals that

$$\begin{aligned} G(4) &= 4\left\{8+\alpha^2 - \left[4-\alpha^2(1-\beta^2)\right]\left[\sqrt{4-\alpha^2(1-\beta^2)}-\alpha\beta\right]^2\right\} \\ &\leq 4\left(8+\alpha^2-9\right) = -4(1-\alpha^2) \leq 0, \end{aligned} \tag{C14}$$

where we have used the assumption that $\alpha\beta \leq 0$ in the last step, and where we note that the equality holds if $\alpha = 1$ and $\beta = 0$. Therefore, $x_{ms} \geq 4$ for retrograde orbits. Together with Eq. (C13) this yields

$$\lambda w_{\alpha,\beta,\lambda}(x) \geq \frac{4}{3}\sqrt{\frac{5}{2}} > 1. \tag{C15}$$

This shows that the right-hand side of Eq. (C12) is also positive for retrograde orbits.

In order to prove the unboundedness property, consider the limit

$$\lim_{\lambda\to\infty} \frac{x^2}{\lambda} w_{\alpha,\beta,\lambda}(x) = \alpha\beta + \sqrt{x^2-2x+\alpha^2}. \tag{C16}$$

The right-hand side is again manifestly positive when $\alpha\beta \geq 0$. When $\alpha\beta < 0$ we use the identity

$$h(x) = \overline{\Delta}(x) - \left[\sqrt{x-\alpha^2(1-\beta^2)}-\alpha\beta\right]^2, \tag{C17}$$

to conclude that $h(2) \leq -(1-\alpha^2) \leq 0$, which shows that $x_{mb} > x_{ph} \geq 2$, such that the right-hand side of Eq. (C16) is again positive. □

Coming back to the question regarding the invertibility of the map $T_\alpha : (\beta, \lambda, \varepsilon) \mapsto (\beta, p, e)$, for what follows we can fix $\beta \in (-1, 1)$ since β transforms trivially with respect to this map. Introducing the sets

$$\mathcal{D}_{\alpha,\beta} := \{(\lambda, \varepsilon) : \lambda > \lambda_{ms}(\alpha, \beta), \varepsilon_{min}(\lambda) < \varepsilon < \min\{1, \varepsilon_{max}(\lambda)\}\}, \tag{C18}$$

and

$$\mathcal{E}_{\alpha,\beta} := \{(p, e) : 0 < e < 1, p > p_{ISO}(\alpha, \beta, e)\}, \tag{C19}$$

our task is to determine the function $p_{ISO}(\alpha, \beta, e)$ and to prove that the map $T_{\alpha,\beta} : \mathcal{D}_{\alpha,\beta} \to \mathcal{E}_{\alpha,\beta}$ is invertible. Note first that this map is well defined if we replace $\mathcal{E}_{\alpha,\beta}$ with $(0, \infty) \times (0, 1)$, since it follows from Lemma 21 that for given $(\lambda, \varepsilon) \in \mathcal{D}_{\alpha,\beta}$ there exist unique turning points $x_2 > x_1 > x_{mb}(\alpha, \beta)$ which are determined by the roots of the equation $w_{\alpha,\beta,\lambda}(x) = \varepsilon$. The key question is whether the converse holds as well: given $x_2 > x_1 > x_{mb}(\alpha, \beta)$, do there exist unique values $(\lambda, \varepsilon) \in \mathcal{D}_{\alpha,\beta}$ such that x_1 and x_2 are the turning point of $w_{\alpha,\beta,\lambda}(x) = \varepsilon$? The first observation is that this property does not hold without further restriction of x_1 and x_2. Indeed, when x_1 lies within the range (x_{mb}, x_{ms}), x_2 cannot approach x_1 since $x_2 > x_{min} > x_{ms}$. As the next lemma shows, the closest x_2 can get to x_1 occurs when $\lambda = \lambda_{sph}(x_1)$ is minimized, such that x_1 corresponds to the inner radius of an ISO. For the following, denote for each $x_1 \in (x_{mb}, x_{ms})$ by $X_{2,ISO}(x_1) > x_{ms}$ the right turning point of $w_{\alpha,\beta,\lambda_{sph}(x_1)}(x) = \varepsilon_{sph}(x_1)$. Then, one can show:

Proposition 7. *Let $\alpha \in [0, 1)$ and $\beta \in [-1, 1]$ be fixed. Given $x_2 > x_1 > x_{mb}(\alpha, \beta)$ with the restriction $x_2 > X_{2,ISO}(x_1)$ if $x_1 \in (x_{mb}, x_{ms})$, there exist unique values $(\lambda, \varepsilon) \in \mathcal{D}_{\alpha,\beta}$ such that x_1, x_2 are the turning points of $w_{\alpha,\beta,\lambda}(x) = \varepsilon$. Conversely, given $(\lambda, \varepsilon) \in \mathcal{D}_{\alpha,\beta}$, it follows that the turning points of the orbit $w_{\alpha,\beta,\lambda}(x) = \varepsilon$ satisfy $x_2 > X_{2,ISO}(x_1)$ if $x_1 \in (x_{mb}, x_{ms})$.*

Proof. Suppose $x_2 > x_1 > x_{mb}(\alpha, \beta)$ with the restriction $x_2 > X_{2,ISO}(x_1)$ if $x_1 \in (x_{mb}, x_{ms})$ are given. Since x_1 must lie between the maximum and the minimum of $w_{\alpha,\beta,\lambda}$, the value of λ must satisfy $\lambda \geq \lambda_1 := \lambda_{sph}(x_1)$. Next, introduce the smooth function

$$\varepsilon_1(\lambda) := w_{\alpha,\beta,\lambda}(x_1), \qquad \lambda \geq \lambda_1, \tag{C20}$$

According to the previous lemma this function is monotonously increasing and unbounded.

Consider first the case $x_1 > x_{ms}$. Then, $\varepsilon_1(\lambda_1) < 1$ since x_1 is the location of the local minimum of $w_{\alpha,\beta,\lambda_1}$ when $\lambda = \lambda_1$. As λ increases, the location of the local minimum moves to the right (see Lemma 21); hence x_1 must be the left turning point of $w_{\alpha,\beta,\lambda}(x) = \varepsilon_1(\lambda)$. Since $\varepsilon_1(\lambda) \to \infty$ monotonically as $\lambda \to \infty$, there exists a unique $\lambda_2 > \lambda_1$ such that $\varepsilon_1(\lambda_2) = 1$. Next, denote for each $\lambda \in (\lambda_1, \lambda_2)$ by $X_2(\lambda)$ the location of the right turning point of $w_{\alpha,\beta,\lambda}(x) = \varepsilon_1(\lambda)$. Because $\varepsilon_1(\lambda) \to 1$ as $\lambda \to \lambda_2$ it follows that $X_2(\lambda) \to \infty$ as $\lambda \to \lambda_2$. Furthermore, $X_2(\lambda_1) = x_1$. Therefore, there exists $\lambda \in (\lambda_1, \lambda_2)$ such that $X_2(\lambda) = x_2$.

It remains to show that this λ is unique. For this, it is sufficient to prove that the function $X_2(\lambda)$ is increasing. To prove this, differentiate both sides of the equation

$$w_{\alpha,\beta,\lambda}(X_2(\lambda)) = w_{\alpha,\beta,\lambda}(x_1)$$

with respect to λ, which yields

$$\frac{\partial w_{\alpha,\beta,\lambda}}{\partial x}(X_2)\frac{dX_2}{d\lambda} = \frac{\partial w_{\alpha,\beta,\lambda}}{\partial \lambda}(x_1) - \frac{\partial w_{\alpha,\beta,\lambda}}{\partial \lambda}(X_2).$$

Using Eq. (C12) this can be rewritten as

$$\frac{\partial w_{\alpha,\beta,\lambda}}{\partial x}(X_2)\frac{dX_2}{d\lambda} = \frac{\lambda\varepsilon_1(\lambda)+\alpha\beta}{(\lambda^2+x_1^2)\left[\lambda^2+X_2(\lambda)^2\right]}\left[X_2(\lambda)^2 - x_1^2\right] > 0. \tag{C21}$$

Since the first factor on the left-hand side is positive (being X_2 the right turning point) we conclude that $X_2(\lambda)$ is an increasing function of λ, and hence the solution $X_2(\lambda) = x_2$ is unique.

Next, we analyze the case for which $x_1 \in (x_{mb}, x_{ms})$ and $x_2 > x_{2,ISO}(x_1)$. Now x_1 describes the location of the local maximum of $w_{\alpha,\beta,\lambda_1}$ and thus the range of the function ε_1 in Eq. (C20) is restricted to the interval $(\lambda_1, \lambda_{mb})$ with $\lambda = \lambda_1$ corresponding to the situation for which x_1 is the inner radius of the ISOs. As before, denote by $X_2(\lambda)$ the right turning point of $w_{\alpha,\beta,\lambda}(x) = \varepsilon_1(\lambda)$. As λ increases from λ_1 to λ_{mb}, ε_1 increases monotonously to 1 and hence $X_2(\lambda)$ increases monotonously from $X_{2,ISO}(x_1)$ to infinity. Therefore, there exists a unique $\lambda \in (\lambda_1, \lambda_{mb})$ such that $X_2(\lambda) = x_2$.

Conversely, let $(\lambda, \varepsilon) \in \mathcal{D}_{\alpha,\beta}$ be given and denote by $x_2 > x_1$ the turning points of $w_{\alpha,\beta,\lambda}(x) = \varepsilon$. Suppose $x_1 \in (x_{mb}, x_{ms})$. Then, $\lambda \in (\lambda_1, \lambda_{mb})$, $x_2 = X_2(\lambda)$, and it follows from the monotonicity property of $X_2(\lambda)$ that $X_2(\lambda) > X_{2,ISO}(x_1)$. This concludes the proof of the proposition. □

Before we proceed, we show the following property of the function $X_{2,ISO}(x_1)$:

Lemma 23. *Let $\alpha \in [0, 1)$ and $\beta \in [-1, 1]$ be fixed. The function $(x_{mb}, x_{ms}) \to \mathbb{R}$, $x \mapsto X_{2,ISO}(x)$ is a smooth monotonously decreasing function satisfying $X_{2,ISO}(x) \to \infty$ as $x \to x_{mb}$ and $X_{2,ISO}(x) \to x_{ms}$ as $x \to x_{ms}$.*

Proof. The smoothness property and the limits is a consequence of the definition of $X_{2,ISO}$ and the fact that it is an isolated root of the polynomial (C5). To prove the monotonicity property, differentiate both sides of the equation

$$w_{\alpha,\beta,\lambda_{sph}(x_1)}(X_{2,ISO}(x_1)) = \varepsilon_{sph}(x_1), \qquad x_{mb} < x_1 < x_{ms}, \tag{C22}$$

with respect to x_1, which yields (setting $x_2 := X_{2,ISO}(x_1)$):

$$\left.\frac{\partial w_{\alpha,\beta,\lambda}}{\partial x}(x_2)\right|_{\lambda=\lambda_{sph}(x_1)} \frac{dX_{2,ISO}}{dx}(x_1) = \varepsilon'_{sph}(x_1) - \left.\frac{\partial w_{\alpha,\beta,\lambda}}{\partial \lambda}(x_2)\right|_{\lambda=\lambda_{sph}(x_1)} \lambda'_{sph}(x_1).$$

Using Eqs. (B12,B13,B23,C12) one can rewrite the right-hand side as

$$\begin{aligned}&\left.\frac{\partial w_{\alpha,\beta,\lambda}}{\partial x}(x_2)\right|_{\lambda=\lambda_{sph}(x_1)} \frac{dX_{2,ISO}}{dx}(x_1)\\ &= \frac{\sqrt{x_1-\alpha^2(1-\beta^2)}}{x_1^2}\left[1 - \frac{x_1^2+\lambda_{sph}(x_1)^2}{x_2^2+\lambda_{sph}(x_1)^2}\right]\lambda'_{sph}(x_1), \qquad x_2 = X_{2,ISO}(x_1),\end{aligned} \tag{C23}$$

for all $x_{mb} < x_1 < x_{ms}$. It follows from the fact that $x_1 < x_2$, $\lambda'_{sph}(x_1) < 0$ and that the first factor on the left-hand side of Eq. (C23) is positive that $dX_{2,ISO}/dx(x_1) < 0$, and this concludes the proof of the lemma. □

As a consequence of Proposition 7 and the last lemma one has:

Proposition 8. *(Invertibility of the maps $T_{\alpha,\beta}$) Let $\alpha \in [0,1)$ and $\beta \in [-1,1]$ be fixed. There exists a continuous function $p_{ISO} : [0,1] \to \mathbb{R}$, $e \mapsto p_{ISO}(\alpha,\beta,e)$ satisfying $p_{ISO}(\alpha,\beta,0) = x_{ms}(\alpha,\beta)$ and $p_{ISO}(\alpha,\beta,1) = 2x_{mb}(\alpha,\beta)$ such that the map*

$$T_{\alpha,\beta} : \mathcal{D}_{\alpha,\beta} \to \mathcal{E}_{\alpha,\beta}, (\lambda,\varepsilon) \mapsto (p,e), \tag{C24}$$

with $\mathcal{D}_{\alpha,\beta}, \mathcal{E}_{\alpha,\beta}$ as defined in Eqs. (C18,C19) is a diffeomorphism.

Proof. Introduce the open set

$$\mathcal{F}_{\alpha,\beta} := \left\{(x_1,x_2) : x_2 > x_1 > x_{mb} \text{ and } x_2 > X_{2,ISO}(x_1) \text{ if } x_1 < x_{ms}\right\}. \tag{C25}$$

It follows from the last proposition that the map

$$\Phi : \mathcal{D}_{\alpha,\beta} \to \mathcal{F}_{\alpha,\beta}, \quad (\varepsilon,\lambda) \mapsto (x_1,x_2) \tag{C26}$$

which maps $(\varepsilon,\lambda) \in \mathcal{D}_{\alpha,\beta}$ to the turning points x_1, x_2 of $w_{\alpha,\beta,\lambda}(x) = \varepsilon$, is invertible. Furthermore, since x_1 and x_2 are isolated roots of the polynomial (C5) it follows that this map is smooth.

Next, consider the smooth map

$$\Psi : \{(x_1,x_2) : x_2 > x_1 > 0\} \to \{(p,e) : p > 0, 0 < e < 1\}, \tag{C27}$$

$$(x_1,x_2) \mapsto (p,e) = \left(\frac{2x_1x_2}{x_1+x_2}, \frac{x_2-x_1}{x_1+x_2}\right), \tag{C28}$$

whose inverse is given by

$$\Psi^{-1}(p,e) = \left(\frac{p}{1+e}, \frac{p}{1-e}\right), \qquad p > 0, \quad 0 < e < 1. \tag{C29}$$

Then, it follows that the map $T_{\alpha,\beta} : \mathcal{D}_{\alpha,\beta} \to \mathcal{E}_{\alpha,\beta} := \Psi(\mathcal{F}_{\alpha,\beta})$, $(\varepsilon,\lambda) \mapsto (p,e) := \Psi \circ \Phi(\varepsilon,\lambda)$ is a diffeomorphism.

It remains to prove that the set $\mathcal{E}_{\alpha,\beta} = \Psi(\mathcal{F}_{\alpha,\beta})$ has the form given in Eq. (C19). For this, consider the image of the curve $x_2 = X_{2,ISO}(x_1)$ under the map Ψ:

$$\mathcal{B} : (x_{mb}, x_{ms}) \to \mathbb{R}^2 : x_1 \mapsto (\mathcal{B}_1(x_1), \mathcal{B}_2(x_1)) := \Psi(x_1, X_{2,ISO}(x_1)). \tag{C30}$$

Note that $\mathcal{B}(x_1) \to (2x_{mb}, 1)$ when $x_1 \to x_{mb}$ and $\mathcal{B}(x_1) \to (x_{ms}, 0)$ when $x_1 \to x_{ms}$. Furthermore, the image of $\mathcal{B}$ describes the boundary of $\mathcal{E}_{\alpha,\beta}$ in $(0,\infty) \times (0,1)$. In view of Lemma 23, $X'_{2,ISO}(x_1) \le 0$, and hence it follows that

$$\frac{\partial \mathcal{B}_2}{\partial x_1}(x_1) = \frac{\partial}{\partial x_1}\frac{X_{2,ISO}(x_1) - x_1}{X_{2,ISO}(x_1) + x_1} = 2\frac{x_1 X'_{2,ISO}(x_1) - X_{2,ISO}(x_1)}{\left[X_{2,ISO}(x_1) + x_1\right]^2} < 0,$$

which shows that e decreases with respect to x_1. Hence, the boundary curve $\mathcal{B}$ can be re-parametrized in terms of e. □

Since the roots x_1 and x_2 also depend smoothly on β, it follows immediately that the map $T_\alpha : \mathcal{D}_\alpha \to \mathcal{E}_\alpha$ is invertible and smooth for each $\alpha \in [0, 1)$. The function $p_{ISO}(\alpha, \beta, e)$ and the inverse map T_α^{-1} can be determined in the following way. From Eq. (C2) one has $x_1 + x_2 = 2p/(1-e^2)$ and $x_1 x_2 = p^2/(1-e^2)$. Setting $w_+ := x_3 + x_4$ and $w_\times := x_3 x_4$ one obtains from Eqs. (C7,C8) a linear relation between w_+ and $w_\times$:

$$w_\times = \frac{\kappa^2 p}{2(p-\kappa^2)} w_+, \tag{C31}$$

where we have abbreviated $\kappa := \alpha\sqrt{1-\beta^2}$. This relation allows one to express $w_\times$ in terms of (κ, p, w_+). Note that $w_\times = 0$ for equatorial orbits.

For ISOs one has $x_4 = x_1 = p/(1+e)$. Thus, Eq. (C31) implies that

$$x_3|_{ISO} = \frac{\kappa^2}{2p - \kappa^2(3+e)} p \Big|_{p=p_{ISO}(\alpha,\beta,e)}. \tag{C32}$$

This in turn, implies that $w_+ = x_3 + x_4$ is equal to

$$w_+|_{ISO} = \frac{2(p-\kappa^2)}{2p-\kappa^2(3+e)} \frac{p}{1+e}\Big|_{p=p_{ISO}(\alpha,\beta,e)} \tag{C33}$$

for ISOs. The expression in Eq. (C33) motivates the introduction of a new parameter u_+, defined through the relation

$$w_+ = \frac{2(p-\kappa^2)}{2p-\kappa^2(3+e)} \frac{p}{1+e} \frac{1}{u_+}, \tag{C34}$$

such that $u_+ = 1$ for ISOs. For general bound orbits, Eqs. (C6–C9) imply the following algebraic equation for u_+:

$$\begin{aligned} &p^2(p-4) + \alpha^2 p(1-e^2) + \kappa^2\left[p(3+e^2) - \alpha^2(1-e^2)\right] \\ &\quad -(p-\alpha^2)\left[2p - \kappa^2(3+e)\right](1+e)u_+ \\ &\quad +2\alpha\beta p\sqrt{1+e}\sqrt{(1-e)p(p-\kappa^2) + (p-1+e^2)\left[2p-\kappa^2(3+e)\right]u_+} = 0. \end{aligned} \tag{C35}$$

Setting $u_+ = 1$, one obtains the ISO limit $p = p_{ISO}(\alpha, \beta, e)$ as a zero of the function

$$\begin{aligned} H(\alpha, \beta, e, p) := {} & p^2(p-6-2e) + \alpha^2 p(3-e)(1+e) + 2\kappa^2\left[p(3+2e+e^2) - 2\alpha^2(1+e)\right] \\ & +2\alpha\beta p\sqrt{1+e}\sqrt{(3-e)p^2 - 2p(1-e^2) - \kappa^2\left[4p - (3+e)(1-e^2)\right]} \end{aligned} \tag{C36}$$

for fixed (α, β, e).

In the Schwarzschild limit $\alpha = 0$, Eqs. (C35,C36) simplify considerably and one obtains

$$u_+ = \frac{p-4}{2(1+e)}, \quad w_+ = \frac{2p}{p-4}, \quad p_{ISO}(e) = 6 + 2e, \quad \lim_{\alpha\to 0} \frac{w_\times}{\alpha^2} = (1-\beta^2)\frac{p}{p-4}. \tag{C37}$$

To treat the case $\alpha > 0$ one rewrites Eq. (C35) in the form

$$a - bu_+ + 2\alpha\beta p\sqrt{(1-e^2)c + \nu b u_+} = 0, \tag{C38}$$

with the coefficients

$$a := p^2(p-4) + \alpha^2 p(1-e^2) + \kappa^2\left[p(3+e^2) - \alpha^2(1-e^2)\right], \tag{C39}$$

$$b := (1+e)(p-\alpha^2)\left[2p - \kappa^2(3+e)\right], \tag{C40}$$

$$c := p(p-\kappa^2), \tag{C41}$$

$$\nu := \frac{p-1+e^2}{p-\alpha^2}. \tag{C42}$$

By squaring Eq. (C35) and solving the resulting quadratic equation, one obtains

$$u_+ = \frac{1}{b}\left[a + 2\alpha^2\beta^2 p^2\nu + 2\alpha\beta p\sqrt{(1-e^2)c + a\nu + \alpha^2\beta^2 p^2\nu^2}\right], \tag{C43}$$

where the correct sign can be determined by taking the limits $\alpha \to 0$ or $p \to \infty$.

Eqs. (C2,C31,C34,C43) allow one to determine the four roots x_1, x_2, x_3 and x_4 explicitly in terms of the parameters (β, p, e). The constants of motion ε and λ can be determined from these quantities using Eqs. (C6,C8), which yield

$$\varepsilon^2 = 1 - \frac{1-e^2}{p}\frac{1}{1+\frac{1-e^2}{2p}w_+}, \qquad \lambda^2 = \frac{p}{1+\frac{1-e^2}{2p}w_+}\frac{w_\times}{\kappa^2}. \tag{C44}$$

Appendix D: Details Regarding the Computation of the Generalized Action-Angle Variables

In this appendix we provide the necessary details for the computation of the generalized action-angle variables (J_α, Q^α). For this, recall the generating function $S(\gamma_x; I_\alpha)$ in Eq. (55) which depends on the two line integrals (see Eq. (74))

$$S_r(\gamma_r; I_\alpha) = \int_{\gamma_r} V\frac{dr}{\Delta}, \qquad S_\vartheta(\gamma_\vartheta; I_\alpha) := \int_{\gamma_\vartheta} p_\vartheta d\vartheta, \tag{D1}$$

corresponding to the radial and polar motion, respectively. Also recall the relation between the quantities I_α defined in Eqs. (49–52) and the constants of motion $C = (C_\alpha) = (m, E, L_z, L)$, such that $I_0(C) = m$, $I_1(C) = L_z$, $I_2(C) = S_\vartheta(\circ; I_\alpha)/(2\pi)$ and $I_3(C) = S_r(\circ; I_\alpha)/(2\pi)$ where the symbol $\circ$ indicates that one takes a closed loop in the line integrals (D1). Therefore, the strategy consists in first computing the functions S_r and S_ϑ and their partial derivatives with respect to C_α (which have the form of open line integrals) and then to compute the action variables I_α and their derivatives with respect to C_α by "closing" the integrals.

Partial differentiation of S_ϑ with respect to $(C_\alpha) = (m, E, L_z, L)$ and taking into account the relation $p_\vartheta^2 = L^2 - K(\vartheta)$ with the functions $K(\vartheta)$ defined in Eq. (25) yields

$$\frac{\partial S_\vartheta}{\partial m} = -a_H^2 m\int_{\gamma_\vartheta}\cos^2\vartheta\frac{d\vartheta}{p_\vartheta}, \tag{D2}$$

$$\frac{\partial S_\vartheta}{\partial E} = a_H \int_{\gamma_\vartheta} (L_z - a_H E \sin^2\vartheta)\frac{d\vartheta}{p_\vartheta}, \tag{D3}$$

$$\frac{\partial S_\vartheta}{\partial L_z} = -\int_{\gamma_\vartheta} (L_z - a_H E \sin^2\vartheta)\frac{d\vartheta}{\sin^2\vartheta\, p_\vartheta}, \tag{D4}$$

$$\frac{\partial S_\vartheta}{\partial L} = L\int_{\gamma_\vartheta} \frac{d\vartheta}{p_\vartheta}. \tag{D5}$$

Similarly, taking into account the relation $V^2 = R(r)$ with $R(r)$ defined in Eq. (28), one obtains

$$\frac{\partial S_r}{\partial m} = -m \int_{(r,p_r)} \frac{r^2 dr}{V}, \tag{D6}$$

$$\frac{\partial S_r}{\partial E} = \int_{(r,p_r)} \frac{(r^2 + a_H^2)(r^2 E - a_H \hat{L}_z)}{\Delta}\frac{dr}{V}, \tag{D7}$$

$$\frac{\partial S_r}{\partial L_z} = -a_H \int_{(r,p_r)} \frac{r^2 E - a_H \hat{L}_z}{\Delta}\frac{dr}{V}, \tag{D8}$$

$$\frac{\partial S_r}{\partial L} = -L \int_{(r,p_r)} \frac{dr}{V}. \tag{D9}$$

For the following, we express these integrals in terms of Legendre's elliptic integrals. We find it convenient to work in terms of the dimensionless quantities defined in Eq. (B1).

Polar integrals. We start with the computation of the polar integrals, determined by the generating function $S_\vartheta(\vartheta; I_\alpha)$ and its partial derivatives with respect to $(C_\alpha) = (m, E, L_z, L)$. For this we set $\zeta := \cos\vartheta$ and write

$$p_\vartheta^2 = L^2 - K(\vartheta) = \left(\frac{M_H m}{\sin\vartheta}\right)^2 q(\zeta), \tag{D10}$$

with the polynomial

$$q(\zeta) := \alpha^2(1-\varepsilon^2)\zeta^4 - \left(\lambda^2 + 2\alpha\beta\varepsilon\lambda + \alpha^2\right)\zeta^2 + \lambda^2(1-\beta^2). \tag{D11}$$

Since $q(0) > 0$ and $q(1) = -\lambda_z^2 < 0$, this polynomial has two positive roots ζ_1, ζ_2 satisfying $0 < \zeta_1 < 1 < \zeta_2$, and the motion is restricted to the interval $[-\zeta_1, \zeta_1]$ which corresponds to $[\vartheta_1, \pi - \vartheta_1]$ in terms of the polar angle. Writing $q(\zeta) = \alpha^2(1-\varepsilon^2)(\zeta^2 - \zeta_1^2)(\zeta^2 - \zeta_2^2)$ one finds that the roots satisfy the relations

$$\zeta_1^2 + \zeta_2^2 = \frac{\lambda^2 + 2\alpha\beta\varepsilon\lambda + \alpha^2}{\alpha^2(1-\varepsilon^2)}, \tag{D12}$$

$$\zeta_1^2\zeta_2^2 = \frac{\lambda^2(1-\beta^2)}{\alpha^2(1-\varepsilon^2)}, \tag{D13}$$

when $\alpha \neq 0$, while in the non-rotating limit $\alpha = 0$ the polynomial q has the single root $\zeta_1 = \sqrt{1-\beta^2}$. In terms of the angle ϕ introduced in Eqs. (66,67) one finds the following expressions for the generating function S_ϑ:

$$S_\vartheta(\gamma_\vartheta; I_\alpha) = M_H m \frac{\lambda\sqrt{1-\beta^2}}{\zeta_1^3}\Big[\zeta_1^2\mathbb{E}_*(\phi,k_1) - k_1^2(1-\zeta_1^2)\mathbb{F}_*(\phi,k_1) \\ -(1-\zeta_1^2)(\zeta_1^2-k_1^2)\Pi_*(\phi,\zeta_1^2,k_1)\Big], \tag{D14}$$

where we recall that $k_1 = \zeta_1/\zeta_2$ and where the notation $\mathbb{E}_*(\phi,k)$ refers to the same integral as in Eq. (E6) with the lower integration limit replaced with $-\pi/2$, such that $\mathbb{E}_*(\phi,k_1) := \mathbb{E}(\phi,k_1) + \mathbb{E}(k_1)$, and similarly for $\mathbb{F}_*(\phi,k_1)$ and $\Pi_*(\phi,\zeta_1^2,k_1)$.

Similarly, one obtains from Eqs. (D2–D5),

$$\frac{\partial S_\vartheta}{\partial m} = M_H\mathbb{G}^0(\phi), \quad \frac{\partial S_\vartheta}{\partial E} = M_H\mathbb{G}^1(\phi), \quad \frac{\partial S_\vartheta}{\partial L_z} = \mathbb{G}^2(\phi), \quad \frac{\partial S_\vartheta}{\partial L} = \mathbb{G}^3(\phi), \tag{D15}$$

with the functions $\mathbb{G}^\alpha(\phi)$ defined by

$$\mathbb{G}^0(\phi) := -\frac{\alpha^2\zeta_1^3}{\lambda\sqrt{1-\beta^2}}\mathbb{D}_*(\phi,k_1), \tag{D16}$$

$$\mathbb{G}^1(\phi) := \frac{\alpha\beta\zeta_1}{\sqrt{1-\beta^2}}\mathbb{F}_*(\phi,k_1) - \varepsilon\mathbb{G}^0(\phi), \tag{D17}$$

$$\mathbb{G}^2(\phi) := \frac{\zeta_1}{\lambda\sqrt{1-\beta^2}}\Big[\alpha\varepsilon\mathbb{F}_*(\phi,k_1) - \lambda_z\Pi_*(\phi,\zeta_1^2,k_1)\Big], \tag{D18}$$

$$\mathbb{G}^3(\phi) := \frac{\zeta_1}{\sqrt{1-\beta^2}}\mathbb{F}_*(\phi,k_1). \tag{D19}$$

In the limit $\beta \to \pm 1$ of equatorial orbits it follows from Eqs. (D12,D13) that $\zeta_1 \to 0$ while ζ_2 and $\zeta_1/\sqrt{1-\beta^2}$ have finite limits, such that $k_1 = 0$, and in this case one finds that $\mathbb{G}^0 = 0$ vanishes, while $\mathbb{G}^1(\phi) = -\alpha\mathbb{G}^2(\phi)$, $\mathbb{G}^3(\phi) = -\beta\mathbb{G}^2(\phi)$ and $\mathbb{G}^2(\phi) = -\hat{\lambda}_z(\phi+\pi/2)/\sqrt{\lambda_z^2+\alpha^2(1-\varepsilon^2)}$.

In the non-rotating limit $\alpha \to 0$ one has $\zeta_1 \to \sqrt{1-\beta^2}$ and $\zeta_2 \to \infty$ such that $k_1 \to 0$ which implies that $\mathbb{G}^0(\phi)$ and $\mathbb{G}^1(\phi)$ vanish identically, whereas $\mathbb{G}^2(\phi) = -\beta\Pi_*(\phi,1-\beta^2,0)$ and $\mathbb{G}^3(\phi) = \phi + \pi/2$.

Radial integrals. Next, we compute the generating function $S_r(\gamma_r; I_\alpha)$ and its partial derivatives with respect to C_α. For this, recall that

$$V^2 = R(r) = (Er^2 - a_H\hat{L}_z)^2 - \Delta(r)(m^2r^2 + L^2). \tag{D20}$$

As discussed in the previous appendix, for $(m, E, L_z, L) \in \Omega$ the polynomial on the right-hand side has four real roots r_i, $i = 1, 2, 3, 4$, satisfying the inequalities

$$0 \leq r_3 < r_- < r_+ < r_4 < r_1 < r_2. \tag{D21}$$

Recalling the definitions of the elliptic integrals in Eqs. (E5–E8) (see also Eqs. (E1–E4) and (E9,E10)), the integrals in Eqs. (D6–D9) can be expressed in terms of the π-periodic angle χ introduced in Eqs. (62,63) and the quantities b, k and $\mathcal{C}$ defined in Eqs. (64) as follows:

$$\frac{\partial S_r}{\partial m} = M_H \mathbb{H}^0(\chi), \quad \frac{\partial S_r}{\partial E} = M_H \mathbb{H}^1(\chi), \quad \frac{\partial S_r}{\partial L_z} = \mathbb{H}^2(\chi), \quad \frac{\partial S_r}{\partial L} = \mathbb{H}^3(\chi), \tag{D22}$$

with the functions $\mathbb{H}^\alpha(\chi)$ defined by[16]

$$\begin{aligned}\mathbb{H}^0(\chi) := -\frac{\mathcal{C}}{2}\{&(x_4x_{124} - x_1x_2)\mathbb{F}(\chi,k) + (x_1-x_3)(x_2-x_4)\mathbb{E}(\chi,k)\\ &+(x_1-x_4)x_{1234}\Pi(\chi,b^2,k)\\ &-\frac{1}{2}(x_1-x_3)(x_2-x_1)\frac{\sin(2\chi)}{1-b^2\sin^2\chi}\Big\},\end{aligned} \tag{D23}$$

$$\begin{aligned}\mathbb{H}^1(\chi) := 2\mathcal{C}\Bigg\{&\left[\frac{x_4(\varepsilon x_4^2 - \alpha\beta\lambda)}{(x_4-x_+)(x_4-x_-)} - \frac{1}{2}\alpha\beta\lambda\right]\mathbb{F}(\chi,k) + \varepsilon(x_1-x_4)\Pi(\chi,b^2,k)\\ &-\frac{x_1-x_4}{x_+-x_-}\left[\frac{x_+(\varepsilon x_+^2-\alpha\beta\lambda)}{(x_1-x_+)(x_4-x_+)}\Pi(\chi,b_+^2,k) - (+\leftrightarrow -)\right]\Bigg\} - \varepsilon\mathbb{H}^0(\chi),\end{aligned} \tag{D24}$$

$$\begin{aligned}\mathbb{H}^2(\chi) := -\alpha\mathcal{C}\Bigg\{&\frac{\varepsilon x_4^2 - \alpha\beta\lambda}{(x_4-x_+)(x_4-x_-)}\mathbb{F}(\chi,k) - \frac{x_1-x_4}{x_+-x_-}\left[\frac{\varepsilon x_+^2-\alpha\beta\lambda}{(x_1-x_+)(x_4-x_+)}\right.\\ &\left.\Pi(\chi,b_+^2,k) - (+\leftrightarrow -)\right]\Bigg\},\end{aligned} \tag{D25}$$

$$\mathbb{H}^3(\chi) := -\lambda\mathcal{C}\mathbb{F}(\chi,k), \tag{D26}$$

where we have set

$$b_\pm := \sqrt{\frac{x_4-x_\pm}{x_1-x_\pm}}\,b. \tag{D27}$$

Note that in the non-rotating limit $\alpha \to 0$ or the limit of equatorial orbits $\beta \to \pm 1$ it follows that $x_3 \to 0$. It is also possible to compute the generating functions S_r itself. Based on the observation that

$$S_r(\gamma_r; \mathbb{I}(\mu m, \mu E, \mu L_z, \mu L)) = \mu S_r(\gamma_r; \mathbb{I}(m, E, L_z, L)) \tag{D28}$$

for all $\mu > 0$, which is a manifestation of the weak equivalence principle, one obtains the relation

$$S_r(\gamma_r; \mathbb{I}(m, E, L_z, L)) = m\frac{\partial S_r}{\partial m} + E\frac{\partial S_r}{\partial E} + L_z\frac{\partial S_r}{\partial L_z} + L\frac{\partial S_r}{\partial L}, \tag{D29}$$

[16] These functions are related to the functions $\mathbb{H}_0$, $\mathbb{H}_1$ and $\mathbb{H}_2$ introduced in [30] for equatorial orbits, in which case $x_3 = 0$ and x_4 was denoted by x_0. In fact, when S_r is restricted to $L = \pm\hat{L}_z = \pm(L_z - aE)$, the partial derivatives of S_r with respect to (m, E, L_z) obtained from Eq. (D22) are found to agree with the corresponding expressions in Eq. (A7) of Ref. [30].

which allows one to compute S_r from Eqs. (D22,D23–D26). After some simplifications based on the identity (C5) one finds

$$S_r(\gamma_r; I_\alpha) = \frac{M_H m \mathcal{C}}{x_{1234}} \{(x_1 - x_4)(x_2 - x_4)\mathbb{F}(\chi, k) - (x_1 - x_3)(x_2 - x_4)\mathbb{E}(\chi, k) + (x_1 - x_4)(x_{1234} - 4)\Pi(\chi, b^2, k) + \frac{1}{2}(x_1 - x_3)(x_2 - x_1)\frac{\sin(2\chi)}{1 - b^2 \sin^2 \chi} - 2\frac{x_1 - x_4}{x_+ - x_-}\left[(x_+ - x_3)(x_2 - x_+)\Pi(\chi, b_+^2, k) - (+ \leftrightarrow -)\right]\Big\}. \quad \text{(D30)}$$

Appendix E: List of Relevant Elliptic Integrals

In this appendix we briefly summarize some of the elliptic integral expressions that are relevant for the results in this article. The starting point is the fourth-order polynomial

$$\mathcal{R}(x) = (x_2 - x)(x - x_1)(x - x_3)(x - x_4),$$

where we assume that the four roots are real and ordered such that $x_3 < x_4 < x_1 < x_2$. Introducing the constants

$$k := \sqrt{\frac{x_4 - x_3}{x_1 - x_3}}b, \qquad b := \sqrt{\frac{x_2 - x_1}{x_2 - x_4}},$$

satisfying $0 < k < b < 1$, the variable substitution

$$\chi := \arcsin\left(\sqrt{\frac{x - x_1}{x_2 - x_1}\frac{x_2 - x_4}{x - x_4}}\right), \qquad x_1 < x < x_2,$$

leads to

$$\frac{dx}{\sqrt{\mathcal{R}(x)}} = \tilde{\mathcal{C}}\frac{d\chi}{\sqrt{1 - k^2 \sin^2 \chi}}. \qquad \tilde{\mathcal{C}} := \frac{2}{\sqrt{(x_1 - x_3)(x_2 - x_4)}}.$$

From this, one obtains the following integral expressions (see [37,59,60] for more details) which are valid for $x_1 < x < x_2$:

$$\int_{x_1}^{x} \frac{dy}{\sqrt{\mathcal{R}(y)}} = \tilde{\mathcal{C}}\mathbb{F}(\chi, k), \quad \text{(E1)}$$

$$\int_{x_1}^{x} \frac{y dy}{\sqrt{\mathcal{R}(y)}} = \tilde{\mathcal{C}}\left[x_4\mathbb{F}(\chi, k) + (x_1 - x_4)\Pi(\chi, b^2, k)\right], \quad \text{(E2)}$$

$$\int_{x_1}^{x} \frac{y^2 dy}{\sqrt{\mathcal{R}(y)}} = \frac{\tilde{\mathcal{C}}}{2}\left[(x_4 x_{124} - x_1 x_2)\mathbb{F}(\chi, k) + (x_1 - x_3)(x_2 - x_4)\mathbb{E}(\chi, k) + (x_1 - x_4)x_{1234}\Pi(\chi, b^2, k) - (x_2 - x_1)(x_1 - x_3)\frac{\cos\chi \sin\chi}{1 - b^2 \sin^2 \chi}\sqrt{1 - k^2 \sin^2 \chi}\right], \quad \text{(E3)}$$

$$\int_{x_1}^{x} \frac{1}{y-x_0}\frac{dy}{\sqrt{\mathcal{R}(y)}} = \frac{\tilde{\mathcal{C}}}{x_4-x_0}\left[\mathbb{F}(\chi,k) - \frac{x_1-x_4}{x_1-x_0}\Pi(\chi,b_0^2,k)\right], \tag{E4}$$

where here we have abbreviated $x_{124} := x_1+x_2+x_4$ and $x_{1234} := x_1+x_2+x_3+x_4$, x_0 is an arbitrary real constant smaller than x_4,

$$b_0 := \sqrt{\frac{x_4-x_0}{x_1-x_0}}b,$$

and where Legendre's integrals $\mathbb{F}$, $\mathbb{E}$ Π and $\mathbb{D}$ are defined by [61]

$$\mathbb{F}(\phi,k) := \int_0^{\phi} \frac{d\theta}{\sqrt{1-k^2\sin^2\theta}}, \qquad \mathbb{K}(k) := \mathbb{F}(\pi/2,k), \tag{E5}$$

$$\mathbb{E}(\phi,k) := \int_0^{\phi} \sqrt{1-k^2\sin^2\theta}\,d\theta, \qquad \mathbb{E}(k) := \mathbb{E}(\pi/2,k), \tag{E6}$$

$$\Pi(\phi,b^2,k) := \int_0^{\phi} \frac{d\theta}{\sqrt{1-k^2\sin^2\theta}(1-b^2\sin^2\theta)}, \qquad \Pi(k) := \Pi(\pi/2,k), \tag{E7}$$

$$\mathbb{D}(\phi,k) := \int_0^{\phi} \frac{\sin^2\theta\, d\theta}{\sqrt{1-k^2\sin^2\theta}}, \qquad \mathbb{D}(k) := \mathbb{D}(\pi/2,k). \tag{E8}$$

From Eq. (E4) one also obtains the integrals

$$\int_{x_1}^{x} \frac{1}{(y-x_+)(y-x_-)}\frac{dy}{\sqrt{\mathcal{R}(y)}} = \tilde{\mathcal{C}}\left\{\frac{\mathbb{F}(\chi,k)}{(x_4-x_+)(x_4-x_-)} - \frac{x_1-x_4}{x_+-x_-}\left[\frac{\Pi(\chi,b_+^2,k)}{(x_1-x_+)(x_4-x_+)} - (+\leftrightarrow -)\right]\right\}, \tag{E9}$$

$$\int_{x_1}^{x} \frac{y}{(y-x_+)(y-x_-)}\frac{dy}{\sqrt{\mathcal{R}(y)}} = \tilde{\mathcal{C}}\left\{\frac{x_4\mathbb{F}(\chi,k)}{(x_4-x_+)(x_4-x_-)} - \frac{x_1-x_4}{x_+-x_-}\left[\frac{x_+\Pi(\chi,b_+^2,k)}{(x_1-x_+)(x_4-x_+)} - (+\leftrightarrow -)\right]\right\}, \tag{E10}$$

for arbitrary $0 < x_- < x_+ < x_4$.

Index

$(\mathbf{P},\mathbf{q})$:	variables on reduced phase space $\hat{\Gamma}$ (Eq. 107)
C_α:	constants of motion (Eq. 42)
E:	particle energy (Eq. 12)
E_{ms}:	energy of marginally stable orbits (Page 12)
F_0, F_1, F_2, F_3:	integrals of motion (Eq. 15)
$H(x,p)$:	free particle Hamiltonian (Eq. 2)

J_α: generalized action variables (Eq. 45)
$K(\vartheta)$: potential for the polar motion (Eq. 25)
L: square root of Carter constant (Eq. 14)
L_z: azimuthal angular momentum of a particle (Eq. 13)
L_{ms}: square root of Carter constant for marginally stable orbits (Lemma 4)
M_H, a_H: Kerr black hole mass and rotation parameter (Eq. 7)
P_α: integrals of motion corresponding to C_α (Eq. 42)
Q^α: generalized angle variables (Eq. 47)
$R(r)$: polynomial associated with the radial motion (Eq. 28)
$S(\gamma_x; I_\alpha)$: generating function (Eq. 48)
$U(t)$: propagator describing the Liouville flow (Eq. 113)
$W_\pm(r)$: auxiliary functions relevant in the factorization of $R(r)$ (Eq. 40)
X, Y: special vector fields in the Kerr spacetime (Eq. 9)
X_H: Hamiltonian vector field associated with H (Eq. 2)
X_α: Hamiltonian vector fields generated by the integrals of motion F_α (Proposition 2)
Δ: Kerr metric function $\Delta(r) = r^2 - 2M_H r + a_H^2$ (Eq. 9)
Γ: relativistic one-particle phase space (Eq. 1)
$\Gamma^{(ext)}_{m,E,L_z,L}$: unique connected component of $\Gamma_{m,E,L_z,L}$ which lies entirely in the exterior region $r > r_+$ (Proposition 3)
Γ_0: a dense subset of Γ on which X_H is integrable (Proposition 2)
Γ_{bound}: phase space corresponding to spatially bound future-directed timelike geodesics which are confined to the exterior region (Eq. 41)
$\Gamma_{m,E,L_z,L}$: invariant subset of Γ of constant $C = (m, E, L_z, L)$ (Eq. 16)
Ω: range for the constants of motion corresponding to bound orbits (Proposition 3)
Ω_s: symplectic form on cotangent bundle T^*M (Page 6)
Θ: Poincaré one-form on T^*M (Eq. 5)
α: dimensionless rotation parameter (Proposition 3)
β: ratio $\hat{L}_z/L$ (Eq. B1)
η^1, η^2, η^3: Derivatives of Carter constant with respect to action variables (Eq. 98)
η_Γ: volume form on Γ (Eq. 6)
$\hat{\Gamma}$: reduced phase space (Eq. 110)
$\hat{\eta}$: volume form on $\hat{\Gamma}$ (Eq. 110)
κ: abbreviation for $\alpha\sqrt{1-\beta^2}$ (Eq. C31)
$\lambda_{sph}(x)$: dimensionless square root of Carter constant for spherical orbits with dimensionless radius x (Eq. B12)
$\omega^1, \omega^2, \omega^3$: fundamental frequencies associated with the azimuthal, polar and radial motion, respectively (Eq. 97)
ρ: Kerr metric function defined by $\rho^2(r, \vartheta) = r^2 + a_H^2 cos^2\vartheta$ (Eq. 7)
$\varepsilon_{sph}(x)$: dimensionless energy for spherical orbits with dimensionless radius x (Eq. B13)
m: particle rest mass (Eq. 11)
$p_{r\pm}(r)$: expression for the radial momentum (Eq. 37)
$q(\zeta)$: polynomial associated with the polar motion (Eq. D11)
q^1, q^2, q^3: angle variables associated with the azimuthal, polar and radial motion, respectively (Eqs. 100–102)
$r_\pm$: radii of inner and outer horizons (Eq. 7)

r_{max}:	radius of maximum of potential (Lemma 4)
r_{ms}:	radius of marginally stable orbits (Lemma 4)
r_{ph}:	radius of photon orbits (Lemma 4)
x_{mb}:	dimensionless radius of marginally bound orbits (Page 54)
x_{ms}:	dimensionless radius of marginally stable orbits (Page 54)
x_{ph}:	dimensionless radius of photon orbit (Page 54)
$\mathbf{A}$:	Jacobi matrix of the fundamental frequencies with respect to the action variables (Eq. 114)
$\mathbf{B}$:	Jacobi matrix of (η^1, η^2, η^3) with respect to the action variables (Eq. 114)
$\mathcal{K}$:	Carter constant (Eq. 14)
$\hat{L}_z$:	shifted azimuthal angular momentum $L_z - a_H E$ (Eq. 38)

References

1. Andréasson, H.: The Einstein-Vlasov system/kinetic theory. Living Rev. Relativ. **14**(4), 1–55 (2011)
2. Carter, B.: Global structure of the Kerr family of gravitational fields. Phys. Rev. **174**, 1559–1571 (1968)
3. Walker, M., Penrose, R.: On quadratic first integrals of the geodesic equations for type [22] spacetimes. Commun. Math. Phys. **18**, 265–274 (1970)
4. Sarbach, O., Zannias, T.: The geometry of the tangent bundle and the relativistic kinetic theory of gases. Class. Quantum Grav. **31**, 085013 (2014)
5. Bondi, H.: On spherically symmetrical accretion. Monthly Notices Roy Astronom. Soc. **112**, 195–204 (1952)
6. Michel, F.C.: Accretion of matter by condensed objects. Astrophys. Space Sci. **15**, 153–160 (1972)
7. Hoyle, F., Lyttleton, R.A.: The effect of interstellar matter on climatic variation. Proc. Camb. Philos. Soc. **35**, 405 (1939)
8. Bondi, H., Hoyle, F.: On the Mechanism of Accretion by Stars. Mon. Not. R. Astron. Soc. **104**(5), 273–282 (1944)
9. Rioseco, P., Sarbach, O.: Accretion of a relativistic, collisionless kinetic gas into a Schwarzschild black hole. Class. Quantum Grav. **34**(9), 095007 (2017)
10. Rioseco, P., Sarbach, O.: Spherical steady-state accretion of a relativistic collisionless gas into a Schwarzschild black hole. J. Phys. Conf. Ser. **831**(1), 012009 (2017)
11. Mach, P., Odrzywołek, A.: Accretion of the relativistic Vlasov gas onto a moving Schwarzschild black hole: Exact solutions. Phys. Rev. D **103**, 024044 (2021)
12. Mach, P., Odrzywołek, A.: Accretion of dark matter onto a moving Schwarzschild black hole: An exact solution. Phys. Rev. Lett. **126**, 101104 (2021)
13. Mach, P., Odrzywołek, A.: Accretion of the relativistic Vlasov gas onto a moving Schwarzschild black hole: low-temperature limit and numerical aspects. *Acta Phys. Pol. B Proc. Suppl.*, 15(1-A7), 2022. Presented at the 7th conference of the Polish Society on Relativity, Łódź, Poland, 20-23 (september 2021)
14. Gamboa, A., Gabarrete, C., Domínguez-Fernández, P., Núñez, D., Sarbach, O.: Accretion of a Vlasov gas onto a black hole from a sphere of finite radius and the role of angular momentum. Phys. Rev. D **104**, 083001 (2021)
15. Cieślik, A., Mach, P., Odrzywolek, A.: Accretion of the relativistic Vlasov gas in the equatorial plane of the Kerr black hole. Phys. Rev. D **106**, 104056 (2022)
16. Lebowitz, J.L., Penrose, O.: Modern ergodic theory. Phys. Today **26**(2), 23–29 (1973)
17. Cornfeld, I.P., Fomin, S.V., Sinai, Ya.G.: Ergodic Theory. Springer-Verlag, New York (1982)
18. Lynden-Bell, D.: The stability and vibrations of a gas of stars. Mon. Notices R. Astronom. Soc. **124**, 279–296 (1962)
19. Lynden-Bell, D.: Statistical mechanics of violent relaxation in stellar systems. Mon. Notices R. Astronom. Soc. **136**, 101–121 (1967)
20. Tremaine, S., Hénon, M., Lynden-Bell, D.: H-functions and mixing in violent relaxation. Mon. Notices R. Astronom. Soc. **219**, 285–297 (1986)
21. Merritt, D.: Elliptical galaxy dynamics. Publ. Astron. Soc. Pac. **111**(756), 129–168 (1999)
22. Tremaine, S.: The geometry of phase mixing. Mon. Notices R. Astronom. Soc. **307**, 877–883 (1999)
23. Mouhot, C., Villani, C.: On Landau damping. Acta Math. **207**, 29–201 (2011)
24. Young, B.: Landau damping in relativistic plasmas. J. Math. Phys. **57**, 021502 (2016)

25. Mathew, R., Tiesinga, E.: Phase-space mixing in dynamically unstable, integrable few-mode quantum systems. Phys. Rev. A **96**, 013604 (2017)
26. Dudnikova, T.V., Komech, A.I., Kopylova, E.A., Suhov, Y.M.: On convergence to equilibrium distribution, I. The Klein-Gordon equation with mixing. Comm. Math. Phys. **225**, 1–32 (2002)
27. Dudnikova, T.V., Komech, A.I., Ratanov, N.E., Suhov, Y.M.: On convergence to equilibrium distribution, II. The wave equation in odd dimensions, with mixing. J. Stat. Phys. **108**, 1219–1253 (2002)
28. Mitchell, C.: Weak convergence to equilibrium of statistical ensembles in integrable Hamiltonian systems. J. Math. Phys. **60**(15), 052702 (2019)
29. Rioseco, P., Sarbach, O.: Phase space mixing in external gravitational central potentials. Class. Quantum Grav. **37**(19), 195027 (2020)
30. Rioseco, P., Sarbach, O.: Phase space mixing in the equatorial plane of a Kerr black hole. Phys. Rev. D **98**(12), 124024 (2018)
31. Andersson, L., Blue, P., Joudioux, J.: Hidden symmetries and decay for the Vlasov equation on the Kerr spacetime. Comm. Partial Differ. Equ. **43**, 47–65 (2018)
32. Bigorgne, L.: Decay estimates for the massless Vlasov equation on Schwarzschild spacetimes. Ann. Henri Poincaré **24**(11), 3763–3836 (2023)
33. Andréasson, H.: Existence of steady states of the massless Einstein-Vlasov system surrounding a Schwarzschild black hole. Ann. Henri Poincaré **22**(12), 4271–4297 (2021)
34. Jabiri, F.E.: Stationary axisymmetric Einstein-Vlasov bifurcations of the Kerr spacetime. 2 (2022). arXiv:2202.10245 [math.AP]
35. Schmidt, W.: Celestial mechanics in Kerr space-time. Class. Quantum Grav. **19**, 2743–2764 (2002)
36. Hinderer, T., Flanagan, E.E.: Two timescale analysis of extreme mass ratio inspirals in Kerr. I. Orbital Motion. Phys. Rev. D **78**, 064028 (2008)
37. Fujita, R., Hikida, W.: Analytical solutions of bound timelike geodesic orbits in Kerr spacetime. Class. Quant. Grav. **26**, 135002 (2009)
38. Fiorani, E., Giachetta, G., Sardanashvily, G.: The Liouville-Arnold-Nekhoroshev theorem for non-compact invariant manifolds. J. Phys. A **36**, L101–L107 (2003)
39. Brink, J., Geyer, M., Hinderer, T.: Orbital resonances around black holes. Phys. Rev. Lett. **114**, 081102 (2015)
40. Brink, J., Geyer, M., Hinderer, T.: Astrophysics of resonant orbits in the Kerr metric. Phys. Rev. D **91**(8), 083001 (2015)
41. Acuña-Cárdenas, R., Gabarrete, C., Sarbach, O.: An introduction to the relativistic kinetic theory on curved spacetimes. Gen. Relativ. Gravit. **54**, 23 (2022)
42. Misner, C.W., Thorne, K.S., Wheeler, J.A.: Gravitation. W. H. Freeman, New York (1973)
43. Zehnder, E.: Lectures on Dynamical Systems: Hamiltonian Vector Fields and Symplectic Capacities. European Mathematical Society, Zurich (2010)
44. Arnold, V.I.: Mathematical Methods of Classical Mechanics. Springer-Verlag, New York (1989)
45. Mityagrin, B.S.: The zero set of a real analytic function. Math. Notes **107**, 529–530 (2020)
46. Lynden-Bell, D.: Stellar dynamics. Only isolating integrals should be used in Jeans theorem. Mon. Notices R. Astronom. Soc. **124**, 1–9 (1962)
47. Mo, H., van den Bosch, F., White, S.: Galaxy Formation and Evolution. Cambridge University Press, Cambridge (2010)
48. Poisson, E., Will, C.M.: Gravity. Cambridge University Press, Cambridge (2014)
49. Gabarrete, C., Sarbach, O.: Axisymmetric, stationary collisionless gas configurations surrounding Schwarzschild black holes. Class. Quant. Grav. **40**(5), 055012 (2023)
50. Gabarrete, C., Sarbach, O.: Kinetic gas disks surrounding Schwarzschild black holes. *Acta Phys. Pol. B Proc. Suppl.*, 15(1-A10), January 2022. Presented at the 7th conference of the Polish Society on Relativity, Łódź, Poland, 20-23 (september 2021)
51. Batt, J., Faltenbacher, W., Horst, E.: Stationary spherically symmetric models in stellar dynamics. E. Arch. Rational Mech. Anal. **93**, 159–183 (1986)
52. Schaeffer, J.: A class of counterexamples to Jeans' theorem for the Vlasov-Einstein system. Comm. Math. Phys. **204**, 313–327 (1999)
53. Chaturvedi, S., Luk, J.: Phase mixing for solutions to 1d transport equation in a confining potential. (2021)
54. Moreno, M., Rioseco, P., Van Den Bosch, H.: Mixing in an anharmonic potential well. J. Math. Phys. **63**, 071502 (2022)
55. Chandrasekhar, S.: The Mathematical Theory of Black Holes. Oxford University Press, Oxford (1992)
56. O'Neill, B.: The Geometry of the Kerr Black Holes. Dover Publications Inc, Mineola (2015)
57. Tejeda, E., Taylor, P.A., Miller, J.C.: An analytic toy model for relativistic accretion in Kerr spacetime. Mon. Not. R. Astron. Soc. **429**, 925 (2013)
58. Bardeen, J., Press, W., Teukolsky, S.: Rotating black holes: locally nonrotating frames, energy extraction, and scalar synchrotron radiation. Astrophys. J. **178**, 347–370 (1972)
59. Erdélyi, A. (ed.): Higher Transcendental Functions, vol. II. McGraw-Hill, New York (1953)

60. Abramowitz, M., Stegun, I.A.: Pocketbook of Mathematical Functions. Harri Deutsch, Thun (1984)
61. Digital library of mathematical functions. http://dlmf.nist.gov/

Communicated by E. Smith

Linear stability of nonrelativistic self-interacting boson stars

Emmanuel Chávez Nambo,[1] Alberto Diez-Tejedor,[2] Armando A. Roque,[3,2] and Olivier Sarbach[1]

[1]*Instituto de Física y Matemáticas, Universidad Michoacana de San Nicolás de Hidalgo, Edificio C-3, Ciudad Universitaria, 58040 Morelia, Michoacán, México*

[2]*Departamento de Física, División de Ciencias e Ingenierías, Campus León, Universidad de Guanajuato, C.P. 37150, León, México*

[3]*Unidad Académica de Física, Universidad Autónoma de Zacatecas, 98060 Zacatecas, México*

(Received 15 February 2024; accepted 2 April 2024; published 6 May 2024)

In this paper, we study the linear stability of self-interacting boson stars in the nonrelativistic limit of the Einstein-Klein-Gordon theory. For this purpose, based on a combination of analytic and numerical methods, we determine the behavior of general linear perturbations around the stationary and spherically symmetric solutions of the Gross-Pitaevskii-Poisson system. In particular, we conclude that ground state configurations are linearly stable if the self-interaction is repulsive, whereas there exists a state of maximum mass that divides the stable and the unstable branches in case the self-interaction is attractive. Regarding the excited states, they are in general unstable under generic perturbations, although we identify a stability band in the first excited states of the repulsive theory. This result is independent of the mass of the scalar field and the details of the self-interaction potential, and it is in contrast to the situation of vanishing self-interaction, in which excited states are always unstable.

DOI: 10.1103/PhysRevD.109.104011

I. INTRODUCTION

The Einstein-Klein-Gordon system constitutes a nonlinear field theory that allows regular and localized configurations that do not disperse in time [1,2]. These configurations are usually referred to as boson stars [3–9], and their theoretical existence is possible due to the equilibrium between the repulsive "pressure" of the scalar field and the attractive nature of the gravitational interaction. In its simplest realization, the Klein-Gordon equation consists only of the kinetic and the mass term, although boson star solutions also exist if self-interactions are included [10–19].

The phenomenological relevance of boson stars depends crucially on their stability properties. Spherically symmetric ground state configurations are known to consist of a stable and an unstable branch [20] divided by the state of maximum mass [21]. This holds true in absence of self-interactions, as well as for the theory with a quartic self-interaction potential $\lambda|\phi|^4$, and has been established through a combination of semianalytic studies of the linearized equations [20,21] and numerical simulations [22,23] of the fully nonlinear field equations in spherical symmetry. Regarding the excited states, there exist different studies in the literature with different conclusions. On the one hand, in Ref. [24], Jetzer argues that for the spherically symmetric excited states, there also exist stable and unstable branches that are divided by the state of maximum mass, similarly to what happens for ground state configurations, although his analysis relies on a pulsation equation that is singular at the nodes. In Ref. [25], Lee and Pang use different analytical arguments to conclude that, on the contrary, excited states are unstable, at least in absence of self-interactions. Finally, based on numerical evolutions of the spherically symmetric Einstein-Klein-Gordon equations, Balakrishna *et al.* [26] have confirmed that excited configurations are unstable, even if quartic self-interactions are considered. Full 3D numerical evolutions are currently available and lead to similar conclusions regarding the stability of boson stars under generic perturbations (for details, see, e.g., Sec. 4 of [7] and references therein).

However, in a series of recent papers, Sanchis-Gual *et al.* [27] and Brito *et al.* [28] have argued that if the self-interaction is repulsive and strong enough, excited boson stars may be stable. Their conclusion is based on the numerical evolution of perturbed boson stars in the spherically symmetric sector of the fully nonlinear Einstein-Klein-Gordon theory with quartic self-interactions. In particular, they find excited configurations in which no apparent instabilities are manifest during the time span of the evolution, indicating that these states are either stable or are unstable with a large time scale associated with the unstable modes. Of course, the restriction to spherical symmetry leaves open the possibility that such excited states, although stable with respect to radial perturbations, suffer from instabilities with respect to generic perturbations.

The purpose of this paper is to shed new light on the stability problem of excited boson stars in the self-interacting case. For this, we concentrate on the Newtonian limit of the theory, where the complications of relativistic

effects are absent and which, as we show, allows for a systematic study of this problem in the linearized case. In the nonrelativistic limit, the Einstein-Klein-Gordon system reduces to the Gross-Pitaevskii-Poisson [8,29,30] or the Schrödinger-Poisson [31–33] system, depending on whether or not the theory includes a self-interaction term. The Gross-Pitaevskii-Poisson system is particularly relevant for the study of axion dark matter candidates (see, for instance, Refs. [34–43]), and it is the main target of this paper. In galaxies, and leaving the central region apart (which is baryon dominated), visible matter moves at velocities that are much smaller than the speed of light, signaling that it might be sufficient to describe dark matter haloes using Newtonian physics. In addition, since the axion potential is nonlinear [44], self-interactions are indeed expected to play a relevant role.

In particular, our study is based on some analytic and numerical methods that have been previously developed to analyze the linear stability of the equilibrium configurations of the Schrödinger-Poisson system [45,46]. When applied to the Gross-Pitaevskii-Poisson system, we obtain that spherically symmetric ground state configurations are stable if the self-interaction is repulsive, in analogy to what happens in the non-self-interacting case, and there exists a state of maximum mass that divides the stable and the unstable branch in the case of an attractive self-interaction [12,13]. This is similar to what happens for relativistic nonself-interacting boson stars, although it is important to stress that the existence of a maximum mass state is now determined by the attractive self-interaction and not by relativistic effects. Furthermore, our analysis allows us to consider generic linear perturbations and is not restricted to the radial case.

Regarding the excited states, our study reveals that, even if they are, in general, unstable, there exist configurations belonging to the first excited state that remain stable under generic linear perturbations when the effects of a repulsive self-interaction become significant. More specifically, for the solution space that we have explored in this paper, if the self-interaction is attractive, as well as in absence of self-interactions, spherically symmetric excited boson stars are unstable under radial perturbations and hence generically unstable. However, in case that the self-interaction is repulsive, there exist excited configurations that remain stable under radial perturbations, at least for the first two excited states that we have considered. The existence of radially stable excited states is consistent with the results reported in Refs. [27,28], as will be discussed. Furthermore, we extend this analysis to consider generic perturbations that do not necessarily respect the spherical symmetry of the stationary states and conclude that only a small region in the solution space corresponding to the first excited states remains stable under generic perturbations.

In this paper, we work in natural units where $c = \hbar = 1$ and use the $(-,+,+,+)$ signature convention for the spacetime metric. For convenience, we sometimes express Newton's constant G in terms of the Planck mass, $M_{\rm Pl} \equiv 1/\sqrt{G}$.

II. SELF-INTERACTING SCALAR FIELDS

Our starting point is the Einstein-Klein-Gordon theory for a complex scalar field $\phi(t,\vec{x})$ of mass m_0 and quartic self-interaction $\lambda|\phi|^4$. This theory is described in terms of the action

$$S[g_{\mu\nu},\phi] = \int d^4x\sqrt{-g}\left(\frac{1}{16\pi G}R + \mathcal{L}_M\right), \tag{1a}$$

which consists on the Einstein-Hilbert term with matter sector

$$\mathcal{L}_M = -\nabla_\mu\phi^*\nabla^\mu\phi - m_0^2|\phi|^2 - \lambda|\phi|^4. \tag{1b}$$

As usual, g is the determinant of the spacetime metric $g_{\mu\nu}$, R is the Ricci scalar, and ϕ^* denotes the complex conjugate of ϕ, with $|\phi|^2$ its modulus square. The coupling constant λ is dimensionless and can take both signs, depending on whether the self-interaction is repulsive ($\lambda > 0$) or attractive ($\lambda < 0$). In case that λ vanishes, we recover a theory with no self-interactions, where the scalar field is only coupled to gravity. For illustrative purposes, we have restricted ourselves to a quartic self-interaction, although our conclusions are independent of the potential, as we clarify in the next subsection and the Appendix A.

A. Nonrelativistic limit

In the nonrelativistic regime we are interested in, it is convenient to write the spacetime line element in the form[1]

$$ds^2 = -[1+2\Phi(t,\vec{x})]dt^2 + [1-2\Psi(t,\vec{x})]\delta_{ij}dx^i dx^j, \tag{2a}$$

and decompose the scalar field into

$$\phi(t,\vec{x}) = \frac{1}{\sqrt{2m_0}}e^{-im_0t}\psi(t,\vec{x}), \tag{2b}$$

where $\Phi(t,\vec{x})$ and $\Psi(t,\vec{x})$ are the gravitational potentials, and $\psi(t,\vec{x})$ is the wave function. In the nonrelativistic limit, the different quantities scale as $\partial_t \sim \epsilon^{1/2}\partial_i \sim \epsilon m_0$, $\Phi \sim \Psi \sim \epsilon$ and $\psi \sim \sqrt{M_{\rm Pl}^2 m_0}\epsilon$, with ϵ a small positive number.

[1]Equation (2a), which is expressed in the Newtonian gauge, codifies only the scalar degrees of freedom of the gravitational field [i.e., for fixed t, the fields $\Phi(t,\vec{x})$ and $\Psi(t,\vec{x})$ transform as scalars under spatial rotations]. Vector and tensor modes do not couple to nonrelativistic matter, and we have not included them here for simplicity.

Introducing the decomposition (2) into the action (1) and working to the lowest orders in ϵ we arrive at

$$S[\Phi,\Psi,\psi]=\int dt\int d^3x\left[\frac{1}{8\pi G}\Psi\Delta(2\Phi-\Psi)+\psi^*\left(i\frac{\partial}{\partial t}+\frac{1}{2m_0}\Delta-\frac{\lambda}{4m_0^2}|\psi|^2\right)\psi-m_0\Phi|\psi|^2\right], \tag{3}$$

where Δ refers to the three-dimensional flat Laplace operator. In order of appearance, the first term of this equation describes the gravitational field, the second term the matter sector, and the last one the interaction between the two. Note that there are no time derivatives of the gravitational potentials in the action of Eq. (3). This is a consequence of the fact that gravity is not dynamical in the nonrelativistic limit.

Equation (3) is cubic in the small parameter ϵ, except for the self-interaction term, which contains four powers of ϵ, which suggests that its effect is negligible for small field amplitudes. However, this term is multiplied by the coupling constant λ, which indicates that it starts to contribute when the amplitude of the field is sufficiently large, such that $\epsilon\sim m_0^2/(\lambda M_{\rm Pl}^2)$. This allows us to introduce the self-interaction parameter

$$\Lambda\coloneqq\frac{|\lambda|M_{\rm Pl}^2}{2\pi m_0^2}, \tag{4}$$

which is dimensionless and measures the "strength" of the self-interaction. Note that, given that m_0 is expected to be much smaller than the Planck mass, the parameter Λ is naturally large. In Appendix A, we argue that Eq. (3) is, in fact, valid for potentials $V(\phi)$, which are more general than the quartic self-interaction one.

The variation of Eq. (3) with respect to the wave function ψ results in the Gross-Pitaevskii equation [47,48]

$$i\frac{\partial\psi}{\partial t}=-\frac{1}{2m_0}\Delta\psi\pm\frac{\pi\Lambda}{M_{\rm Pl}^2}|\psi|^2\psi+m_0\mathcal{U}\psi, \tag{5a}$$

whereas the variation with respect to Ψ yields (after integration by parts and discarding boundary terms) $\Delta(\Phi-\Psi)=0$. Assuming that Φ and Ψ vanish at infinity, this implies that $\Phi=\Psi$. Finally, variation of Eq. (3) with respect to Φ results in the Poisson equation

$$\Delta\mathcal{U}=4\pi G m_0|\psi|^2 \tag{5b}$$

for the gravitational potential $\mathcal{U}\coloneqq\Phi=\Psi$. The $\pm$ signs in Eq. (5a) make reference to the repulsive (+) and attractive (−) cases. We will refer to the system of equations (5) as the Gross-Pitaevskii-Poisson system. Note that if the self-interaction term vanishes, i.e., $\Lambda=0$, this reduces to the more familiar Schrödinger-Poisson system.

The nonrelativistic action, Eq. (3), is invariant under time translations, which means that the evolution of the system is not affected by shifts in the time parameter t. Associated to this symmetry, we can define the total energy of the configuration,

$$\mathcal{E}=\int\left(\frac{1}{2m_0}|\nabla\psi|^2\pm\frac{\pi\Lambda}{2M_{\rm Pl}^2}|\psi|^4+\frac{1}{2}m_0\mathcal{U}|\psi|^2\right)d^3x, \tag{6}$$

which is conserved during the evolution. In addition, Eq. (3) is also invariant under continuous shifts in the phase of the wave function, $\psi\mapsto e^{i\alpha}\psi$, with α a real constant, which results in the conservation of the particle number

$$N=\int|\psi|^2d^3x. \tag{7}$$

Other conserved quantities associated with the Galilei group do exist; however, they will not be used in this article. For a systematic study of symmetries and conserved quantities for $\Lambda=0$, see Refs. [49–51].

B. Reformulation in terms of dimensionless quantities

In this section, we formulate the Gross-Pitaevskii-Poisson system in a more convenient form. To proceed, we introduce the dimensionless quantities

$$\bar{t}\coloneqq\frac{2m_0}{\Lambda}t,\qquad \bar{x}\coloneqq\frac{2m_0}{\Lambda^{1/2}}x, \tag{8a}$$

$$\bar{\mathcal{U}}\coloneqq\frac{\Lambda}{2}\mathcal{U},\qquad \bar{\psi}\coloneqq\left(\frac{\pi\Lambda^2}{2M_{\rm Pl}^2m_0}\right)^{1/2}\psi. \tag{8b}$$

In terms of these new variables, the Gross-Pitaevskii (5a) and Poisson (5b) equations simplify to

$$i\frac{\partial\psi}{\partial t}=(-\Delta\pm|\psi|^2+\mathcal{U})\psi, \tag{9a}$$

$$\Delta\mathcal{U}=|\psi|^2, \tag{9b}$$

where we have omitted the bars in order to simplify the presentation (from now on, we will denote dimensionfull quantities with the superscript *phys* whenever necessary).

Equivalently, Eq. (9) can be expressed as an integro-differential nonlinear equation

$$i\frac{\partial\psi}{\partial t}=\hat{\mathcal{H}}(\psi)\psi, \tag{10}$$

where we have defined the dimensionless operator

$$\hat{\mathcal{H}}(\psi)\coloneqq-\triangle\pm|\psi|^2+\triangle^{-1}(|\psi|^2), \tag{11}$$

and where for a generic function $f(\vec{x})$, we have introduced

$$\Delta^{-1}(f)(\vec{x}) \coloneqq -\frac{1}{4\pi}\int \frac{f(\vec{y})}{|\vec{x}-\vec{y}|}d^3y. \tag{12}$$

Note that in terms of the variables (8), the parameter Λ disappears from our equations; hence, all possible values of the coupling constant λ can be explored at the same time, implying that our results do not depend on the strength of the self-interaction.

In terms of the dimensionless quantities, the conserved energy functional (6) $\mathcal{E}^{\text{phys}}[\psi^{\text{phys}}] = [M_{\text{Pl}}^2/(m_0\Lambda^{3/2}\pi)]\mathcal{E}[\psi]$ can be expressed in the form

$$\mathcal{E}[\psi] = T[\psi] \pm F[n] - D[n,n], \qquad n \coloneqq |\psi|^2, \tag{13}$$

where the functionals T, F, and D are defined by

$$T[\psi] \coloneqq \frac{1}{2}\int |\nabla\psi(\vec{x})|^2 d^3x, \tag{14a}$$

$$F[n] \coloneqq \frac{1}{4}\int n(\vec{x})^2 d^3x, \tag{14b}$$

$$D[n,n] \coloneqq \frac{1}{16\pi}\int\int \frac{n(\vec{x})n(\vec{y})}{|\vec{x}-\vec{y}|}d^3yd^3x. \tag{14c}$$

Furthermore, the first and second variations of the energy functional are given by (see Appendix B of Ref. [45] for some details on a similar calculation)

$$\delta\mathcal{E} = \text{Re}(\hat{\mathcal{H}}(\psi)\psi, \delta\psi), \tag{15a}$$

$$\delta^2\mathcal{E} = \text{Re}(\hat{\mathcal{H}}(\psi)\psi, \delta^2\psi) + (\hat{\mathcal{H}}(\psi)\delta\psi, \delta\psi) \pm 2F[\delta n] - 2D[\delta n, \delta n], \tag{15b}$$

with $\delta n \coloneqq 2\text{Re}(\psi^*\delta\psi)$ and $(\psi,\phi) = \int \psi^*\phi d^3x$ denoting the standard L^2-scalar product between ψ and ϕ, such that $(\psi,\psi) = N$.

III. STATIONARY STATES AND THEIR LINEAR STABILITY

In this section, we focus on scalar field configurations of the form

$$\psi(t,\vec{x}) = e^{-iEt}\sigma^{(0)}(\vec{x}), \tag{16}$$

where $\sigma^{(0)}$ is a real-valued function of $\vec{x}$ and E a real constant.[2] Introducing this ansatz into Eq. (10) we arrive at the nonlinear eigenvalue problem:

$$E\sigma^{(0)} = \hat{\mathcal{H}}(\sigma^{(0)})\sigma^{(0)}. \tag{17}$$

The integro-diferential equation (17) determines the stationary solutions to the Gross-Pitaevskii-Poisson system.

The stability of these solutions is determined by the behavior of the small deviations about Eq. (16). To proceed, we linearize the integro-differential equation (10) following the procedure presented in Refs. [33,45]. With this in mind, we propose the following ansatz for the wave function

$$\psi(t,\vec{x}) = e^{-iEt}[\sigma^{(0)}(\vec{x}) + \epsilon\sigma(t,\vec{x}) + \mathcal{O}(\epsilon^2)], \tag{18}$$

where ϵ is a small positive parameter. Here, $(E,\sigma^{(0)})$ is a solution of the nonlinear eigenvalue problem (17), and σ is a complex-valued function depending on $(t,\vec{x})$ that describes the linear perturbation.

Introducing the ansatz (18) into Eq. (10), one obtains, to linear order in ϵ,

$$i\frac{\partial\sigma}{\partial t} = (\hat{\mathcal{H}}^{(0)} - E)\sigma + 2\sigma^{(0)}\hat{K}[\sigma^{(0)}\text{Re}(\sigma)], \tag{19}$$

with the linear operators $\mathcal{H}^{(0)} \coloneqq \mathcal{H}(\sigma^{(0)})$ and

$$\hat{K} \coloneqq \pm 1 + \triangle^{-1}. \tag{20}$$

To separate the temporal from the spatial parts of σ, we use the mode ansatz (see also Sec. 5.2 in [52] for details):

$$\sigma(t,\vec{x}) = [A(\vec{x}) + B(\vec{x})]e^{\lambda t} + [A(\vec{x}) - B(\vec{x})]^* e^{\lambda^* t}, \tag{21}$$

where A and B are complex-valued functions depending only on $\vec{x}$ and λ is a complex constant [not to be confused with the self-interaction coupling constant λ of Eq. (1b)]. Substituting Eq. (21) into Eq. (19) and setting the coefficients in front of $e^{\lambda^* t}$ and $e^{\lambda t}$ to zero, we arrive at

$$i\lambda A = (\hat{\mathcal{H}}^{(0)} - E)B, \tag{22a}$$

$$i\lambda B = (\hat{\mathcal{H}}^{(0)} - E)A + 2\sigma^{(0)}\hat{K}[\sigma^{(0)}A]. \tag{22b}$$

This system constitutes a linear eigenvalue problem for the constant λ. Notice that linear instability is signaled by the existence of solutions with a positive real part λ_R of λ. The lifetime of the unstable configurations is expected to be of the order of $t_{\text{life}} \sim 1/\lambda_R^{\max}$, with $\lambda^{\max}$ the eigenvalue with the largest real part.

A. Basic properties of the stationary states

Next, we present some basic properties satisfied by the solutions of Eq. (17), based on a simple scaling argument similar to the one used in Ref. [53]. In Sec. IV B, these properties will be used to shed light on the stability of stationary states in the attractive case.

[2]Since the operator $\hat{\mathcal{H}}(\sigma^{(0)})$ is real, in the sense that $\hat{\mathcal{H}}(\sigma^{(0)})\psi^* = (\hat{\mathcal{H}}(\sigma^{(0)})\psi)^*$, there is no restriction in demanding that $\sigma^{(0)}$ is real valued.

To explain our scaling argument, recall that stationary states are critical points of the energy functional (13), assuming that the particle number $N = (\psi, \psi)$ is fixed. To show this, we may use Eqs. (15a) and (17), which imply that stationary states (16) satisfy $\delta\mathcal{E} = E\mathrm{Re}(\sigma^{(0)}, \sigma)$. On the other hand, since N is fixed, $0 = \mathrm{Re}(\psi, \delta\psi) = \mathrm{Re}(\sigma^{(0)}, \sigma)$, which implies that $\delta\mathcal{E} = 0$.

Now, let $\nu > 0$ be an arbitrary real and positive parameter and $\psi(t, \vec{x})$ a given wave function. Consider the rescaled function

$$\psi_\nu(t, \vec{x}) \coloneqq \nu^{3/2}\psi(t, \nu\vec{x}), \tag{23}$$

which leaves the particle number invariant: $(\psi_\nu, \psi_\nu) = (\psi, \psi)$. Under this rescaling, the energy functional (13) transforms as

$$\mathcal{E}[\psi_\nu] = \nu^2 T[\psi] \pm \nu^3 F[n] - \nu D[n, n], \tag{24}$$

and the first and second variations of $\mathcal{E}[\psi_\nu]$ at $\psi_{\nu=1} = \psi$ are

$$\frac{d}{d\nu}\mathcal{E}[\psi_\nu]\Big|_{\nu=1} = 2T[\psi] \pm 3F[n] - D[n, n], \tag{25a}$$

$$\frac{d^2}{d\nu^2}\mathcal{E}[\psi_\nu]\Big|_{\nu=1} = 2T[\psi] \pm 6F[n]. \tag{25b}$$

In particular, if ψ is a stationary solution, the first variation is zero, which yields the relation

$$D[n, n] = 2T[\psi] \pm 3F[n]. \tag{26}$$

This expression is valid for any stationary solution and allows one to eliminate $D[n, n]$ in the energy functional and compute the energy for such states solely in terms of $T[\psi]$ and $F[n]$ according to

$$\mathcal{E}[\psi] = -T[\psi] \mp 2F[n]. \tag{27}$$

This expression implies that the energy of the stationary states is always negative in the repulsive case. In the attractive case, it follows from Eq. (24) that $\mathcal{E}[\psi_\nu]$ is not bounded from below, since it can be made arbitrarily negative by choosing ν large. According to Eq. (25b), the critical point at $\nu = 1$ corresponds to a local minimum of $\mathcal{E}[\psi_\nu]$ if $T - 3F > 0$ and to a local maximum if $T - 3F < 0$. It follows from these observations that in the attractive case, a stationary state ψ cannot be a (local) minimum of the energy functional if $T < 3F$, that is, when the self-interaction term dominates the kinetic term.

B. Basic properties of the linearized equations

We close this section by reviewing some properties of the solutions to the system of Eq. (22) that describe the behavior of linear perturbations. These properties and their derivation are completely analogous to the ones reported in [46]; hence, we only mention the most relevant ones.

First, note that there always exists the zero-mode solution $(\lambda, A, B) = (0, 0, \beta\sigma^{(0)})$, with β an arbitrary complex constant. This corresponds to the trivial perturbation that rotates the real function $\sigma(\vec{x})$ into the complex plane, resulting in a new configuration $\psi(t, \vec{x})$ that is indistinguishable from (16).

Second, the solutions to the Eq. (22) appear always in quadruples; that is, if (λ, A, B) is a solution, then $(-\lambda, A, -B)$, $(\lambda^*, A^*, -B^*)$ and $(-\lambda^*, A^*, B^*)$ are also solutions. This implies that the eigenvalues λ appear always in the form $\{\lambda, -\lambda, \lambda^*, -\lambda^*\}$. Linear stability requires that all eigenvalues λ are purely imaginary. In the remainder of this work, we shall count the number of unstable modes by the number of eigenvalues with distinct real part. Hence, when both the real and imaginary parts of λ are different from zero, we count the pair of eigenvalues λ and λ^* as one unstable mode, although they may belong to two linearly independent eigenfunctions.

Third, from Eq. (15b), we obtain the following expression for the second variation of the energy functional,

$$\delta^2\mathcal{E} = (\delta\psi, [\hat{\mathcal{H}}^{(0)} - E]\delta\psi) \pm 2F[\delta n] - 2D[\delta n, \delta n], \tag{28}$$

which is quadratic in $\delta\psi$. Note that we have used the second variation of $(\psi, \psi) = N = \text{const}$ to eliminate the term containing $\delta^2\psi$, and recall that $\delta n = 2\mathrm{Re}(\psi^*\delta\psi)$. The second variation of the energy functional $\delta^2\mathcal{E}$ is related to the linearized equations in the following way: Multiplying Eq. (22b) by A^* and Eq. (22a) by B^* and integrating, one obtains

$$i\lambda(A, B) = \delta^2\mathcal{E}[A_R] + \delta^2\mathcal{E}[A_I], \tag{29a}$$

$$i\lambda(B, A) = (B, [\hat{\mathcal{H}}^{(0)} - E]B), \tag{29b}$$

where A_R, A_I denotes the real and imaginary parts of A, respectively, and $\delta^2\mathcal{E}[A_R]$ is given by Eq. (28) replacing $\delta\psi$ with A_R. The right-hand sides of the previous equations are real; thus,

$$-\lambda^2|(A, B)|^2 \in \mathbb{R}. \tag{30}$$

Finally, if λ is real, one can choose A real and B purely imaginary. Eliminating $i\lambda A$ on the left-hand side of Eq. (29a) and using Eq. (22a), one gets

$$-(B, [\hat{\mathcal{H}}^{(0)} - E]B) = \delta^2\mathcal{E}[A]. \tag{31}$$

Equations (29)–(31) are useful to rule out the existence of certain unstable modes. For example, consider a stationary state for which E is the ground state energy of the Schrödinger operator $\hat{\mathcal{H}}^{(0)}$. Then, $(B, [\hat{\mathcal{H}}^{(0)} - E]B) \geq 0$ with

equality if and only if B lies in the kernel of $\hat{\mathcal{H}}^{(0)} - E$. This immediately excludes the existence of modes with $\lambda_R \neq 0$ and $\lambda_I \neq 0$ since in this case, Eq. (30) would imply that $(A, B) = 0$, and then one could infer that $A = B = 0$ using Eqs. (22) and (29b). If, in addition, this state is a local minimum of the energy functional, such that $\delta^2\mathcal{E}$ is positive or zero, then unstable modes with $\lambda_I = 0$ are also ruled out since in this case, Eqs. (22) and (31) imply that $A = B = 0$. These arguments show that stationary ground state configurations can have only real or purely imaginary λ and that real eigenvalues are excluded if these configurations are a local minimum of the energy functional $\mathcal{E}$.

Similar arguments will be applied to exclude other types of unstable modes in the next section.

IV. STATIONARY AND SPHERICALLY SYMMETRIC SOLUTIONS

For the remainder of this article, we focus on stationary solutions which are spherically symmetric, i.e., $\sigma^{(0)}(\vec{x}) = \sigma^{(0)}(r)$. In the next subsection, we discuss the background (unperturbed) solutions, whereas some properties of the linearized perturbations are discussed in subsequent subsections. A detailed study of the linear stability based on a numerical analysis is presented in Sec. V.

A. Background configurations

Instead of solving directly the integro-differential equation (17), for a numerical analysis, it is more convenient to work with the original Gross-Pitaevskii-Poisson system (9). Introducing the harmonic ansatz (16) into Eq. (9) and defining the shifted potential $u^{(0)}(r) \coloneqq E - \mathcal{U}(r)$, the dimensionless Gross-Pitaevskii-Poisson equations take the form

$$\Delta_s \sigma^{(0)} = \left(\pm\sigma^{(0)2} - u^{(0)}\right)\sigma^{(0)}, \tag{32a}$$

$$\Delta_s u^{(0)} = -\sigma^{(0)2}, \tag{32b}$$

where $\Delta_s \coloneqq \frac{1}{r}\frac{d^2}{dr^2}r$ denotes the radial Laplace operator.

The system of equations (32) must be solved for some appropriate boundary conditions. Regularity at the origin demands $\sigma^{(0)}(r=0) = \sigma_0$, $\sigma^{(0)\prime}(r=0) = 0$, $u^{(0)}(r=0) = u_0$, and $u^{(0)\prime}(r=0) = 0$. (Here and in the following, the prime refers to derivation with respect to r.) Then, given u_0, the central amplitude of the field σ_0 is fine-tuned using a numerical shooting methodology based on the condition $\lim_{r\to\infty}\sigma(r) = 0$ at spatial infinity, which is required for the solution to be localized.

The system (32) is solved numerically using an adaptive explicit 5(4)-order Runge-Kutta routine [54–56], where we rewrite the equations as a first-order system for the fields $(\sigma^{(0)}, u^{(0)})$. For the shooting, we use a methodology similar to the one described in [32], based on bisection.

Some representative solutions of the stationary and spherically symmetric Gross-Pitaevskii-Poisson system are shown in Figs. 1 and 2 for the ground ($n = 0$) and the first excited ($n = 1$) states, respectively.

In these figures, the mass of the configurations M^{phys} has been calculated as their particle number Eq. (7) times the mass m_0 of the individual particles, which leads to $M^{\text{phys}} = [M_{\text{Pl}}^2/(4\pi m_0 \Lambda^{1/2})]M$, where $M \coloneqq 4\pi\int_0^\infty [\sigma^{(0)}(r)]^2 r^2 dr$ is the dimensionless mass. Note that, formally, the radius of a

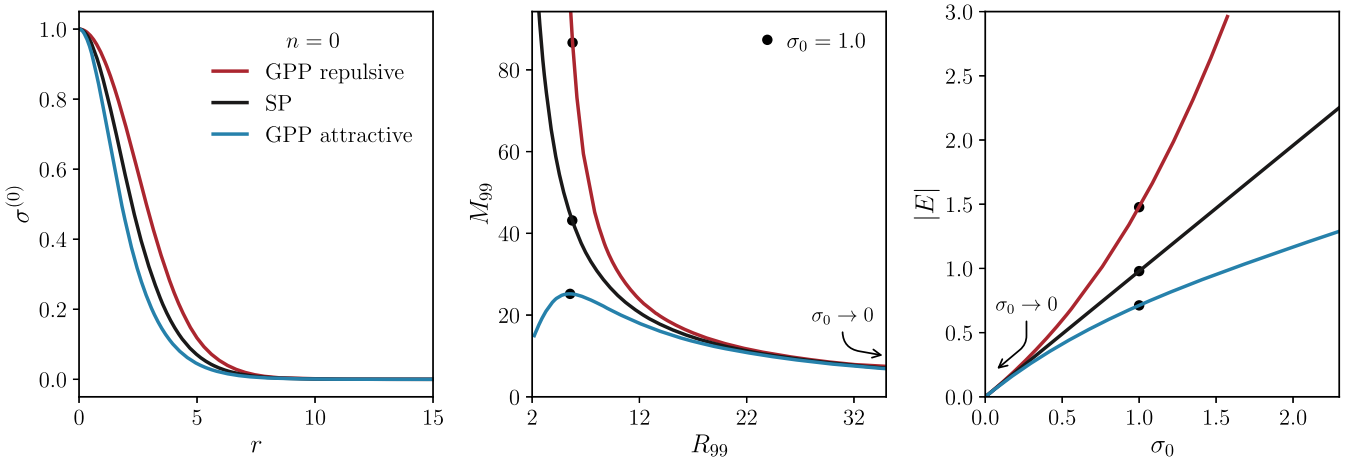

FIG. 1. Ground state configurations: Stationary and spherically symmetric solutions of the Gross-Pitaevskii-Poisson system with no nodes ($n = 0$). Red (blue) lines correspond to the repulsive (attractive) case, and we have included the solutions to the Schrödinger-Poisson system (black lines) for reference. Left panel: the profile of the wave function $\sigma^{(0)}(r)$ for a central value of unity, $\sigma_0 = 1$. Center panel: the effective mass of the configurations M_{99} as a function of the effective radius R_{99}. Right panel: the magnitude of the energy eigenvalue $|E|$ as a function of the central amplitude σ_0. The dots in the last two panels correspond to the configurations of unit amplitude. For $\sigma_0 \to 0$, the effects of the self-interactions become negligible.

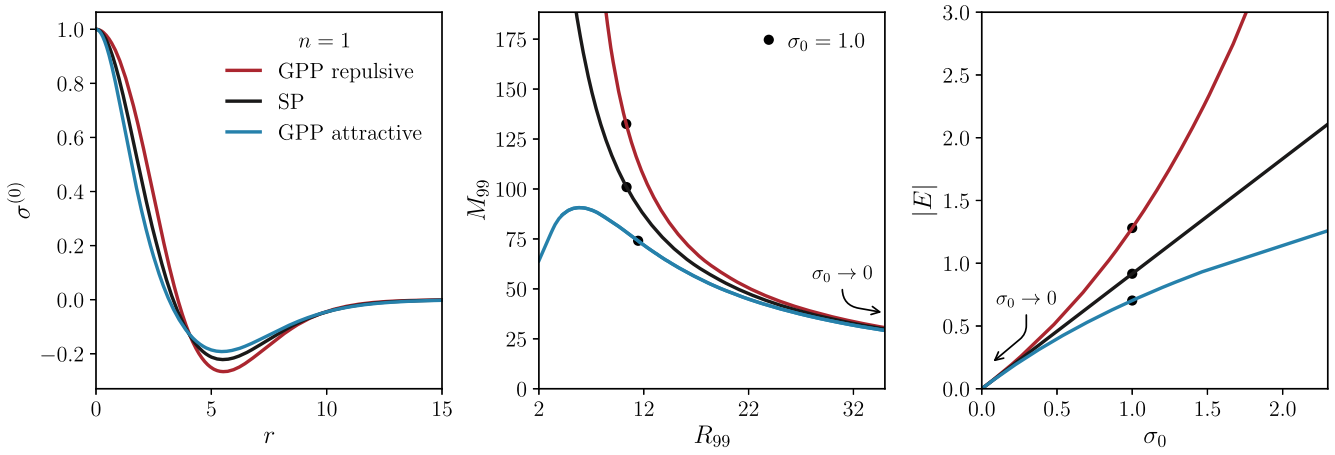

FIG. 2. First excited state configurations: Same as in Fig. 1 but for the stationary and spherically symmetric solutions of the Gross-Pitaevskii-Poisson system with one node ($n = 1$).

boson star extends to infinity, and for that reason, we have defined the effective radius R_{99} as the one encompassing 99% of the total mass of the configuration, M_{99}. On the other hand, the energy eigenvalue $E^{\rm phys} = [2m_0/\Lambda]E$ associated with the state $\sigma^{(0)}(r)$ can be computed from the formula (see Appendix C in Ref. [45] for more details)

$$E = u_0 - \int_0^\infty [\sigma^{(0)}(r)]^2 r dr. \tag{33}$$

As expected, the profile of the configurations expands (shrinks) if the self-interaction is repulsive (attractive), as can be appreciated in the left panels of Figs. 1 and 2. Furthermore, in the repulsive case, the configurations become more compact as we increase the value of the central amplitude, as also occurs for the stationary and spherically symmetric solutions of the Schrödinger-Poisson system, whereas in the case in which the self-interaction is attractive, there exists a state of maximum mass corresponding to a central amplitude $\sigma_0^{M_{99}^{\rm max}}$; see the central panel of Figs. 1 and 2 and Refs. [12,13,18]. Finally, it is also interesting to stress that in the limit $\sigma_0 \to 0$, the attractive and the repulsive configurations approach the solutions to the Schrödinger-Poisson system; see the central and right panels of the same figures. This implies that the effects of the self-interactions become negligible in the limit of low amplitudes, as is also apparent from the Gross-Pitaevskii-Poisson system (5).

In Fig. 3, we plot the total energy $\mathcal{E}$ of the configurations as a function of the total number of particles N for the ground and first two excited states. Note that the energy functional (6) consists of three terms: The first of them is a consequence of the "quantum pressure" and is positive definite. The second one is associated with the self-interaction and can be positive or negative, depending on whether the self-interaction is repulsive or attractive, respectively. Finally, the last term is associated with the gravitational interaction, which is attractive and negative definite. It is interesting to note that in the repulsive case, as well as if there are no self-interactions, the total energy is negative definite, and its magnitude increases with the number of particles. Furthermore, for a given value of N, the energy also increases with the number of nodes n in the configuration. This allows us to label the number of the excited states with n, as is usually done. However, this behavior changes for the case of an attractive self-interaction, where, for a given n, there is a state of minimum energy (which coincides with the state of maximum mass), and from this point onward, the energy increases up to positive values.

B. Stability properties based on a scaling argument (attractive case)

Recall from Sec. III A that in the attractive case, a stationary configuration cannot be a local minimum of the energy functional if $T - 3F < 0$. When the central value of the scalar field σ_0 is small, the configurations resemble the ones of the Schrödinger-Poisson system, and hence, the self-interaction term F is negligible, such that $T > 3F$ is expected to hold. In contrast, as σ_0 grows, the influence of the self-interaction becomes more pronounced (see Figs. 1 and 2), and one expects $3F$ to surpass the value of T after some critical value of σ_0.

The plots in Fig. 4 show that these expectations are indeed fulfilled. Interestingly, the critical value of σ_0 for which $T - 3F = 0$ seems to coincide with the maximum of the mass in the center panels of Figs. 1 and 2. As will be discussed in the next section, when this critical value is surpassed, the number of unstable modes grows by one.

For completeness, Fig. 5 shows the behavior of the energy functional under the rescaling (23) and illustrates that stationary states with positive (negative) values of $T - 3F$ represent a local minimum (maximum) with respect to this particular variation.

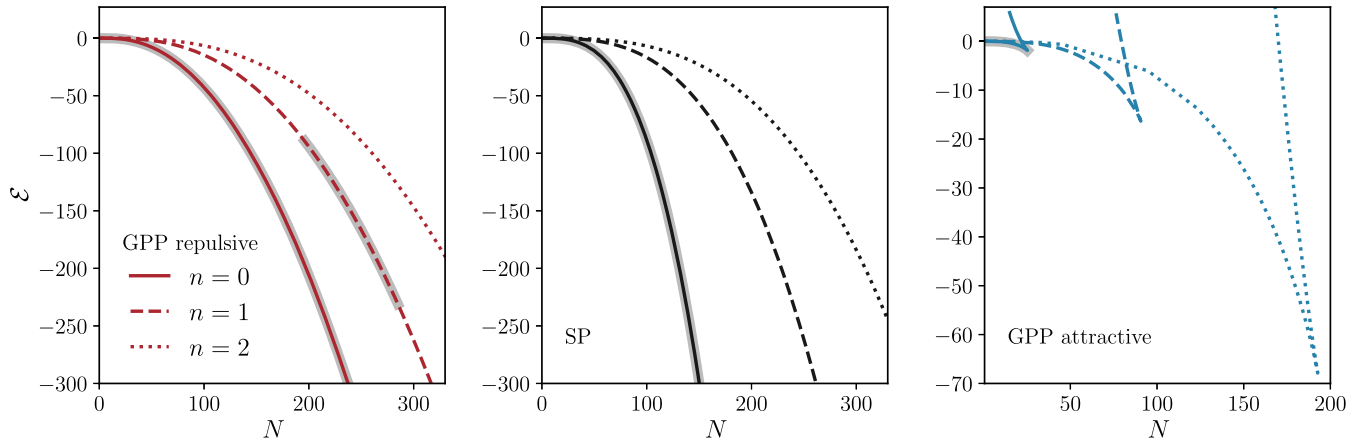

FIG. 3. The energy $\mathcal{E}$ of the states as a function of their number of particles N: Relationship between the energy functional (27) and the particle number N for states with zero, one, and two nodes in the repulsive, non-self-interacting and attractive cases. Note that in the attractive case, the number of nodes n does not necessarily label the number of the excited state. The shaded regions represent the stability bands with respect to generic linear perturbations discussed in Sec. V.

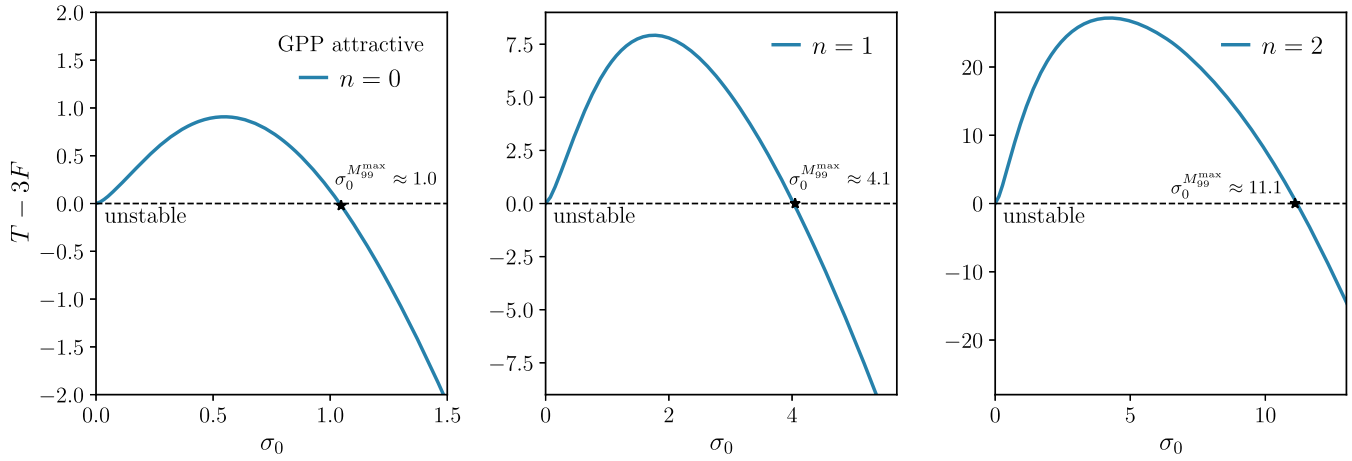

FIG. 4. The combination $T - 3F$ as a function of the central amplitude σ_0 for different values of the node number n in the attractive case: Configurations with a negative value of $T - 3F$ correspond to stationary states that represent critical points of the energy functional that cannot be local minima, and hence, they are expected to be unstable. The stars denote the maximum mass configurations at $\sigma_0 = \sigma_0^{M_{99}^{\max}}$; see also Fig. 5, which complements these plots.

C. Decomposition of the linearized system into spherical harmonics

Since the background solution is spherically symmetric, the linearized equations can be decoupled into a family of purely radial systems by expanding the perturbations in terms of spherical harmonics Y^{LM}. In particular, the field $A(\vec{x})$ can be expanded as

$$A(\vec{x}) = \sum_{LM} A_{LM}(r) Y^{LM}(\vartheta, \varphi), \tag{34}$$

and similarly for $B(\vec{x})$. This reduces Eq. (22) to the following system:

$$i\lambda A_{LM} = (\hat{\mathcal{H}}_L^{(0)} - E) B_{LM}, \tag{35a}$$

$$i\lambda B_{LM} = (\hat{\mathcal{H}}_L^{(0)} - E) A_{LM} + 2\sigma^{(0)} \hat{K}_L [\sigma^{(0)} A_{LM}], \tag{35b}$$

with the operators $\hat{\mathcal{H}}_L^{(0)}$ and $\hat{K}_L$ defined by

$$\hat{\mathcal{H}}_L^{(0)} := -\triangle_L \pm \sigma^{(0)2} + \triangle_s^{-1}(\sigma^{(0)2}), \tag{36a}$$

$$\hat{K}_L := \pm 1 + \triangle_L^{-1}, \tag{36b}$$

where $\triangle_L := \triangle_s - L(L+1)/r^2$ and

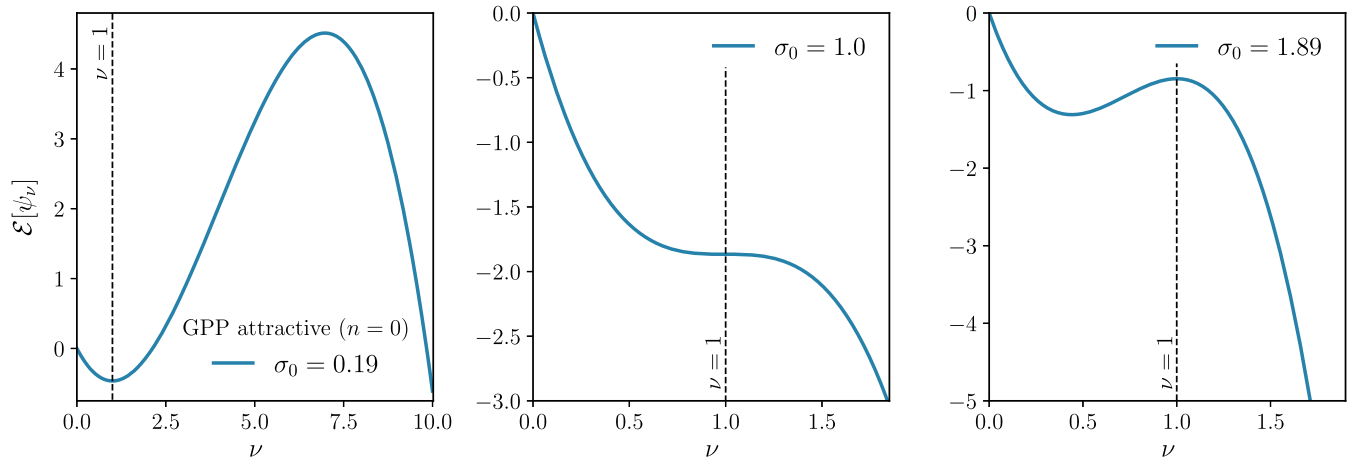

FIG. 5. Scaling the energy functional as $\psi_\nu(t,\vec{x}) = \nu^{3/2}\psi(t,\nu\vec{x})$ for attractive ground state configurations: The energy functional $\mathcal{E}[\psi_\nu]$ as a function of ν for three ground state configurations. Left panel: stationary state with $\sigma_0 = 0.19 < \sigma_0^{M_{99}^{\max}}$ giving $T = 0.558$ and $F = 0.047$. This state could be a local (but not a global) minimum of the energy functional and hence could be stable. Center panel: stationary state with $\sigma_0 = 1.0 = \sigma_0^{M_{99}^{\max}}$ giving $T = 5.641$ and $F = 1.887$. This state resembles a saddle point of the energy functional. Right panel: stationary state with $\sigma_0 = 1.89$ giving $T = 11.411$ and $F = 5.282$. This state cannot be a local minimum of the energy functional and is expected to be unstable.

$$\triangle_L^{-1}(f)(r) := -\frac{1}{2L+1}\int_0^\infty \frac{r_<^L}{r_>^{L+1}} f(\tilde{r})\tilde{r}^2 d\tilde{r}, \tag{37}$$

with $r_< := \min\{r,\tilde{r}\}$ and $r_> := \max\{r,\tilde{r}\}$. Note, in particular, that $\Delta_s = \Delta_{L=0}$.

In the next section, this system will be solved numerically for $L = 0, 1, 2, \ldots$. Before doing that, however, we prove that no unstable modes are present if L is large enough, which, in principle, reduces the numerical analysis to a finite number of L values.

D. Nonexistence of unstable modes for sufficiently large L

In this subsection, we show that if the orbital angular momentum L of the perturbation is large enough, then there are no unstable modes. The arguments below generalize the ones in Sec. IV. C of Ref. [46] to include the self-interaction term.

Using the estimate (E8) for $D[\delta n, \delta n]$ in Appendix E of Ref. [46], one obtains from Eq. (28) the inequality[3]

$$\delta^2\mathcal{E} \geq \frac{1}{2}(\nabla\delta\psi, \nabla\delta\psi) + (\delta\psi, [\pm\sigma^{(0)2} + U_0 - E]\delta\psi) - C_1(\delta\psi/f, \delta\psi/f) \pm 2F[\delta n], \tag{38}$$

where $U_0 := \triangle^{-1}(|\sigma^{(0)}|^2)$, $C_1 > 0$ is a positive constant, and $f(\vec{x}) := \sqrt{1+|\vec{x}|^2}$. In the repulsive case, the term $+2F[\delta n]$ on the right-hand side of Eq. (38) is positive and hence can be discarded without altering the inequality. In the attractive case, we use the estimate $|\delta n|^2 \leq 4|\psi|^2|\delta\psi|^2$, which implies

$$F[\delta n] \leq \max_{\vec{x}\in\mathbb{R}^3}[(1+|\vec{x}|^2)|\psi(\vec{x})|^2](\delta\psi/f, \delta\psi/f). \tag{39}$$

Since $|\psi|$ is smooth and decays exponentially to zero as $|\vec{x}| \to \infty$, the maximum is finite. Therefore, the negative term $-2F[n]$ on the right-hand side of Eq. (38) can be removed after making the constant C_1 larger.

Based on these results, we can prove that $\delta^2\mathcal{E}$ is positive definite for sufficiently large values of the orbital angular momentum L. To this purpose, we expand $\delta\psi$ in spherical harmonics

$$\delta\psi = \sum_{LM} h_{LM}(r)Y^{LM}(\vartheta,\varphi). \tag{40}$$

Substituting this in expression (38) and discarding the terms that involve $|h'_{LM}(r)|^2$, one gets

$$\delta^2\mathcal{E} \geq \sum_{LM}\left\{\int_0^\infty |h_{LM}(r)|^2\left[\frac{L(L+1)}{2} - C_1\right]dr + \int_0^\infty |h_{LM}(r)|^2[\pm\sigma^{(0)}(r)^2 + U_0(r) - E]r^2 dr\right\}. \tag{41}$$

First we look at the integrand in the second line and observe that the function $g(r) := [\pm\sigma^{(0)}(r)^2 + U_0(r) - E]r^2$ satisfies $g(0) = 0$ since $\sigma^{(0)}$ and U_0 are regular at the center, whereas $g(r)$ is positive for large enough r. This implies (since U_0 is continuous) that $g(r)$ has a minimum; that is,

[3]Note that the left-hand side of Eq. (E8) in [46] should read $D[\delta n, \delta n]$ instead of $D[\delta u, \delta u]$.

$g(r) \geq C_2$ for all $r \geq 0$ for some negative constant C_2. Using these properties, the estimate (41) yields

$$\delta^2\mathcal{E} \geq \sum_{LM} \int_0^\infty |h_{LM}(r)|^2 \left[\frac{L(L+1)}{2} - C_1 + C_2\right] dr. \quad (42)$$

Therefore, $\delta^2\mathcal{E}$ is positive definite if h_{LM} is identically zero for all L with $L(L+1)/2 - C_1 + C_2 \leq 0$. This proves that the second variation of the energy functional is positive definite on the subspace of perturbations with large enough values of L.

Now we can prove the nonexistence of unstable modes for large L. We proceed by contradiction. If λ has real and imaginary parts different from zero, then Eq. (30) yields $(A, B) = 0$, and in this case, Eq. (29) and the positivity of $\delta^2\mathcal{E}$ imply that $A = B = 0$. On the other hand, if λ is real, Eq. (31) leads to a contradiction since the right-hand side is positive, whereas the left-hand side is negative for sufficiently large values of L.

V. NUMERICAL STUDY OF THE LINEARIZED SYSTEM

To find the eigenvalues λ of the system (35), we use the methodology described in Refs. [45,46], for which it is convenient to write the system of equations in a more appropriate form. For this, we define the new rescaled functions $a_L(r) \coloneqq rA_{LM}(r)$ and $b_L(r) \coloneqq rB_{LM}(r)$, in terms of which the system (35) reduces to

$$b_L'' \mp |\sigma^{(0)}|^2 b_L + U_L^{\text{eff}} b_L = -i\lambda a_L, \quad (43a)$$

$$a_L'' + U_L^{\text{eff}} a_L \mp 3|\sigma^{(0)}|^2 a_L - 2\alpha\sigma^{(0)}\left(\frac{d^2}{dr^2} - \frac{L(L+1)}{r^2}\right)^{-1}[\sigma^{(0)} a_L] = -i\lambda b_L. \quad (43b)$$

Here, we have introduced the effective potential $U_L^{\text{eff}}(r) \coloneqq u^{(0)}(r) - L(L+1)/r^2$, and the operator $(d^2/dr^2 - L(L+1)/r^2)^{-1} = r\triangle_L^{-1} r^{-1}$ denotes the inverse of $r\triangle_L(r^{-1})$ with homogeneous Dirichlet boundary conditions at $r = 0$ and $r \to \infty$. Given that the system (35) is independent of the magnetic quantum number M, we have omitted this label in Eq. (43).

These equations must be solved for some appropriate boundary conditions. To determine these conditions, one can study (heuristically) the dominant terms near the origin and at spatial infinity. Near $r = 0$, the equations are dominated by the centrifugal term $L(L+1)/r^2$ of the effective potential U_L^{eff}, which means that regular solutions at the center must behave as $(a_L, b_L) \sim (r^{L+1}, r^{L+1})$. This leads to the following boundary conditions at the origin:

$$a_L(r=0) = 0, \qquad b_L(r=0) = 0. \quad (44a)$$

On the other hand, in the asymptotic region, the radial profile of the background field $\sigma^{(0)}(r)$ decays exponentially to zero and $u^{(0)}(r)$ approaches E. This implies that the fields (a_L, b_L) must vanish at infinity,

$$\lim_{r\to\infty} a_L(r) = 0, \qquad \lim_{r\to\infty} b_L(r) = 0, \quad (44b)$$

in order to have solutions with finite total energy.

To numerically solve the system (43) with the Dirichlet boundary conditions (44), we employ the following approach: First, the background profiles $\sigma^{(0)}(r)$ and $u^{(0)}(r)$ are computed following the method described in Sec. IV, and they are extended to large values of r using the procedure described in Sec. III.A of [45]. Second, these background profiles, as well as the perturbed fields a_L, b_L and the different operators, e.g., the derivative and its inverse, are discretized in terms of Chebyshev polynomials using a standard spectral method (see, e.g., Ref. [57]), which leads to a finite-dimensional eigenvalue problem. For details of the numerical discretization procedure, we refer the reader to Sec. IV of Ref. [45].

The discrete version of the system (43) can be written as

$$\begin{pmatrix} 0 & \tilde{\mathbb{D}}_{\mathsf{N}}^2 \mp \Sigma_0^2 + \mathsf{U}_L^{\text{eff}} \\ \tilde{\mathbb{D}}_{\mathsf{N}}^2 \mp 3\Sigma_0^2 + \mathsf{U}_L^{\text{eff}} - 2\alpha\Sigma_0(\tilde{\mathbb{D}}_{\mathsf{N}}^2 - \mathbb{L})^{-1}\Sigma_0 & 0 \end{pmatrix} \begin{pmatrix} \mathsf{a}_L \\ \mathsf{b}_L \end{pmatrix} = -i\lambda \begin{pmatrix} \mathsf{a}_L \\ \mathsf{b}_L \end{pmatrix}, \quad (45)$$

where here 0 represents the $(\mathsf{N}-1)\times(\mathsf{N}-1)$ zero matrix, with N the number of Chebyshev points distributed as $x_j = \cos(j\pi/\mathsf{N})$, $j = 0, 1, \ldots, \mathsf{N}$. The quantities

$$\Sigma_0 \coloneqq \mathbf{diag}\big(\sigma^{(0)}(x_1), \sigma^{(0)}(x_2), \ldots, \sigma^{(0)}(x_{\mathsf{N}-1})\big),$$
$$\mathsf{U}_L^{\text{eff}} \coloneqq \mathbf{diag}\big(U_L^{\text{eff}}(x_1), U_L^{\text{eff}}(x_2), \ldots, U_L^{\text{eff}}(x_{\mathsf{N}-1})\big),$$
$$\mathbb{L} \coloneqq \mathbf{diag}\left(\frac{L(L+1)}{x_1^2}, \frac{L(L+1)}{x_2^2}, \ldots, \frac{L(L+1)}{x_{\mathsf{N}-1}^2}\right)$$

are the discrete representation of the background quantities and centrifugal term, respectively, and the discrete operator $\tilde{\mathbb{D}}_{\mathsf{N}}$ is defined in [45]. The vector

$$\begin{pmatrix} \mathsf{a}_L \\ \mathsf{b}_L \end{pmatrix} \coloneqq (a_L(x_1), \ldots, a_L(x_{\mathsf{N}-1}), b_L(x_1), \ldots, b_L(x_{\mathsf{N}-1}))^T$$

represents the eigenfields $r(A_{LM}, B_{LM})^T$. We solve the discrete eigenvalue problem (45) using the SciPy library [54]. Our code is publicly available in [58].

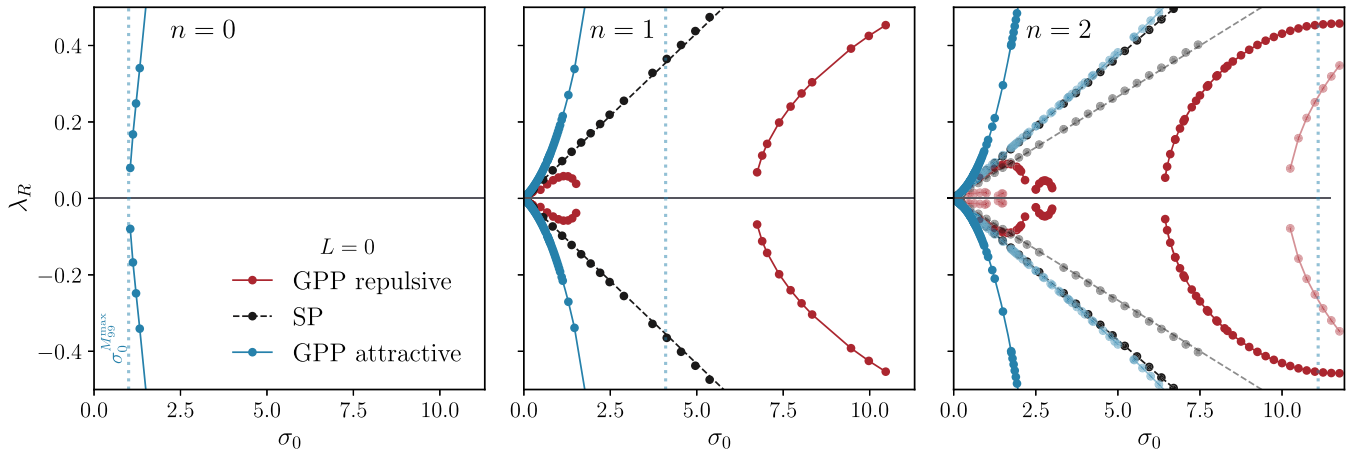

FIG. 6. Spherically symmetric perturbations: The real part of the frequency λ as a function of the central amplitude σ_0 for perturbations with $L = 0$ in configurations with $n = 0$, 1, and 2 nodes. The existence of modes with a real positive part of the frequency indicates the existence of an instability. The different color shades correspond to different unstable modes, and for reference, we have included dotted vertical lines in blue to indicate the state of maximum mass $\sigma_0^{M_{99}^{\max}}$ in the attractive case. The circles denote our numerical results, whereas the dashed lines represent the scaled results of the n unstable modes reported in Ref. [46] for the Schrödinger-Poisson system. For the repulsive and the attractive cases, we use straight solid lines to connect the numerical results and improve the visualization. Ground state configurations ($n = 0$) are stable for any value of the amplitude if the self-interaction is repulsive, or if there is no self-interaction, and they are unstable for large enough amplitudes ($\sigma_0 \gtrsim \sigma_0^{M_{99}^{\max}} \approx 1.0$) if the self-interaction is attractive. Excited states ($n \neq 0$) are in general unstable, although certain bands of stability in the amplitude σ_0 appear if the self-interaction is repulsive.

In the following subsections, we present the results of the eigenvalue problem, first for the ground state configurations and then for the excited states.

A. Ground state

As we have discussed in previous sections, the Gross-Pitaevskii-Poisson system describes three possible scenarios: one characterized by the absence of self-interactions (where the Gross-Pitaevskii-Poisson equations reduce to the Schrödinger-Poisson system), another where the self-interaction is repulsive, and a third scenario where the self-interaction is attractive.

For ground state configurations ($n = 0$), we have found that, for the explored range of the parameter space ($0 < \sigma_0 < 10$, $0 \leq L \leq 12$ for the repulsive and $0 < \sigma_0 < 5$, $0 \leq L \leq 6$ for the attractive case), the first two scenarios exhibit a similar behavior under linear perturbations. In particular, the configurations are always stable under spherically symmetric perturbations ($L = 0$), as can be appreciated from the left panel of Fig. 6. Furthermore, nonspherical perturbations ($L \neq 0$) do not either exhibit unstable modes that grow in time, at least for $L \leq 12$, as can be seen in the left panel of Fig. 7 for $L = 1$ and the left panel of Fig. 8 for other values of L in the repulsive case. The results corresponding to the scenario without self-interactions are consistent with those reported in [46] and coincide with the repulsive and the attractive cases in the limit $\sigma_0 \to 0$.

Contrary to the first two scenarios, the case with an attractive self-interaction presents ground state configurations that are unstable under radial perturbations ($L = 0$). More precisely, we found unstable modes with $\lambda_R > 0$ when $\sigma_0 \gtrsim 1$; see the left panel of Fig. 6. This gives rise to a family of solutions that is stable for $\sigma_0 \lesssim 1$ and unstable for $\sigma_0 \gtrsim 1$. Interestingly, the division between the stable and unstable states seems to coincide with the maximum mass configuration at $\sigma_0 = \sigma_0^{M_{99}^{\max}} \approx 1$. This is consistent with the turning-point principle; see Refs. [59–61], the Appendix C2 of the published version of [62], and in particular Ref. [21] for a discussion in the context of relativistic boson stars. Regarding nonspherical perturbations, no unstable modes appear when $L = 1$, as is appreciated from the left panel of Fig. 7. Based on a more extensive study within the aforementioned parameter range, we found no unstable modes for $L > 0$, as can be seen from the left panel of Fig. 9.

B. Excited states (spherical perturbations)

The excited states of the Schrödinger-Poisson system are known to be unstable under radial perturbations [33]. However, in presence of self-interactions, our analysis (carried out in the range $0 < \sigma_0 < 14$ with $0 \leq L \leq 12$ and $0 \leq L \leq 6$ in the repulsive and attractive cases, respectively) reveals an interesting pattern of stability and instability bands, with a particular relevance for the case where the self-interaction is repulsive. Our study focuses on the first two excited states ($n = 1$ and $n = 2$) of the Gross-Pitaevskii-Poisson equations; however, we expect that the behavior discussed below will continue to be valid for higher excited states.

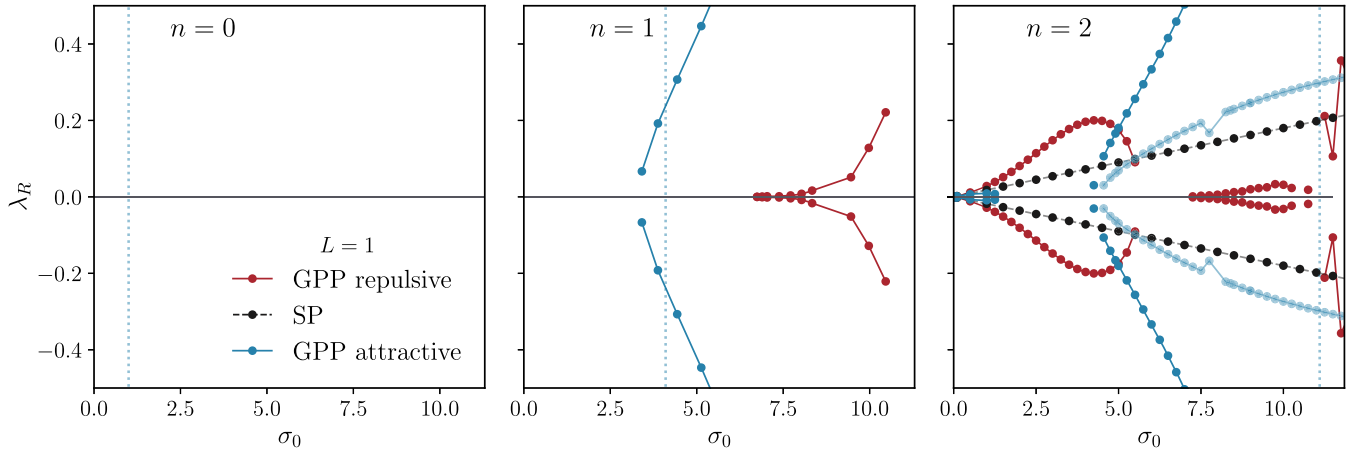

FIG. 7. Nonspherical perturbations ($L = 1$): Same as in Fig. 6 but for perturbations with $L = 1$. The ground state ($n = 0$) is always stable under such perturbations, no matter if the self-interaction is attractive, repulsive, or absent. Excited states ($n \neq 0$) present stability bands for the repulsive and attractive cases.

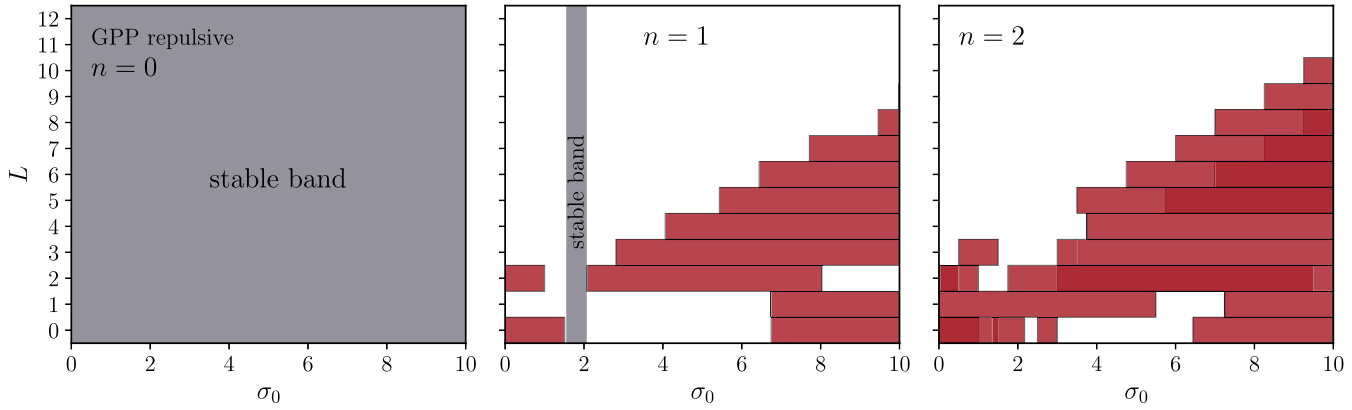

FIG. 8. Stability band structure (repulsive case): The shaded regions in red represent, for different values of L in the interval from 0 to 12, the amplitudes σ_0 for which the system posses unstable modes. Lighter (darker) colors indicate the presence of one (two) unstable mode(s). Note that the ground state ($n = 0$) does not present unstable modes for any value of σ_0 or L, so we can conclude that it is stable. In contrast, the first excited state ($n = 1$) presents a common stability band in the interval $1.55 \lesssim \sigma_0 \lesssim 2.07$, whereas this band is empty for the second excited state ($n = 2$).

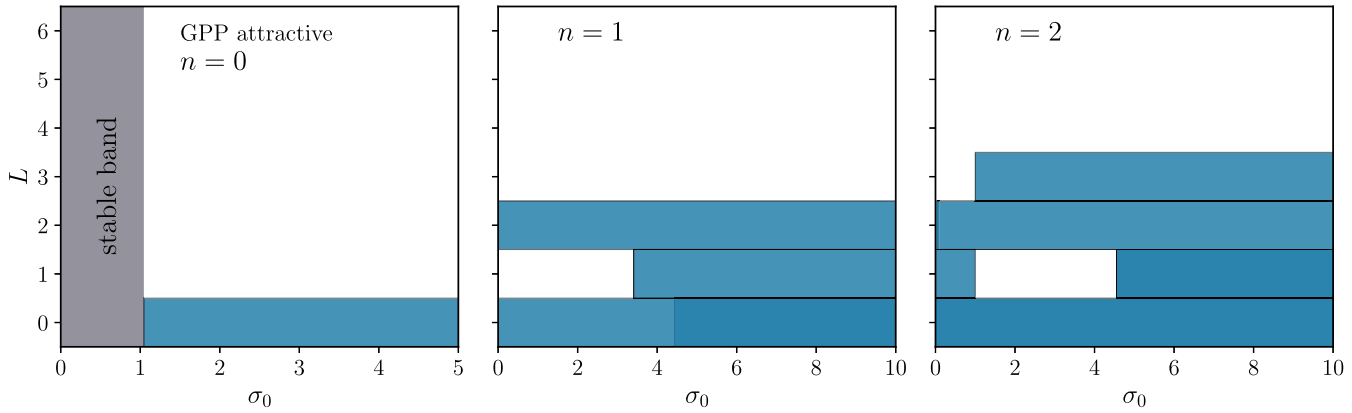

FIG. 9. Stability band structure (attractive case): Same as in Fig. 8 but for the attractive case. Note that the common stability band is empty for the first and second excited states and that no unstable modes are found for $L > 3$. Note also that for $n = 2$ and $L = 2$, there are two unstable modes in the interval $0 < \sigma_0 < 0.1$, although they are barely visible.

The central and right panels of Fig. 6 present the results obtained for radial perturbations. As can be observed, there exist unstable modes with $\lambda_R > 0$ in the attractive, the repulsive as well as in the non-self-interacting case. In the first and third cases, we have identified an unstable band that spans all values of the central amplitude σ_0 that we have explored. For the nth excited state, this band consists of n unstable modes that grow exponentially in time. In the attractive scenario, for one of these modes, λ_R grows rapidly as σ_0 increases, signaling that the solutions have a lifetime that is much shorter than the state with the same central amplitude in the non-self-interacting theory. Indeed, in absence of self-interactions, one observes a linear relationship between the real part of the mode(s) frequency λ_R and the central amplitude σ_0. This relationship arises from an inherent scaling freedom in the Schrödinger-Poisson system. For further details regarding this symmetry, we refer the reader to Refs. [32,45]. The dashed lines represent the scaled results of the n unstable modes reported in Ref. [46], while the dark circles denote our numerical results. As can be seen, both sets of results are in agreement.

A more interesting pattern appears for the repulsive scenario, in which the unstable radial modes cover only localized intervals of σ_0, resulting in stability bands where $\lambda_R = 0$[4]; see the central and right panels of Fig. 6. It's worth noting that, unlike ground state configurations, the boundary between stable and unstable solutions is not determined by a maximum mass state. The relation of these results with those of Refs. [27,28] will be discussed in the conclusion section and Appendix B.

C. Excited states (nonspherical perturbations)

Next, we address the problem of what happens to the stability bands of the previous subsection when nonspherical perturbations are considered. Specifically, the relevant question is whether unstable modes with $L > 0$ appear inside these bands, which would imply that the configurations are unstable with respect to generic linear perturbations.

The central and right panels of Fig. 7 show unstable modes with $L = 1$ appearing in certain intervals of σ_0, giving rise to new stability bands. Interestingly, such bands appear in the repulsive as well as in the attractive case, whereas for $L = 0$, they only occurred in the former case. Further stability bands arise as L increases. The central and right panels of Figs. 8 and 9 show the different stability bands (white regions) for different values of L. Notice that for high enough values of L, the stable band covers entirely the region of the parameter space we have explored, which is compatible with the result obtained in Sec. IV D.

Furthermore, it is interesting to compare the colored regions of instability shown in Figs. 8 and 9 for small values of σ_0. In this limit, the self-interaction term of the Gross-Pitaevskii equation (5) is subdominant, which would lead to all scenarios being equivalent (see the overlapping region in Figs. 1 and 2). As a consequence, one observes from Figs. 8 and 9 that in the limit $\sigma_0 \to 0$, the instability bands (including the number of unstable modes) transit continuously to the corresponding instability bands belonging to the configurations of the Schrödinger-Poisson system. For the particular cases $n = 0$ and $n = 1$, we refer the reader to Fig. 4 of Ref. [46] for the case $\ell = 0$ where the respective regions of instability for the Schrödinger-Poisson system are reported.

We conclude this section by emphasizing that only configurations lying in the intersection of the stability bands for all L are stable with respect to generic linear perturbations. For $n = 1$, the resulting common stability band turns out to be very narrow in the repulsive case, as shown in Fig. 8, whereas it is empty in the attractive case; see Fig. 9. For $n = 2$, there are no stable configurations, neither in the repulsive nor in the attractive case. Similar results are expected for higher excited states.

VI. CONCLUSIONS

In this paper, we have analyzed the impact of a self-interaction potential on the linear stability of boson stars, with particular interest on the excited states. In absence of self-interactions, it is known that excited boson stars are unstable, as has been confirmed using semianalytical techniques, both in the nonrelativistic [33] and the relativistic [25] regimes, and numerical simulations [26,33]. This has led to the belief that this result is general and holds true in the presence of a self-interaction potential, as has been observed using numerical evolutions of the spherically symmetric Einstein-Klein-Gordon equations in the $\lambda|\phi|^4$ theory [26].

However, in a series of recent papers, performing a more systematic study of the numerical evolutions of self-interacting excited boson star configurations, the authors of Refs. [27,28] have concluded that, for strong enough repulsive quartic self-interaction, these configurations remain stable under spherical perturbations, at least for times of the order of $10^4 m_0^{-1}$.

Motivated by these recent findings, and using a combination of analytic and numerical methods, we have analyzed the linear stability of the stationary and spherically symmetric solutions of the Gross-Pitaevskii-Poisson system that describes the nonrelativistic limit of the Einstein-Klein-Gordon theory in the presence of a quartic or more general potential term. Furthermore, we have been able to extend our analysis to include perturbations that do not necessarily respect the spherical symmetry of the unperturbed system, and in this sense, it goes beyond the radial stability study of the excited states performed in [27,28].

In particular, if the self-interaction is repulsive, we have found that ground state configurations are stable under

[4]Note that the occurrence of such localized stability bands is excluded in the non-self-interacting case due to the aforementioned rescaling freedom of the Schrödinger-Poisson system.

generic linear perturbations, a result that is consistent with the idea that these states represent a global minimum of the energy functional for fixed particle number (cf. the left panel of Fig. 3). For the excited states, however, there exists a series of stability and instability bands in the central amplitude σ_0 of the background field that depends on the particular value of the angular momentum number L associated with the perturbation. This series disappears for high enough values of L, since in this case, there are no unstable modes, as we have been able to prove. The stability under generic linear perturbations is determined by the common band that results from the intersection of the stability bands associated with each different L. For the first excited state, we have determined the existence of a common stability band in the range $1.55 \lesssim \sigma_0 \lesssim 2.07$, whereas this band is empty for the second excited state. These results are summarized in Fig. 8, and they are independent of the mass of the scalar field and the strength of the self-interaction (as long as they are different from zero). This is a consequence of the fact that for the Gross-Pitaevskii-Poisson system, m_0 and Λ can be absorbed in the dimensionless variables. We expect a similar behavior for higher excited states.

In contrast, if the self-interaction is attractive, ground state configurations are only stable if they are located to the right of the maximum mass configuration in the M_{99} vs R_{99} curve (see the center panel of Fig. 1). Regarding the excited states, and similar to what occurs in the repulsive case, for each value of the angular momentum number L of the perturbations, there exists a series of stability and instability bands in the central amplitude σ_0. However, the common stability band is empty, at least for the first two excited states; see Fig. 9 for details. Again, similar results are expected for higher excited states.

It is reasonable to think that the stability bands we have found persist in the Einstein-Klein-Gordon theory, at least as long as we are not too far from the nonrelativistic limit. Related to this point, it is interesting to compare our results with those reported in Refs. [27,28]. In [27], the authors construct solutions of the Einstein-Klein-Gordon equations for the first excited state ($n = 1$) and different values of the self-interaction parameter Λ and frequency ω, whereas in [28], for the states $n = 1, \ldots, 10$, the frequency ω is fixed, and the self-interaction parameter is varied. In particular, it is found in [28] that for sufficiently large values of Λ, the excited states are stable under radial perturbations. Additionally, for the case of the first excited states, stability bands can be identified from Fig. 3 and Table 1 in [27].

Although the existence of excited stable states and the occurrence of stability bands is compatible with the results reported in Refs. [27,28], a direct comparison is challenging due to the relativistic effects that we have neglected in our results. Furthermore, the fact that the Gross-Pitaevskii-Poisson system can be rewritten in a form that is independent of the mass and the self-interaction parameter reduces the problem to one with a single continuous parameter (the field's central amplitude); hence, exploring the solution space in the same form as in [27,28] is unnatural in our setting. For the second excited states, a rough comparison of our results with those of Ref. [28] is presented in Appendix B, although it is important to stress that, in the nonrelativistic limit, these states are unstable with respect to generic linear perturbations (see the right panel of Fig. 8 for reference).

Finally, it is interesting to stress that, contrary to what happens in the relativistic theory, the conclusions that we have presented in this paper are generic and can be extended to other potentials different from the quartic self-interaction one that have been analyzed in, e.g., Refs. [26–28]. Again, this is due to some of the peculiarities of the nonrelativistic limit of the Einstein-Klein-Gordon theory, as we clarify in Appendix A. Boson stars resulting from higher-rank fields, both in the absence and presence of self-interactions, have been explored in e.g. Refs. [63–66].

ACKNOWLEDGMENTS

We are grateful to Nicolas Sanchis-Gual, Marco Brito, Carlos Herdeiro, Eugen Radu, and Miguel Zilhão for bringing to our attention the existence of stability/instability bands within the relativistic framework and to Mudit Jain and Pierre Chavanis for correspondence. This work was partially supported by CONAHCyT Projects No. 376127 "Sombras, lentes y ondas gravitatorias generadas por objetos compactos astrofísicos" and No. 286897 "Materia oscura: Implicaciones de sus propiedades fundamentales en las observaciones astrofísicas y cosmológicas," and by CONAHCyT-SNII. E. C. N. was supported by a CONAHCyT doctoral scholarship. A. D. T. acknowledges support from DAIP. A. A. R. also acknowledges funding from a postdoctoral fellowship from "Estancias Posdoctorales por México para la Formación y Consolidación de las y los Investigadores por México." O. S. was partially supported by a CIC grant to Universidad Michoacana de San Nicolás de Hidalgo. We also acknowledge the use of the computing server COUGHS from the UGDataLab at the Physics Department of Guanajuato University.

APPENDIX A: GENERIC SELF-INTERACTION POTENTIAL

Consider a self-interaction potential of the general form

$$V(\phi) = M^4 \sum_{n=2}^{\infty} \frac{v_{2n}}{(2n)!} \left| \frac{\phi}{M} \right|^{2n}, \tag{A1}$$

where v_{2n} are dimensionless constant parameters, and M is a characteristic mass scale. Under the assumption that the coefficients v_{2n} do not grow too fast such that the convergence radius is different from zero, this is the most general potential that respects the internal $U(1)$ symmetry and is analytic in $|\phi|^2$ in a vicinity of $\phi = 0$. Furthermore,

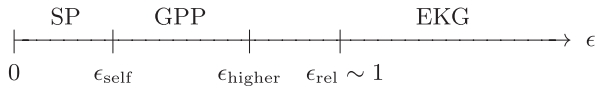

FIG. 10. The effect of the higher self-interaction terms. The different regimes of the Einstein-Klein-Gordon theory, showing the scales at which the quartic self-interaction term ($\epsilon_{\rm self}$) and the higher-order terms ($\epsilon_{\rm higher}$) become important. Notice the model independence that the Einstein-Klein-Gordon theory exhibits at scales below $\epsilon_{\rm higher}$. This regime is characterized in terms of two parameters: the mass of the scalar field and the coupling constant λ. For the quartic self-interaction potential, $\epsilon_{\rm higher} \to \infty$, whereas for a generic potential, $\epsilon_{\rm higher}$ is expected to be of order $\epsilon_{\rm rel} \sim 1$.

we have assumed that the constant term $n = 0$ is zero and have excluded the $n = 1$ term in Eq. (A1) since its contribution is already included in the mass of the scalar field m_0. Note that the first term of this series corresponds to the quartic $\lambda|\phi|^4$ self-interaction potential of Eq. (1b), with $\lambda = v_4/4!$; however, now we have an infinite number of additional self-interaction terms that also contribute to the potential energy of the field.

After introducing this potential into the action (1) and working out the nonrelativistic approximation as we described in Sec. II A, the self-interaction term in Eq. (3) is modified to

$$-\frac{\lambda}{4m_0^2}|\psi|^4\left[1+\frac{v_6}{240v_4}\frac{|\psi|^2}{m_0M^2}+\ldots\right]. \tag{A2}$$

In the nonrelativistic limit, $\psi \sim \sqrt{M_{\rm Pl}^2 m_0}\epsilon$, and the second term in the square bracket starts to contribute to the equations of motion when $\epsilon \sim \epsilon_{\rm higher} = \sqrt{240v_4/v_6}(M/M_{\rm Pl})$, which should be compared with $\epsilon_{\rm self} = m_0^2/(\lambda M_{\rm Pl}^2)$, which signals the onset of the quartic self-interaction and is naturally smaller. For instance, if $M \sim M_{\rm Pl}$ and all the coefficients v_{2n} are of the same order, then the higher orders of the potential show up at the same scale than the relativistic effects, when $\epsilon \sim \epsilon_{\rm rel} = 1$. This leads to the conclusion that the nonrelativistic limit that we have introduced in Eq. (3) is generic and valid beyond the quartic self-interaction theory $\lambda|\phi|^4$. These observations are illustrated pictorially in Fig. 10.

APPENDIX B: COMPARISON WITH THE WORK IN REFS. [27,28]

The Einstein-Klein-Gordon action in Eq. (1) of our paper coincides with that of Eq. (1) in Refs. [27,28] provided we perform the following identifications: $M_{\rm Pl} = 1$, $m_0 = \mu$ and $\phi = \frac{1}{\sqrt{2}}\Phi$. However, there is a factor 2 of difference in our definition of the self-interaction parameter (4); i.e., $\Lambda_{\rm ours} = 2\Lambda_{\rm their}$. Taking this into account, it is possible to conclude that, in the nonrelativistic limit [cf. Eqs. (8) and (16)],

$$\bar{\sigma}_0 = \left(\frac{\pi\Lambda_{\rm ours}^2}{2M_{\rm Pl}^2 m_0}\right)^{1/2}\sigma_0 = \sqrt{2\pi}\Lambda_{\rm their}\frac{|\Phi_0|}{M_{\rm Pl}}, \tag{B1}$$

where in this appendix, we have reintroduced the overbar to indicate dimensionless quantities. Given that the authors of Refs. [27,28] work in Planck units, $M_{\rm Pl} = 1$, we can relate field amplitudes in our paper to those of Refs. [27,28] through $\bar{\sigma}_0 = \sqrt{2\pi}\Lambda_{\rm their}|\Phi_0|$.

In Ref. [28] it is reported that, for second excited states ($n = 2$) with frequency $\omega = 0.92$ and $\mu = 1$, the minimum value of the self-interaction parameter for which a configuration is stable under radial perturbations is $\Lambda_{\rm their} = 150$, corresponding to a central amplitude of approximately $\Phi_0 \approx 1.3 \times 10^{-2}$ (see Fig. 7 in [28]), which translates to $\bar{\sigma}_0 \approx 4.9$ in our paper. We can compare this result with the stability bands at $L = 0$ that we have identified in the right panel of Fig. 8, i.e. $2.2 < \bar{\sigma}_0 < 2.5$, and $3 < \bar{\sigma}_0 < 6.4$. Even if the correspondence is only at the order of magnitude level, it is important to stress that the configurations with $\omega = 0.92$ are relativistic, so we do not expect a perfect match.

Furthermore, evidence of stability/instability bands can be also inferred from the results presented in Ref [27]. In Fig. 3 of this reference, the authors explore the solution space corresponding to the first excited states ($n = 1$) by varying the self-interaction parameter Λ and the frequency ω. For instance, choosing $\Lambda = 75$, a stability band emerges as we decrease the frequency from $\omega = 0.92$ to $\omega = 0.90$, leading to excited states that are stable under radial perturbations. However, further decrease in ω leads again to unstable solutions. Table 1 of this reference confirms the same pattern.

[1] D. J. Kaup, Klein-Gordon geon, Phys. Rev. **172**, 1331 (1968).
[2] R. Ruffini and S. Bonazzola, Systems of self-gravitating particles in general relativity and the concept of an equation of state, Phys. Rev. **187**, 1767 (1969).
[3] P. Jetzer, Boson stars, Phys. Rep. **220**, 163 (1992).
[4] T. D. Lee and Y. Pang, Nontopological solitons, Phys. Rep. **221**, 251 (1992).
[5] A. R. Liddle and M. S. Madsen, The structure and formation of boson stars, Int. J. Mod. Phys. D **01**, 101 (1992).

[6] F. E. Schunck and E. W. Mielke, General relativistic boson stars, Classical Quantum Gravity **20**, R301 (2003).
[7] S. L. Liebling and C. Palenzuela, Dynamical boson stars, Living Rev. Relativity **26**, 1 (2023).
[8] H. Zhang, Axion stars, Symmetry **12**, 25 (2019).
[9] L. Visinelli, Boson stars and oscillatons: A review, Int. J. Mod. Phys. D **30**, 2130006 (2021).
[10] M. Colpi, S. L. Shapiro, and I. Wasserman, Boson stars: Gravitational equilibria of self-interacting scalar fields, Phys. Rev. Lett. **57**, 2485 (1986).
[11] F. E. Schunck and D. F. Torres, Boson stars with generic self-interactions, Int. J. Mod. Phys. D **09**, 601 (2000).
[12] P.-H. Chavanis, Mass-radius relation of Newtonian self-gravitating Bose-Einstein condensates with short-range interactions. I. Analytical results, Phys. Rev. D **84**, 043531 (2011).
[13] P.-H. Chavanis and L. Delfini, Mass-radius relation of Newtonian self-gravitating Bose-Einstein condensates with short-range interactions. II. Numerical results, Phys. Rev. D **84**, 043532 (2011).
[14] J. Eby, C. Kouvaris, N. G. Nielsen, and L. C. R. Wijewardhana, Boson stars from self-interacting dark matter, J. High Energy Phys. 02 (2016) 028.
[15] P.-H. Chavanis, Phase transitions between dilute and dense axion stars, Phys. Rev. D **98**, 023009 (2018).
[16] E. D. Schiappacasse and M. P. Hertzberg, Analysis of dark matter axion clumps with spherical symmetry, J. Cosmol. Astropart. Phys. 01 (2018) 037.
[17] N. Siemonsen and W. E. East, Stability of rotating scalar boson stars with nonlinear interactions, Phys. Rev. D **103**, 044022 (2021).
[18] P.-H. Chavanis, Maximum mass of relativistic self-gravitating Bose-Einstein condensates with repulsive or attractive $|\bar{\varphi}|^4$ self-interaction, Phys. Rev. D **107**, 103503 (2023).
[19] M. Jain, W. Wanichwecharungruang, and J. Thomas, Kinetic relaxation and nucleation of Bose stars in self-interacting wave dark matter, Phys. Rev. D **109**, 016002 (2024).
[20] M. Gleiser, Stability of boson stars, Phys. Rev. D **38**, 2376 (1988); **39**, 1257(E) (1989).
[21] M. Gleiser and R. Watkins, Gravitational stability of scalar matter, Nucl. Phys. **B319**, 733 (1989).
[22] E. Seidel and W.-M. Suen, Dynamical evolution of boson stars. 1. Perturbing the ground state, Phys. Rev. D **42**, 384 (1990).
[23] F. S. Guzmán, The three dynamical fates of boson stars, Rev. Mex. Fis. **55**, 321 (2009).
[24] P. Jetzer, Stability of excited bose stars, Nucl. Phys. B, Proc. Suppl. **14**, 265 (1990).
[25] T. D. Lee and Y. Pang, Stability of mini—boson stars, Nucl. Phys. **B315**, 477 (1989).
[26] J. Balakrishna, E. Seidel, and W.-M. Suen, Dynamical evolution of boson stars. II. Excited states and self-interacting fields, Phys. Rev. D **58**, 104004 (1998).
[27] N. Sanchis-Gual, C. Herdeiro, and E. Radu, Self-interactions can stabilize excited boson stars, Classical Quantum Gravity **39**, 064001 (2022).
[28] M. Brito, C. Herdeiro, E. Radu, N. Sanchis-Gual, and M. Zilhão, Stability and physical properties of spherical excited scalar boson stars, Phys. Rev. D **107**, 084022 (2023).
[29] A. H. Guth, M. P. Hertzberg, and C. Prescod-Weinstein, Do dark matter axions form a condensate with long-range correlation?, Phys. Rev. D **92**, 103513 (2015).
[30] A. S. Dmitriev, D. G. Levkov, A. G. Panin, E. K. Pushnaya, and I. I. Tkachev, Instability of rotating Bose stars, Phys. Rev. D **104**, 023504 (2021).
[31] P. Tod and I. M. Moroz, An analytical approach to the Schrödinger-Newton equations, Nonlinearity **12**, 201 (1999).
[32] I. M. Moroz, R. Penrose, and P. Tod, Spherically symmetric solutions of the Schrodinger-Newton equations, Classical Quantum Gravity **15**, 2733 (1998).
[33] R. Harrison, I. M. Moroz, and P. Tod, A numerical study of the Schrödinger Newton equations, Nonlinearity **16**, 101 (2002).
[34] P. Sikivie, Axion cosmology, Lect. Notes Phys. **741**, 19 (2008).
[35] W. Hu, R. Barkana, and A. Gruzinov, Fuzzy cold dark matter: The wave properties of ultralight particles, Phys. Rev. Lett. **85**, 1158 (2000).
[36] T. Matos and L. A. Ureña López, Further analysis of a cosmological model with quintessence and scalar dark matter, Phys. Rev. D **63**, 063506 (2001).
[37] A. Arvanitaki, S. Dimopoulos, S. Dubovsky, N. Kaloper, and J. March-Russell, String axiverse, Phys. Rev. D **81**, 123530 (2010).
[38] A. Suárez, V. H. Robles, and T. Matos, A review on the scalar field/Bose-Einstein condensate dark matter model, Astrophys. Space Sci. Proc. **38**, 107 (2014).
[39] D. J. E. Marsh, Axion cosmology, Phys. Rep. **643**, 1 (2016).
[40] L. Hui, J. P. Ostriker, S. Tremaine, and E. Witten, Ultralight scalars as cosmological dark matter, Phys. Rev. D **95**, 043541 (2017).
[41] J. C. Niemeyer, Small-scale structure of fuzzy and axion-like dark matter, Prog. Part. Nucl. Phys. **113**, 103787 (2020).
[42] L. A. Ureña López, Brief review on scalar field dark matter models, Front. Astron. Space Sci. **6**, 47 (2019).
[43] E. G. M. Ferreira, Ultra-light dark matter, Astron. Astrophys. Rev. **29**, 7 (2021).
[44] G. Grilli di Cortona, E. Hardy, J. Pardo Vega, and G. Villadoro, The QCD axion, precisely, J. High Energy Phys. 01 (2016) 034.
[45] A. A. Roque, E. C. Nambo, and O. Sarbach, Radial linear stability of nonrelativistic ℓ-boson stars, Phys. Rev. D **107**, 084001 (2023).
[46] E. C. Nambo, A. A. Roque, and O. Sarbach, Are non-relativistic ground state ℓ-boson stars only stable for $\ell = 0$ and $\ell = 1$?, Phys. Rev. D **108**, 124065 (2023).
[47] E. P. Gross, Structure of a quantized vortex in boson systems, Il Nuovo Cimento (1955–1965) **20**, 454 (1961).
[48] L. P. Pitaevskii, Vortex lines in an imperfect Bose gas, Sov. Phys. JETP **13**, 451 (1961).
[49] O. Robertshaw and P. Tod, Lie point symmetries and an approximate solution for the Schrödinger–Newton equations, Nonlinearity **19**, 1507 (2006).

[50] D. Giulini and A. Großardt, Gravitationally induced inhibitions of dispersion according to the Schrödinger–Newton equation, Classical Quantum Gravity **28**, 195026 (2011).
[51] C. Duval and S. Lazzarini, On the Schrödinger–Newton equation and its symmetries: A geometric view, Classical Quantum Gravity **32**, 175006 (2015).
[52] J. Yang, *Nonlinear Waves in Integrable and Non-Integrable Systems* (Society for Industrial and Applied Mathematics, USA, 2010), 10.1112/blms/bdu100.
[53] G. H. Derrick, Comments on nonlinear wave equations as models for elementary particles, J. Math. Phys. (N.Y.) **5**, 1252 (1964).
[54] P. Virtanen, R. Gommers *et al.*, SciPy 1.0: Fundamental algorithms for scientific computing in Python, Nat. Methods **17**, 261 (2020).
[55] J. Dormand and P. Prince, A family of embedded Runge-Kutta formulae, J. Comput. Appl. Math. **6**, 19 (1980).
[56] F. S. Lawrence, Some practical Runge-Kutta formulas, Math. Comput. **46**, 135 (1986).
[57] L. N. Trefethen, *Spectral Methods in MATLAB*, EngineeringPro collection (Society for Industrial and Applied Mathematics, 2000), 10.1137/1.9780898719598.
[58] Repository, http://Github.com/Mandy8808/Implementation.git (2024).
[59] Y. B. Zel'dovich, Hydrodynamical stability of star, Vopr. Kosmog. **9**, 157 (1963).
[60] B. K. Harrison, K. S. Thorne, M. Wakano, and J. A. Wheeler, *Gravitation Theory and Gravitational Collapse* (University of Chicago Press, Chicago, 1965).
[61] N. Straumann, *General Relativity and Relativistic Astrophysics*, Texts and Monographs in Physics (Springer-Verlag, Berlin, 1984), 10.1007/978-3-642-84439-3.
[62] G. Alberti and P.-H. Chavanis, Caloric curves of self-gravitating fermions in general relativity, Eur. Phys. J. B **93**, 208 (2020).
[63] M. Jain and M. A. Amin, Polarized solitons in higher-spin wave dark matter, Phys. Rev. D **105**, 056019 (2022).
[64] P. Adshead and K. D. Lozanov, Self-gravitating vector dark matter, Phys. Rev. D **103**, 103501 (2021).
[65] H.-Y. Zhang, M. Jain, and M. A. Amin, Polarized vector oscillons, Phys. Rev. D **105**, 096037 (2022).
[66] M. Jain, Soliton stars in Yang-Mills-Higgs theories, Phys. Rev. D **106**, 085011 (2022).

Wave propagation through a spacetime containing thin concentric shells of matter

Rubén O. Acuña-Cárdenas,[1] Olivier Sarbach,[1,2] and Luca Tessieri[3]

[1]*Instituto de Física y Matemáticas, Universidad Michoacana de San Nicolás de Hidalgo, Edificio C-3, Ciudad Universitaria, 58040 Morelia, Michoacán, Mexico*

[2]*Departamento de Matemáticas Aplicadas y Sistemas, Universidad Autónoma Metropolitana-Cuajimalpa, 05348, Cuajimalpa de Morelos, Ciudad de México, Mexico*

[3]*Facultad de Ciencias Físico-Matemáticas, Universidad Michoacana de San Nicolás de Hidalgo, Edificio Alfa, Ciudad Universitaria, 58040 Morelia, Michoacán, Mexico*

(Received 3 July 2024; accepted 21 October 2024; published 25 November 2024)

The interaction between waves and matter in the Universe is a fundamental but very challenging problem, since one needs to consistently solve the Einstein-matter equations in a dynamical regime. To shed some light on this problem, we investigate the transmission of scalar, electromagnetic, and linearized odd-parity gravitational waves in a toy model. This model consists of a static spacetime satisfying Einstein's field equations which is characterized by a spherical distribution of matter in the form of thin concentric equidistant shells of equal mass which is perturbed by a linear wave. More specifically, we assume that the central region has zero mass, and we verify that the resulting spacetime is stable with respect to small perturbations of the shell radii as long as the gravitational field is sufficiently weak. We focus on the transmission of monochromatic waves emitted from the center and propagating through a succession of N shells. Analytical expressions for the transmission and reflection coefficients are obtained and their dependency on the frequency, the number of shells and their mutual distance is analyzed. In particular, in the high-frequency limit, we observe that the reflection coefficient decays with the fourth power of the frequency. Increasing the number of shells initially produces oscillations in the transmission coefficient; however, as N grows, this coefficient rapidly stabilizes at a constant positive value. We attribute this property to the fact that reflections are mainly determined by the surface density of the shells, which decreases as the inverse square of their radii.

DOI: 10.1103/PhysRevD.110.104064

I. INTRODUCTION

The study of wave propagation in spacetime has intensified in recent years, as a consequence of the groundbreaking experimental observation of gravitational waves [1–3] and important advances in numerical relativity simulations [4–6]. The detection of gravitational waves has provided new tools to explore the Universe [7] and has increased the interest in the propagation of waves of all kind in relativistic spacetimes and in their interaction with different forms of matter, see for instance Refs. [8–13]. However, in spite of contemporary advances, our theoretical understanding of the influence that matter exerts on wave propagation is still far from complete.

Initial steps in this direction have been performed by Esposito [14] and by Ehlers and collaborators [15,16], who demonstrated that an ideal fluid cannot extract energy from gravitational waves. However, when traversing a *dissipative* fluid, gravitational waves are expected to be attenuated due to shear viscosity. This mechanism has been studied by several groups in the context of cosmology, see for instance Refs. [8,17–21]. More recently, Bishop *et al.* [9] analyzed the interaction of a gravitational wave produced by a source surrounded by a shell of dust matter. They found that the energy exchange is zero, in agreement with the conclusion from the aforementioned work, and that the wave undergoes modifications in its frequency, phase, and magnitude. In [10] some astrophysical scenarios were proposed in which these effects could be important, including echoes in LIGO events or gravitational waves produced by core collapse supernovae. The last scenario was further explored in [11] for a viscous fluid shell, and other potential applications such a gravitational wave heating of a shell of matter and the damping of primordial gravitational waves were discussed in Refs. [22,13].

In this article, we discuss an entirely different mechanism that could lead to the attenuation of gravitational waves, namely the scattering of waves by thin shells of matter. These shells represent discontinuities in the spacetime curvature and their simple structure makes it possible to simplify the theoretical analysis of the interaction of matter with gravitational, electromagnetic, and scalar waves. Thin-shell models [23–27] have been applied to the analysis of

various dynamical phenomena, including cosmological scenarios [28], the stability of wormholes [29,30], the study of the behavior of shells around black holes [31–34], gravitational collapse [35,36], and mass inflation [37].

More specifically, we study the propagation of scalar, electromagnetic, and linearized odd-parity gravitational waves through a stationary spacetime composed of thin spherical and concentrical shells of equal mass. These shells serve as interfaces connecting Schwarzschild spacetimes of varying masses. We assume that the Israel junction conditions [38–40] hold and that on each shell the surface energy-momentum tensor satisfies a polytropic equation of state. The model under study has a massless central region, and its stability against small perturbations of the shell radii under weak gravitational fields is examined. We focus on the transmission of monochromatic waves originating from the center across an array of N shells. Applying the Regge-Wheeler (RW) equation to the case of a weak gravitational background field and using the formalism introduced in Refs. [41,42], we derive analytical expressions for the transmission and reflection coefficients. These results allow us to determine how the transmission properties depend on the wave frequency, the number of thin shells, and the distance between neighboring shells. In particular, we show that the reflection coefficient tends to vanish in the high-frequency limit and that the transmission coefficient tends to a nonzero constant asymptotic value when the number of shells increases. In principle, our results might be applied to the interpretation of experimental data for waves propagating through spherically distributed matter; in this case, they could provide insight on the inner features of the scattering mass distribution.

The treatment of linearized gravitational waves with even parity requires a more complex analysis, since in this case the waves interact with the shells, inducing (non-spherical) deformations of them, and the resulting effects need to be analyzed separately. Although the techniques employed in this article could be generalized to describe this situation, the resulting perturbation equations are more complicated, and for this reason we leave it to future work. Still, the results obtained in the present article provide a detailed calculation for the attenuation of the outgoing odd-parity gravitational wave due to reflections at the thin shells. Furthermore, our findings also apply to (even and odd) electromagnetic waves and to scalar waves. The result for the second type of waves might be relevant for scalar field dark matter models which have attracted considerable interest in recent years (see, for instance, Refs. [43–46] for recent reviews).

The remainder of this work is organized as follows: in Sec. II we specify our background spacetime on which the wave propagation will be studied and discuss its stability and weak-field limit. In Sec. III we construct approximate solutions of the RW equation for a spin S field which are valid in the weak-field limit. Next, in Sec. IV we work out the relevant matching conditions at each shell and introduce the transfer matrix formalism. The resulting reflection and transmission coefficients are computed in Sec. V and their behavior is analyzed in detail in Sec. VI. Conclusions are drawn in Sec. VII, where we also discuss possible extensions of this work. Finally, technical issues are considered in appendices A, B, C, D, and E.

In this work, we use geometrized units in which the gravitational constant G and the speed of light c are one, and we use the signature convention $(-,+,+,+)$ for the spacetime metric.

II. SPACETIME STRUCTURE, STABILITY, AND WEAK-FIELD LIMIT

In this section we specify the field equations for a spherically symmetric spacetime composed of a series of N thin concentric shells with vacuum regions in between. According to Birkhoff's theorem, these shells must connect Schwarzschild spacetimes of distinct masses, and their dynamics must adhere to Israel's junction conditions [38–40] with a suitable surface energy-momentum tensor which is assumed here to obey a polytropic-type equation of state. The central region is assumed to be flat (Minkowski) spacetime, see Fig. 1 for a depiction of the spacetime structure. In particular, we determine the equilibrium configurations leading to a static spacetime and analyze the stability of the resulting model. Finally, we take the weak-field limit of our model which greatly simplifies the subsequent analysis, and we show that the aforementioned stability conditions are automatically satisfied in this limit.

A. Spacetime construction

Our spacetime consists of $N+1$ copies of Schwarzschild spacetimes of increasing masses $0=m_0<m_1<\ldots<m_N$.

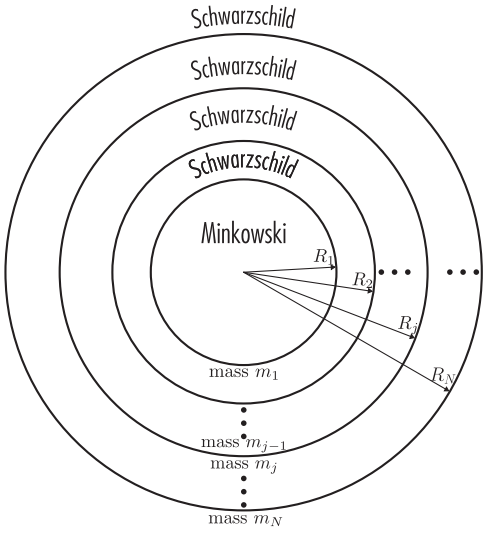

FIG. 1. Illustration for the spacetime structure consisting of N thin concentric shells of matter.

The spacetimes are glued together at three-dimensional hypersurfaces of the form $\Sigma_j \coloneqq \{r = \mathcal{R}_j(t)\}$ with the shells' radii satisfying the inequalities

$$0 < \mathcal{R}_1(t) < \mathcal{R}_2(t) < \ldots < \mathcal{R}_N(t) \tag{1}$$

for every time t. More precisely, the spacetime manifold is $\mathbb{R}^4$, equipped with the metric

$$g = -\left(1 - \frac{2m(t,r)}{r}\right)dt^2 + \frac{dr^2}{1 - \frac{2m(t,r)}{r}} + r^2 d\Omega^2. \tag{2}$$

In Eq. (2), $t \in \mathbb{R}$ is the time, $r > 0$ the areal radial coordinate, $d\Omega^2 = d\vartheta^2 + \sin^2\vartheta d\varphi^2$ is the standard metric on the unit two-sphere in spherical coordinates (ϑ, φ), and the mass function $m(t,r)$ is defined as follows

$$m(t,r) \coloneqq m_j, \qquad \mathcal{R}_j(t) < r < \mathcal{R}_{j+1}(t), \tag{3}$$

with $j = 0, 1, 2, \ldots, N$. In Eq. (3) it is understood that $\mathcal{R}_0 \equiv 0$ and $\mathcal{R}_{N+1} \equiv \infty$. Furthermore, we assume that $2m(t,r) < r$ everywhere, i.e., that there are no horizons.

The dynamics of the shells is determined by Israel's junction conditions [38,39], which ensures the satisfaction of Einstein's field equations at the interfaces Σ_j. In terms of the first and second fundamental forms h_{ab} and K_{ab} of Σ_j these conditions are

$$[h_{ab}] = 0, \tag{4}$$

$$h_{ab}[K] - [K_{ab}] = 8\pi S_{ab}. \tag{5}$$

In Eqs. (4) and (5) we use the symbol $[X]$ to denote the discontinuity of any field X across the surface Σ_j, i.e.,

$$[X] \coloneqq X_+|_{\Sigma_j} - X_-|_{\Sigma_j}, \tag{6}$$

with X_+ and X_- respectively representing the value of X on the outer and inner border of Σ_j. The symbols

$$K \coloneqq h^{ab}K_{ab} \tag{7}$$

and S_{ab} stand for the trace of K_{ab} and for the surface energy-momentum tensor. We will assume that S_{ab} has the form associated to a perfect surface fluid:

$$S_{ab} = (\sigma + p)u_a u_b + p h_{ab}, \tag{8}$$

with σ, p, and u^a respectively denoting the surface energy density, the surface pressure, and the three-velocity of the fluid (taken to coincide with the velocity of the comoving observers). As a consequence of the Codazzi-Mainardi equations and Einstein's equations, S_{ab} is divergence-free.

The first and second fundamental form of the jth shell Σ_j, as embedded into the metric (2) are given by

$$h_{ab}dx^a dx^b|_\pm = -d\tau^2 + \mathcal{R}^2 d\Omega^2, \tag{9}$$

$$K_{ab}dx^a dx^b|_\pm = -\frac{1}{\mathcal{K}_\pm}\left(\ddot{\mathcal{R}} + \frac{m_\pm}{\mathcal{R}^2}\right)d\tau^2 + \mathcal{K}_\pm \mathcal{R} d\Omega^2, \tag{10}$$

where we have set $\mathcal{K}_\pm \coloneqq \sqrt{1 - 2m_\pm/\mathcal{R} + \dot{\mathcal{R}}^2}$ and suppressed the index j. Here and in the rest of this paper, the dot denotes derivation with respect to proper time τ measured by observers which are comoving with the shells, rather than Schwarzschild time t. Introducing the expressions (9), (10) into Eqs. (4), (5) yields, after some manipulations [25,33,38,47]

$$\dot{\mathcal{R}}_j^2 = \frac{m_{\Sigma_j}^2}{4\mathcal{R}_j^2} + \frac{m_j + m_{j-1}}{\mathcal{R}_j} + \frac{(m_j - m_{j-1})^2}{m_{\Sigma_j}^2} - 1, \tag{11}$$

$$\dot{\sigma}_j = -2\frac{\dot{\mathcal{R}}_j}{\mathcal{R}_j}(\sigma_j + p_j), \tag{12}$$

where we have abbreviated

$$m_{\Sigma_j} \coloneqq 4\pi \mathcal{R}_j^2 \sigma_j. \tag{13}$$

To close the system, one needs to specify an equation of state for the surface fluid. In this work, we propose a polytropic-type equation of state, for which

$$\sigma_j = \sigma_{\mathrm{rest},j} + \sigma_{\mathrm{int},j}, \tag{14}$$

with vanishing pressure associated with the rest energy $p_{\mathrm{rest},j} = 0$, and a pressure associated with the internal energy of the form

$$p_{\mathrm{int},j} = \alpha \sigma_{\mathrm{int},j}. \tag{15}$$

In the previous equation α is a constant which takes the same value for all the shells. In Sec. II B and II C we will analyze the range of the physically acceptable values of α. We require $\sigma_{\mathrm{rest},j}$ and $\sigma_{\mathrm{int},j}$ to be positive. Note that the dominant (and hence also the weak) energy condition is satisfied if $|\alpha| \leq 1$ (see, for instance Sec. IX. 2 in Ref. [48]). It follows from Eq. (12) that the surface energy density evolves in time according to

$$\sigma_j(\tau) = \sigma_{\mathrm{rest},j}(0)\left(\frac{\mathcal{R}_j(0)}{\mathcal{R}_j(\tau)}\right)^2 + \sigma_{\mathrm{int},j}(0)\left(\frac{\mathcal{R}_j(0)}{\mathcal{R}_j(\tau)}\right)^{2(1+\alpha)}. \tag{16}$$

After substituting this expression into Eq. (11) one obtains the equation of motion for the jth shell which has the same

form as the equation for a one-dimensional mechanical particle in an external potential. In what follows we explicitly derive the form of this dynamical equation and determine the equilibrium points and their stability.

B. Equilibrium configurations

In this subsection we determine the conditions under which the shells are in equilibrium (so that the resulting spacetime is static) and, furthermore, they are stable with respect to small radial perturbations. We shall denote the radii of the static shells with the italic symbols R_j and introduce the new variables $z_j \coloneqq \mathcal{R}_j/R_j$. Using Eqs. (11), (16) we can rewrite the jth shell's equation of motion as

$$R_j^2 \dot{z}_j^2 + V_j(z_j) = 0, \tag{17}$$

with the effective potential

$$V_j(z) \coloneqq 1 - \left[1 - \frac{(k_j^+)^2 + (k_j^-)^2}{2}\right]\frac{1}{z} - \frac{(a_{\mathrm{rest},j} + a_{\mathrm{int},j} z^{-2\alpha})^2}{z^2} - \frac{[(k_j^-)^2 - (k_j^+)^2]^2}{16(a_{\mathrm{rest},j} + a_{\mathrm{int},j} z^{-2\alpha})^2}. \tag{18}$$

To simplify the notation, in Eq. (18) we have introduced the dimensionless variables $a_{\mathrm{rest},j} \coloneqq 2\pi R_j \sigma_{\mathrm{rest},j}$, $a_{\mathrm{int},j} \coloneqq 2\pi R_j \sigma_{\mathrm{int},j}$, and

$$k_j^- \coloneqq \sqrt{1 - \frac{2m_{j-1}}{R_j}}, \qquad k_j^+ \coloneqq \sqrt{1 - \frac{2m_j}{R_j}}. \tag{19}$$

The equilibrium points are determined by the conditions $V_j(1) = V_j'(1) = 0$. After performing some tedious but straightforward calculations, one obtains

$$k_j^- - k_j^+ = 4\pi R_j(\sigma_{\mathrm{rest},j} + \sigma_{\mathrm{int},j}), \tag{20}$$

$$k_j^- k_j^+ = \frac{\sigma_{\mathrm{rest},j} + \sigma_{\mathrm{int},j}}{\sigma_{\mathrm{rest},j} + \sigma_{\mathrm{int},j}(1+4\alpha)}. \tag{21}$$

Since $k_j^\pm < 1$, the constant α in Eq. (15) must be positive, $\alpha > 0$. The physical content of equilibrium conditions (20) and (21) will be discussed in Sec. II D, where the weak-field limit is considered.

C. Stability

The stability of the static configurations with respect to radial fluctuations of the shells can be determined by analyzing the sign of the second derivative of the effective potential V_j at the equilibrium point. More precisely, the condition $V_j''(1) > 0$ guarantees stability. In our analysis of the stability of spherical shells connecting two Schwarzschild spacetimes we follow the previous works on the subject [25,27,32]. Computing the second derivative of V_j and using the equilibrium conditions (20), (21) to eliminate $a_{\mathrm{rest},j}$ and $a_{\mathrm{int},j}$ leads to

$$V_j''(1) = 2 + 2\alpha - (1+4\alpha)\frac{k_j^+ k_j^-}{2} - \frac{(k_j^+)^2 + (k_j^-)^2 + k_j^+ k_j^-}{2(k_j^+ k_j^-)^2}. \tag{22}$$

This expression allows one to determine the stability region in terms of the two parameters $k_j^\pm$ which satisfy $0 < k_j^+ < k_j^- < 1$. In the weak-field regime, $k_j^- = 1 - m_{j-1}/R_j + \mathcal{O}(\varepsilon^2)$ and $k_j^+ = 1 - m_j/R_j + \mathcal{O}(\varepsilon^2)$ with $\varepsilon = m_j/R_j$, and a short calculation gives

$$V_j''(1) = (2\alpha - 1)\frac{m_{j-1} + m_j}{R_j} + \mathcal{O}(\varepsilon^2), \tag{23}$$

which is positive as long as $\alpha > 1/2$. In the limit $k_j^- = k_j^+$, which corresponds to shells with vanishing surface energy density, one finds that the second derivative is positive if and only if $\alpha > 1/2$ and

$$\sqrt{\frac{3}{1+4\alpha}} < k_j^+ < 1. \tag{24}$$

Finally, in the limit $k_j^- = 1$ one finds that $V_j''(1) > 0$ if and only if $\alpha > 1/2$ and

$$\frac{1 + \sqrt{2(1+2\alpha)}}{1+4\alpha} < k_j^+ < 1. \tag{25}$$

Figure 2 shows the stability regions for different values of α.

D. Weak-field limit and specific model

To avoid mathematical complications which could obscure the physical results, in what follows we shall restrict ourselves to spacetimes with *weak* gravitational field and whose shells have surface energy dominated by their rest component, i.e.,

$$\frac{2m_j}{R_j} \ll 1, \tag{26}$$

$$\sigma_{\mathrm{int},j} \ll \sigma_{\mathrm{rest},j}. \tag{27}$$

As shown in the previous subsection, the conditions (26), (27) ensures that the configuration is stable as long as $\alpha > 1/2$. In this limit, Eqs. (20) and (21) reduce to the much simpler conditions

$$m_j - m_{j-1} = 4\pi R_j^2 \sigma_{\mathrm{rest},j}, \tag{28}$$

$$m_j + m_{j-1} = 4R_j \frac{p_j}{\sigma_{\mathrm{rest},j}}. \tag{29}$$

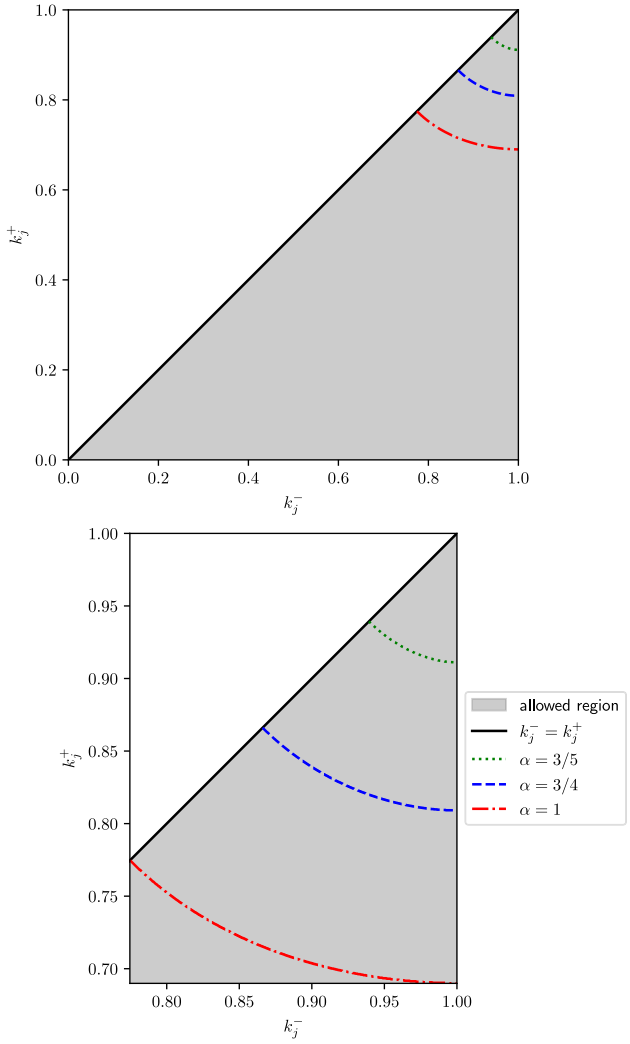

FIG. 2. Stability regions within the triangular zone $0 < k_j^- < k_j^+ < 1$ (in gray) associated with physically allowed realizations for a static shell in the (k_j^-, k_j^+) plane. The solid black line $k_j^- = k_j^+$ corresponds to the limit of shells with vanishing surface energy density. Stable shells lie in the region above the colored dotted, dashed, or dash-dotted curves, indicated here for values of α equal to $3/5$, $3/4$ and 1, respectively. The bottom panel shows an enlargement of the top panel, to make the stability regions more visible.

The first condition has an obvious interpretation; it states that the masses m_j and m_{j-1} differ by the total mass of the jth shell. The second condition originates from the requirement of hydrostatic equilibrium, and it can be derived using purely Newtonian arguments (see Refs. [27,33] and Appendix A for a more detailed discussion).

From now on, we shall focus on a system of thin equidistant shells of equal masses. We would like to stress that our techniques make possible to analyze models of a more general nature; however, we restrict our attention to this specific case for the sake of simplicity. Hence, we assume that the masses m_j and radii R_j are of the form

$$m_j = j\Delta m, \qquad R_j = R_1 + (j-1)\Delta R, \tag{30}$$

for $j = 1, 2, \ldots, N$. The positive constants Δm, ΔR, and R_1 in Eq. (30) are required to satisfy the conditions

$$\frac{\Delta m}{R_1} \ll 1, \qquad \frac{\Delta m}{\Delta R} \ll 1, \tag{31}$$

for consistency with the weak-field limit (26). It follows from Eqs. (28) and (29) that

$$\sigma_{\mathrm{rest},j} = \frac{\Delta m}{4\pi R_j^2}, \qquad p_j = \frac{(2j-1)(\Delta m)^2}{16\pi R_j^3}, \tag{32}$$

for $j = 1, 2, \ldots, N$. For large j the ratio $p_j/\sigma_{\mathrm{rest},j}$, which is proportional to the temperature of the shell, and the compactness ratio $2m_j/R_j$ are given by

$$\lim_{j\to\infty} \frac{p_j}{\sigma_{\mathrm{rest},j}} = \frac{\Delta m}{2\Delta R} \ll 1, \tag{33}$$

$$\lim_{j\to\infty} \frac{2m_j}{R_j} = 2\frac{\Delta m}{\Delta R} \ll 1. \tag{34}$$

The first condition implies that we are working in the low temperature limit, whereas the second one allows us to consider spacetimes with an arbitrarily high number of shells within the weak-field approximation. For large N, these shells have compactness ratio and temperature approaching a constant value as j becomes large. In contrast to this, note that the surface mass density decays as $1/j^2$ for large j. This property will turn out to be important when we analyze the transmission of waves through a large number of shells (see Sec. VI).

To sum up, Eq. (30) defines a static spacetime consisting of N spherical concentric and equidistant shells of equal mass. Provided conditions (31) are satisfied, this spacetime is stable with respect to small fluctuations of the shells' radii and the gravitational field is weak everywhere. In the rest of this article we shall study the propagation of linear waves emanating from the central region.

III. APPROXIMATE SOLUTIONS OF THE REGGE-WHEELER EQUATION

The propagation of scalar, electromagnetic and linearized gravitational waves in a spherically symmetric spacetime background is described by the RW equation [49] and its generalizations (see, for instance, Refs. [50,51] and references therein). The RW equation is a wave-type "master" equation for a gauge-invariant field Φ from which the original (scalar, electromagnetic, or linearized metric) field can be reconstructed. In this section we construct explicit monochromatic incoming and outgoing solutions of the RW master equation assuming a background

spacetime of the form considered in the previous section and depicted in Fig. 1. Since the RW equation belongs to the confluent Heun class (see, for instance [52]), it is in principle possible to construct *exact* solutions which, however, present a significant interpretative challenge when one considers the nature of incoming and outgoing waves at infinity. For this reason, we adopt a different approach in this article: we focus on the weak-field limit and perform an expansion of the incoming and outgoing solutions in terms of $2m/r$. For a Schwarzschild spacetime, such an expansion can be worked out in a systematic way and leads to a convergent series when done appropriately [53]. However, for the purpose of this article it is sufficient to consider only the zeroth and the first-order terms in $2m/r$, since higher-order corrections have already been neglected when taking the weak-field limit in Sec. II D.

When decomposed into spherical harmonics, the RW master equation for a field of spin S propagating on the spacetime background (2) reads

$$\left[\frac{\partial^2}{\partial t^2}-\frac{\partial^2}{\partial r_*^2}+\left(1-\frac{2m(r)}{r}\right)\left(\frac{\ell(\ell+1)}{r^2}+(1-S^2)\frac{2m(r)}{r^3}\right)\right]\times\Phi_\ell(t,r)=0. \tag{35}$$

In Eq. (35), $\ell \geq S$ denotes the total angular momentum of the field and we do not label the field Φ_ℓ with the magnetic quantum number m since it does not enter the equation. The number S takes the values

$$S := \begin{cases} 0 & \text{scalar,} \\ 1 & \text{electromagnetic,} \\ 2 & \text{odd-parity linearized gravitational,} \end{cases} \tag{36}$$

and r_* is the tortoise coordinate, defined as

$$r_* := \int_{r_0}^{r}\left(1-\frac{2m(x)}{x}\right)^{-1}dx, \tag{37}$$

with an arbitrary constant $r_0 > 0$. Note that in Eqs. (35) and (37) we have written $m(r)$ rather than $m(t,r)$ since the spacetime is static. We will stick to this convention in the rest of the paper. Since the mass function vanishes in the central region we can take $r_0 = 0$; evaluation of the resulting integral yields

$$r_* = r + 2\sum_{k=1}^{j-1} m_k \log\left(\frac{R_{k+1}-2m_k}{R_k-2m_k}\right) + 2m_j\log\left(\frac{r-2m_j}{R_j-2m_j}\right), \tag{38}$$

for $R_j < r < R_{j+1}$. In Eq. (38) and in the rest of this paper, we adopt the convention that a sum is zero if the upper bound is smaller than the lower one. Hence, $r_* = r$ inside the first shell ($0 < r < R_1$) and $r_* = r + 2m_1\log(\frac{r-2m_1}{R_1-2m_1})$ in the region $R_1 < r < R_2$ between the first and second shell. Note that r_* is a continuous function of r; however, its first derivative jumps at each shell.

In what follows, we represent the solution to Eq. (35) as a sum of incoming ($\Phi_{\searrow,\ell}$) and outgoing ($\Phi_{\nearrow,\ell}$) wave functions, with respective amplitudes Λ_ℓ and Υ_ℓ

$$\Phi_\ell(t,r) = \Lambda_\ell\Phi_{\searrow,\ell}(t,r) + \Upsilon_\ell\Phi_{\nearrow,\ell}(t,r). \tag{39}$$

In the next four subsections we construct these functions in the region between two shells, where m is constant, whereas the matching conditions for the function Φ_ℓ across the shells are worked out in Sec. III E.

A. Perturbative setting

As mentioned above, we construct the functions $\Phi_{\searrow,\ell}$ and $\Phi_{\nearrow,\ell}$ using a perturbative approach based on the method developed in [53]. We follow closely the presentation and notation introduced in [41,42]. However, whereas the last two references only consider the cases $S = \ell = 2$ and $S = \ell = 0$, here we generalize these results to arbitrary values of S and ℓ.

As a first step, we change the Schwarzschild coordinates (t,r) to the new coordinates (τ,ρ), defined by[1]

$$\tau := t - r_* + r, \qquad \rho := r. \tag{40}$$

This allows one to rewrite the RW master equation (35) in the form

$$\mathcal{L}_\ell\Phi_\ell(\tau,\rho) = -\frac{2m}{\rho}\mathcal{B}\Phi_\ell(\tau,\rho), \tag{41}$$

where $\mathcal{L}_\ell$ denotes the (spherically reduced) wave operator in flat spacetime,

$$\mathcal{L}_\ell := \frac{\partial^2}{\partial\tau^2}-\frac{\partial^2}{\partial\rho^2}+\frac{\ell(\ell+1)}{\rho^2}, \tag{42}$$

and the operator $\mathcal{B}$ is defined as

$$\mathcal{B} := \left(\frac{\partial}{\partial\tau}+\frac{\partial}{\partial\rho}\right)^2 - \frac{1}{\rho}\left(\frac{\partial}{\partial\tau}+\frac{\partial}{\partial\rho}\right)+\frac{1-S^2}{\rho^2}. \tag{43}$$

The representation (41) in which the small parameter $2m/\rho$ appears on the right-hand side of the equation allows one to seek the outgoing solution in the form

$$\Phi_{\nearrow,\ell}(\tau,\rho) = h_{\nearrow,\ell}(\tau,\rho) + \sum_{k=1}^{\infty}\left(\frac{2m}{R}\right)^k g_{k,\ell}(\tau,\rho). \tag{44}$$

[1]Note that these coordinates are related to the outgoing Eddington-Finkelstein coordinates $(u,r) = (t - r_*, r)$.

In Eq. (44) R is a typical radius ($R \approx R_j$ for our problem), the functions $g_{k,\ell}$ are to be determined, and $h_{\nearrow,\ell}$ is the outgoing solution of the flat wave equation which is constructed in the next subsection. Substituting the ansatz (44) into Eq. (41) results in an infinite hierarchy of wave equations

$$\mathcal{L}_\ell g_{k,\ell} = -\frac{R}{\rho}\mathcal{B} g_{k-1,\ell}, \quad k = 1, 2, 3, \ldots, \tag{45}$$

with $g_0 := h_{\nearrow,\ell}$. As stated previously, in this work we only solve the first of these equations.

B. Flat spacetime outgoing solution

The flat spacetime outgoing solution can be generated from a smooth function U_0 depending only on (minus) retarded time $-u = r_* - t = \rho - \tau$. For $\ell = 0$ it is sufficient to define $h_{\nearrow,\ell}(\tau,\rho) := U_0(\rho-\tau)$, since $\mathcal{L}_0 U_0(\rho-\tau) = 0$. For $\ell > 0$ the solutions can be obtained by successive application of the "creation" operators $a_\ell^\dagger$, where

$$a_\ell := \frac{\partial}{\partial\rho} + \frac{\ell}{\rho}, \qquad a_\ell^\dagger := -\frac{\partial}{\partial\rho} + \frac{\ell}{\rho} \tag{46}$$

satisfy

$$a_{\ell+1} a_{\ell+1}^\dagger = a_\ell^\dagger a_\ell = -\frac{\partial^2}{\partial\rho^2} + \frac{\ell(\ell+1)}{\rho^2}, \tag{47}$$

from which it follows that $\mathcal{L}_\ell a_\ell^\dagger a_{\ell-1}^\dagger \cdots a_1^\dagger = a_\ell^\dagger a_{\ell-1}^\dagger \cdots a_1^\dagger \mathcal{L}_0$. Therefore, the function

$$\begin{aligned} h_{\nearrow,\ell}(\tau,\rho) &:= a_\ell^\dagger a_{\ell-1}^\dagger \cdots a_1^\dagger U_0(\rho-\tau) \\ &= \sum_{k=0}^{\ell} \frac{(\ell+k)!}{k!(\ell-k)!}\frac{(-1)^\ell}{(-2\rho)^k}\frac{d^{\ell-k}}{d\rho^{\ell-k}} U_0(\rho-\tau) \end{aligned} \tag{48}$$

satisfies the flat wave equation $\mathcal{L}_\ell h_{\nearrow,\ell} = 0$.

Similarly, incoming solutions can be constructed by changing the sign of τ. For the next subsection the following solution will play an important role

$$\begin{aligned} K_\ell(\tau,\rho,x) &:= a_\ell^\dagger a_{\ell-1}^\dagger \cdots a_1^\dagger \frac{1}{(\tau+\rho+x)^2} \\ &= \frac{1}{(2\rho)^{\ell+2}} \sum_{k=0}^{\ell} \frac{(2\ell-k)!(k+1)}{(\ell-k)!}\left(\frac{2\rho}{\tau+\rho+x}\right)^{k+2}. \end{aligned} \tag{49}$$

Using the binomial identity

$$\sum_{k=0}^{p}\binom{\ell+k}{k} = \binom{\ell+1+p}{p}, \quad p = 0, 1, 2, \ldots, \tag{50}$$

it is not difficult to verify that

$$\left(\frac{\partial}{\partial\tau} + \frac{\partial}{\partial\rho}\right) K_\ell(\tau,\rho,x)\Big|_{x=\rho-\tau} = -\frac{(2\ell+1)!}{2^{\ell+1}\ell!}\frac{1}{\rho^{\ell+3}}, \tag{51}$$

from which one obtains the following identity

$$\mathcal{L}_\ell \int_{\rho-\tau}^{\infty} K_\ell(\tau,\rho,x) U_0(x) dx = -\frac{(2\ell+1)!}{2^\ell \ell!}\frac{U_0(\rho-\tau)}{\rho^{\ell+3}}, \tag{52}$$

valid for any smooth function $U_0(x)$ which is bounded for $x \to \infty$. This identity will be useful in the next subsection, when computing the first-order correction terms.

C. Outgoing solution including first-order correction terms

The first-oder correction term $g_{1,\ell}$ is determined by Eq. (45) for $k = 1$, that is,

$$\mathcal{L}_\ell g_{1,\ell} = -\frac{R}{\rho}\mathcal{B} h_{\nearrow,\ell}, \tag{53}$$

where $h_{\nearrow,\ell}$ is given by Eq. (48). Using Eqs. (43) and (48) one finds

$$\begin{aligned} &\mathcal{B} h_{\nearrow,\ell}(\tau,\rho) \\ &= \frac{(-1)^\ell}{\rho^2}\sum_{k=0}^{\ell}\frac{(\ell+k)!}{k!(\ell-k)!}\frac{k(k+2)+1-S^2}{(-2\rho)^k}\frac{d^{\ell-k}}{d\rho^{\ell-k}} U_0(\rho-\tau). \end{aligned} \tag{54}$$

Motivated by this form and the results in Sec. 5.2 of Ref. [41] and the appendix in Ref. [42], we propose the following ansatz for $g_{1,\ell}(\tau,\rho)$:

$$g_{1,\ell}(\tau,\rho) = R\left(\phi_\ell(\tau,\rho) + \beta\int_{\rho-\tau}^{\infty} K_\ell(\tau,\rho,x) U_0(x) dx\right), \tag{55}$$

where

$$\phi_\ell(\tau,\rho) := \sum_{k=0}^{\ell}\frac{\gamma_{\ell k}}{(k+1)!}\frac{(-1)^{\ell+1}}{(-2\rho)^{k+1}}\frac{d^{\ell-k}}{d\rho^{\ell-k}} U_0(\rho-\tau), \tag{56}$$

the integral kernel K_ℓ is given by Eq. (49), and the constants β and $\gamma_{\ell k}$ need to be adjusted. Substituting this ansatz into Eq. (53) yields $\beta = 1$ and $\gamma_{\ell,0} = 0$, whereas the remaining constants are obtained from the recurrence relation

$$\gamma_{\ell k} = \frac{2k(\ell+k-1)!}{(\ell-k+1)!}(k^2 - S^2) + (\ell-k)(\ell+k+1)\gamma_{\ell,k-1}, \tag{57}$$

for $k = 1, 2, \ldots, \ell$. Using the previous results, one can write the outgoing wave solution as

$$\Phi_{\nearrow,\ell}(\tau,\rho) = (-1)^\ell \sum_{k=0}^{\ell} \left\{ \left[\frac{(\ell+k)!}{k!(\ell-k)!} + \frac{m}{\rho}\frac{\gamma_{\ell k}}{(k+1)!} \right] \frac{1}{(-2\rho)^k} \frac{d^{\ell-k}}{d\rho^{\ell-k}} U_0(\rho-\tau) + \frac{m}{\rho}\frac{(2\ell-k)!(k+1)}{(\ell-k)!(-2\rho)^\ell} \int_1^\infty U_0(2\rho y - \tau - \rho)\frac{dy}{y^{k+2}} \right\} + \mathcal{O}\left(\frac{2m}{R}\right)^2. \tag{58}$$

The terms in the first line include the first-order correction in $2m/R$ from the curvature of the background and obey Huygens' principle, whereas the terms on the second line describe the leading-order effects from the backscatter. Notice that these terms are present for all $\ell \geq S$; hence backscatter is always present for linear waves of spin S fields on a Schwarzschild background. For dipolar electromagnetic radiation, $\ell = S = 1$ and one finds $\gamma_{1,0} = \gamma_{1,1} = 0$, whereas for quadrupolar linearized gravitational waves one has $\ell = S = 2$, and therefore

$$\gamma_{2,0} = \gamma_{2,2} = 0, \qquad \gamma_{2,1} = -6, \tag{59}$$

and Eq. (58) coincides with the outgoing solution on page 6735 of Ref. [41].

In what follows, we consider a monochromatic plane wave of frequency ω, for which the function U_0 is given by

$$U_0(x) := \frac{e^{-sx}}{s^\ell}, \qquad s := -i\omega, \tag{60}$$

such that

$$U_0(\rho-\tau) = \frac{1}{s^\ell} e^{-i\omega(\tau-\rho)} = \frac{1}{s^\ell} e^{-i\omega(t-r_*)}. \tag{61}$$

Substituting this into Eq. (58) and expressing the result in terms of the original coordinates (t, r) yields the outgoing solution

$$\Phi_{\nearrow,\ell}(t,r) = e^{-i\omega t} X_{\nearrow,\ell}(r), \tag{62}$$

with

$$X_{\nearrow,\ell}(r) = e^{i\omega r_*} \sum_{k=0}^{\ell} \left\{ \left[\frac{(\ell+k)!}{k!(\ell-k)!} + \frac{m}{r}\frac{\gamma_{\ell k}}{(k+1)!} \right] \frac{1}{(2sr)^k} + \frac{m}{r}\frac{(2\ell-k)!(k+1)}{(\ell-k)!(2sr)^\ell} e^{2sr} E_{k+2}(2sr) \right\} + \mathcal{O}\left(\frac{2m}{r}\right)^2, \tag{63}$$

where we recall that $s = -i\omega$ and where E_p refers to the generalized exponential integrals, defined by [54][pg. 185]

$$E_p(z) := \int_1^\infty \frac{e^{-zy}}{y^p} dy, \quad p = 0, 1, 2, \ldots \tag{64}$$

They are holomorphic for $\mathrm{Re}(z) > 0$, finite for $\mathrm{Re}(z) \geq 0$ when $p \geq 2$, satisfy the recurrence relation

$$pE_{p+1}(z) = e^{-z} - zE_p(z), \tag{65}$$

and behave as $E_p(z) \sim e^{-z}/z$ for $z \to \infty$.

This concludes our discussion of the outgoing solution including the first-order correction terms in $2m/r$.

D. Incoming solution including first-order correction terms

Taking advantage of the fact that the RW equation (35) is invariant with respect to the inversion of time $t \mapsto -t$, the incoming solution $\Phi_{\nwarrow,\ell}$ can be obtained from the outgoing one as follows:

$$\Phi_{\nwarrow,\ell}(t,r) = \overline{\Phi_{\nearrow,\ell}(-t,r)} = e^{-i\omega t}\overline{X_{\nearrow,\ell}(r)}. \tag{66}$$

Therefore, the incoming solution is obtained by replacing $X_{\nearrow,\ell}$ by its complex conjugate. Note that in Eq. (66) we use the symbol $\overline{(\cdots)}$ to denote the complex conjugate. We shall follow this convention throughout this paper.

Accordingly, Eq. (39) can be rewritten in the form

$$\Phi_\ell(t,r) = e^{-i\omega t} X_\ell(r), \qquad X_\ell(r) := \Lambda_\ell X_{\nwarrow,\ell}(r) + \Upsilon_\ell X_{\nearrow,\ell}(r) \tag{67}$$

with $X_{\nearrow,\ell}$ given by Eq. (63) and

$$X_{\nwarrow,\ell}(r) = \overline{X_{\nearrow,\ell}(r)}. \tag{68}$$

E. Matching conditions at the shells

So far, the incoming and outgoing solutions have been constructed in the regions between the shells, where m is constant. Here, we discuss the matching conditions that allow one to join the solutions at the shells. We shall use the symbol $X_{\ell,j}(r)$ for the solution (67) within the region $R_j < r < R_{j+1}$ and we will represent the amplitudes of the corresponding in- and outgoing waves with $\Lambda_{\ell,j}$ and $\Upsilon_{\ell,j}$.

Note that the total mass inside this region is $m = m_j$. The matching conditions are understood best when looking at the RW equation (35) in terms of the coordinates (t, r_*). Recall that r_* is a continuous monotonously increasing function of r, such that r also depends continuously on r_*. However, the function $m(r)$ jumps at each shell; thus, when introducing the monochromatic ansatz $\Phi_\ell(t,r) = e^{-i\omega t}X_\ell(r)$, one obtains a time-independent Schrödinger equation with a potential that jumps at each shell. As is well known, for such problems the correct matching conditions are the requirements that both $X_\ell(r)$ and its first derivative (with respect to r_*) must be continuous, which leads to

$$X_{\ell,j}(R_j) = X_{\ell,j-1}(R_j), \tag{69}$$

and

$$\left.\frac{dX_{\ell,j}(r)}{dr_*}\right|_{r=R_j} = \left.\frac{dX_{\ell,j-1}(r)}{dr_*}\right|_{r=R_j} \tag{70}$$

for all $j = 1, 2, \ldots, N$. However, note that the derivative of $X_\ell(r)$ with respect to the areal radius r jumps since dr_*/dr involves the function $m(r)$ [see Eq. (37)].

Using Eq. (67), the matching conditions (69), (70) can be reformulated in terms of the coefficients $\Lambda_{\ell,j}$ and $\Upsilon_{\ell,j}$ as follows:

$$\mathbb{D}_{\ell,j}(R_j)\begin{pmatrix}\Upsilon_{\ell,j}\\ \Lambda_{\ell,j}\end{pmatrix} = \mathbb{D}_{\ell,j-1}(R_j)\begin{pmatrix}\Upsilon_{\ell,j-1}\\ \Lambda_{\ell,j-1}\end{pmatrix}, \tag{71}$$

where

$$\mathbb{D}_{\ell,j}(r) \coloneqq \begin{pmatrix} X_{\nearrow\ell,j}(r) & X_{\nwarrow\ell,j}(r)\\ \frac{dX_{\nearrow\ell,j}}{dr_*}(r) & \frac{dX_{\nwarrow\ell,j}}{dr_*}(r)\end{pmatrix}. \tag{72}$$

The determinant of the matrix (72) is independent of r, since both $e^{st}X_{\nearrow\ell,j}(r)$ and $e^{st}X_{\nwarrow\ell,j}(r)$ are solutions of the RW equation (35). Evaluating the determinant (for fixed mass) in the limit $r \to \infty$ one finds

$$\det\left(\mathbb{D}_{\ell,j}(r)\right) = 2s, \tag{73}$$

and thus the matrix is invertible as long as $s = -i\omega \neq 0$.

Finally, for future reference, we write the explicit form of the tortoise coordinate r_* at each shell. Using Eq. (38), one obtains

$$r_*(R_j) = R_j + 2\sum_{k=1}^{j-1} m_k \log\left(\frac{R_{k+1}-2m_k}{R_k-2m_k}\right), \tag{74}$$

for $j = 1, 2, \ldots, N$.

IV. TRANSFER MATRIX METHOD

In this section we introduce the transfer matrix formalism, and we compute the explicit form of the transfer matrices using a perturbative approach. To this purpose it is convenient to rewrite Eq. (71) in the form

$$\begin{pmatrix}\Upsilon_{\ell,j}\\ \Lambda_{\ell,j}\end{pmatrix} = \mathbb{M}_j\begin{pmatrix}\Upsilon_{\ell,j-1}\\ \Lambda_{\ell,j-1}\end{pmatrix}, \tag{75}$$

where we have introduced the transfer matrix

$$\mathbb{M}_j \coloneqq \mathbb{D}_{\ell,j}(R_j)^{-1}\mathbb{D}_{\ell,j-1}(R_j). \tag{76}$$

The transfer matrix (76) matches the amplitudes of the in- and out-going waves on both sides of the jth shell. The explicit form of this matrix is

$$\mathbb{M}_j = \begin{pmatrix}(\mathbb{M}_j)_{11} & (\mathbb{M}_j)_{12}\\ (\mathbb{M}_j)_{21} & (\mathbb{M}_j)_{22}\end{pmatrix}. \tag{77}$$

with

$$(\mathbb{M}_j)_{11} = \frac{1}{2s}\left(\frac{dX_{\nwarrow\ell,j}}{dr_*}X_{\nearrow\ell,j-1} - X_{\nwarrow\ell,j}\frac{dX_{\nearrow\ell,j}}{dr_*}\right), \tag{78}$$

$$(\mathbb{M}_j)_{12} = \frac{1}{2s}\left(\frac{dX_{\nwarrow\ell,j}}{dr_*}X_{\nwarrow\ell,j-1} - X_{\nwarrow\ell,j}\frac{dX_{\nwarrow\ell,j}}{dr_*}\right), \tag{79}$$

$$(\mathbb{M}_j)_{21} = \frac{1}{2s}\left(-\frac{dX_{\nearrow\ell,j}}{dr_*}X_{\nearrow\ell,j-1} + X_{\nearrow\ell,j}\frac{dX_{\nearrow\ell,j}}{dr_*}\right), \tag{80}$$

$$(\mathbb{M}_j)_{22} = \frac{1}{2s}\left(-\frac{dX_{\nearrow\ell,j}}{dr_*}X_{\nwarrow\ell,j-1} + X_{\nearrow\ell,j}\frac{dX_{\nwarrow\ell,j}}{dr_*}\right), \tag{81}$$

where it is understood that the expressions on the right-hand side are evaluated at $r = R_j$.

Taking into account Eq. (68) and the fact that $s = -i\omega$ is purely imaginary it is easy to see that

$$(\mathbb{M}_j)_{22} = \overline{(\mathbb{M}_j)_{11}}, \tag{82}$$

$$(\mathbb{M}_j)_{21} = \overline{(\mathbb{M}_j)_{12}}. \tag{83}$$

From Eq. (73) it also follows immediately that the determinant of $\mathbb{M}_j(r)$ is unitary

$$\det(\mathbb{M}_j) = 1. \tag{84}$$

By multiplying successive transfer matrices, one obtains the total transfer matrix

$$\mathbb{M}_T \coloneqq \mathbb{M}_N\mathbb{M}_{N-1}\cdots\mathbb{M}_1, \tag{85}$$

which connects the amplitudes $\Upsilon_{\ell,0}$ and $\Lambda_{\ell,0}$ in the inner Minkowski space with the amplitudes $\Upsilon_{\ell,N}$ and $\Lambda_{\ell,N}$ of the waves outside of the Nth shell

$$\begin{pmatrix} \Upsilon_{\ell,N} \\ \Lambda_{\ell,N} \end{pmatrix} = \mathbb{M}_T \begin{pmatrix} \Upsilon_{\ell,0} \\ \Lambda_{\ell,0} \end{pmatrix}. \tag{86}$$

Note that the total transfer matrix (85) also satisfies the properties (82), (83), and (84).

A. Perturbative expansion of transfer matrices

It is useful to write the matrix $\mathbb{D}_{\ell,j}$ as the sum of two terms

$$\mathbb{D}_{\ell,j}(r) = \mathbb{D}^{(0)}_\ell(r) + \frac{2m_j}{r}\frac{\mathbb{D}^{(1)}_\ell(r)}{\omega r}, \tag{87}$$

where the first matrix on the right-hand side of Eq. (87) does not depend on the mass function $m(r)$, while the second summand is proportional to the weak-field term $2m(r)/r$. After introducing the matrix

$$\mathbb{B}_\ell(r) \coloneqq [\mathbb{D}^{(0)}_\ell(r)]^{-1}\mathbb{D}^{(1)}_\ell(r), \tag{88}$$

one can factor out $\mathbb{D}^{(0)}_\ell(r)$ in Eq. (87) and write

$$\mathbb{D}_{\ell,j}(r) = \mathbb{D}^{(0)}_\ell(r)\left(\mathbb{1} + \frac{2m_j}{r}\frac{\mathbb{B}_\ell(r)}{\omega r}\right). \tag{89}$$

This makes possible to express the transfer matrix (76) as

$$\mathbb{M}_j = \left[\mathbb{1} + \frac{2m_j}{R_j}\frac{\mathbb{B}_\ell(R_j)}{\omega R_j}\right]^{-1}\left[\mathbb{1} + \frac{2m_{j-1}}{R_j}\frac{\mathbb{B}_\ell(R_j)}{\omega R_j}\right]. \tag{90}$$

It is important to observe that the matrix (88) is bounded for finite values of ωr. It remains bounded in the limit $\omega r \to \infty$ as can be seen from the high-frequency asymptotic expansion

$$\mathbb{B}_\ell(r) = \mathbb{B}^{(0)}_\ell(r) + \frac{1}{\omega r}\mathbb{B}^{(1)}_\ell(r) + \mathcal{O}\left(\frac{1}{(\omega r)^2}\right) \tag{91}$$

with

$$\mathbb{B}^{(0)}_\ell(r) = \frac{1-S^2}{4}\begin{pmatrix} i & 0 \\ 0 & -i \end{pmatrix} \tag{92}$$

and

$$\mathbb{B}^{(1)}_\ell(r) = -\frac{\ell(\ell+1)-1+S^2}{4}\begin{pmatrix} 0 & e^{-2i\omega r_*} \\ e^{2i\omega r_*} & 0 \end{pmatrix}. \tag{93}$$

Note that the zeroth order term (92) gives the dominant contribution in the high-frequency limit for scalar ($S = 0$) and gravitational fields ($S = 2$), whereas it vanishes for an electromagnetic field ($S = 1$). In the latter case the first-order term, proportional to the matrix (93), provides the leading contribution.

The fact that the matrix (88) is bounded allows one to expand the right-hand side of Eq. (90) in the weak field limit (26) and approximate the single-shell transfer matrix as

$$\mathbb{M}_j = \mathbb{1} - \frac{2\Delta m_j}{\omega R_j^2}\mathbb{B}_\ell(R_j) + \mathcal{O}\left(\left(\frac{2m_j}{\omega R_j^2}\mathbb{B}_\ell(R_j)\right)^2\right), \tag{94}$$

where the matrix $\mathbb{B}_\ell(R_j)$ must be understood as a shorthand notation for the truncated expansion (91).

Equation (94) shows that the single-shell transfer matrices share two features: (a) they are "close" to the unit matrix, i.e., they have the form

$$\mathbb{M}_j = \mathbb{1} - \epsilon_j\mathbb{B}_\ell(R_j) + \ldots, \tag{95}$$

and (b) their "distance" from the unit matrix, which is measured by the parameter ϵ_j, decreases as $1/j^2$. As discussed in Appendix B, these two features ensure that the total transfer matrix (85) can be written in the form

$$\mathbb{M}_T = \mathbb{1} - 2\sum_{k=1}^{N}\frac{\Delta m}{\omega(R_1+(k-1)\Delta R)^2}\mathbb{B}_\ell(R_k) + \mathcal{O}\left(\left(\frac{\Delta m}{\omega(\Delta R)^2}\right)^2\right). \tag{96}$$

We remark that condition (a), in itself, does not guarantee the validity of the expansion (96); it is also necessary that the parameters ϵ_j decrease sufficiently fast for increasing values of j. In the present case both conditions are fulfilled.

V. TRANSMISSION AND REFLECTION COEFFICIENTS

We now analyze the transport properties of the spacetime defined in Sec. II. We focus our attention on the propagation of a monochromatic spherical wave of frequency ω and total angular momentum ℓ. We consider a wave which, after being radiated from the center of the inner Minkowski space, crosses N thin concentric shells. Our purpose is to compute the corresponding transmission and reflection coefficients.

To achieve this goal, we first have to determine the energy flux associated with a spherical wave. In the case of scalar ($S = 0$) and electromagnetic ($S = 1$) waves, incoming and outgoing fluxes can be computed in a straightforward way by means of the energy-momentum tensor associated with the field. The case of linearized gravitational waves ($S = 2$) is more delicate, because for gravitational radiation there is not an energy-momentum tensor

with the properties of being covariantly defined, local, and divergence-free (see, for instance, Refs. [55]). Nevertheless, as discussed below, the covariant interpretation of the RW equation (35) [51,56] allows one to introduce a universal *effective* energy-momentum tensor $T_{\mu\nu}$ which gives rise to a conserved current when contracted with the timelike Killing vector field of the Schwarzschild spacetime, even if the tensor $T_{\mu\nu}$ has a nonvanishing divergence. In this way it is possible to compute the desired conserved flux for fields of arbitrary spin S. For $S=0$, the effective $T_{\mu\nu}$ coincides with the usual energy-momentum tensor of the scalar field (which is divergence-free), whereas for $S=1$ it is shown in Appendix C that the resulting fluxes agree (up to a constant factor) with those associated with the Poynting vector.

Our universal approach is based on rewriting the RW equation (35) in the covariant form [51,57]

$$\Box\Psi + V(r)\Psi = 0, \qquad V(r) = -\frac{2m(r)S^2}{r^3}, \tag{97}$$

where $\Box := -\nabla^\mu\nabla_\mu$ is the curved spacetime d'Alembert operator and Ψ is a (real-valued) scalar function which admits the series representation

$$\Psi(t,r,\vartheta,\varphi) = \frac{1}{r}\sum_{\ell=S}^{\infty}\sum_{m=-\ell}^{\ell}\Phi_{\ell m}(t,r)Y^{\ell m}(\vartheta,\varphi). \tag{98}$$

In Eq. (98) the functions $\Phi_{\ell m}$ are solutions of the RW equation (35), while the functions $Y^{\ell m}$ are standard spherical harmonics, and we have momentarily reintroduced the magnetic quantum number m which should not be confused with the mass function $m(r)$. The functions $\Phi_{\ell m}$ should be chosen such that $\overline{\Phi_{\ell m}} = (-1)^m\Phi_{\ell,-m}$ in order to guarantee that Ψ is real-valued. Equation (97) describes a scalar field Ψ which is subject to the external effective potential $V(r)$. Note that for $S=0$ this potential vanishes and Eq. (97) reduces to the standard wave equation.

Motivated by these observations, we introduce the effective energy-momentum tensor

$$T_{\mu\nu} := (\nabla_\mu\Psi)(\nabla_\nu\Psi) - \frac{1}{2}g_{\mu\nu}[(\nabla^\alpha\Psi)(\nabla_\alpha\Psi) + V(r)\Psi^2] \tag{99}$$

which is symmetric by definition and, according to Eq. (97), satisfies the divergence law

$$\nabla^\mu T_{\mu\nu} = -\frac{1}{2}\frac{dV}{dr}(r)(\nabla_\nu r)\Psi^2. \tag{100}$$

As stated above, the right-hand side is only zero in the scalar case, i.e., when $S=0$. However, when both sides of Eq. (100) are contracted with the timelike Killing vector field $k := \partial/\partial t$, one obtains the conservation law

$$\nabla_\mu J^\mu_\epsilon = 0, \qquad J^\mu_\epsilon := -T^\mu{}_\nu k^\nu, \tag{101}$$

since $k[r] = k^\nu\nabla_\nu r = 0$. As shown below, the presence of this conserved current allows one to compute the in- and outflow of scalar, electromagnetic and linearized "gravitational" energy across surfaces with a fixed radius over a given time period in a fully covariant way. This finding underscores that the presence of a divergence-free energy-momentum tensor is not a prerequisite for defining conserved currents. Nonetheless, the physical nature of the effective tensor (99) remains elusive.

A. Energy flux through a sphere

The energy that is radiated through a sphere S^2_r of constant radius r during the time interval Δt is given by the flux integral

$$\Delta F = \int_{[t,t+\Delta t]\times S^2_r} J^\mu_\epsilon n_\mu d\Sigma, \tag{102}$$

over the three-dimensional hypersurface $[t, t+\Delta t]\times S^2_r$. In Eq. (102) $d\Sigma$ denotes a surface element and n_μ is the unit outward covector to this surface. For the spacetime with metric (2) one has

$$n_\mu = \frac{\nabla_\mu r}{\sqrt{1-\frac{2m(r)}{r}}}, \qquad d\Sigma = \sqrt{1-\frac{2m(r)}{r}}r^2 dt d\Omega, \tag{103}$$

and hence the average energy radiated per unit time is given by

$$\frac{\Delta F}{\Delta t} = \frac{r^2}{\Delta t}\int_t^{t+\Delta t} dt \int_{S^2_r} d\Omega J^r_\epsilon. \tag{104}$$

Note that this average only depends on the radial component of the current, which is equal to

$$J^r_\epsilon = -T^r{}_t = -\left(\frac{\partial\Psi}{\partial r_*}\right)\left(\frac{\partial\Psi}{\partial t}\right). \tag{105}$$

We remind the reader that the tortoise coordinate r_* is defined by Eq. (37). We next introduce the expansion (98) in Eq. (105) and integrate the radial current over a sphere. With the help of the orthonormality relations of the spherical harmonics, we obtain

$$r^2\int_{S^2_r} d\Omega J^r_\epsilon = -\sum_{\ell=S}^{\infty}\sum_{m=-\ell}^{\ell}\mathrm{Re}\left[\left(\frac{\partial\overline{\Phi_{\ell m}}}{\partial r_*}\right)\left(\frac{\partial\Phi_{\ell m}}{\partial t}\right)\right] + \frac{1}{r}\left(1-\frac{2m(r)}{r}\right)\sum_{\ell=S}^{\infty}\sum_{m=-\ell}^{\ell}\mathrm{Re}\left(\overline{\Phi_{\ell m}}\frac{\partial\Phi_{\ell m}}{\partial t}\right). \tag{106}$$

Taking into account the monochromatic ansatz (67) and the identity (68), we conclude that the second series in the right-hand side of Eq. (106) vanishes, while the summands in the first series are equal to

$$\frac{i\omega}{2}(|\Lambda_{\ell m}|^2-|\Upsilon_{\ell m}|^2)\det\begin{pmatrix} X_{\nearrow,\ell m} & X_{\nwarrow,\ell m} \\ \frac{\partial X_{\nearrow,\ell m}}{\partial r_*} & \frac{\partial X_{\nwarrow,\ell m}}{\partial r_*}\end{pmatrix}. \tag{107}$$

The Wronskian in the previous expression is equal to the determinant of the matrix (72), i.e., to $2s=-2i\omega$. One is thus led to the conclusion that the average energy flux through a sphere of constant radius r is

$$\frac{\Delta F}{\Delta t}=\omega^2\sum_{\ell=S}^{\infty}\sum_{m=-\ell}^{\ell}(|\Upsilon_{\ell m}|^2-|\Lambda_{\ell m}|^2). \tag{108}$$

Note that the flux (108) does not depend on the surface radius r; it is proportional to the square of the frequency ω, and positive for purely outgoing waves and negative for incoming ones.

As an additional remark, we observe that Eq. (108) makes possible to prove that the conservation law (101) is consistent with the unimodularity of the transfer matrices, see Eq. (84). In fact, when the condition of flux conservation (101) is applied to a monochromatic wave crossing the jth shell, one obtains

$$|\Upsilon_{\ell m,j}|^2-|\Lambda_{\ell m,j}|^2=|\Upsilon_{\ell m,j-1}|^2-|\Lambda_{\ell m,j-1}|^2. \tag{109}$$

With the help of Eq. (75), one can write the previous identity as

$$\begin{aligned}&[|(\mathbb{M}_j)_{11}|^2-|(\mathbb{M}_j)_{12}|^2][|\Upsilon_{\ell m,j-1}|^2-|\Lambda_{\ell m,j-1}|^2]\\&\quad=|\Upsilon_{\ell m,j-1}|^2-|\Lambda_{\ell m,j-1}|^2,\end{aligned} \tag{110}$$

which leads to the conclusion that

$$|(\mathbb{M}_j)_{11}|^2-|(\mathbb{M}_j)_{12}|^2=1. \tag{111}$$

Eq. (111), together with conditions (82) and (83), implies that the determinant of the transfer matrix $\mathbb{M}_j$ is equal to one.

B. Transmission and reflection coefficients

The transmission and reflection coefficients across N shells are defined as follows:

$$\mathscr{T}:=\frac{\text{Transmitted flux}}{\text{Incident flux}}, \tag{112}$$

$$\mathscr{R}:=\frac{|\text{Reflected flux}|}{\text{Incident flux}}. \tag{113}$$

Taking into account Eq. (108), for a monochromatic wave of angular momentum ℓ and magnetic quantum number m, these coefficients become

$$\mathscr{T}=\frac{|\Upsilon_{\ell m,N}|^2}{|\Upsilon_{\ell m,0}|^2},\qquad \mathscr{R}=\frac{|\Lambda_{\ell m,0}|^2}{|\Upsilon_{\ell m,0}|^2}. \tag{114}$$

Equation (86) shows that the amplitudes of the impinging, reflected, and transmitted waves are linked by the total transfer matrix. Assuming that no incoming radiation reaches the outer Nth shell from the external region, Eq. (86) can be written as

$$0=(M_T)_{11}\Lambda_{\ell m,0}+(M_T)_{12}\Upsilon_{\ell m,0}, \tag{115}$$

$$\Upsilon_{\ell m,N}=(M_T)_{21}\Lambda_{\ell m,0}+(M_T)_{22}\Upsilon_{\ell m,0}. \tag{116}$$

These equations, together with the properties (82), (83), and (84) of the total transfer matrix, make possible to write the transmission and reflection coefficients as

$$\mathscr{R}=\frac{|(M_T)_{12}|^2}{|(M_T)_{11}|^2},\qquad \mathscr{T}=\frac{1}{|(M_T)_{11}|^2}. \tag{117}$$

Note that the condition of unitary determinant implies that

$$\mathscr{T}+\mathscr{R}=1, \tag{118}$$

as expected.

VI. RESULTS

In this section we present the most relevant results for the reflection and transmission coefficients in the weak field limit. We provide explicit expressions for $\mathscr{R}$ and $\mathscr{T}$ for scalar, electromagnetic and odd-parity linearized gravitational radiation fields with total angular momentum number ℓ satisfying $S\le\ell\le 4$. Furthermore, we analyze in greater detail the transmission properties of our model in the high-frequency limit.

To compute the transmission and reflection coefficients one must insert the elements of the transfer matrix (96) into Eq. (117), which yields

$$\mathscr{T}=\frac{1}{\left|1-\frac{2\Delta m}{\omega}\sum_{k=1}^{N}\frac{(\mathbb{B}_\ell(R_k))_{11}}{(R_1+(k-1)\Delta R)^2}\right|^2}+\mathcal{O}\left(\left(\frac{\Delta m}{\omega\Delta R^2}\right)^2\right), \tag{119}$$

$$\mathscr{R}=\frac{\left|\frac{2\Delta m}{\omega}\sum_{k=1}^{N}\frac{(\mathbb{B}_\ell(R_k))_{12}}{(R_1+(k-1)(\Delta R))^2}\right|^2}{\left|1-\frac{2\Delta m}{\omega}\sum_{k=1}^{N}\frac{(\mathbb{B}_\ell(R_k))_{11}}{(R_1+(k-1)\Delta R)^2}\right|^2}+\mathcal{O}\left(\left(\frac{\Delta m}{\omega(\Delta R)^2}\right)^3\right). \tag{120}$$

It is important to observe that the matrices $\mathbb{B}_\ell(R_k)$ have purely imaginary diagonal elements, as can be

deduced from the properties of the matrices $\mathbb{D}_{\ell,j}(r)$, see Appendix D. As a consequence, the denominators on the right-hand sides of Eqs. (119) and (120) differ from one by a term which is quadratic rather than linear in the expansion parameter $\Delta m/(\omega(\Delta R)^2)$. Since we have determined $\mathbb{B}_\ell(R_k)$ only up to first-order terms, we cannot use Eq. (119) to determine the leading-order correction of the transmission coefficient. However, we can use Eq. (120) to compute the reflection coefficient in the second-order approximation and then obtain $\mathscr{T}$ from the property (118) of flux conservation.

A. Weak field reflection coefficient

Using Eqs. (63), (72), (87), (88), one obtains from Eq. (120) the following explicit expressions for the reflection coefficient, neglecting third or higher order terms in the expansion parameter:

(1) For the case $\ell = S = 0$,

$$\mathscr{R} \simeq \left(\frac{\Delta m}{\omega}\right)^2 \left| \sum_{k=1}^{N} \frac{e^{2i\omega(R_k - r_*(R_k))} E_3(2i\omega R_k)}{(R_1 + (k-1)\Delta R)^2} \right|^2 . \quad (121)$$

(2) For the case $\ell = 1$ and $S = 0$ or $S = 1$

$$\mathscr{R} \simeq \left(\frac{\Delta m}{\omega}\right)^2 \left| \sum_{k=1}^{N} \frac{e^{-2i\omega r_*(R_k)}}{(R_1 + (k-1)\Delta R)^2} \times \left[\frac{S^2}{4(\omega R_k)^2}(i - 2\omega R_k) - i e^{2i\omega R_k} E_3(2i\omega R_k) \right] \right|^2 . \quad (122)$$

(3) For the case $\ell = 2$ and $S = 0$, 1 or 2,

$$\mathscr{R} \simeq \left(\frac{\Delta m}{\omega}\right)^2 \left| \sum_{k=1}^{N} \frac{e^{-2i\omega r_*(R_k)}}{(R_1 + (k-1)\Delta R)^2} \times \left[\frac{3(S^2+3)}{2(\omega R_k)^4}(2\omega R_k - i) + \frac{3(S^2+10)i}{4(\omega R_k)^2} - \frac{S^2+6}{2\omega R_k} + i e^{2i\omega R_k} E_3(2i\omega R_k) \right] \right|^2 . \quad (123)$$

(4) For the case $\ell = 3$ and $S = 0$, 1 or 2,

$$\mathscr{R} \simeq \left(\frac{\Delta m}{\omega}\right)^2 \left| \sum_{k=1}^{N} \frac{e^{-2i\omega r_*(R_k)}}{(R_1 + (k-1)\Delta R)^2} \times \left[\frac{225(S^2+8)}{8(\omega R_k)^6}(i - 2\omega R_k) - \frac{15(13S^2+106)i}{4(\omega R_k)^4} + \frac{15(3S^2+26)}{2(\omega R_k)^3} + \frac{21(S^2+10)i}{4(\omega R_k)^2} - \frac{S^2+10}{2\omega R_k} - i e^{2i\omega R_j} E_3(2i\omega R_k) \right] \right|^2 . \quad (124)$$

(5) For the case $\ell = 4$ and $S = 0$, 1 or 2,

$$\mathscr{R} \simeq \left(\frac{\Delta m}{\omega}\right)^2 \left| \sum_{k=1}^{N} \frac{e^{-2i\omega r_*(R_k)}}{(R_1 + (k-1)\Delta R)^2} \times \left[\frac{2205(S^2+15)}{2(\omega R_k)^8}(2\omega R_k - i) + \frac{315(51S^2+770)i}{8(\omega R_k)^6} - \frac{105(41S^2+630)}{4(\omega R_k)^5} - \frac{15(97S^2+1544)i}{4(\omega R_k)^4} + \frac{3(51S^2+860)}{2(\omega R_k)^3} + \frac{37S^2+660}{4(\omega R_k)^2} i - \frac{S^2+20}{2\omega R_k} + i e^{2i\omega R_k} E_3(2i\omega R_k) \right] \right|^2 . \quad (125)$$

In these formulas the exponential term $e^{-2i\omega r_*(R_k)}$ can be computed with the help of Eq. (74), which yields

$$\exp\left(-2i\omega r_*(R_k)\right) = \exp\left[-2i\omega R_1 \left(1 + (k-1)\frac{\Delta R}{R_1}\right)\right] \times \exp\left[-4i\omega\Delta m \sum_{j=1}^{k-1} j \log\left(\frac{1 + j(\frac{\Delta R}{R_1} - \frac{2\Delta m}{R_1})}{1 - \frac{\Delta R}{R_1} + j(\frac{\Delta R}{R_1} - \frac{2\Delta m}{R_1})}\right)\right] . \quad (126)$$

Interestingly, for scalar waves ($S = 0$), the reflection coefficients for monopolar ($\ell = 0$) and dipolar ($\ell = 1$) waves are identical to each other.

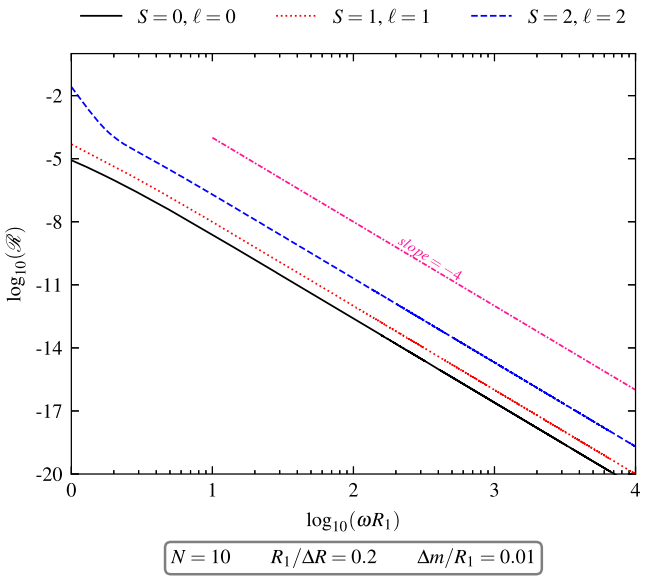

FIG. 3. Reflection coefficient versus the dimensionless frequency in a log-log scale for different values of $S = \ell$ and the parameter values $N = 10$, $R_1/\Delta R = 0.2$, and $\Delta m/R_1 = 0.01$. For reference, we also display a line with slope −4 corresponding to the power law decay $(\omega R_1)^{-4}$.

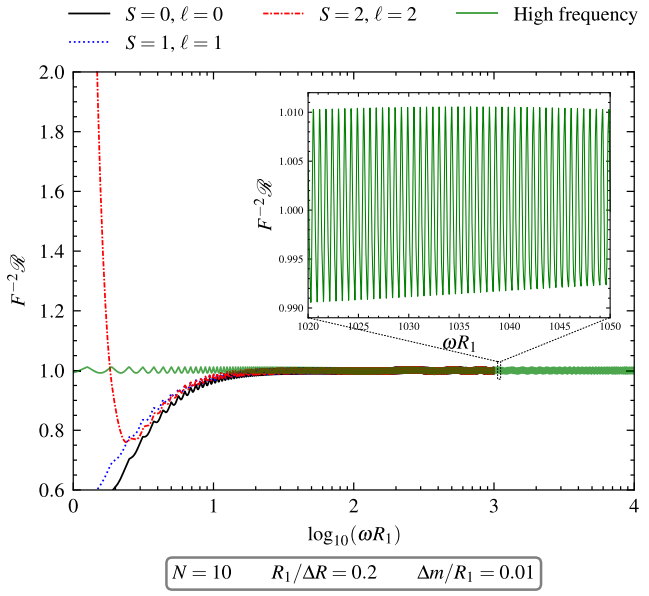

FIG. 4. Rescaled reflection coefficient versus the dimensionless frequency in a semilog scale for different values of $S=\ell$ and the parameter values $N=10$, $R_1/\Delta R=0.2$, $\Delta m/R_1=0.01$. Also shown is the high-frequency expression from Eq. (127). The inset represents a zoom in a linear scale over the interval $\omega R_1 \in [1020, 1050]$.

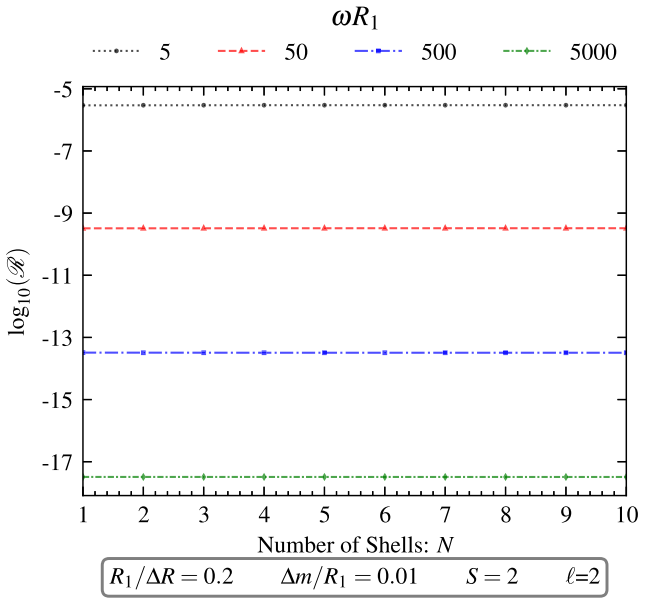

FIG. 5. Reflection coefficient versus the number of shells for different values for the dimensionless frequency ωR_1 and the parameters $R_1/\Delta R=0.2$, $\Delta m/R_1=0.01$, $S=2$, and $\ell=2$. The change in the reflection coefficient with respect to N is imperceptible (less than 1%), its value saturating from the first shell on. To better illustrate this fact, we have connected the data points at integer values of N with dotted or dashed lines.

B. High frequency reflection coefficient

The analysis of the behavior of the reflection coefficient in the high-frequency limit (HFL) is particularly significant for several reasons. First, the outcomes observed under the HFL are consistent with those predicted by the Wentzel-Kramers-Brillouin (WKB) method worked out in Appendix E. This consistency underlines the reliability of the HFL approach in our analysis. Second, the HFL proves to be a valuable tool for understanding the behavior of both transmission and reflection across various types of radiation discussed in this work, irrespective of their total angular momentum. To illustrate the utility of the HFL further, consider the following equation, which encapsulates the derived relationships and quantifies the reflection coefficients in a concise mathematical form

$$\mathscr{R} = F^2 \left| \sum_{k=1}^{N} \frac{e^{-2i\omega r_*(R_k)}}{(1+(k-1)\frac{\Delta R}{R_1})^3} \right|^2, \tag{127}$$

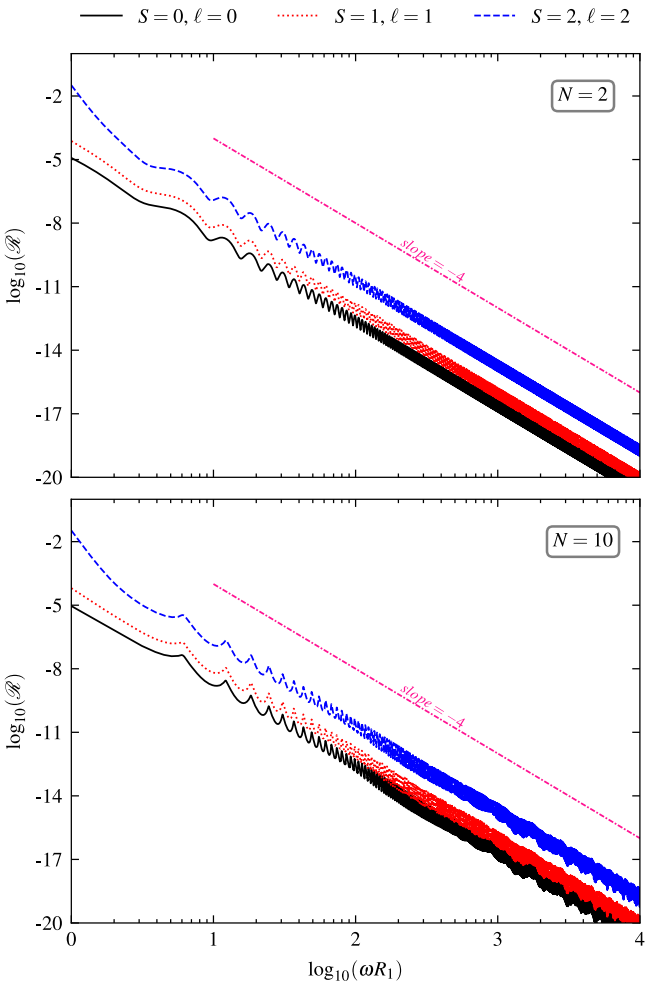

FIG. 6. Reflection coefficient versus dimensionless frequency on a log-log scale for different values of $S=\ell$. The parameters are $R_1/\Delta R=2$ and $\Delta m/R_1=0.01$ and $N=2$ (top panel) and $N=10$ (bottom panel).

where the factor F is given by

$$F := \frac{\Delta m}{R_1}\frac{\ell(\ell+1)-1+S^2}{2(\omega R_1)^2}. \tag{128}$$

It is remarkable that the dependency on the angular momentum and spin only appears in the factor F, which allows us to study the dependency on ω and N by considering only the second factor in Eq. (127). In view of this, it will turn out to be convenient to analyze the quantity $F^{-2}\mathscr{R}$ instead of $\mathscr{R}$, as the former becomes independent of ℓ and S in the HFL.

C. Numerical results

In what follows, we analyze the behavior of the reflection coefficient using the expressions (121), (122), (123), and (127), as a function of the following dimensionless parameters

(i) ωR_1 (dimensionless frequency),
(ii) $\Delta m/R_1$ (perturbative parameter),
(iii) $\Delta R/R_1$ (distance between the shells in units of R_1).

Note that $\Delta R/R_1$ determines the average mass density of the system (i.e., its total mass divided by its volume), small values corresponding to high average densities and vice-versa. As we will see, this density influences the qualitative behavior of the reflection coefficient. To illustrate this point, we exhibit our results for three different configurations: low average density ($R_1/\Delta R = 0.2$), medium average density ($R_1/\Delta R = 2$), and high average density ($R_1/\Delta R = 20$). In each case we show results for the reflection coefficient for waves with $S = 0$, 1, 2, and for definiteness we restrict ourselves to $\ell = S$ (however, note that in the HFL, the value of ℓ only affects the factor F). A direct comparison between the low, medium, and high average density systems will also be provided at the end of this section.

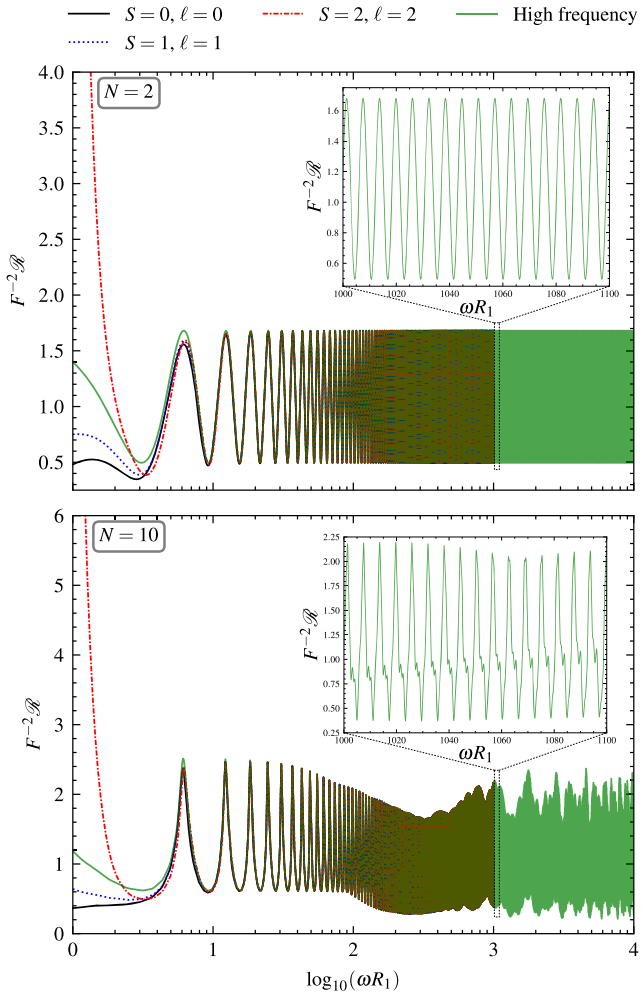

FIG. 7. Rescaled reflection coefficient versus the dimensionless frequency in a semilog scale for different values of $S = \ell$ and the parameter values $R_1/\Delta R = 2$, $\Delta m/R_1 = 0.01$ and $N = 2$ (top panel) or $N = 10$ (bottom panel). Also shown is the high-frequency limit obtained from the expression in Eq. (127). The insets in both panels provide a zoomed view in a linear scale over the interval $\omega R_1 \in [1000, 1100]$.

1. Low average density

Figure 3 shows the reflection coefficient as a function of the frequency on a log-log scale for $N = 10$ shells. We observe that for fixed ω, this coefficient becomes larger as S and ℓ increase, as is expected from the behavior of the function F in the HFL. Furthermore, a slope of approximately -4 is observed, indicating that the reflection

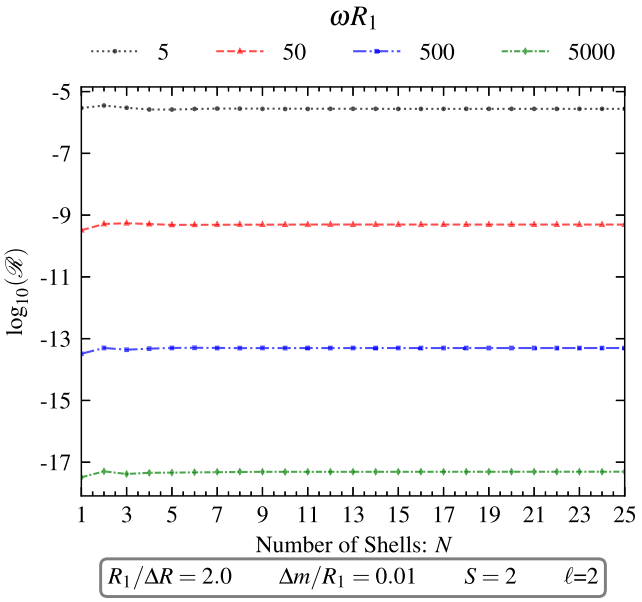

FIG. 8. Reflection coefficient versus the number of shells for different values of the dimensionless frequency ωR_1 and the parameters $R_1/\Delta R = 2$, $\Delta m/R_1 = 0.01$, and $S = \ell = 2$. Small fluctuations in the reflection coefficient are observed in the first 5 shells; however from the sixth shell on these fluctuations are smaller than about 2%.

coefficient decays according to the power law $(\omega R_1)^{-4}$. This can again be attributed to the expression for the factor F in the HFL, see Eqs. (127) and (128). Figure 4 shows the rescaled reflection coefficient $F^{-2}\mathscr{R}$ as a function of the frequency in a semi-log scale, along with the HFL expression (127). As expected, the exact coefficients converge to the ones obtained in the HFL for large values of ωR_1. Note also that the reflection coefficient exhibits an oscillatory behavior in the frequency, albeit with a tiny amplitude.

We have also varied the number of shells N from 1 to 100 and found the same qualitative behavior as the one shown in Figs. 3 and 4, with variations of the reflection coefficient of less than 1%. This is further illustrated in Fig. 5. The fact that for the low average density case the reflection coefficient is nearly independent of N can be understood by looking at the HFL expression (127). Indeed, for $\Delta R/R_1 = 5$, the second term in the sum is smaller in magnitude than the first term by a factor of at least $6^3 = 216$.

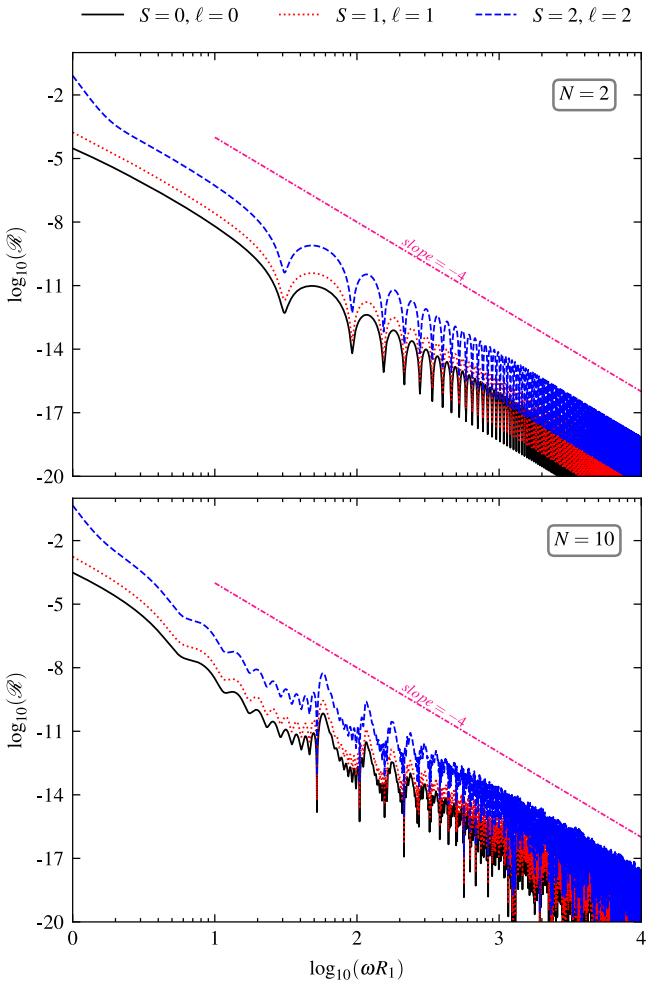

FIG. 9. Reflection coefficient versus the dimensionless frequency in a log-log scale for different values of $S = \ell$ and parameters $R_1/\Delta R = 20$, $\Delta m/R_1 = 0.01$ and $N = 2$ (top panel) and $N = 10$ (bottom panel).

2. Medium average density

Figures 6–8 show the behavior of the reflection coefficient for the medium average density case, and they should be compared with the corresponding Figs. 3–5 for low average density. As can be seen from this comparison, the medium average density reflection coefficient decays again as $(\omega R_1)^{-4}$, as predicted from the factor F in the HFL. However, in contrast to the low average density case, the reflection coefficient exhibits oscillations in the frequency with a much larger amplitude which originate from the sum in the second factor of Eq. (127). Furthermore, one observes that these oscillations become more irregular when the number of shells increases from $N = 2$ to $N = 10$. This effect is particularly visible from the plots in Fig. 7 and the inset in the bottom panel of that figure which shows that the oscillations are not sinusoidal.

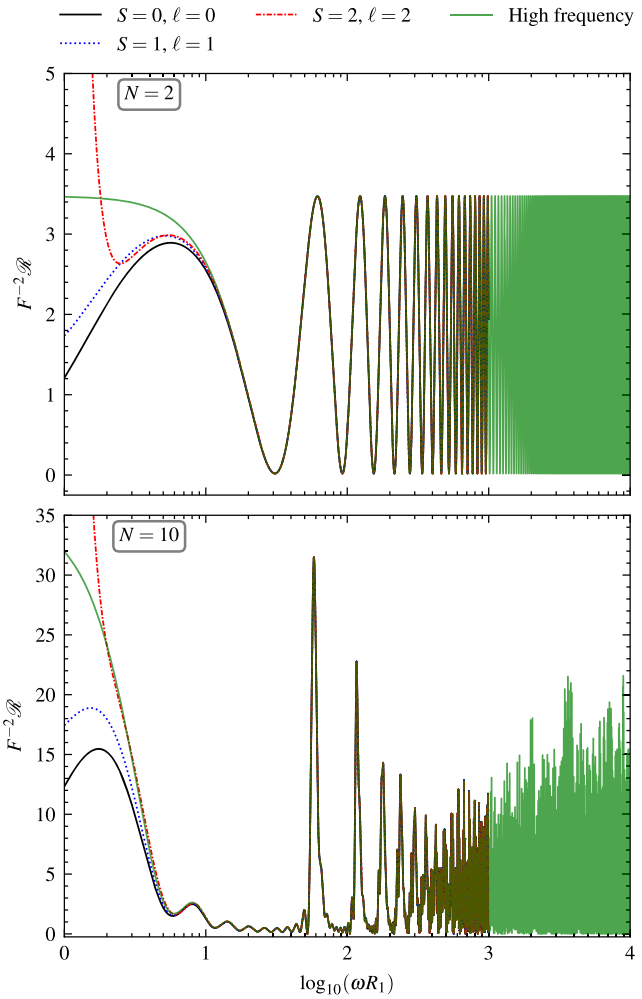

FIG. 10. Rescaled reflection coefficient versus the dimensionless frequency in a semilog scale for different values of $S = \ell$ and the parameter values $R_1/\Delta R = 20$, $\Delta m/R_1 = 0.01$ and $N = 2$ (top panel) and $N = 10$ (bottom panel). Also shown is the high-frequency limit obtained from the expression in Eq. (127).

From Fig. 8 we see that the reflection coefficient shows small fluctuations as a function of N up to the first 6 shells, after which it saturates to a constant value. As in the previous case, this can be understood by looking at the HFL expression (127), for which $\Delta R/R_1 = 1/2$ in the medium average density case, such that the seventh term in the sum is smaller than the first one by a factor of at least $4^3 = 64$, which is consistent with the 2% bound observed for $N \geq 6$.

3. High average density

Figures 9–11 show the behavior of the reflection coefficient for a system with high average density. As these figures show, the oscillations' amplitude is even larger than in the medium average density case. They are still regular for $N = 2$; however for $N = 10$ they present an irregular pattern, as in the medium average density case. Regarding the saturation of the reflection coefficient with the number of shells shown in Fig. 11, we see that it occurs at about $N = 60$. Comparing the sixty-first term in the sum in Eq. (127) with $\Delta R/R_1 = 1/20$, we obtain a factor of $4^3 = 64$ relative to the first term in the sum, which is consistent with the 2% bound observed for $N \geq 60$.

4. Direct comparison between low, medium, and high average density

Finally, we show in Fig. 12 a comparison of the rescaled reflection coefficient $F^{-2}\mathscr{R}$ between the low, medium and high average density systems, as a function of $\omega\Delta R$. As observed previously, in the low density case the reflection coefficient oscillates with a very small amplitude which is not visible in this plot, whereas the oscillations are more pronounced in the medium and high density cases. As can be observed, the (rescaled) period of the oscillations in the medium and high density cases are similar; however the oscillations in the latter case are much more irregular.

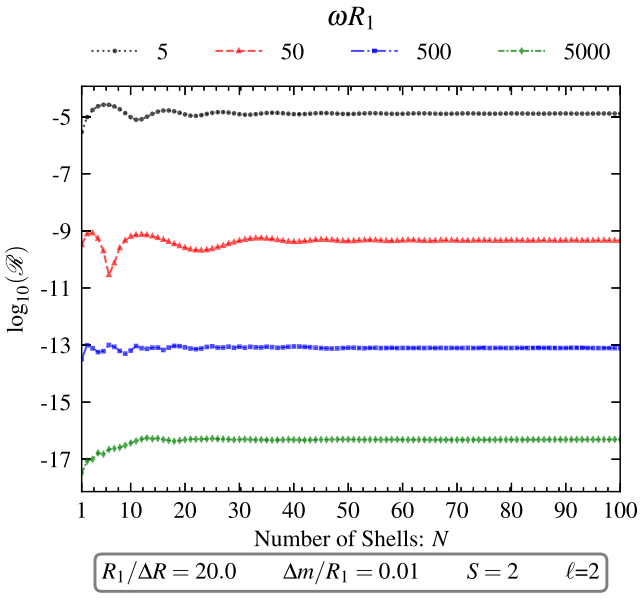

FIG. 11. Reflection coefficient versus the number of shells for different values of the dimensionless frequency ωR_1 and the parameters $R_1/\Delta R = 20$, $\Delta m/R_1 = 0.01$, and $S = \ell = 2$. Moderate fluctuations in the reflection coefficient are observed in the first 50 shells; however from the sixtieth shell on these fluctuations are smaller than about 2%.

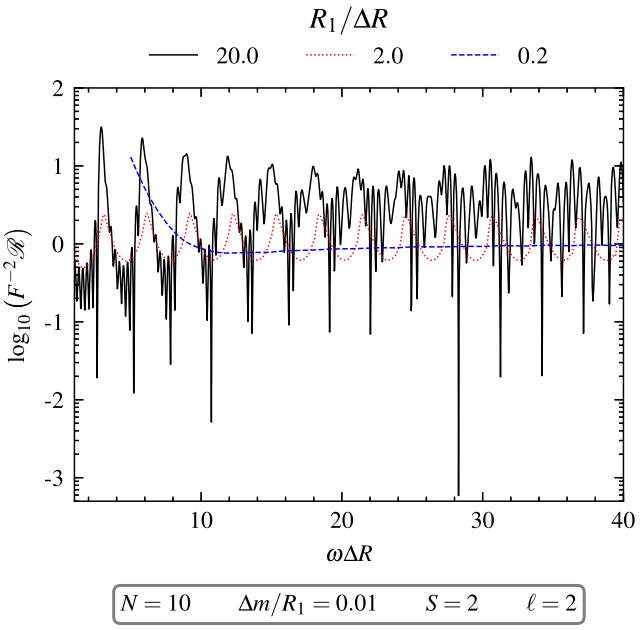

FIG. 12. Rescaled reflection coefficient versus the rescaled frequency $\omega\Delta R = \frac{\Delta R}{R_1} \cdot \omega R_1$ in a semilogarithmic scale for fixed parameters $N = 10$, $\Delta m/R_1 = 0.01$, $S = 2$, and $\ell = 2$ and different values of $R_1/\Delta R$.

VII. CONCLUSIONS

In this work, we have considered a spacetime consisting of N thin spherical concentric shells of matter separated by vacuum regions. By specifying an appropriate equation of state for this matter and based on the Israel junction formalism and the work in Refs. [27,32], we have derived the relevant equilibrium conditions [see Eqs. (20) and (21)] leading to static configurations and analyzed their stability with respect to small spherical perturbations of the shells. In the regime of a weak gravitational field and low temperature (i.e., the internal surface energy is much smaller than the rest one), the hydrostatic equilibrium conditions simplify considerably [see Eqs. (28) and (29)] and can be interpreted in terms of Newtonian physics. Furthermore, we have shown that in this limit, the stability conditions are automatically satisfied.

In particular, we have shown that by choosing a configuration consisting of equidistant shells of equal mass, the low-temperature weak field limit can be maintained independently of the number of shells N.

This allowed us to study the transmission properties of an outgoing monochromatic wave emanating from a source located at the center of the configuration and propagating through a configuration with an arbitrary number of shells. We solved the Regge-Wheeler equation perturbatively to first order in the small parameter $2m/r$ for a field with arbitrary spin S and angular momentum number $\ell \geq S$ [see Eqs. (62) and (63)]. To the best of our knowledge, the generalization to arbitrary values of ℓ is a new result. We also note that, since we have analytical formulas with fast-converging series for the reflection coefficient, the computational costs of evaluating the transmission and reflection coefficients are totally negligible.

By using the transfer matrix formalism, we performed a comprehensive study of the transmission and reflection coefficients as a function of the frequency, the distance between the shells and the number of shells.

Our study revealed that the qualitative properties of the transmission and reflection coefficients depend fundamentally on the ratio between the areal radius of the first shell and the distance between the shells, which determines the average mass density of the system. While for low average density the reflection coefficient decays as $(\omega R_1)^{-4}$ and is almost independent of N, systems with high average density still decay in the same fashion but are modulated by wide oscillations in ωR_1 which become more and more pronounced as N increases. Most of these effects can be understood from the expression in Eq. (127) in the high-frequency limit.

In all cases we have studied, the reflection and transmission coefficients approach a finite value as N becomes large. In particular, the transmission coefficient does not converge to zero in this limit. We attribute this to the fact that the transmission through the jth shell is determined by its surface density $\Delta m/(4\pi R_j)^2$ [cf. Eqs. (91), (96), and (119)]. Since in our model Δm is constant and R_j grows linearly with j, the shells become progressively less dense and, therefore, more transparent which leads to the observed saturation as N increases.

Future research could study the generalization of the present analysis to include even-parity linearized gravitational waves and different scenarios, like the propagation of a monochromatic plane wave from infinity through the spacetime region shaped by N thin spherical concentric shells. Furthermore, it would be interesting to consider models with random fluctuations of the masses of the shells and the distances between them. Specifically, one could analyze in such a model the transmission properties of outgoing waves, and investigate whether disorder can produce localization effects [58–61].

ACKNOWLEDGMENTS

We thank Francisco Astorga, Alberto Diez-Tejedor, Ulises Nucamendi, and Emilio Tejeda for fruitful discussions. R. O. A. C. was supported by a CONAHCyT doctoral scholarship. This work was partially supported by CONAHCyT Projects No. CF 2019/376127 and No. CBF-2023-2024-3116 and by CIC Grant No. 18090 and No. 18315 of the Universidad Michoacana de San Nicolás de Hidalgo.

APPENDIX A: HYDROSTATIC EQUILIBRIUM FOR THIN NEWTONIAN SHELLS

In this appendix we show that Eq. (29) which was obtained in Sec. II D by taking the nonrelativistic limit of the Israel junction conditions can also be directly derived from the condition of hydrostatic equilibrium of a thin shell in a purely Newtonian setting. Our arguments are based on Secs. II A and B of [27] and generalize the results of that work to the case in which the shell surrounds a spherical concentric mass distribution.

Hence, we consider a thin spherical shell of matter of mass m_s and radius R which is subject to two forces: the force due to the push of matter in the outward radial direction, generated by the surface pressure p, and the gravitational force which is directed toward the center of the configuration. Let us denote the radial components of these forces by F_p and F_g, respectively, such that the total force acting on the shell is

$$F = F_p + F_g. \tag{A1}$$

The force F_p is obtained by analyzing the work done by the surface pressure due to an increase dA of the area of the shell

$$dW = p \cdot dA = p \cdot 8\pi R dR, \tag{A2}$$

resulting in the net radial force being

$$F_p = 8\pi p R. \tag{A3}$$

To calculate the gravitational force, it is convenient to perform the calculation starting from a shell of finite width 2ε, as illustrated in Fig. 13, and taking the limit $\varepsilon \to 0$ at the end of the calculation. We assume that the shell has the following mass density profile

$$\rho(r) \coloneqq \begin{cases} \frac{\sigma}{2\varepsilon}, & R-\varepsilon < r < R+\varepsilon, \\ 0, & \text{otherwise}, \end{cases} \tag{A4}$$

where σ denotes the surface density in the limit $\varepsilon \to 0$. Accordingly, the total mass contained in a sphere of radius r lying in the interval $R-\varepsilon < r < R+\varepsilon$ is

$$m(r) = m_{\text{int}} + 4\pi\sigma \frac{r^3 - (R-\varepsilon)^3}{6\varepsilon}, \tag{A5}$$

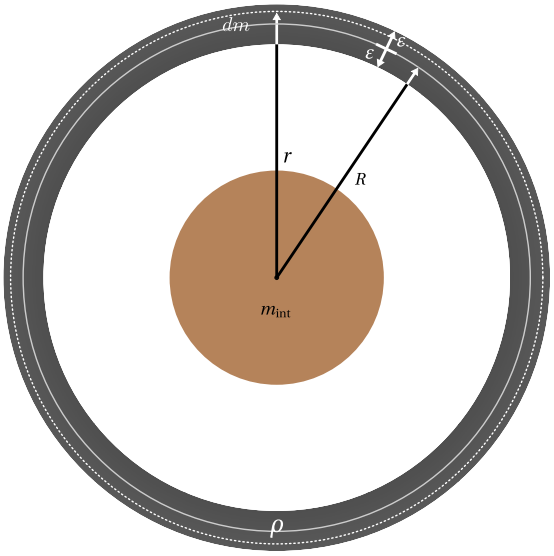

FIG. 13. Configuration consisting of a spherical shell of width 2ε with a central object of mass m_{int} in its center.

with m_{int} the mass of the central object. Note that the mass of the shell, $m_s = m(R+\varepsilon) - m(R-\varepsilon)$, converges to $4\pi R^2\sigma$ in the limit $\varepsilon \to 0$, as required. The gravitational force acting on the layer of radius r is

$$dF_g = -\frac{Gm(r)dm(r)}{r^2}, \qquad dm(r) = 4\pi r^2\rho(r)dr. \tag{A6}$$

Hence, the total gravitational force acting on the shell is

$$\begin{aligned} F_g &= -4\pi G \int_{R-\varepsilon}^{R+\varepsilon} m(r)\rho(r)dr \\ &= -4\pi G\sigma\left[m_{\text{int}} + \frac{2\pi\sigma}{3}(3R^2 - 2R\varepsilon + \varepsilon^2)\right]. \end{aligned} \tag{A7}$$

Taking the limit $\varepsilon \to 0$ we obtain for the total force

$$F = 8\pi pR - 2\pi G\sigma(2m_{\text{int}} + m_s), \tag{A8}$$

and hence the condition for hydrostatic balance is

$$2m_{\text{int}} + m_s = \frac{4R}{G}\frac{p}{\sigma}. \tag{A9}$$

To apply this result to the jth shell of the configurations in Sec. II we substitute $m_{\text{int}} \mapsto m_{j-1}$, $m_s \mapsto m_j - m_{j-1}$, $R \mapsto R_j$, $p \mapsto p_j$, $\sigma \mapsto \sigma_{\text{rest},j}$ and use geometrized units $G = 1$. This leads to Eq. (29) as was to be shown.

APPENDIX B: ERROR ESTIMATE FOR THE LINEAR APPROXIMATION OF FINITE MATRIX PRODUCTS

In this appendix we consider a finite product of matrices of the form

$$\mathbb{M}_N := (\mathbb{1} + \epsilon_N\mathbb{B}_N)(\mathbb{1} + \epsilon_{N-1}\mathbb{B}_{N-1})\cdots(\mathbb{1} + \epsilon_1\mathbb{B}_1), \tag{B1}$$

with a decreasing sequence $\epsilon := \epsilon_1 > \epsilon_2 > \ldots > \epsilon_{N-1} > \epsilon_N > 0$ of positive small numbers and uniformly bounded matrices $\mathbb{B}_j$, i.e., there is a constant b such that

$$\|\mathbb{B}_k\| \le b \tag{B2}$$

for all $k \ge 1$. Consider the first-order approximation

$$\mathbb{M}_N^{(1)} := \mathbb{1} + \sum_{j=1}^{N} \epsilon_j\mathbb{B}_j, \tag{B3}$$

such that $\mathbb{M}_N = \mathbb{M}_N^{(1)} + \mathcal{O}(\epsilon^2)$. In general the quadratic error term $\mathcal{O}(\epsilon^2)$ depends on N. However, we show in the following that if the sequence ϵ_k falls off sufficiently fast, then the error term has an upper bound proportional to ϵ^2 that is independent of N.

To analyze this, we note that the residual $R_N := \mathbb{M}_N - \mathbb{M}_N^{(1)}$ can be written as

$$\begin{aligned} R_N = &\sum_{k_1>k_2} \epsilon_{k_1}\epsilon_{k_2}\mathbb{B}_{k_1}\mathbb{B}_{k_2} + \sum_{k_1>k_2>k_3} \epsilon_{k_1}\epsilon_{k_2}\epsilon_{k_3}\mathbb{B}_{k_1}\mathbb{B}_{k_2}\mathbb{B}_{k_3} \\ &+ \cdots + \epsilon_N\epsilon_{N-1}\cdots\epsilon_1\mathbb{B}_N\mathbb{B}_{N-1}\cdots\mathbb{B}_1. \end{aligned} \tag{B4}$$

Taking into account Eq. (B2) and defining $s_N := \sum_{k=1}^{N}\epsilon_k$ one finds

$$\begin{aligned} \|R_N\| &\le b^2 \sum_{k_1>k_2} \epsilon_{k_1}\epsilon_{k_2} + b^3 \sum_{k_1>k_2>k_3} \epsilon_{k_1}\epsilon_{k_2}\epsilon_{k_3} \\ &\quad + \cdots + b^N\epsilon_N\epsilon_{N-1}\cdots\epsilon_1 \\ &\le \frac{b^2}{2}s_N^2 + \frac{b^3}{3!}s_N^3 + \cdots + \frac{b^N}{N!}s_N^N \\ &\le h(bs_N), \end{aligned} \tag{B5}$$

with the function $h(x) := e^x - 1 - x$. Using the estimate $h(x) \le \frac{1}{2}x^2e^x$ one concludes that

$$\|R_N\| \le \frac{1}{2}(bs_N)^2e^{bs_N}, \qquad s_N := \sum_{k=1}^{N}\epsilon_k, \tag{B6}$$

for all $N \in \mathbb{N}$. In particular, if

$$s_\infty := \sum_{k=1}^{\infty}\epsilon_k < \infty \tag{B7}$$

converges, it follows that R_N has an upper bound that is independent of N. For the calculations in Sec. IV, the relevant model is $\epsilon_k = \epsilon/k^2$; therefore $s_\infty = \epsilon \times \pi^2/6$ and one obtains the uniform bound

$$\|R_N\| \leq \frac{\pi^4 b^2}{36}\epsilon^2, \tag{B8}$$

for all $N \in \mathbb{N}$ and small enough $\epsilon > 0$ such that $\pi^2 b\epsilon \leq 6\log(2)$.

If ϵ_k is small but is not summable one cannot expect such a uniform bound in general. For example, if all $\mathbb{B}_k$'s are equal to the identity matrix and $\epsilon_k = \epsilon/k$, then it follows from Eq. (B4) that

$$\begin{aligned}\|R_N\| &\geq 1 + \sum_{k_1>k_2} \epsilon_{k_1}\epsilon_{k_2} \\ &= 1 + \frac{\epsilon^2}{2}\left[\left(\sum_{k=1}^{N}\frac{1}{k}\right)^2 - \sum_{k=1}^{N}\frac{1}{k^2}\right], \\ &\geq 1 + \frac{\epsilon^2}{2}\left[\left(\sum_{k=1}^{N}\frac{1}{k}\right)^2 - \frac{\pi^2}{6}\right],\end{aligned} \tag{B9}$$

which diverges like $(\log N)^2$ when $N \to \infty$ even if ϵ is small.

APPENDIX C: ELECTROMAGNETIC FLUX THROUGH A SPHERE

In this appendix we show that the electromagnetic flux through a sphere computed from the electromagnetic energy-momentum tensor is, up to a factor, equal to the expression obtained from the effective energy-momentum tensor with $S = 1$ in Sec. V.

Recall that in terms of the electromagnetic field tensor $F_{\mu\nu}$ the electromagnetic energy-momentum tensor $T^{\mu\nu}_{em}$ is given by

$$(T_{em})^\mu{}_\nu = F^{\mu\alpha}F_{\nu\alpha} - \frac{1}{4}\delta^\mu{}_\nu F_{\alpha\beta}F^{\alpha\beta}, \tag{C1}$$

and recall that only its rt-component is needed to compute the average energy flow per unit time from Eq. (104). In particular, the radial component of the electromagnetic current is

$$J^r_{(\mathrm{em})} = -(T_{em})^r{}_t = -F^{rA}F_{tA}, \tag{C2}$$

where $A = \vartheta, \varphi$ refer to the spherical components. In the following, we express this quantity in terms of the functions $\Phi_{\ell m}$ that appear in Eq. (98).

To this purpose, it is necessary to know the relation between the components F_{tA} and F_{rA} of the electromagnetic field tensor and the functions $\Phi_{\ell m}$. From Sec. III B in Ref. [51] one can deduce the relation between $F_{\mu\nu}$ and the master scalars $\Phi^{(\pm)}$ in the even- and odd-parity sectors (denoted by Φ and $\nu^{(inv)}$ in [51]), which are related to our functions $\Phi_\ell(t,r) = \Phi^{(\pm)}_{\ell m}(t,r)$ satisfying the RW equation (35) with $S = 1$ according to

$$\Phi^{(\pm)}(t,r,\vartheta,\varphi) = \sum_{\ell=1}^{\infty}\sum_{m=-\ell}^{\ell}\Phi^{(\pm)}_{\ell m}(t,r)Y^{\ell m}(\vartheta,\varphi). \tag{C3}$$

In terms of these master scalars one has

$$F_{tA} = -\hat{\nabla}_A\hat{\Delta}^{-1}(\tilde{\varepsilon}^a{}_t\partial_a\Phi^{(+)}) + \hat{\varepsilon}_A{}^B\hat{\nabla}_B\partial_t\Phi^{(-)}, \tag{C4}$$

$$F_{rA} = -\hat{\nabla}_A\hat{\Delta}^{-1}(\tilde{\varepsilon}^a{}_r\partial_a\Phi^{(+)}) + \hat{\varepsilon}_A{}^B\hat{\nabla}_B\partial_r\Phi^{(-)}, \tag{C5}$$

where $\hat{\nabla}_A$, $\hat{\Delta}$, $\hat{\varepsilon}_{AB}$ are the covariant derivative, the Laplacian, and the volume form associated with the unit two-sphere S^2, respectively, and $\tilde{\varepsilon}_{ab}$ is the volume form with respect to the two-metric $\tilde{g}_{ab}dx^a dx^b = -\mathcal{N}(r)dt^2 + dr^2/\mathcal{N}(r)$, $\mathcal{N}(r) := 1 - 2m(r)/r$.

Using the fact that $\tilde{\varepsilon}_{tr} = -\tilde{\varepsilon}_{rt} = 1$ and substituting Eqs. (C4), (C5) into Eq. (C2) yields, after integrating and using integration by parts,

$$\int_{S^2_r} d\Omega r^2 J^r_{(\mathrm{em})} = \sum_{\pm}\int_{S^2_r} d\Omega\left(\frac{\partial\Phi^{(\pm)}}{\partial r_*}\right)\hat{\Delta}^{\mp 1}\left(\frac{\partial\Phi^{(\pm)}}{\partial t}\right). \tag{C6}$$

Introducing the expansion (C3) into the above and using the orthonormality property of the spherical harmonics yields

$$\int_{S^2_r} d\Omega r^2 J^r_{(\mathrm{em})} = -\mathrm{Re}\sum_{\ell m\pm}[\ell(\ell+1)]^{\mp 1}\left(\overline{\frac{\partial\Phi^{(\pm)}_{\ell m}}{\partial r_*}}\right)\left(\frac{\partial\Phi^{(\pm)}_{\ell m}}{\partial t}\right). \tag{C7}$$

Up to the factors $[\ell(\ell+1)]^{\mp 1}$ (which can be absorbed into the definitions of $\Phi^{(\pm)}_{\ell m}$) this agrees precisely with the expression on the first line of Eq. (106). Therefore, for $S = 1$, we obtain expressions for the electromagnetic flux which are equivalent to the ones derived in Sec. V A. In particular, the reflection and transmission coefficients defined in Eq. (114) yield identical results in both cases.

APPENDIX D: PROPERTIES OF AUXILIARY MATRICES

In this appendix it will be shown that the diagonal elements of the matrix $\mathbb{B}_\ell(R_j)$ defined in Eq. (88) are purely imaginary. This is based on the fact that the parameter $2m_j/R_j$ is small and it is known that the elements of the matrix $\mathbb{D}_\ell(R_j)$ satisfy

$$[\mathbb{D}_\ell(R_j)]_{12} = \overline{[\mathbb{D}_\ell(R_j)]_{11}}, \tag{D1}$$

$$[\mathbb{D}_\ell(R_j)]_{22} = \overline{[\mathbb{D}_\ell(R_j)]_{21}}, \tag{D2}$$

as follows from the definition in Eq. (72) and the symmetry (68) between the in- and outgoing solutions. Of course, the properties (D1), (D2) also apply to the matrices $\mathbb{D}_\ell(R_j)^{(0)}$ and $\mathbb{D}_\ell(R_j)^{(1)}$ in the sum (87). Furthermore, recall that the matrices $\mathbb{D}_\ell(R_j)$ and $\mathbb{D}_\ell(R_j)^{(0)}$ have determinant $2s = -2i\omega$. As a consequence, one can verify that the matrix elements of $[\mathbb{D}_\ell(R_j)^{(0)}]^{-1}$ satisfy

$$[\mathbb{D}_\ell(R_j)^{(0)}]^{-1}_{21} = \overline{[\mathbb{D}_\ell(R_j)^{(0)}]^{-1}_{11}}, \tag{D3}$$

$$[\mathbb{D}_\ell(R_j)^{(0)}]^{-1}_{22} = \overline{[\mathbb{D}_\ell(R_j)^{(0)}]^{-1}_{12}}, \tag{D4}$$

which implies that

$$[\mathbb{B}_\ell(R_j)]_{22} = \overline{[\mathbb{B}_\ell(R_j)]_{11}}, \tag{D5}$$

$$[\mathbb{B}_\ell(R_j)]_{21} = \overline{[\mathbb{B}_\ell(R_j)]_{12}}. \tag{D6}$$

Finally, applying the determinant to both sides of Eq. (89) and using the aforementioned properties one finds

$$1 = \det\left(\mathbb{1} + \frac{2m_j}{\omega R_j^2}\mathbb{B}_\ell(R_j)\right) \tag{D7}$$

$$= 1 + \frac{2m_j}{\omega R_j^2}\operatorname{tr}\mathbb{B}_\ell(R_j) + \mathcal{O}\left(\left(\frac{2m_j}{\omega R_j^2}\right)^2\right), \tag{D8}$$

showing that the trace of $\mathbb{B}_\ell(R_j)$ is zero. Together with Eq. (D5) this yields

$$[\mathbb{B}_\ell(R_j)]_{11} + \overline{[\mathbb{B}_\ell(R_j)]_{11}} = 0, \tag{D9}$$

which implies that the diagonal elements of $\mathbb{B}_\ell(R_j)$ are purely imaginary numbers.

APPENDIX E: INDEPENDENT WKB CALCULATION FOR THE TRANSFER MATRIX

In this appendix we perform an independent calculation for the transfer matrix in the high-frequency limit which is based on the WKB approximation. The calculation does not make use of the expansion of the RW equation in $2M/r$, and hence it provides an independent verification for the results obtained in Sec. IV for high frequencies.

We start by introducing the ansatz $\Phi_\ell(t,r) = e^{-i\omega t}u(r)$ into the RW equation (35), where from now on we drop the index ℓ for notational simplicity. This yields the time-independent Schrödinger equation

$$\left[-\frac{\partial^2}{\partial r_*^2} + V(r)\right]u(r) = Eu(r), \tag{E1}$$

with $E = \omega^2$ and the potential

$$V(r) \coloneqq \mathcal{N}(r)\left[\frac{\ell(\ell+1)}{r^2} + (1-S^2)\frac{2m(r)}{r^3}\right]. \tag{E2}$$

As in Appendix C, $\mathcal{N}(r)$ refers to the function $\mathcal{N}(r) \coloneqq 1 - 2m(r)/r$, and we also recall that the relation between the tortoise coordinate r_* and the areal radial coordinate r is given by Eq. (37) or (38). As in Sec. III we first compute the solution in the region between two shells, where m is constant and the potential $V(r)$ is smooth and then match the solutions across the shells using the matching conditions derived in Sec. III E.

In the WKB approximation (see for instance chapters 6 and 7 in Ref. [62]) the in- and outgoing solutions of Eq. (E1) in the region $R_j < r < R_{j+1}$ are given by

$$u_{\nwarrow,j}(r) \coloneqq \frac{e^{-i\phi_j(r)}}{\sqrt{k_j(r)}}, \qquad u_{\nearrow,j}(r) \coloneqq \frac{e^{i\phi_j(r)}}{\sqrt{k_j(r)}}, \tag{E3}$$

with the phase function

$$\phi_j(r) \coloneqq \int^r k_j(s)ds_*. \tag{E4}$$

Here, $k_j(r) \coloneqq \sqrt{E - V_j(r)}$ with V_j being the potential V in the region $R_j < r < R_{j+1}$ where $m(r) = m_j$ is constant, and $ds_* = ds/\mathcal{N}_j(s)$. The approximation is valid as long as

$$\left|\frac{\mathcal{N}_j(r)k_j'(r)}{k_j(r)^2}\right| = \frac{1}{2}\frac{|\mathcal{N}_j(r)V_j'(r)|}{|E - V_j(r)|^{3/2}} \ll 1, \tag{E5}$$

where the prime denotes differentiation with respect to r. In particular, the condition (E5) is satisfied for $E = \omega^2 \gg V(r)$.

In analogy with Eq. (67) the WKB solution in the region $R_j < r < R_{j+1}$ is

$$u_j(r) = \Lambda_j u_{\nwarrow,j}(r) + \Upsilon_j u_{\nearrow,j}(r), \tag{E6}$$

and the matching conditions can be written in the same form as Eq. (71), that is

$$\mathbb{D}_j(R_j)\begin{pmatrix}\Upsilon_j\\ \Lambda_j\end{pmatrix} = \mathbb{D}_{j-1}(R_j)\begin{pmatrix}\Upsilon_{j-1}\\ \Lambda_{j-1}\end{pmatrix}, \tag{E7}$$

with

$$\mathbb{D}_j(r) \coloneqq \begin{pmatrix} u_{\nearrow,j}(r) & u_{\nwarrow,j}(r) \\ \mathcal{N}_j(r)u_{\nearrow,j}'(r) & \mathcal{N}_j(r)u_{\nwarrow,j}'(r)\end{pmatrix}. \tag{E8}$$

Using Eq. (E3) one finds

$$\mathcal{N}_j(r)u'_{\nearrow,j}(r) = \left[ik_j(r) - \frac{1}{2}\frac{\mathcal{N}_j(r)k'_j(r)}{k_j(r)}\right]u_{\nearrow,j}(r), \tag{E9}$$

and similarly for the derivative of $u_{\nwarrow,j}(r)$. Owing to condition (E5) one can neglect the second term on the right-hand side, which leads to the following simplification

$$\mathbb{D}_j(r) = \begin{pmatrix} u_{\nearrow,j}(r) & u_{\nwarrow,j}(r) \\ ik_j(r)u_{\nearrow,j}(r) & -ik_j(r)u_{\nwarrow,j}(r) \end{pmatrix}. \tag{E10}$$

Note that $\det(\mathbb{D}_j(r)) = -2i$. From this, one finds

$$\begin{pmatrix} \Upsilon_j \\ \Lambda_j \end{pmatrix} = \mathbb{M}_j \begin{pmatrix} \Upsilon_{j-1} \\ \Lambda_{j-1} \end{pmatrix}, \tag{E11}$$

with the WKB transfer matrix

$$\mathbb{M}_j := \begin{pmatrix} \cosh(\Theta_j)e^{-i\Delta_j} & \sinh(\Theta_j)e^{-i\Sigma_j} \\ \sinh(\Theta_j)e^{i\Sigma_j} & \cosh(\Theta_j)e^{i\Delta_j} \end{pmatrix} \tag{E12}$$

where Θ_j, Δ_j, and Σ_j are defined as

$$e^{\Theta_j} := \sqrt{\frac{k_j(R_j)}{k_{j-1}(R_j)}}, \tag{E13}$$

$$\Delta_j := \phi_j(R_j) - \phi_{j-1}(R_j), \tag{E14}$$

$$\Sigma_j := \phi_j(R_j) + \phi_{j-1}(R_j). \tag{E15}$$

In the high-frequency limit $\omega^2 \gg V_j(r)$ we can expand

$$k_j(r) = \omega\sqrt{1 - \frac{V_j(r)}{\omega^2}} = \omega\left[1 - \frac{V_j(r)}{2\omega^2} + \mathcal{O}\left(\frac{V_j(r)^2}{\omega^4}\right)\right], \tag{E16}$$

which yields

$$e^{\pm\Theta_j} = 1 \mp \frac{V_j(R_j) - V_{j-1}(R_j)}{4\omega^2} + \mathcal{O}\left(\frac{V_j^2}{\omega^4}\right). \tag{E17}$$

Using Eq. (E2), recalling $m_j - m_{j-1} = \Delta m$ and abbreviating $\mu_j := (m_j + m_{j+1})/R_j$, one finds

$$\cosh(\Theta_j) = 1 + \mathcal{O}\left(\frac{V_j^2}{\omega^4}\right), \tag{E18}$$

$$\sinh(\Theta_j) = \frac{\Delta m}{2R_j^3\omega^2}[\ell(\ell+1) - (1-S^2)(1-2\mu_j)] + \mathcal{O}\left(\frac{V_j^2}{\omega^4}\right). \tag{E19}$$

Furthermore, after integrating Eq. (E16) and adjusting the integration constant, one obtains

$$\phi_j(r) = \omega r_* + \frac{1}{2\omega}\left[\frac{\ell(\ell+1)}{r} + \frac{(1-S^2)m_j}{r^2}\right] + \mathcal{O}\left(\frac{V_j^2 R_j}{\omega^3}\right). \tag{E20}$$

This implies

$$\Delta_j = \frac{1-S^2}{2\omega R_j}\frac{\Delta m}{R_j} + \mathcal{O}\left(\frac{V_j^2 R_j}{\omega^3}\right), \tag{E21}$$

$$\Sigma_j = 2\omega r_*|_{R_j} + \frac{1}{\omega R_j}[\ell(\ell+1) + (1-S^2)\mu_j] + \mathcal{O}\left(\frac{V_j^2 R_j}{\omega^3}\right). \tag{E22}$$

Taking into account that V_j is of the order $2m_j/R_j^3 \leq 1/R_j^2$ when $\ell = 0$ and of the order $1/R_j^2$ when $\ell \geq 1$, one obtains the following matrix elements

$$M_{j,11} = 1 - i\frac{1-S^2}{2\omega R_j}\frac{\Delta m}{R_j} - \frac{1}{2}\left(\frac{1-S^2}{2\omega R_j}\frac{\Delta m}{R_j}\right)^2 + \mathcal{O}\left(\frac{1}{\omega^3 R_j^3}\right), \tag{E23}$$

$$M_{j,12} = \frac{\Delta m}{2\omega^2 R_j^3}[\ell(\ell+1) - (1-S^2)(1-2\mu_j)]e^{-2i\omega r_*|_{R_j}} + \mathcal{O}\left(\frac{1}{\omega^3 R_j^3}\right). \tag{E24}$$

The terms that are zeroth and first order in $\Delta m/R_j$ agree precisely with the results obtained in the high-frequency limit in Sec. IV A, see Eqs. (92), (93), (94).

[1] B. P. Abbott *et al.*, Observation of gravitational waves from a binary black hole merger, Phys. Rev. Lett. **116**, 061102 (2016).

[2] B. P. Abbott *et al.*, Tests of general relativity with GW150914, Phys. Rev. Lett. **116**, 221101 (2016).

[3] B. P. Abbott *et al.*, Multi-messenger observations of a binary neutron star merger*, Astrophys. J. Lett. **848**, L12 (2017).

[4] F. Pretorius, Binary black hole coalescence, in *Physics of Relativistic Objects in Compact Binaries: From Birth to Coalescence* (Springer, New York, 2009), pp. 305–369.

[5] I. Hinder, The current status of binary black hole simulations in numerical relativity, Classical Quantum Gravity **27**, 114004 (2010).

[6] M. D. Duez and Y. Zlochower, Numerical relativity of compact binaries in the 21st century, Rep. Prog. Phys. **82**, 016902 (2018).

[7] P. Amaro-Seoane, J. Andrews, M. Arca Sedda, A. Askar, Q. Baghi *et al.*, Astrophysics with the laser interferometer space antenna, Living Rev. Relativity **26**, 2 (2023).

[8] G. Baym, S. P. Patil, and C. J. Pethick, Damping of gravitational waves by matter, Phys. Rev. D **96**, 084033 (2017).

[9] N. T. Bishop, P. J. van der Walt, and M. Naidoo, Effect of a low density dust shell on the propagation of gravitational waves, Gen. Relativ. Gravit. **52**, 1 (2020).

[10] M. Naidoo, N. T. Bishop, and P. J. van der Walt, Modifications to the signal from a gravitational wave event due to a surrounding shell of matter, Gen. Relativ. Gravit. **53**, 77 (2021).

[11] N. T. Bishop, P. J. van der Walt, and M. Naidoo, Effect of a viscous fluid shell on the propagation of gravitational waves, Phys. Rev. D **106**, 084018 (2022).

[12] R. Lieu, K. Lackeos, and B. Zhang, Damping of long wavelength gravitational waves by the intergalactic medium, Classical Quantum Gravity **39**, 075014 (2022).

[13] N. T. Bishop, V. Kakkat, A. S. Kubeka, M. Naidoo, and P. J. van der Walt, The interaction of gravitational waves with matter, arXiv:2405.07743.

[14] F. P. Esposito, Interaction of gravitational radiation with an inviscid fluid in simple motion, Astrophys. J. **168**, 495 (1971).

[15] J. Ehlers, A. R. Prasanna, and R. A. Breuer, Propagation of gravitational waves through pressureless matter, Classical Quantum Gravity **4**, 253 (1987).

[16] J. Ehlers and A. R. Prasanna, A WKB formalism for multicomponent fields and its application to gravitational and sound waves in perfect fluids, Classical Quantum Gravity **13**, 2231 (1996).

[17] S. W. Hawking, Perturbations of an expanding universe, Astrophys. J. **145**, 544 (1966).

[18] F. P. Esposito, Absorption of gravitational energy by a viscous compressible fluid, Astrophys. J. **165**, 165 (1971).

[19] J. Madore, The absorption of gravitational radiation by a dissipative fluid, Commun. Math. Phys. **30**, 335 (1973).

[20] A. M. Anile and V. Pirronello, High-frequency gravitational waves in a dissipative fluid, Nuovo Cimento B (1971–1996) **48**, 90 (1978).

[21] A. Prasanna, Propagation of gravitational waves through a dispersive medium, Phys. Lett. A **257**, 120 (1999).

[22] V. Kakkat, N. T. Bishop, and A. S. Kubeka, Gravitational wave heating, Phys. Rev. D **109**, 024013 (2024).

[23] K. G. Zloshchastiev, Barotropic thin shells with linear eos as models of stars and circumstellar shells in general relativity, Int. J. Mod. Phys. D **08**, 549 (1999).

[24] S. Khakshournia and R. Mansouri, Dynamics of general relativistic spherically symmetric dust thick shells, Gen. Relativ. Gravit. **34**, 1847 (2002).

[25] J. Kijowski, G. Magli, and D. Malafarina, Relativistic dynamics of spherical timelike shells, Gen. Relativ. Gravit. **38**, 1697 (2006).

[26] J. Kijowski, G. Magli, and D. Malafarina, The Hamiltonian formulation for the dynamics of a multishell self-gravitating system, J. Math. Phys. (N.Y.) **51**, 072504 (2010).

[27] P. LeMaitre and E. Poisson, Equilibrium and stability of thin spherical shells in Newtonian and relativistic gravity, Am. J. Phys. **87**, 961 (2019).

[28] V. P. Frolov, M. A. Markov, and V. F. Mukhanov, Black holes as possible sources of closed and semiclosed worlds, Phys. Rev. D **41**, 383 (1990).

[29] E. Poisson and M. Visser, Thin-shell wormholes: Linearization stability, Phys. Rev. D **52**, 7318 (1995).

[30] F. S. N. Lobo and P. Crawford, Stability analysis of dynamic thin shells, Classical Quantum Gravity **22**, 4869 (2005).

[31] J. Frauendiener, C. Hoenselaers, and W. Konrad, A shell around a black hole, Classical Quantum Gravity **7**, 585 (1990).

[32] P. R. Brady, J. Louko, and E. Poisson, Stability of a shell around a black hole, Phys. Rev. D **44**, 1891 (1991).

[33] S. M. C. V. Gonçalves, Relativistic shells: Dynamics, horizons, and shell crossing, Phys. Rev. D **66**, 084021 (2002).

[34] J. P. Pereira, J. G. Coelho, and J. A. Rueda, Stability of thin-shell interfaces inside compact stars, Phys. Rev. D **90**, 123011 (2014).

[35] R. Gautreau and J. M. Cohen, Gravitational collapse in a single coordinate system, Am. J. Phys. **63**, 991 (1995).

[36] R. J. Adler, J. D. Bjorken, P. Chen, and J.-S. Liu, Simple analytical models of gravitational collapse, Am. J. Phys. **73**, 1148 (2005).

[37] E. Poisson and W. Israel, Internal structure of black holes, Phys. Rev. D **41**, 1796 (1990).

[38] W. Israel, Singular hypersurfaces and thin shells in general relativity, Nuovo Cimento B (1965–1970) **44**, 1 (1966).

[39] W. Israel, Gravitational collapse and causality, Phys. Rev. **153**, 1388 (1967).

[40] M. Mars and J. M. M. Senovilla, Geometry of general hypersurfaces in spacetime: Junction conditions, Classical Quantum Gravity **10**, 1865 (1993).

[41] L. T. Buchman and O. C. Sarbach, Towards absorbing outer boundaries in general relativity, Classical Quantum Gravity **23**, 6709 (2006).

[42] L. T. Buchman and O. C. Sarbach, Improved outer boundary conditions for Einstein's field equations, Classical Quantum Gravity **24**, S307 (2007).

[43] D. J. E. Marsh, Axion cosmology, Phys. Rep. **643**, 1 (2016).

[44] E. Ferreira, Ultra-light dark matter, Astron. Astrophys. Rev. **29**, 1 (2021).

[45] *The Search for Ultralight Bosonic Dark Matter*, edited by D. J. Kimball and K. van Bibber (Springer, New York, 2023).

[46] T. Matos, L. Ureña-López, and J.-W. Lee, Short review of the main achievements of the scalar field, fuzzy, ultralight, wave, BEC dark matter model, Front. Aston. Space Sci. **11**, 1 (2024).
[47] M. Khorrami and R. Mansouri, Spherically symmetric thin walls, Phys. Rev. D **44**, 557 (1991).
[48] R. M. Wald, *General Relativity* (University of Chicago Press, Chicago, IL, 2010).
[49] T. Regge and J. A. Wheeler, Stability of a Schwarzschild singularity, Phys. Rev. **108**, 1063 (1957).
[50] S. Chandrasekhar, The mathematical theory of black holes, in *General Relativity and Gravitation: Invited Papers and Discussion Reports of the 10th International Conference on General Relativity and Gravitation, Padua*, edited by B. Bertotti, F. de Felice, and A. Pascolini (Springer Netherlands, Dordrecht, 1984), pp. 5–26.
[51] E. Chaverra, N. Ortiz, and O. Sarbach, Linear perturbations of self-gravitating spherically symmetric configurations, Phys. Rev. D **87**, 044015 (2013).
[52] P. P. Fiziev, Exact solutions of Regge-Wheeler equation and quasi-normal modes of compact objects, Classical Quantum Gravity **23**, 2447 (2006).
[53] J. M. Bardeen and W. H. Press, Radiation fields in the Schwarzschild background, J. Math. Phys. (N.Y.) **14**, 7 (1973).
[54] F. W. Olver, D. W. Lozier, R. F. Boisvert, and C. W. Clark, *NIST Handbook of Mathematical Functions Hardback and CD-ROM* (Cambridge University Press, Cambridge, England, 2010).
[55] N. Straumann, *General Relativity*, Graduate Texts in Physics (Springer Science+Business Media, Dordrecht, 2013), ISBN 978-94-007-5409-6.
[56] O. Sarbach and M. Tiglio, Gauge-invariant perturbations of Schwarzschild black holes in horizon-penetrating coordinates, Phys. Rev. D **64**, 084016 (2001).
[57] N. Ortiz and O. Sarbach, Cauchy horizon stability in a collapsing spherical dust cloud: II. Energy bounds for test fields and odd-parity gravitational perturbations, Classical Quantum Gravity **35**, 025010 (2017).
[58] M. C. W. van Rossum and T. M. Nieuwenhuizen, Multiple scattering of classical waves: Microscopy, mesoscopy, and diffusion, Rev. Mod. Phys. **71**, 313 (1999).
[59] A. Ishimaru, *Electromagnetic Wave Propagation, Radiation, and Scattering* (Prentice-Hall, Englewood Cliffs, NJ, 1991).
[60] P. Sheng, *Introduction to Wave Scattering, Localization, and Mesoscopic Phenomena*, 2nd ed. (Springer, Berlin, 2006).
[61] P. Markoš and C. M. Soukoulis, *Wave Propagation: from Electrons to Photonic Crystals and Left-Handed Materials* (Princeton University Press, Princeton, NJ, 2008).
[62] F. Olver, *Introduction to Asymptotics and Special Functions* (Academic Press, New York, 1974).